



**This electronic thesis or dissertation has been
downloaded from Explore Bristol Research,
<http://research-information.bristol.ac.uk>**

Author:
Dornan, Tracey

Title:
Southern Ocean mesopelagic fish

Scales, drivers and the effects of environmental variability

General rights

Access to the thesis is subject to the Creative Commons Attribution - NonCommercial-No Derivatives 4.0 International Public License. A copy of this may be found at <https://creativecommons.org/licenses/by-nc-nd/4.0/legalcode>. This license sets out your rights and the restrictions that apply to your access to the thesis so it is important you read this before proceeding.

Take down policy

Some pages of this thesis may have been removed for copyright restrictions prior to having it been deposited in Explore Bristol Research. However, if you have discovered material within the thesis that you consider to be unlawful e.g. breaches of copyright (either yours or that of a third party) or any other law, including but not limited to those relating to patent, trademark, confidentiality, data protection, obscenity, defamation, libel, then please contact collections-metadata@bristol.ac.uk and include the following information in your message:

- Your contact details
- Bibliographic details for the item, including a URL
- An outline nature of the complaint

Your claim will be investigated and, where appropriate, the item in question will be removed from public view as soon as possible.

Southern Ocean mesopelagic fish:
Scales, drivers and the effects of
environmental variability

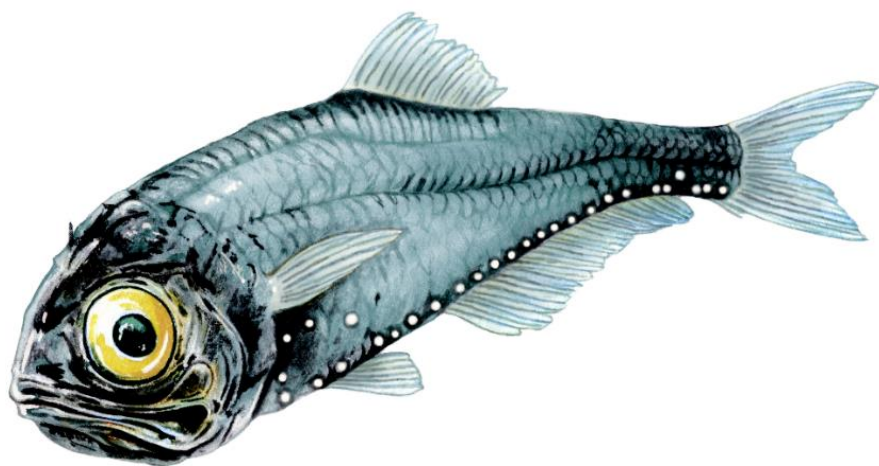
Tracey Dornan

A dissertation submitted to the University of Bristol in accordance with
the requirements for award of the degree of Doctor of Philosophy (PhD)
in the Faculty of Life Sciences.

School of Biological Sciences

November 2019

Word count: 59,706



Reproduced with the kind permission of the Government of the British Antarctic Territory.

Abstract

In the Southern Ocean, the mesopelagic zone 200 – 1000 m below sea level holds vast resources of fish, yet they remain one of the least investigated components of the Antarctic ecosystem. Sampling challenges have led to considerable uncertainty regarding mesopelagic fish biomass, limiting our ability to monitor populations or quantify their contribution to ecosystem function. Active acoustic methods, where pulses of sound are transmitted into the water column and the “backscattered” signal from organisms are detected by a transducer, enable us to sample the water column at greater spatial and temporal scales than conventional net sampling. However, to reliably interpret acoustic data we require information on the species present and their acoustic properties, which has been lacking for the Southern Ocean region. In this thesis I document the use of X-ray computed tomography scans to clarify swimbladder morphology of members of the mesopelagic fish community. I report a switch from fish possessing gas-filled swimbladders that contribute strongly to backscatter at low latitudes, to fish lacking gas-filled swimbladders at high latitudes. This contributes to the ubiquitous southward decline in acoustic backscatter that contrasts with latitudinal biomass patterns recorded from net samples. Patterns in acoustic data indicate that diel vertical migration of fish may be suppressed at high latitudes, which has implications for biogeochemical cycling. Acoustic backscatter was strongly related to sea surface temperature, daylight hours and sea ice extent. These relationships, coupled with taxon-specific calculations of acoustic Target Strength, yielded Southern Ocean mesopelagic fish biomass estimates considerably greater than previous net-based estimates. Overall, these findings indicate that knowledge of the acoustic properties of mesopelagic species, alongside core information on their relative abundance in the environment, can enable active acoustic data to become a powerful tool for researching, monitoring and managing the Southern Ocean ecosystem.

Dedication and acknowledgements

Firstly, I'd like to thank my supervisors **Sophie Fielding**, **Martin Genner** and **Ryan Saunders**. I am hugely grateful to Sophie, who has been fundamental to my development as a scientist, passing on her wealth of acoustics knowledge and experience, challenging my work to make it better, and giving me the opportunity to experience the beauty of the Southern Ocean, twice, thank you for everything. I am fortunate to have had **Martin** as my 'Bristol' supervisor, who has helped me when I couldn't see the wood for the trees, and encouraged me to think much bigger than I would have dared. **Ryan** has assisted me on my myctophid discovery, constructively commenting on drafts, and processing numerous fish samples over the years, which have made this research possible.

I gratefully acknowledge the support of my funders. Thank you to **NERC GW4+ DTP** for funding my research and professional development, and the **University of Bristol Alumni Foundation** for providing additional funds towards attending MEASO 2018. I am also grateful to the **British Antarctic Survey**, my academic home for the duration of my PhD.

Several people have helped me along the way. Particular thanks go to **John Horne**, who taught me to 'believe' in the sonar equation, and spent hours with me x-raying myctophids in the surgery of the RRS James Clark Ross, and developing film in the confines the 'darkroom' (a.k.a. the bathroom). Thank you to **Tom Davies** (University of Bristol), who worked with me as we learned how best to CT scan a fish, and went over and above to help me get the scans I needed. Thanks also to **Ket Smithson** (University of Cambridge) for helping to capture the final scans. **Tim Stanton** cheerfully took time to talk me through the acoustic models and methods I was using.

My research has depended on the collection of acoustic data and net samples, for which I thank the dedicated **crew and scientists of the RRS James Clark Ross and Polar Data Centre**. I am also indebted to all of the people who contribute to the upkeep of open-access environmental datasets. Thank you to all of the scientists on cruises JR15004 and JR16003, who shared their knowledge and love of the Southern Ocean and its inhabitants. Particular thanks go to **Gabbi Stowasser**, who taught me how to dissect a fish and somehow manages to capture the appropriate data amid the excitement of a catch landing on deck.

My friends and family deserve a special mention. Thanks to the maths legend that is **Emily Potter**, who helped me solve my (rarely simple) mathematical queries, with calm logic, patience, and when those failed - a pint. Thanks to the excellent early career researchers at the British Antarctic Survey, for making this journey so enjoyable. Thank you to my family, for their unconditional love and support. The **Ladies of the North** are a continuous source of inspiration and laughter, I doubt I would be on this path if it hadn't been for their presence in my life. My final deepest thanks are reserved **James**, for his unfailing belief, love and patience.

Author's declaration

I declare that the work in this dissertation was carried out in accordance with the requirements of the University's Regulations and Code of Practice for Research Degree Programmes and that it has not been submitted for any other academic award. Except where indicated by specific reference in the text, the work is the candidate's own work. Work done in collaboration with, or with the assistance of, others, is indicated as such. Any views expressed in the dissertation are those of the author.

SIGNED:

DATE: 8th November 2019

Table of contents

Abstract.....	i
Dedication and acknowledgements	ii
Author’s declaration.....	iii
Table of contents.....	iv
List of tables	viii
List of figures	xi
List of abbreviations.....	xvi
Chapter 1 General introduction.....	1
1.1 Overview	2
1.2 The Southern Ocean and Scotia Sea	3
1.2.1 Hydrography	3
1.2.2 Southern Ocean circulation	4
1.2.3 Water masses and fronts	5
1.2.4 Seasonal effects and climate change	8
1.3 The Southern Ocean ecosystem.....	8
1.4 Mesopelagic fish species overview	10
1.4.1 Global perspective.....	10
1.4.2 Southern Ocean and Scotia Sea species and distribution	11
1.4.3 Myctophids in the Southern Ocean food web.....	16
1.4.4 Behaviour and life history.....	16
1.4.5 Diet	18
1.4.6 Morphology.....	18
1.5 Methodologies for studying mesopelagic species/data.....	20
1.5.1 Net sampling.....	20
1.5.2 Acoustics – theory and practise.....	20
1.5.3 Abundance and Biomass estimation	24
1.5.4 Fish Target Strength estimates.....	25
1.5.5 Acoustics for studying spatial and temporal trends.....	26
1.6 Thesis outline.....	27
Chapter 2 Swimbladder morphology masks Southern Ocean mesopelagic fish biomass	29
2.1 Abstract	30

2.2	Introduction.....	30
2.3	Methods	32
2.3.1	Acoustic surveys.....	32
2.3.2	Net sampling.....	33
2.3.3	Swimbladder gas assessment.....	34
2.3.4	Statistical analysis	35
2.4	Results	36
2.4.1	Acoustic backscatter declines with latitude	36
2.4.2	Gas presence and absence of key mesopelagic fish species	37
2.4.3	Changing community structure	38
2.4.4	Effects of changing community on acoustic signal – less backscatter, not fewer fish	38
2.5	Discussion	39
2.5.1	Poleward loss of gas-filled swim bladders.	40
2.5.2	Ontogenetic shifts in distribution and swimbladder morphology.	40
2.5.3	Challenges for acoustic studies of mesopelagic fish.....	41
2.5.4	Implications for monitoring and modelling.....	42
2.6	Conclusions.....	43
	Acknowledgements.....	43
	Supplementary material.....	44
Chapter 3 Vertical migration behaviour and environmental drivers of mesopelagic fish distribution		57
3.1	Abstract	58
3.2	Introduction.....	58
3.3	Methods	61
3.3.1	Acoustic data collection.....	61
3.3.2	Acoustic data processing	62
3.3.3	Diel Vertical Migration	64
3.3.3.1	<i>Day night total water column backscatter</i>	66
3.3.4	Environmental drivers of backscatter	66
3.3.5	Modelling environmental drivers of water column backscatter	68
3.4	Results	70
3.4.1	Diel Vertical Migration	70
3.4.2	Environmental drivers of acoustic backscatter.....	76

3.5 Discussion	79
3.5.1 Drivers of DVM change with latitude	79
3.5.1.1 <i>Light</i>	79
3.5.1.2 <i>Temperature</i>	80
3.5.1.3 <i>Food availability</i>	80
3.5.1.4 <i>Non-identification – detectability and behaviour issues</i>	81
3.5.1.5 <i>Additional factors</i>	82
3.5.2 Environmental drivers of acoustic backscatter in the Scotia Sea	82
3.5.2.1 <i>Drivers of backscatter in the Scotia Sea, Southern Ocean and globally</i>	82
3.5.2.2 <i>Biological implications</i>	83
3.6 Conclusions.....	84
Supplementary material.....	85
Chapter 4 How many fish are in the Scotia Sea? An acoustic biomass estimate of mesopelagic fish.....	111
4.1 Abstract	112
4.2 Introduction.....	112
4.3 Methods	115
4.3.1 Net sampling.....	115
4.3.2 Fish properties for TS modelling.....	116
4.3.2.1 <i>Samples analysed</i>	116
4.3.2.2 <i>Tissue density measurements</i>	117
4.3.2.3 <i>Standard length and length to width ratio</i>	118
4.3.2.4 <i>Wet weight and length weight regressions</i>	118
4.3.2.5 <i>Fish swimbladder gas volume</i>	118
4.3.3 Modelling fish TS.....	119
4.3.3.1 <i>Finite cylinder model – Non-gas bearing fish</i>	119
4.3.3.2 <i>Prolate spheroid model – Gas bearing fish</i>	120
4.3.4 Basin scale backscatter, species abundance and biomass prediction.....	121
4.3.4.1 <i>Acoustic backscatter estimation</i>	121
4.3.4.2 <i>Determining fish community composition across the basin.</i>	122
4.3.4.3 <i>Acoustics to biomass</i>	124
4.3.5 Sensitivity analysis	125
4.3.5.1 <i>Altering fish TS – Standard length adjustment</i>	125

4.3.5.2	<i>Other species - Krill adjustment</i>	125
4.4	Results	126
4.4.1	Fish morphological properties	126
4.4.2	Target strength estimates	129
4.4.3	Fish abundance and biomass.....	131
4.4.3.1	<i>Sensitivity analysis - Impact of altering fish standard length (TS)</i>	133
4.4.3.2	<i>Sensitivity analysis - Impact of adding krill</i>	133
4.4.3.3	<i>Basin and ocean scale mesopelagic biomass estimates</i>	134
4.5	Discussion	135
4.5.1	Biomass at the basin and oceanic scale.....	136
4.5.2	Sources of uncertainty	137
4.5.3	Implications for the ecosystem	138
4.6	Conclusions.....	139
	Supplementary material.....	140
	Chapter 5 General discussion	155
5.1	General conclusions.....	156
5.2	From limitations to solutions.....	159
5.3	Exploitation – potential and challenges.....	160
5.4	Climate change and mesopelagic fish.....	162
5.5	Future work.....	164
	Supplementary material.....	167
	References	171
	Appendix I	191

List of tables

<p>Table 1.1 Southern Ocean fronts and water masses. Fronts and zones of ACC (north to south) shaded blue. Water masses of overturning circulation shaded green, see Figure 1.2 (Stein and Heywood, 1994, Orsi et al., 1995, Rintoul et al., 2001, Venables et al., 2012, Post et al., 2014).</p>	7
<p>Table 1.2 Summary of spatial and depth distribution, standard length (SL), lifespan, and depth (0-1000 m) integrated abundance of key myctophid species (Adapted from Saunders et al. (2019) and references therein). Swimbladder status source: Bold Marshall (1960), Non-Bold are assumed based on Marshall (1960) in Collins (2012).</p>	15
<p>Table 3.1 Spatio-temporal summary of acoustic transect data used in DVM and GAMM analysis. All data sets were used in GAMM, data sets used in DVM analysis are shaded. Transect date format year-month-day, and time is hours:minutes:seconds in GMT. Latitude (lat) and longitude (lon) both in decimal degrees South.</p>	61
<p>Table 3.2 Environmental variables considered for inclusion in assessment of environmental drivers of acoustic backscatter.....</p>	67
<p>Table 3.3 Summary of analysis of variance for GLMMs used to investigate effect of day-night and latitude on vertical distribution index.</p>	71
<p>Table 3.4 Summary statistics of day-night mean vertical distribution index, and contrasts within 1° latitude bands, for three DVM scenarios. D - day, N - night, EMM VDI - estimated marginal mean vertical distribution index, SE - standard error, df - degrees of freedom, CL - comparison level, CI - confidence interval. Significance codes: '***' <0.001, '**' <0.01, '*' <0.05, 'NS'≥0.1. Negative contrast (green) consistent with typical DVM, positive (red) inconsistent with typical DVM.</p>	73
<p>Table 3.5 Summary statistics of day-night mean total water column log_e Nautical Scattering Area Coefficient (acoustic backscatter), and contrasts within 1° latitude bands. EMM NASC - estimated marginal mean of total water column log_e Nautical Scattering Area Coefficient, SE - standard error, df - degrees of freedom, CL - comparison level, CI - confidence interval. Significance codes: '***' <0.001, '**' <0.01, '*' <0.05, 'NS'≥0.1. Negative contrast indicates higher total water column backscatter at night (green), positive contrast indicates lower total water column backscatter at night (red).....</p>	75

Table 3.6 Summary of GAMM results. DN – Day night, Chl – \log_e surface chlorophyll (mg m^{-3}), GeoCurr – square root geostrophic current speed (ms^{-1}), SST – sea surface temperature ($^{\circ}\text{C}$), Depth – water depth (m), DistToCoast – distance to coast (km), DHr – Daylight hours, SIP – max percentage sea ice (%). All GAMMs were specified as ‘scaled t’ family, with identity link function. Response variable \log_e NASC. All explanatory variables were treated as smoothing terms ($k=3$) with the exception of binomial term DN.....77

Table 4.1 Overview of fish taxa included in mesopelagic fish biomass assessment. Gas status source: [1] Dornan et al. (2019). [2] Marshall (1960), [3] Post (1990). Current study: ✓ indicates new data collected and/or analysed during this study’s assessment of fish acoustic properties, ‘Est.’ indicates value was estimated from current study data, ‘Lit.’ indicates value was derived from literature. Where ρ_f is fish tissue density and equivalent spherical radius of gas volume for neutral buoyancy, LW_{reg} is Length-Weight regression, LW_{rat} is Length-Width ratio, TS is target strength model..... 116

Table 4.2 Mean abundance of ind. m^{-2} from RMT25 night-time total water column net samples, in each 1°C SST groups. Data were used to apportion predicted Southern Ocean NASC values among species in each 0.25° grid square. BAX – *Bathylagus* spp., ELC – *E. carlsbergi*, ELN L – *E. antarctica* (> 51.378 mm), ELN S – *E. antarctica* (< 51.378 mm), GYF – *G. fraseri*, GYN – *G. nicholsi*, GYR – *G. braueri*, KRA – *K. anderssoni*, NOE – *Notolepis* spp., PRE – *P. tenisoni*, PRM – *P. bolini*, YTX – *Cyclothone* spp. 124

Table 4.3 Linear regression fits for fish density in relation to standard length, plus summary stats for theoretical equivalent spherical radius of gas bubble required to achieve neutral buoyancy in surrounding sea water at atmospheric pressure. Values in ‘red’ are set to zero as these fish do not possess gas-bearing bladders in these size classes or at all in the case of *Bathylagus* spp., ELN summary contains fish in both small (gas-bearing swimbladder) and large (non-gas swimbladder) size classes..... 128

Table 4.4 Table of species morphological parameters and estimated target strengths used in biomass estimation. Taxa: KRA – *K. anderssoni*, PRM- *P. bolini*, PRE – *P. tenisoni*, ELC – *E. carlsbergi*, ELN_S – *E. antarctica* (< 51.378 mm), ELN_L *E. antarctica* (> 51.378 mm), GYR – *G. braueri*, GYF – *G. fraseri*, GYN – *G. nicholsi*, BAX – *Bathylagus* spp., NOE – *Notolepis* spp., YTX – *Cyclothone* spp., KRI – *Euphausia superba* (krill). Mean fish density derived from laboratory measurements with the exception of * which use the mean density of gas or non-

gas fish as appropriate. LWR length to width ratio taken from laboratory measurements (the same values were used for both large and small ELN, [†]digital images, or [‡]estimated mean of all other taxa. Gas is gas status assigned to taxon. Model PS – Prolate Spheroid model for gas bubble (Andreeva, 1964, Holliday, 1972, Kloser et al., 2002), FC is Finite Cylinder model for fish body in non-gas taxa (Stanton et al., 1993). Krill Stochastic Distorted Wave Borne Approximation (SDWBA) model data was taken from (Fielding et al., 2011)..... 130

Table 4.5 Abundance and biomass estimates for median and interquartile range of fish standard lengths (TSs) in the Scotia Sea and the Southern Ocean, assuming that fish are responsible for all of the acoustic backscatter. 133

Table 4.6 Abundance and biomass estimates for median fish in the Scotia Sea and the Southern Ocean when varying abundance of median sized krill m⁻². 134

Table 4.7 Total regional mesopelagic fish and myctophid biomass estimates in million tonnes (Mt), derived by summing the product of each gridded biomass estimate by cell area. Biomass values calculated from target strength (TS) as a function of fish standard length at the median, 25th and 75th percentiles. 135

List of figures

- Figure 1.1** Ocean sectors and major fronts of the Southern Ocean. Eastward flowing Antarctic Circumpolar Current comprising of Sub Antarctic Front (SAF), Polar Front (PF), Southern ACC Front (SACCF), and Southern Boundary of the ACC (SB). Westward flow of Antarctic Slope Current (ASC) indicated by grey dashed line. 4
- Figure 1.2** Schematic of flows of major water masses in meridional overturning circulation (MOC) in the Southern Ocean. Frontal features: STF Sub Tropical Front, SAZ Sub Antarctic Zone, SAF Sub Antarctic Front, PFZ Polar Frontal Zone, PF Polar Front, AZ Antarctic Zone, SACCF Sub-Antarctic Circumpolar Current Front, SB Southern Boundary of ACC, SPZ Sub Polar Zone. Major water masses: SAMW Sub Antarctic Mode Water, AAIW Antarctic Intermediate Mode Water, UCDW Upper Circumpolar Deep Water, LCDW Lower Circumpolar Deep Water, AABW Antarctic bottom water. Small black arrows represent turbulent mixing. Red arrows indicate upper water masses involved in MOC, blue arrows indicate lower MOC water masses. Locations of frontal positions are illustrative only. Adapted from: Post et al. (2014). 6
- Figure 1.3** Schematic of major trophic pathways in part of the Scotia Sea food web, showing contrasts between (a) krill abundant years, and (b) years when krill are scarce. Major pathways shown as black arrows. Reproduced from Murphy et al. (2007). 9
- Figure 1.4** Global capture production of myctophid species, including *Electrona carlsbergi*, *Lampanyctodes hectoris*, and *Benthosema pterotum*. The peak during the years 1989, 1990 and 1991 is predominantly due to a brief *Electrona carlsbergi* fishery operated by the former USSR. This fishery extracted 23438 tonnes in 1989, 71970 tonnes in 1990 and 58568 tonnes in 1991. Data source (FAO, 2019). 11
- Figure 1.5** Summary of the major physical and food-web characteristics in the southern and northern regions of the Scotia Sea. Reproduced from (Ward et al., 2012). 13
- Figure 1.6** Schematic of echosounding. Transducer emits a pulse of sound into the water, echoes are generated when an object of differing acoustic impedance is encountered resulting in a backscattered signal. Adapted from Simmonds and MacLennan (2005). 22
- Figure 1.7** Schematic of the relative frequency response $r(f)$ of marine fauna, dependent upon scattering type. Grey scale at bottom illustrates scattering regions. Horizontal bands indicate

typical scattering regions of selected scattering types when measured at frequencies 18 – 200 kHz. Adapted from Korneliussen (2003).....23

Figure 2.1 Study location in the Scotia Sea, Atlantic sector of the Southern Ocean. RMT25 surface to 1000 m depth net sample locations (yellow diamond). Acoustic transects between the Falkland Islands and the South Orkney Islands (coloured lines), Spring cruises: JR161 (Oct 2006), JR15002 (Nov 2015), Summer cruises JR177 (Jan 2008), JR15004 (Jan & Feb 2016), and Autumn cruise JR200 (Mar 2009). Mean frontal positions are represented in white, SAF (Sub Antarctic Front), PF (Polar Front), SACCF (Southern Antarctic Circumpolar Current Front) and SB (Southern Boundary of the Antarctic Circumpolar Current) (Orsi et al., 1995, Moore et al., 1999, Thorpe et al., 2002). Also shown are the 2° latitudinal bands used in analysis. Map generated in Quantum GIS ver 2.18 (www.qgis.org).33

Figure 2.2 Relationship between the Nautical Area Scattering Coefficient (NASC, m² nmi⁻²), a proxy for biomass, and increasing latitude by cruise number. JR15004 had both North to South (NS) and South to North (SN) transits, all others are one way only. All data shown were collected in water >1000 m depth. Linear regressions (black lines) are statistically significant (p < 0.001).36

Figure 2.3 Single slice Computed Tomography scans of (a) *Electrona antarctica* showing loss of swimbladder gas and (b) *Krefflichthys anderssoni* showing gas presence (dark regions in tissue). (c) Polar plots of standardised proportions of species captured in 2° latitude bins, each colour segment proportionally corresponds to the abundance of individual species.37

Figure 2.4 (a) Mean abundance of fish (individuals per 1000 m³) in RMT25 net samples by latitude. Bars indicate standard deviation between net samples and numbers in columns indicate numbers of individual net strata samples included. (b) Mean biomass of fish (grams per 1000m³) in RMT25 net samples by latitude, box spans interquartile range (IQR), horizontal line is the median, whiskers include values up to 1.5 x IQR, outlying values plotted individually. (c) Relative proportions of fish by swimbladder contents in net samples at latitude. Numbers in columns are the individual number of total water column samples (each comprising of four depth strata) used in analysis.....39

Figure 3.1 Acoustic transects used as part of the current study. All transects (red and yellow lines) were used in GAMM assessment of environmental drivers of acoustic backscatter. Latitudinal patterns in DVM only used transits between Falkland and South Orkney Islands

(red lines). Mean frontal positions are represented in white, SAF (Sub Antarctic Front), PF (Polar Front), SACCF (Southern Antarctic Circumpolar Current Front) and SB (Southern ACC Boundary). Also shown are 2° latitudinal graticules. Map generated in Quantum GIS ver 2.18 (www.qgis.org), projection EPSG:3031..... 62

Figure 3.2 (a) Example echogram of raw calibrated data. (b) Background Noise Removal following De Robertis & Higginbottom (2007), using mean noise (calculated as mean S_v in 20 ping wide by 10 m depth cell minus Time Varied Gain) leaves considerable amount of noise visible at depth. (c) Calculating noise in cell based on 90th percentile (Korneliussen, 2000) results in cleaner data whilst retaining signal. (d) Echogram post-cleaning, black regions are excluded data (e.g. surface near-field, depths >1000 m and false bottom echoes). Colour scale is in dB, visible threshold set to -80 dB. Panel on the right shows effect of data cleaning steps on mean S_v 63

Figure 3.3 Schematic of diel vertical migration behaviour under consideration, (a) daytime occupation by mesopelagic fish of upper and deep mesopelagic water, (b) synchronous migration during night from mesopelagic to epipelagic, (c) migration during night from only the upper-mesopelagic into epipelagic, d) migration during the night from the deep mesopelagic to upper mesopelagic..... 65

Figure 3.4 Representative climatologies of environmental variables used in generalised additive mixed model (GAMM). Actual data used in GAMM were from finer temporal resolution (see Table 3.2 for GAMM data sources). (a) SST climatology for months Oct-Apr 2005-2017, (b) mean sea ice concentration climatology for month of September (2005-2017), (c) \log_e surface chlorophyll concentration (mg m^{-3}) Oct-Apr 2005-2017, (d) mean geostrophic current speed (m s^{-1}), (e) water depth (m) and (f) distance to coast (km) a proxy for predation pressure. See Supplement S.7 for details of the climatology source data..... 69

Figure 3.5 Echograms of mean volume backscattering strength (Mean S_v dB re 1 m^{-1}) of 1 km distance by 10 m depth integrated 38 kHz acoustic data for cruises used in latitudinal DVM assessment. Missing data and data less than -90 dB in white. Day, night and crepuscular periods indicated in top strip. Data processed in Echoview® 8.0.95, plots made in R 3.5.1, package cowplot (Wilke, 2018), ggplot2 (Wickham, 2016), and data.table (Dowle and Srinivasan, 2018)..... 70

Figure 3.6 Left panel (a-c): Day-night difference of Estimated Marginal Means (EMM) of vertical distribution index (VDI) in 1° latitude bands. A higher index at night is conducive with a shallowing of backscatter, typical of DVM. Bars indicate comparison levels, adjusted for multiplicity (Lenth, 2019). Right panel: Contrasts between day night EMM, cyan bars are 95% confidence intervals, red points indicative of significance at <0.05 level. Blue lowest-smoothing line indicative of trend. Points approaching 0 line indicate less difference between day and night. (a) Ratio between Epipelagic (0-230 m) and Mesopelagic (>230 m) backscatter, (b) Epipelagic and Upper-mesopelagic (>230 m ≤580 m), and (c) Upper-mesopelagic and Deep-mesopelagic (>580 m). (d) Day-night difference in total water column backscatter \log_e Nautical Area Scattering Coefficient. Note difference in y-axis scales. 74

Figure 3.7 Effects of sequentially dropping variables from GAMM on model performance (a) Akaike's Information Criterion (AIC) and (b) R^2 values adjusted for degrees of freedom. Full GAMM contains all modelled variables. Four black bars are reduced variable models for the three most influential variables, sea surface temperature (SST), daylight hours (DHr), sea ice percentage (SIP), and final model selection SST, DHr and SIP. 78

Figure 3.8 Estimated smoothing curves for the GAMM fitted to \log_e Nautical Area Scattering Coefficient (NASC $m^2 nmi^{-2}$) (a) sea surface temperature (b) daylight hours and (c) maximum percentage of sea ice. Centred smoothing curves indicate that response variable NASC increases with SST, initially decreases up to 15 hours of DHr, and decreases with SIP. Dotted lines are ± 2 standard errors. Degrees of freedom in parenthesis. Rug plots on x-axis indicate number and distribution of observations. 78

Figure 4.1 Location of night-time RMT25 net samples (red circles), used in assessment of relative abundance of mesopelagic fish taxa in relation to sea surface temperature in the Scotia Sea. Projection WGS84, produced in R version 3.5.1. Sea surface temperature (SST) climatology covers months of Oct-Apr, 2005-2017, from World Ocean Database (Locarnini et al., 2018). White boxes indicate Commission for the Conservation of Antarctic Marine Living Resources (CCAMLR) area 48 boundaries. 115

Figure 4.2 (a) Predicted \log_e NASC for Scotia Sea. CCAMLR areas bounded by white boxes. (b) Southern ocean \log_e NASC, white line indicates approximate mean position of the Polar Front (PF). 122

Figure 4.3 Data processing flow to calculate estimated mesopelagic fish biomass from raw RMT25 night, surface – 1000 m net data and environmental climatologies. SST: sea surface temperature Oct-Apr 2005-2017, mean Daylight hours Oct-Apr, Sea ice conc.: mean sea ice concentration Sept only 2005-2017 (see Chapter 3 supplement S.7 for further details on climatology data). Filled rectangles = data sets, unfilled rounded rectangles = processing step. 123

Figure 4.4 Mesopelagic fish density relationships in relation to standard length. Linear regression lines and 95% confidence interval. *Gymnoscopelus fraseri* (n=3) is not shown..... 127

Figure 4.5 Predicted Scotia Sea abundance (left) and biomass (right) of mesopelagic fish. Top plots assume that all backscatter is from mesopelagic fish. Middle and bottom plots assume that krill contribute to backscatter at a rate of 64 krill m⁻², in the Scotia Sea and Southern Ocean respectively. White regions indicate no data. 131

Figure 4.6 (a) Proportions of fish by swimbladder contents in net samples within 1°C sea surface temperature (SST) groups. Numbers above bars indicate the number of total water column samples in each 1°C group. (b) Acoustic contribution of fish species to mean predicted NASC in 1°C SST groups by swimbladder contents. Acoustic contribution is calculated using species-specific target strength values for median length fish. (c) Relative proportions of gas and non-gas swimbladder fish species contributing to Southern Ocean mean biomass (g m⁻²) as estimated from acoustic backscatter and net proportion data, in 1°C sea surface temperature (SST) groups. Notice that relative proportion of gas bearing species is highest at warmer temperatures but overall contributes less to biomass because of the non-linear effect of gas contribution to backscatter. 132

Figure 4.7 Predicted locations of ‘negative’ abundances of fish when the model is forced to apply krill at rates of 64 krill m⁻² (left) and 128 krill m⁻² (right). All negative values for fish abundance were set to 0 to calculate mean values for fish abundance and biomass. 134

List of abbreviations

AABW	Antarctic Bottom Water
AAIW	Antarctic Intermediate Mode Water
ACC	Antarctic Circumpolar Current
AIC	Akaike's Information Criterion
AOV	Analysis of Variance
AS	Attenuated Signal
ASC	Antarctic Slope Current
AZ	Antarctic Zone
BN	Background Noise
CCAMLR	Commission for the Conservation of Antarctic Marine Living Resources
CT	Computed Tomography
CTD	Conductivity Temperature Depth profiler
DN	Day Night
DVM	Diel Vertical Migration
EGV	Equivalent Gas Volume
EMM	Estimated Marginal Mean
ESR	Equivalent Spherical Radius
FC	Finite Cylinder Model
GAMM	Generalised Additive Mixed Model
GEBCO	General Bathymetric Chart of the Oceans
GLMM	Generalised Linear Mixed Effects Model
DHr	Daylight hours
IN	Impulse Noise
LCDW	Lower Circumpolar Deep Water
LWR	Length to Width Ratio
NASC	Nautical Area Scattering Coefficient
OLZ	Oxygen Limiting Zones
OMZ	Oxygen Minimum Zones
PF	Polar Front
PFZ	Polar Frontal Zone
PS	Prolate Spheroid Model
RMT	Rectangular Mid-water Trawl
SACCF	Southern Antarctic Circumpolar Current Front
SAF	Sub Antarctic Front
SAM	Southern Annular Mode

SAMW	Sub Antarctic Mode Water
SAZ	Sub Antarctic Zone
SB	Southern Boundary of the Antarctic Circumpolar Current
SDWBA	Stochastic Distorted Wave Borne Approximation Model
SIP	Sea Ice Percentage Cover
SIZ	Sea Ice Zone
SL	Standard Length
SNR	Signal to Noise Ratio
SPZ	Sub Polar Zone
SST	Sea Surface Temperature
ST₂₀₀	Sea Temperature at 200 m
STF	Sub-Tropical Front
S_v	Volume Backscattering Strength
TL	Total Length
TS	Target Strength
TWC	Total Water Column
UCDW	Upper Circumpolar Deep Water
VIF	Variance Inflation Factors
WW	Wet Weight

Chapter 1

General introduction

1.1 Overview

The oceans mesopelagic zone, 200-1000 m below sea level, holds potentially vast resources of fish. Globally mesopelagic fish are the most abundant vertebrates on earth, and play vital roles in ecosystem function and biogeochemical cycling. Within the Southern Ocean the mesopelagic fish community is dominated by myctophids in terms of abundance and biomass. These fish occupy a key mid-trophic position in Antarctic food webs, as consumers of zooplankton and prey for higher predators including penguins and seals. Many myctophid fish are also assumed to play a role in the vertical transport of carbon through diel vertical migration (DVM), a daily phenomenon in which animals migrate from deep water to feed in nutrient rich surface waters under the cover of darkness. However, their remote location, biases in traditional net sampling techniques and net avoidance behaviour have left considerable knowledge gaps and uncertainty in our biomass estimates and the extent of vertical migration behaviour. These uncertainties hamper our ability to quantitatively assess their importance in ecosystem functioning or to monitor changes in the community, which are of pressing importance in this changing ocean environment.

Active acoustic methods enable us to sample the water column at larger spatial and temporal scales than traditional net sampling methods. However, to reliably interpret acoustic data we need additional information on the species present and their backscattering properties before biomass estimates can be made, and these data have been lacking for the Southern Ocean. Consequently, unanswered questions remain regarding the status of mesopelagic fish stocks, behaviour, environmental drivers of their distribution, and how they are likely to respond under climatically influenced environmental change.

With a focus on the highly productive Scotia Sea region of the Southern Ocean, this thesis aims to fill these knowledge gaps by 1) identifying the strong and weak backscattering members of the mesopelagic fish community, 2) describing visible DVM patterns in acoustic data and the environmental drivers of horizontal patterns of acoustic backscatter, and 3) combining knowledge of species specific backscatter properties and environmental drivers to assess the biomass of mesopelagic fish in the Scotia Sea and wider Southern Ocean. This chapter provides context for the thesis by i) presenting an overview of the oceanography of the Southern Ocean ecosystem, ii) reviewing current knowledge on Scotia Sea mesopelagic fish species, and iii) introducing fisheries acoustic methods.

1.2 The Southern Ocean and Scotia Sea

1.2.1 Hydrography

The Southern Ocean encircles the Antarctic continent and differs markedly from other global oceans in that its major eastward flowing current, the Antarctic Circumpolar Current (ACC), flows around the globe unbroken by any continental land mass (Rintoul et al., 2001). This connection between the Atlantic, Indian and Pacific basins enables transport of water, nutrients, oxygen and heat between the oceans (Orsi et al., 1995, Marshall and Speer, 2012). As such, the Southern Ocean plays an important role in the global climate, and oceanographic changes here have global implications (Post et al., 2014).

The path of the ACC is strongly linked to bathymetry, which deflects the flow of the ACC to lower latitudes at key locations, such as the Scotia Arc and Kerguelen plateau (Figure 1.1) (Orsi et al., 1995, Rintoul et al., 2001). The complex topography formed by the Drake Passage at the Antarctic Peninsula and the Scotia Arc bounding the Scotia Sea, is particularly influential in Southern Ocean dynamics and is responsible for mixing of three water masses, namely the eastward flowing ACC, the westward flowing Antarctic Slope Current (ASC) and the Weddell Gyre (Figure 1.1) (Stein and Heywood, 1994, Garabato et al., 2004, Venables et al., 2012).

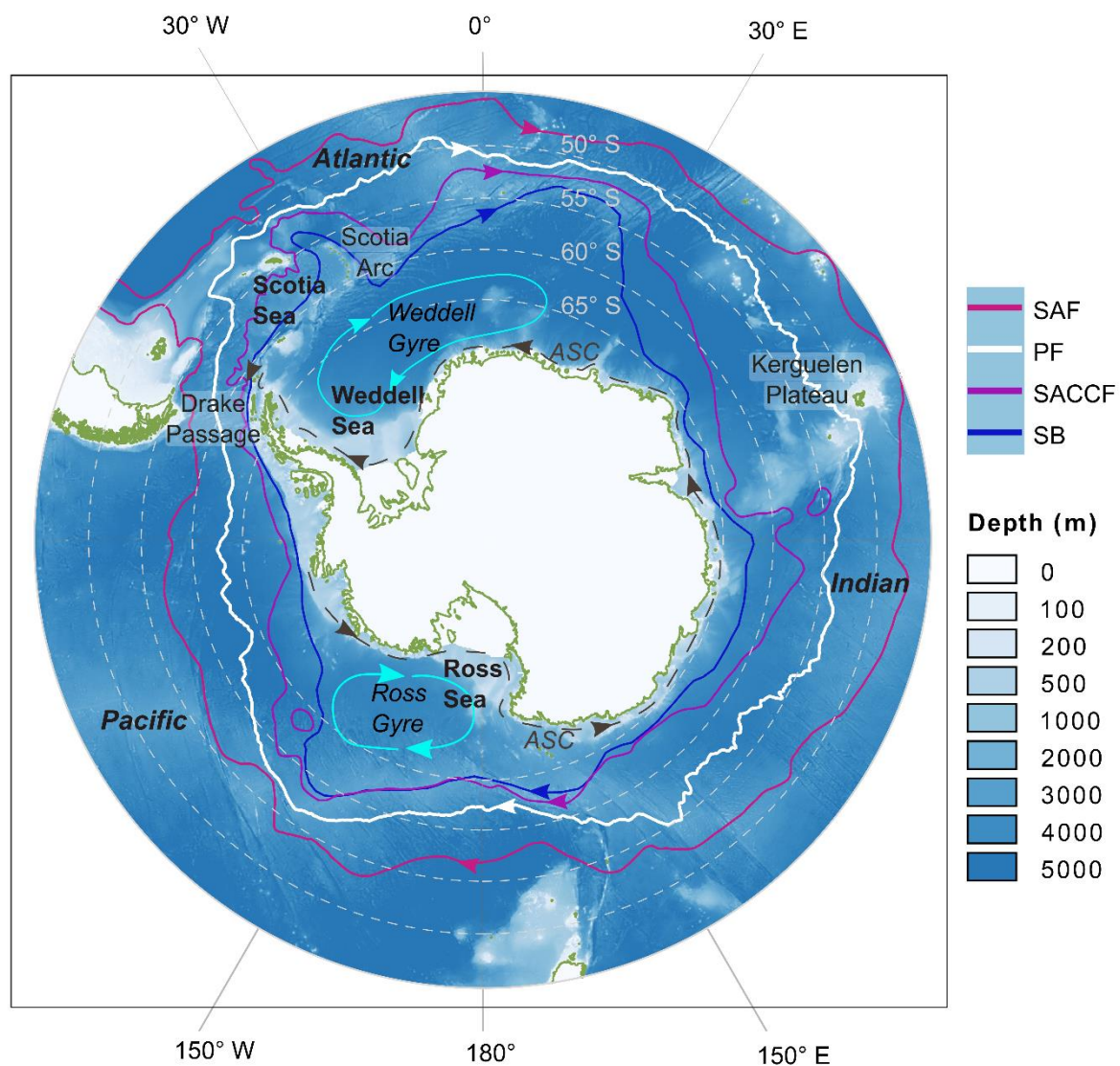


Figure 1.1 Ocean sectors and major fronts of the Southern Ocean. Eastward flowing Antarctic Circumpolar Current comprising of Sub Antarctic Front (SAF), Polar Front (PF), Southern ACC Front (SACC), and Southern Boundary of the ACC (SB). Westward flow of Antarctic Slope Current (ASC) indicated by grey dashed line.

1.2.2 Southern Ocean circulation

Circulation within the Southern Ocean is dynamic and complex, yet it can be simplistically viewed as being governed by (i) wind driven zonal (east-west) advection, which also drives vertical transport via upwelling and (ii) meridional (north-south) transportation, which in part is governed by water density as a result of difference in salinity, pressure and temperature (Arrigo et al., 2008, Marshall and Speer, 2012).

The ACC is driven eastward by strong westerly winds (Trenberth et al., 1990, Orsi et al., 1995), which are affected by the Southern Annular Mode (SAM). In recent years a positive SAM index has resulted in stronger westerlies, shifting poleward directly over the path of the ACC, though it is debated if this is the driving factor for a recent increase in strength of ACC flow (Thompson and Solomon, 2002, Toggweiler and Russell, 2008, Thompson et al., 2011, Watson et al., 2014).

In contrast, the ASC flows westward along the predominantly steep and relatively narrow continental slope. Driven by intensely cold katabatic winds from the continent of Antarctica, it is broken only at the Drake Passage and Western Antarctic Peninsula (Heywood et al., 2014, Post et al., 2014). This contraflow leads to upwelling where ACC and ASC diverge (Post et al., 2014). Two major clockwise gyres exist between the ACC and ASC, namely the Weddell and Ross Sea gyres. The Weddell gyre is a source of Antarctic bottom water into the Scotia Sea (Garabato et al., 2004).

Upper and lower circumpolar deep water are deep meridional flows of dense water, which originate in the tropics and shoal (i.e. shallow) towards the continent (Figure 1.2). Turbulent mixing and mesoscale eddies facilitate the transfer of deep water nutrients to the surface and subduction of surface waters freshens and ventilates deeper waters in global overturning circulation (Post et al., 2014, Stein and Heywood, 1994).

1.2.3 Water masses and fronts

The Southern Ocean is characterised by a number of fast flowing fronts (Figure 1.1), which mark transitions between slower water masses (Figure 1.2) with distinct salinity, oxygen concentration and temperature signatures (Orsi et al., 1995, Venables et al., 2012). A summary of Southern Ocean fronts and water mass properties is outlined in Table 1.1. As water mass boundaries and upwelling zones are known to be highly productive, it is important to have methods for recognising these features to facilitate prey distribution modelling. Orsi et al. (1995), identified and described signatures of temperature, salinity and oxygen gradients in the water column of the ACC from CTD data and water sampling. However, identification of these water masses requires analysis and interpretation of data taken throughout the water column. It has been shown that sea surface temperature derived from satellite data can be used to locate the approximate location of the Polar Front (Moore et al., 1999), and front positions have also been inferred from dynamic height ranges (Venables et al., 2012), where

Chapter 1

the dynamic height is a method of specifying the height of the sea surface from an arbitrary reference point (Table 1.1).

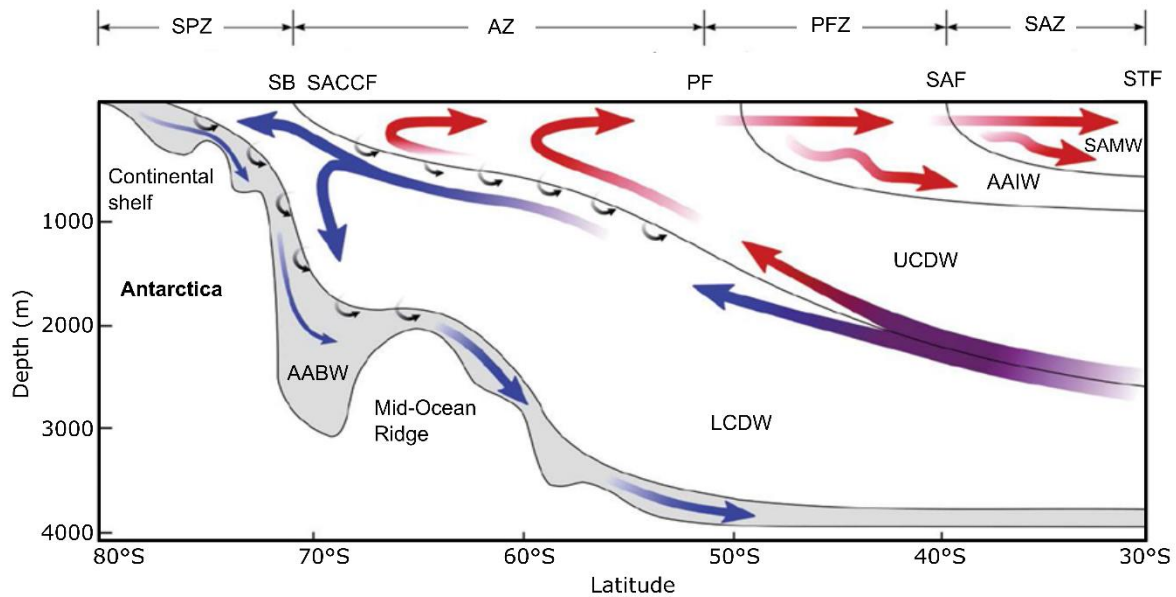


Figure 1.2 Schematic of flows of major water masses in meridional overturning circulation (MOC) in the Southern Ocean. Frontal features: STF Sub Tropical Front, SAZ Sub Antarctic Zone, SAF Sub Antarctic Front, PFZ Polar Frontal Zone, PF Polar Front, AZ Antarctic Zone, SACC Sub-Antarctic Circumpolar Current, SB Southern Boundary of ACC, SPZ Sub Polar Zone. Major water masses: SAMW Sub Antarctic Mode Water, AAIW Antarctic Intermediate Mode Water, UCDW Upper Circumpolar Deep Water, LCDW Lower Circumpolar Deep Water, AABW Antarctic bottom water. Small black arrows represent turbulent mixing. Red arrows indicate upper water masses involved in MOC, blue arrows indicate lower MOC water masses. Locations of frontal positions are illustrative only. Adapted from: Post et al. (2014).

Table 1.1 Southern Ocean fronts and water masses. Fronts and zones of ACC (north to south) shaded blue. Water masses of overturning circulation shaded green, see Figure 1.2 (Stein and Heywood, 1994, Orsi et al., 1995, Rintoul et al., 2001, Venables et al., 2012, Post et al., 2014).

Feature	Abbreviation	Notable features	Dynamic height range (dyn cm)
Sub Tropical Front	STF	Silica limited. Separates Southern Ocean water from warmer saltier subtropical waters.	
Sub Antarctic Zone	SAZ	Presence of warmer SAMW above AAIWs salinity minima.	
Sub Antarctic Front	SAF	Fast flowing surface currents. Sharp temperature changes between SAZ, SAF and PF.	29 to -5
Polar Frontal Zone	PFZ	Zone of mesoscale eddies.	
Polar Front	PF	Fast flowing surface currents.	-45 to -71
Antarctic Zone	AZ	Temperature <2°C at 100–300 m.	
Southern ACC Front	SACCF	Most southerly front of ACC.	-99 to -115
Southern Boundary	SB	Poleward edge of ACC, where circumpolar deep water outcrops to the surface.	-116 to -132
Sub Polar Zone	SPZ	High nutrient, low chlorophyll region.	
Antarctic Slope Current	ASC	Westward current driven along the continental slope by intensely cold katabatic winds.	
Sub Antarctic Mode Water	SAMW	Thick homogenous layer of water extending to 600 m.	
Antarctic Intermediate Mode Water	AAIW	Indicated by a salinity minimum in the water column. Subducted under SAMW near SAF.	
Upper Circumpolar Deep Water	UCDW	Low oxygen and high nutrient concentrations. Abiotic characteristics of this water mass are lost at the Weddell Gyre.	
Lower Circumpolar Deep Water	LCDW	High salinity. Greater depth and density than UCDW. Dense enough to penetrate south of ACC into SPZ.	
Antarctic bottom water	AABW	Very dense water. Formed from cold fresh shelf water and high salinity LCDW.	

1.2.4 Seasonal effects and climate change

The Southern Ocean has an approximate sea ice extent of ~3 million km² in February expanding to ~18 million km² in September (Parkinson and Cavalieri, 2012, Post et al., 2014). Despite significant warming in the ACC in recent decades, extending down to depths beyond 1000 m, there has been a significant trend for increasing sea ice coverage in the Southern Ocean since the 1970s (Parkinson and Cavalieri, 2012, Rintoul et al., 2012). However, this positive trend in sea ice cover was not spatially uniform, with increases in the Ross Sea and Indian Ocean and decreases to the west of the Antarctic Peninsula (Parkinson and Cavalieri, 2012). However, a significant drop in sea ice coverage across the Southern Ocean has been reported since 2014 (Parkinson, 2019). Spatial and temporal changes in sea ice distribution and extent have the potential for profound impact on Antarctic food webs (Massom and Stammerjohn, 2010). This is because sea ice cover affects light available for primary productivity and acts as a growing medium for algae (Rintoul et al., 2012).

Oxygen depletion has been noted throughout global oceans as a result of warming oceans (Schmidtke et al., 2017), which inhibits oxygen solubility (Gilly et al., 2013). This has led to shoaling (shallowing) of oxygen minimum zones (OMZs) and the oxygen limiting zones (OLZs) associated with them. As mesopelagic species often seek refuge in deeper darker water during daylight hours within OLZs, any shoaling will likely compress mesopelagic species refugia (Bianchi et al., 2013a, Gilly et al., 2013). This has the potential to be compounded if increased circumpolar winds lead to an increase in upwelling of nutrients, driving primary productivity and further oxygen depletion.

1.3 The Southern Ocean ecosystem

The Southern Ocean is a high nutrient low chlorophyll system, where there are generally sufficient macronutrients (nitrate, phosphate, silicate) to fuel primary production, but phytoplankton growth is limited by available micronutrients, specifically iron (Martin et al., 1990, Pollard et al., 2006). However, there are regional hotspots within the Southern Ocean, where localised iron enrichment from frontal upwelling or run off can lead to areas of high productivity characterised by high chlorophyll levels (Murphy et al., 2007, Venables and Moore, 2010). The Scotia Sea is one of the most productive regions in the Southern Ocean, supporting high densities of Antarctic krill (*Euphausia superba*), a keystone species in the Antarctic food web (Atkinson et al., 2008). This abundance of krill sustains large populations of higher predators, including fish, seabirds, seals and whales (Atkinson et al., 2012b). The

Southern Ocean's food web is commonly comprised of short energy-efficient food chains linking *phytoplankton – krill – higher predators* (Figure 1.3) (Murphy et al., 2007, Stowasser et al., 2012). However, the ecosystem is complex, with high and mid-level predators able to switch prey depending upon availability (Croxall et al., 1999, Saunders et al., 2019). These alternative trophic pathways, for example *phytoplankton – zooplankton – myctophid fish – higher predators* (Stowasser et al., 2012), can take precedence when krill numbers are low (Murphy et al., 2007). In a rapidly changing ecosystem, where krill distributions are being modified (Atkinson et al., 2004, Flores et al., 2012, Atkinson et al., 2019), alternative pathways are likely to become more important, particularly for land-based breeding predators with limited foraging ranges. However, there is considerable uncertainty regarding mesopelagic fish abundance, behaviour and their ability to compensate for a shift in ecosystem function under scenarios of sustained environmental change.

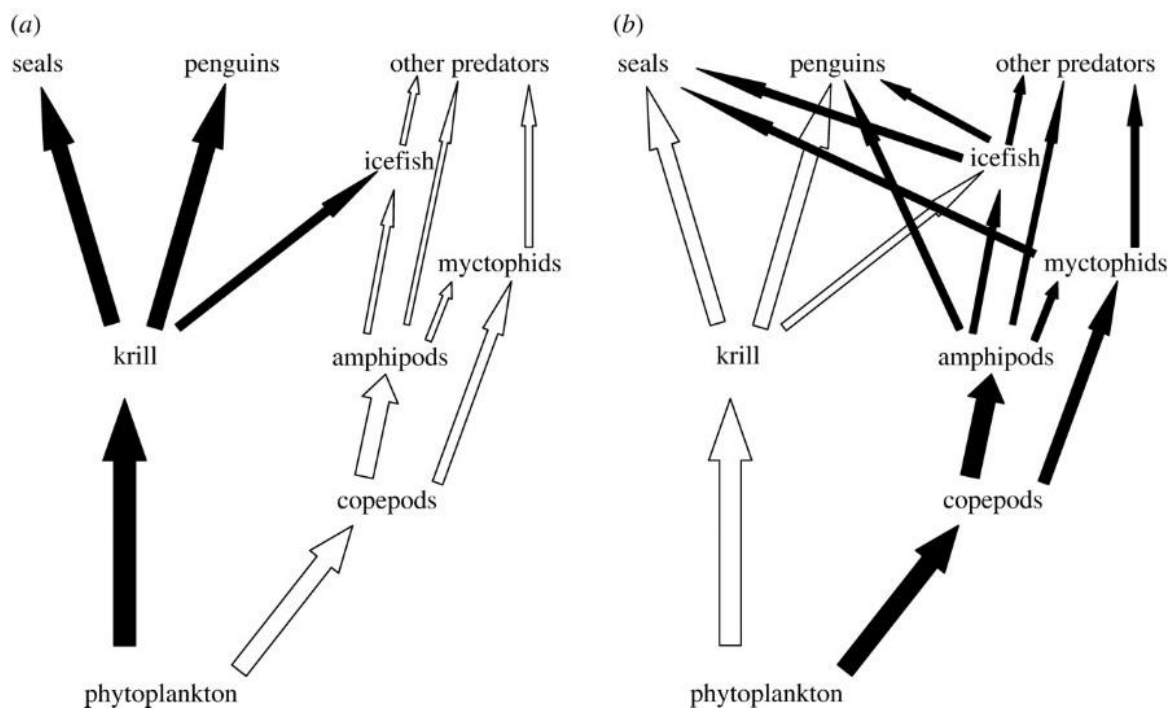


Figure 1.3 Schematic of major trophic pathways in part of the Scotia Sea food web, showing contrasts between (a) krill abundant years, and (b) years when krill are scarce. Major pathways shown as black arrows. Reproduced from Murphy et al. (2007).

Historically ecosystem studies have tended to focus on krill, because of its key role in the function of the Antarctic ecosystems and its value to the commercially important krill fishery (El-Sayed, 1994). However, there has been a rapidly growing interest in mesopelagic fish, in particular myctophids, and their role in ecosystem function, biogeochemical cycling and as an abundant marine resource (St. John et al., 2016).

1.4 Mesopelagic fish species overview

1.4.1 Global perspective

Mesopelagic fish are ubiquitous throughout the world's oceans, while they are represented by ~30 families globally, though they are dominated by the Myctophidae in terms of abundance and biomass (Gjøsaeter and Kawaguchi, 1980). Myctophids are typically small fish (<20 cm), that predominantly spend their days in the oceanic twilight zone 200-1000 m below sea level, where they can aggregate in extensive mixed fauna layers, which are visible on acoustic echograms and can span ocean basins (Gjøsaeter and Kawaguchi, 1980, Irigoien et al., 2014).

Many mesopelagic species undertake a diel vertical migration (DVM), feeding in nutrient rich epipelagic waters at night and returning to the relative safety of the mesopelagic zone by day. This DVM behaviour is widely thought to be a mechanism to avoid predation by visual predators (Robison, 2003). Notably, DVM behaviour in oceanic waters takes a significant role in biogeochemical cycling, by enhancing vertical transport of carbon by up to 40% (Robinson et al., 2010, Bianchi et al., 2013b). Both depth and horizontal distribution have been linked to a number of oceanographic and biogeochemical properties including fronts, primary production and oxygen minimum zones (Opdal et al., 2008, Fielding et al., 2012, Cade and Benoit-Bird, 2015). Aggregation and distribution patterns are also likely to be affected by predation pressure with some species exhibiting schooling behaviour (Saunders et al., 2013).

Net-based biomass estimates of global mesopelagic fish stand at ~1000 million tonnes, with the highest levels of productivity in the tropics and subtropics (Gjøsaeter and Kawaguchi, 1980, FAO, 1997, Lam and Pauly, 2005). However, due to variability in net efficiency, patchy distribution and net avoidance behaviours, acoustic modelling has revealed that mesopelagic biomass may have been underestimated by at least an order of magnitude (Pakhomov and Yamamura, 2010, Kaartvedt et al., 2012, Irigoien et al., 2014). Reducing uncertainty in biomass estimates is vital if we are to effectively account for mesopelagic fish in ecosystem models and monitor change in the community under future warming scenarios.

Given their global ubiquity and large biomass, myctophids offer considerable potential as a capture fishery product and have been harvested to varying degrees since the 1970s (Figure 1.4) (FAO, 2019). The European Commission has recently identified a need to research the potential biological resources held in the oceans mesopelagic zone as part of its

Horizon 2020 Blue Growth – Sustainable harvesting work programme (European Commission, 2018). Studies into the viability of a fishery in the Gulf of Oman revealed an average biomass of 2.3 million tonnes, however experimental catch rates resulted in non-commercially viable yields (Valinassab et al., 2007). Iran maintains a *Benthoosema pterotum* fishery in the West Indian Ocean, which is responsible for the majority of the global myctophid catch since 2008 (FAO, 2019). Historically the former USSR operated global fisheries, with the majority focused in the Southwest Indian Ocean and Southern Atlantic, achieving catches of ~72,000 tonnes in the Atlantic Antarctic in 1990 (FAO, 1997, FAO, 2019). A South African fishery for *Lampanyctodes hectoris* peaked at 30,000 tonnes in 1985, but closed due to difficulties in processing this lipid rich fish (FAO, 1997, FAO, 2019). Should improvements in capture and processing methodologies be developed there is likely to be considerable interest in expansion of mesopelagic capture fishery. However, prior to any renewed exploitation it is essential that we first improve our understanding of myctophid life history, the implications for ecosystem functioning and our ability to accurately monitor stock status.

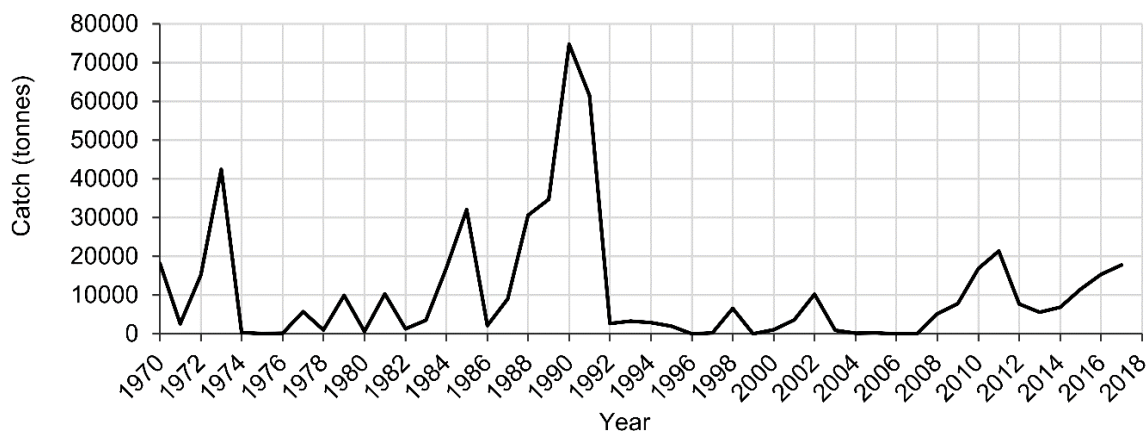


Figure 1.4 Global capture production of myctophid species, including *Electrona carlsbergi*, *Lampanyctodes hectoris*, and *Benthoosema pterotum*. The peak during the years 1989, 1990 and 1991 is predominantly due to a brief *Electrona carlsbergi* fishery operated by the former USSR. This fishery extracted 23438 tonnes in 1989, 71970 tonnes in 1990 and 58568 tonnes in 1991. Data source (FAO, 2019).

1.4.2 Southern Ocean and Scotia Sea species and distribution

The Southern Ocean and Scotia Sea mesopelagic fish communities are also dominated by myctophids, both in number of species and biomass (Gjøsaeter and Kawaguchi, 1980, Pusch et al., 2004, Collins et al., 2012). Net assessments of myctophid biomass within the Southern Ocean have been estimated at ~70 to 130 million tonnes (Lubimova et al., 1987 in Collins et

al., 2012). Scotia Sea myctophid biomass has been conservatively estimated at 4.5 million tonnes (Collins et al., 2012). Modelled acoustic biomass for mesopelagic fish in the West Pacific sector of the Southern Ocean, has recently been estimated as ranging from 6.41 g m⁻² south of 67°S, to 39.31 g m⁻² for off-shelf locations south of 50°S (Escobar-Flores, 2017), where g m⁻² is representative of the biomass of fauna in the water underlying 1 m² of surface area.

Hulley (1990) identified 35 species of myctophid present in the Southern Ocean, however, many of these are relatively rare subtropical species at the southern edge of their range. Of those myctophids commonly found within the Southern Ocean, their distribution is broadly circumpolar (Hulley, 1990). Whilst ranges of many species can extend to the Antarctic Polar Front and beyond, species distribution boundaries tend to be latitudinal, with a general trend towards a decrease in species diversity at colder high latitudes (Collins et al., 2012, Escobar-Flores et al., 2018b). Ward et al. (2012) identify two bioregions within the productive Scotia Sea, supporting distinctly differing food webs (see Figure 1.5), with the region between the SACCF and the edge of the sea ice zone marking the transition between north and south, and the SACCF the site of the highest degree of species range overlap.

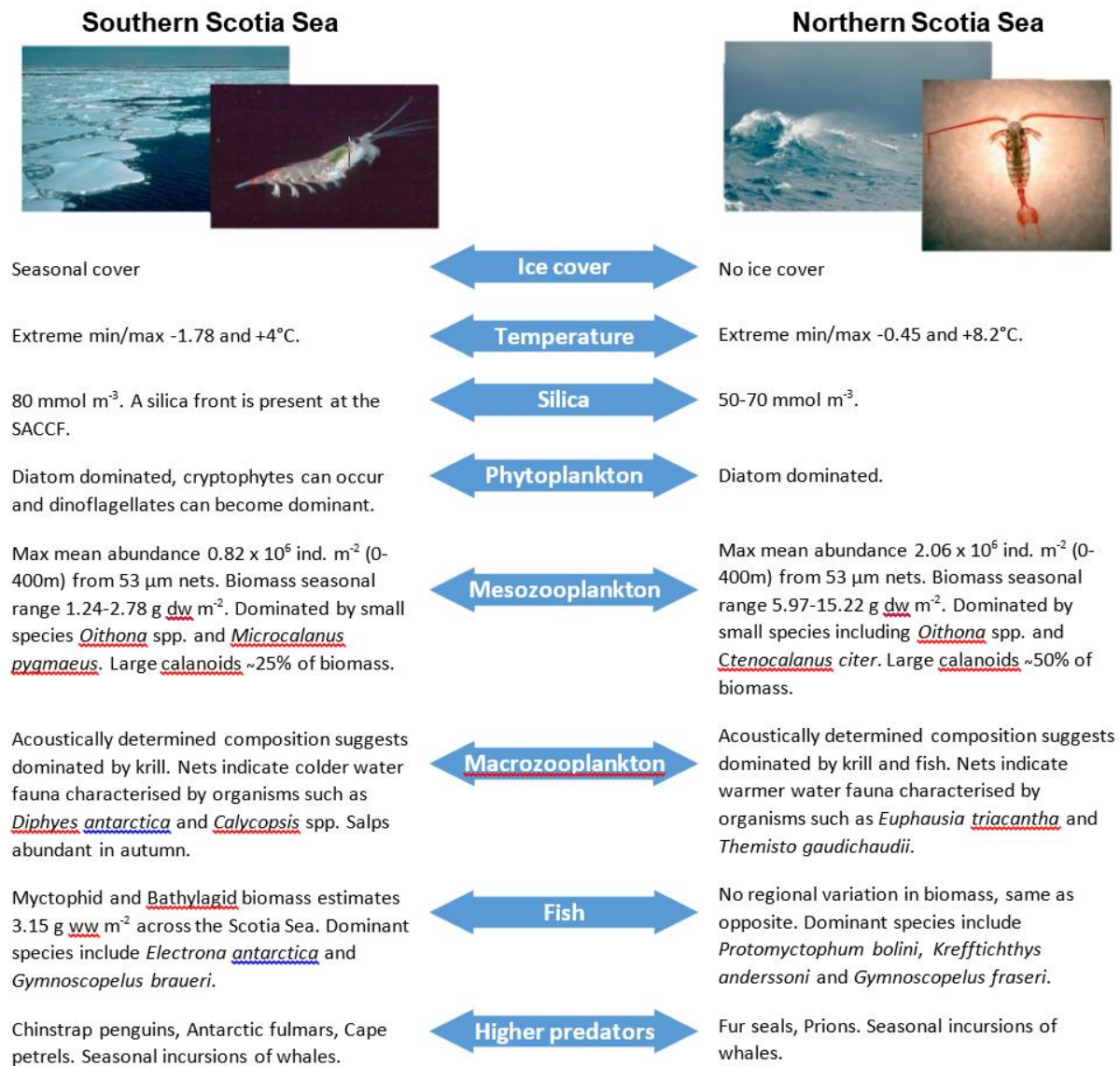


Figure 1.5 Summary of the major physical and food-web characteristics in the southern and northern regions of the Scotia Sea. Reproduced from (Ward et al., 2012).

In terms of myctophid distribution *Electrona antarctica* and *Gymnoscopelus braueri* are the most prevalent species in the seasonally ice-covered Southern Scotia Sea, with *E. antarctica* by far the most abundant, and a true polar species (Collins et al., 2012, Ward et al., 2012, Saunders et al., 2014a, Saunders et al., 2014b, Saunders et al., 2019). *Gymnoscopelus nicholsi* and *Gymnoscopelus opisthopterus* also occur in this southern region but are rarer (Saunders et al., 2014b, Saunders et al., 2019). Whilst these southerly species also occur in the Northern Scotia Sea, the dominant myctophids in these ice-free warmer waters are *Krefftichthys anderssoni*, *Protomyctophum bolini* and *Electrona carlsbergi*, joined by lower abundances of *Protomyctophum tenisoni*, *Gymnoscopelus fraseri*, *Protomyctophum choriodon*

and *Nannobranchium achirus* (Collins et al., 2012, Ward et al., 2012, Saunders et al., 2014a, Saunders et al., 2014b, Saunders et al., 2015b, Lourenço et al., 2016).

Night-time net sampling in the Scotia Sea reveals interspecific differences in both latitudinal and depth strata occupation, which may serve to separate otherwise ecologically similar myctophid species. For example, *E. carlsbergi* has shallower depth range 0-400 m (predominantly 0-200 m) than the closely related polar specialist *E. antarctica*, which is found 0-1000 m (Saunders et al., 2014a). In addition, *E. antarctica* appears to exhibit a seasonal change in its depth preference, being more prevalent in the upper 0-200 m at night during Autumn (Saunders et al., 2014a). *Gymnoscopelus* species are found throughout the 0-1000 m depth range, with the exception of *G. opisthopterus*, which is typically found only at depths >400 m (Saunders et al., 2014b). *Gymnoscopelus fraseri* has been found at 0-700 m and may exhibit a trend for occupying deeper water (200-400 m) in autumn than in summer (0-200 m) (Saunders et al., 2014b). Whilst *Protomyctophum* species have been found throughout the mesopelagic range (0-1000 m), they tend to favour shallower depths. *Protomyctophum tenisoni* and *P. choriodon* have predominantly been found in the 0-200 m depth strata at night, and *P. bolini* are typically most concentrated at 200-400 m (Saunders et al., 2015b). *Krefflichthys anderssoni* has generally been found throughout the 0-1000 m water column, but has been most frequently sampled below 400 m (Collins et al., 2008, Lourenço et al., 2016). Though not common across all myctophids, some species displayed evidence of size, and potentially sex related depth stratification. Around north-west South Georgia in the northern Scotia Sea Collins et al. (2008) found significantly different depth stratification among size classes of *G. braueri*, with smaller fish (80 – 90 mm standard length) captured at the surface at night and larger fish occurring progressively deeper in the water column. Table 1.2, adapted from Saunders et al. (2019), gives an overview of the biogeographic ranges and depth distributions of the most common Scotia Sea myctophid species.

Chapter 1

Table 1.2 Summary of spatial and depth distribution, standard length (SL), lifespan, and depth (0-1000 m) integrated abundance of key myctophid species (Adapted from Saunders et al. (2019) and references therein). Swimbladder status source: **Bold** Marshall (1960), Non-Bold are assumed based on Marshall (1960) in Collins (2012).

Species	Type/Pattern	Approx. distributional range (adults)	Approx. depth distribution (m)	Approx. max. size (SL, mm)	Est. lifespan (year)	Median abundance (ind. m ⁻²)	Abundance 25 th and 75 th percentiles (ind. m ⁻²)	Swimbladder status
<i>Electrona carlsbergi</i>	South temperate	STF to APF	0–400	93	5	0.015	0.002–0.207	Gas
<i>Electrona antarctica</i>	Antarctic	APF to SIZ	0–1000	115	4	0.155	0.003–0.586	Gas*
<i>Gymnoscopelus fraseri</i>	South temperate	STF to APF	0–400	115	3	0.007	0.002–0.048	Regressed
<i>Gymnoscopelus nicholsi</i>	Broadly Antarctic	STF to SIZ	0–1000	165	7	0.004	0.002–0.015	Regressed
<i>Gymnoscopelus braueri</i>	Broadly Antarctic	STF to SIZ	0–1000	162	4	0.078	0.002–0.431	Regressed
<i>Gymnoscopelus opisthopterus</i>	Antarctic	STF to SIZ	400–1000	187	5	0.003	0.002–0.030	Regressed
<i>Krefflichthys anderssoni</i>	Broadly Antarctic	STF to SACCF	200–1000	75	3	0.067	0.002–0.346	Gas
<i>Nannobrachium achirus</i>	South temperate	STF to APF	200–1000	167	4	0.006	0.003–0.033	No data
<i>Protomyctophum bolini</i>	Broadly Antarctic	STF to SACCF	200–700	78	2	0.032	0.002–0.143	Gas
<i>Protomyctophum choriodon</i>	South Temperate	STF to SACCF	0–400	85	4	0.003	0.002–0.030	Gas
<i>Protomyctophum tenisoni</i>	Broadly Antarctic	STF to APF	0–700	58	2	0.006	0.002–0.084	Gas

*reduced in adult

1.4.3 Myctophids in the Southern Ocean food web

Myctophids are a key component in the diet of many Southern Ocean top predators including Antarctic fur seals *Arctocephalus gazelle* (Lea et al., 2002), elephant seals *Mirounga leonina* (Cherel et al., 2008, Guinet et al., 2014), king penguins *Aptenodytes patagonicus* (Duhamel, 1998), procellariiform seabirds (Connan et al., 2007) and squid *Moroteuthis ingens* (Phillips et al., 2001). They also form a component in the diet of the economically valued Patagonian toothfish *Dissostichus eleginoides* (Collins et al., 2007). The Southern Ocean is often viewed as a krill centric food web, and historically the focus of much stock assessment and food web research has focussed on Antarctic krill (*Euphausia superba*) as a keystone species (El-Sayed, 1994). However, there is evidence that predators can switch prey when krill availability is low, with myctophids potentially providing krill-independent energetic pathway (Figure 1.3) (Murphy et al., 2007, Stowasser et al., 2012). With evidence of changes to krill distribution (Atkinson et al., 2019), it is thought that mesopelagic fish may play an important role as an alternative food source (Murphy et al., 2007). However, it remains unclear how much they will be able to meet the energetic demands of higher predators, since larger myctophids are consumers of krill and trophic pathways via myctophids are less energy efficient than direct pathways between krill and higher predators (Saunders et al., 2019).

1.4.4 Behaviour and life history

The most striking behaviour within the mesopelagic community is that of DVM. Whilst it is not completely certain why myctophids would undertake such an energetically demanding daily migration, there is evidence that the primary factor is to avoid visually-cued predators in surface waters during daylight hours (Robison, 2003). However, predator avoidance must be traded-off against the need to intake sufficient food to maintain their body condition and facilitate reproduction. It is therefore possible that mesopelagic fish may exploit dusk and dawn 'anti-predation windows', where light levels are high enough to catch their zooplankton prey but low enough to reduce the chance of being captured themselves, thus optimising their chances of survival (Clark and Levy, 1988). Comparisons of day and night net samples indicate that DVM behaviour is exhibited by the majority of myctophid species in the Scotia Sea. However, it is difficult to untangle a signal of DVM behaviour from that of day-time net avoidance (Collins et al., 2008, Kaartvedt et al., 2012, Saunders et al., 2014a, Lourenço et al., 2016). Moreover, there are apparent spatial differences in the extent of DVM behaviour

observed in mesopelagic assemblages. Of specific relevance here are recent acoustic analyses revealing potential breakdown in consistent DVM behaviour towards the pole (Proud et al., 2018a).

Beyond DVM, relatively little is known of the behaviour of individual myctophid species. An early observational study of myctophid DVM describes short bursts of rapid movement in some species whilst others were observed hanging motionless vertically in the water column (Barham, 1966). More recently there is evidence that outside of DVM at least some myctophid species are largely immobile in the water column unless disturbed e.g. by predators (Kaartvedt et al., 2012, Dypvik et al., 2012).

Another behaviour likely to be involved in predator avoidance is schooling behaviour. At present it is unclear whether Scotia Sea myctophids form single species or mixed assemblage schools, although ground-truthed acoustic marks identified by Collins et al. (2008) appear to show schooling behaviour in *P. choriodon*, which is further evidenced by their occurrence in large numbers in the diet of Antarctic fur seals (*Arctocephalus gazella*) (Reid et al., 2006), despite generally low abundance (Saunders et al., 2015b, Saunders et al., 2019). Other likely candidates for schooling behaviour are *E. carlsbergi* and *K. anderssoni* (Torres et al., 1985, Zasel'sliy et al., 1985, Fielding et al., 2012, Saunders et al., 2013). Acoustic observations in the Scotia Sea indicate that changes in fish school morphology are linked to changes in environmental conditions such as sea temperature and dynamic height, as well as in response to changing predation pressure (Fielding et al., 2012, Saunders et al., 2013). Fielding et al. (2012) found evidence of schooling behaviour was highest in the warmer northern Scotia Sea (where the acoustic backscatter attributable to fish was generally higher), but that school distribution changed seasonally, shifting further south and deeper in autumn than spring. Fish schools also tend to be more compact closer to land, becoming shallower and longer but also more diffuse with increasing distance from shore, presumably as predation pressure from land-based predator colonies decreases (Saunders et al., 2013).

Both myctophid larvae and females of reproductive condition are rarely found in the Scotia Sea, giving rise to the hypothesis that the majority of Scotia Sea myctophids are expatriate migrants in southerly polar waters, originating in more temperate waters further north (Saunders et al., 2017). Exceptions to this rule appear to be *K. anderssoni*, whose larvae have been found around South Georgia (Belchier and Lawson, 2013), and *E. antarctica*, whose larvae have been known to occur around the Antarctic peninsula, South Orkneys and Georgia

basin (Loeb et al., 1993). Notably, the larval life history of *E. antarctica* appears to be linked to the sea ice sector, specifically in the Southern Indian Ocean (Wilkes Land, East Antarctica), where larvae have been found in the top 200 m of water (Moteki et al., 2017).

1.4.5 Diet

Myctophid species have been shown to be opportunistic feeders, preying upon the most locally abundant mesozooplankton including copepods, euphausiids, hyperiids and pteropods (Pakhomov et al., 1996, Pusch et al., 2004). However, diet composition in the Southern Ocean varies interspecifically, seasonally and spatially (Saunders et al., 2018). Size is also a key determinant in myctophid diet, with larger species able to predate larger prey items (Saunders et al., 2014b, Saunders et al., 2015b, Saunders et al., 2015a, Saunders et al., 2019). In the northern Scotia Sea *K. anderssoni*, *P. bolini*, *P. tenisoni*, *P. choriodon*, *N. achirus*, *E. carlsbergi*, *G. fraseri* and *G. nicholsi* have been identified as predominantly consuming copepods, whilst *E. antarctica* and *G. braueri* consume substantial proportions of the amphipod *Themisto gaudichaudii* (Shreeve et al., 2009, Saunders et al., 2018). Smaller euphausiids (*Thysanoessa* spp.) are also important dietary components for the majority of these myctophid species (Saunders et al., 2018). Elsewhere, around the South Shetland Islands and south of the SACCF, *E. antarctica*, *G. braueri*, and *G. nicholsi* feed predominantly on euphausiids, including *Euphausia superba* (Antarctic krill), which accounts for more than 50% (by mass) of *E. antarctica* and *G. nicholsi* diets (Pusch et al., 2004, Saunders et al., 2014a, Saunders et al., 2014b). *Gymnoscopelus opisthopterus* also appears to consume substantial proportions of krill from the few data available (Saunders et al., 2019). Large myctophids are therefore considerable consumers of Antarctic krill and are likely to be directly impacted by long-term changes in krill abundance (Lancraft et al., 1989, Saunders et al., 2019).

1.4.6 Morphology

Knowledge of fish morphology, specifically the presence or absence of a gas-bearing swimbladder, is an important step to adequately interpreting acoustic data (Kloser et al., 2009). Marshall (1960) describes the swimbladders of myctophids as euphysoclist (i.e. double chambered closed swimbladders), whilst Butler and Percy (1972) have described myctophid swimbladders as falling into three main categories: gas-filled, lipid-filled and atrophied (regressed), where lipids may provide buoyancy in species that undertake large DVM. However, mesopelagic fish frequently show a nonlinear relationship between swimbladder

size and growth (Marshall, 1960). There is a paucity of published swimbladder data for the Southern Ocean myctophid community, with limited sample sizes and little published detail on variability between and within species, which could have a significant impact on acoustic backscatter. A summary of swimbladder status in key myctophid species is given in Table 1.2.

Marshall (1960) considers the issue of maintaining a constant volume of gas in physoclist (closed) swimbladders when undergoing DVM, noting that myctophids are rarely brought to the surface with viscera protruding from their mouths. Marshall (1960) attributes this ability to control gas resorption to a number of adaptations, including smaller swimbladders, and an increased capacity for resorption via their well-developed rete mirabile with sizeable blood flow. As mesopelagic fishes typically have a higher ratio of gas resorbing area and capillary bed of the swimbladder, in relation to swimbladder volume, and gas exchange is enhanced by high oxygen partial pressure at depth, Marshall (1960) concludes that this well-developed system may result in gas resorption rates 20-30 times greater in myctophids than freshwater physoclists.

The evolutionary drivers for the loss of swimbladder gas are unclear. While echolocating Odontoceti (toothed whales) may find it easier to locate fish with gas-bearing swimbladders (Tyack, 1997, Jones, 2005), within the Southern Ocean odontocetes are relatively few in number in comparison to Mysticeti (baleen whales), and the dominant species are thought to primarily consume squid (sperm whales *Physeter macrocephalus*), larger fish and marine mammals (killer whales *Orcinus orca*) (van Waerebeek et al., 2010). Exceptions include the smaller hourglass dolphin (*Lagenorhynchus cruciger*), which are known to consume squid and myctophids (Goodall et al., 1997). However, given the limited numbers of fish-eating odontocetes in the Southern Ocean it is likely that the loss of swimbladder gas is an adaptation to vertical migration and their depth of occupation (Priede, 2017), rather than selective predation pressure.

Physically myctophids are highly adapted to life at depth, surviving substantial daily pressure gradients and the near absence of light. All but one of myctophid species have bioluminescent photophores, with variation in the pattern of photophores on the body differing among species, and also between sexes within a species. Myctophid photophores have been proposed to perform both counter illumination and or communication functions (Catul et al., 2011, Warrant and Locket, 2004). Indeed, it has been suggested that myctophid fishes can detect pin point bioluminescence tens of metres away, with an individual fish's

visual acuity being dependent upon both the diameter of the eye and the intensity of downwelling light, which may mask bioluminescence (Warrant and Lockett, 2004). Turner et al. (2009) make a strong case for myctophids being visually-adapted to the detection of bioluminescence by providing evidence that retinal pigmentation of the majority of Southern Ocean myctophid species are tuned to the same wavelengths as blue/green bioluminescence. Turner et al. (2009) predict a maximum visual detection distance of ~15 m for myctophid fishes in Antarctic waters, and acoustic studies in Masfjorden (60° 52' N, 5° 25' E), Norway, have also shown that mesopelagic species can respond to a predatory threat up to 30 m away (Kaartvedt et al., 2012).

1.5 Methodologies for studying mesopelagic species/data

1.5.1 Net sampling

Net sampling is routinely used by scientists and fishery managers to assess population dynamics, community composition, abundance and distribution of fish species. However, micronekton are often patchily distributed and even when repeated measures are conducted nets can only sample a tiny fraction of the pelagic ecosystem (Warren, 2012). Several studies have presented compelling evidence for mesopelagic fish net avoidance, which coupled with the inherent selectivity of gear type has likely led to an underestimation of mesopelagic fish biomass by at least an order of magnitude (Lancraft et al., 1989, Collins et al., 2008, Kaartvedt et al., 2012, Irigoien et al., 2014). Inter-calibration exercises highlight the balance to be struck in selecting sampling gear for micronekton studies, because while larger micronekton have the ability to evade nets, smaller individuals are not retained by large meshed trawl nets. Additionally, towing a gear at higher speeds may reduce evasion leading to greater efficiency (Pakhomov and Yamamura, 2010). Despite these intrinsic issues, net sampling remains essential to ground-truth acoustics data.

1.5.2 Acoustics – theory and practise

The marine biome is the largest ecosystem on earth, yet studying oceanic ecology can be challenging because visual observations are limited due to the rapid attenuation of light in water, and net sampling can only sample a tiny fraction of the pelagic ecosystem (Warren, 2012). In comparison, the development of active acoustics has facilitated the efficient collection of relatively large amounts of temporal and spatial data, enabling us to answer broad ecological questions (Benoit-Bird and Lawson, 2016).

Whilst the speed of sound through water was first calculated experimentally in 1827 by Colladon and Sturm, the innovation of active acoustics, the term applied to the active transmitting and receiving of a sound signal, was not developed until the turn of the 20th century (Simmonds and MacLennan, 2005). The field has principally been driven by advances in technology, specifically the invention of the piezo-electric transducer, and later military innovations aimed at revealing sunken vessels and submarines (Simmonds and MacLennan, 2005). However, it was quickly recognised that this single-beam single-frequency technology was able to detect biological features in water, such as deep scattering layers comprised of fish, squid and zooplankton (Dietz, 1962), leading to the use of echosounders by fisherman and researchers to assess and describe fish stock distributions (Sund, 1935, Balls, 1948). By the mid-20th century methods were being developed for determining fish abundance by automated echo counting of individual fish (Mitson and Wood, 1961), followed by echo integration, which facilitates the estimation of density for aggregations of fish for which individual counting would not be possible (Simmonds and MacLennan, 2005).

The principles of active acoustics are relatively simple: a pulse of sound with known frequency, intensity and duration is transmitted into the water column from a transducer, when it encounters an object, such as the seabed or fish (hereafter target) with a different acoustic impedance the soundwave is scattered and reflected. The time taken for the backscattered pulse or 'echo' to return to the acoustic receiver enables range to the target to be calculated, and the intensity (backscatter) of the received signal gives some indication to the nature of the target encountered (Figure 1.6) (Simmonds and MacLennan, 2005). The combination of range and amplitude of the received signal enables us to build up a 2D acoustic image or 'echogram' of targets in the water column in time (for stationary acoustic platforms e.g. fixed moorings) or in space (for moving platforms e.g. ship hull-mounted transducers).

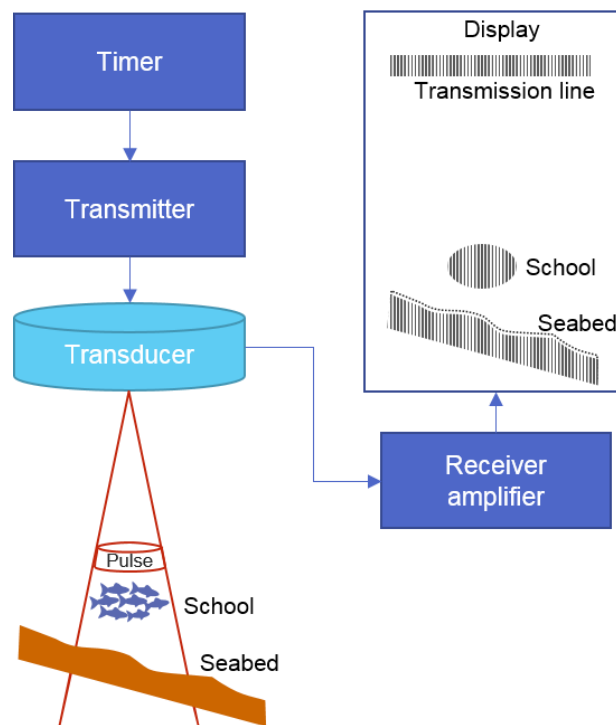


Figure 1.6 Schematic of echosounding. Transducer emits a pulse of sound into the water, echoes are generated when an object of differing acoustic impedance is encountered resulting in a backscattered signal. Adapted from Simmonds and MacLennan (2005).

The return signal is affected by sound speed (which changes with temperature, salinity and depth), transmission losses through friction and geometric spreading, and background noise masking signal, all of which need to be accounted for in data processing. The relationship between the source signal and backscatter received is most simply represented by the active sonar equation:

$$EL = SL - 2TL + TS \quad 1.1$$

Where EL is Echo Level, SL is Source Level, TL is Transmission Loss (2 for two way travel) and TS is Target Strength (Foote and Stanton, 2000).

The amplitude of backscatter from a target, at a specific frequency, received at the transducer is dependent upon i) the target's size, which determines whether the scattering is in the Rayleigh, resonant, transient or geometric region (Figure 1.7), ii) the target's orientation or tilt angle and shape, which alters the cross sectional area presented to the acoustic beam, and iii) the density of, and speed of sound in, the scatterer compared with the surrounding medium (Foote, 1980b, Simmonds and MacLennan, 2005).

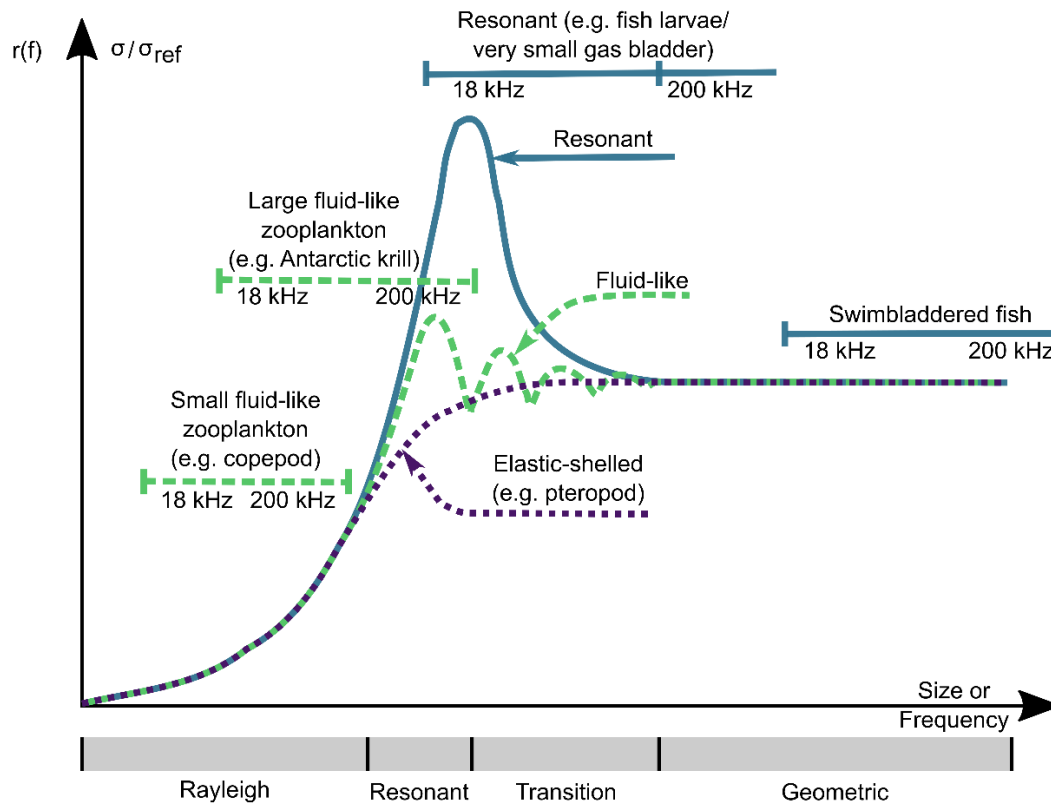


Figure 1.7 Schematic of the relative frequency response $r(f)$ of marine fauna, dependent upon scattering type. Grey scale at bottom illustrates scattering regions. Horizontal bands indicate typical scattering regions of selected scattering types when measured at frequencies 18 – 200 kHz. Adapted from Korneliussen (2003).

The phenomenon of resonance occurs when the natural oscillating frequency of a target, e.g. the gas in a fish's swimbladder, is similar to that of the echosounder frequency with which it is insonified (Simmonds and MacLennan, 2005). At its resonant frequency the movement in a gas bubble wall is greater than at any other frequency, resulting in considerably higher acoustic backscatter (Figure 1.7). Resonant frequency can be affected by changes in bubble volume, and changes in gas pressure. For physoclists, changes in pressure are the most significant factor, as constant volume is generally maintained but gas pressure can be altered with ambient pressure, which changes rapidly with depth (Simmonds and MacLennan, 2005). Resonance is particularly common at low frequencies, in small gas-bladdered species, and during ascent and descent in DVM (Simmonds and MacLennan, 2005, Godø et al., 2009).

The proportion of the incident energy backscattered by a target is described as either the back-scattering cross section (σ_{bs} , m^2), or Target Strength (TS, dB re $1 m^2$). Where TS is a logarithmic measure of the ratio of the reflected soundwave intensity, relative to the

transmitted intensity, at a reference distance of 1 m from the sound source (Foote and Stanton, 2000), represented by:

$$TS = 10\log_{10}(\sigma_{bs}) \quad 1.2$$

In many cases it is not possible to resolve individual targets in acoustic data, for example when the transmitted pulse encounters a krill swarm or fish layers at depth, and in this case the echosounder is measuring the volume backscattering coefficient (s_v , m^{-1}) of these swarms or layers.

$$s_v = \frac{\sum \sigma_{bs}}{V_0} \quad 1.3$$

Frequently s_v is averaged over more than one transmission or ‘ping’ into (Mean) Volume Backscattering Strength (S_v , dB re 1m^{-1} , MVBS when s_v is averaged over a finite volume), where:

$$S_v = 10\log_{10}(s_v) \quad 1.4$$

1.5.3 Abundance and Biomass estimation

In fisheries acoustics the introduction of a standardised calibration method for acoustic data, using a standard reference target, has enabled abundance estimations to be made (Foote, 1982, Simmonds and MacLennan, 2005, Demer et al., 2015).

To estimate the abundance of targets per m^2 (ρ_a , m^{-2}), the area backscattering coefficient (s_a , $\text{m}^2 \text{m}^{-2}$), defined as the integral of s_v with respect to the depth (z , m) of a layer, can be used to estimate the quantity of scatterers in an area, by dividing s_a by the backscattering cross-section σ_{bs} of the scatterers.

$$s_a = \int_{z_1}^{z_2} s_v dz \quad 1.5$$

$$\rho_a = \frac{s_a}{\sigma_{bs}} \quad 1.6$$

Where the σ_{bs} of a target can be calculated either empirically or theoretically (expanded on in section 1.5.4). Equations 1.2 – 1.6 from MacLennan et al. (2002).

While some pelagic organisms form single-species assemblages, e.g. schooling fish, mixed-species assemblages are common, particularly when quantifying the species throughout the water column. In this case, if we have available net data indicating the relative abundance

of each species, the proportion of the backscatter from each group, be that taxonomic or scattering type e.g. gas-bearing or fluid-like (Stanton et al., 1994), can be partitioned to account for each group's differing scattering properties (Nakken and Dommasnes, 1975, Simmonds and MacLennan, 2005). Where, following Proud et al. (2018b), the proportion of the backscatter from the group (P_g) can be defined as:

$$P_g = \frac{n_g \overline{\sigma_{bsg}}}{\sum_{g=1}^G n_g \overline{\sigma_{bsg}}} \quad 1.7$$

Where G is the number of groups, and n_g is the relative number of individuals in that group and $\overline{\sigma_{bsg}}$ is the mean σ_{bs} for the group. The abundance of targets per m^2 , in a group can then be estimated by:

$$\rho_{a,g} = \frac{P_g S_a}{\overline{\sigma_{bsg}}} \quad 1.8$$

Abundance of the group can then be converted to biomass by multiplying by the mean weight of members of the group. Equations 1.7 – 1.8 adapted from Proud et al. (2018b).

1.5.4 Fish Target Strength estimates

TS of a fish can be derived experimentally by i) insonifying free swimming fish, ii) insonifying caged swimming fish, or iii) insonifying tethered fish and manually adjusting tilt angle to mimic natural behaviour (Nakken and Olsen, 1977, Foote, 1980a, Misund and Beltestad, 1996, Simmonds and MacLennan, 2005). Insonifying *in-situ* free-swimming fish is challenging, and while this has been achieved from a manned submersible, fitted with a low-light camera for species identification (Benoit-Bird et al., 2003), the use of unmanned acoustic optical probes or acoustics limits the ability to identify the target to species level (Kloser et al., 2016). Insonifying caged swimming fish facilitates accurate species identification, and incorporates a degree of behaviour (Foote, 1980a), but requires a set-up which may be difficult to achieve at sea. Benoit-Bird and Au (2001), have insonified freshly captured, tethered and manually tilted Myctophidae from the upper 200 m of the water column to estimate TS. However, insonifying both caged and tethered fish, requires good quality samples, acclimatised to surface conditions, which can be difficult to achieve in mesopelagic species. Whilst directly measuring TS of animals behaving naturally is ideal, this may not be reasonably practicable, in such cases theoretical TS can be modelled based on an animal's physiology (Yasuma et al., 2010, Jech et al., 2015).

There are a range of acoustic models for estimating the TS of a species, from simple low-resolution to sophisticated high-resolution models, which vary in accuracy, complexity and computational expense. For example, a fish's swimbladder can be modelled as a simple gas-filled sphere (Anderson, 1950), or its body as a fluid-filled cylinder (Stanton, 1988). As marine fauna are rarely spherical or cylindrical, complexity has been added by extending these models to account for prolate spheroids (Holliday, 1972) and cylinder taper (Stanton et al., 1993). At the more complex end of the modelling spectrum, the Kirchhoff-ray mode backscatter model, models fish bodies in sections, by combining multiple simpler models, each representing different components of sections of the fish body with varying properties, to capture the backscattering complexity of each fish (Clay and Horne, 1994). As a fish's size and swimming behaviour can vastly alter parameters added into more complex models, these can rapidly become computationally intensive. Jech et al. (2015), conducted a comparison of simple and complex models to estimate both the error and computational efficiency of simple approximate models over complex models. They found that some simple models performed as well as more complex models, and had the added benefit of being computationally faster.

1.5.5 Acoustics for studying spatial and temporal trends

Active acoustics are an unparalleled tool for studying the distribution of fish and other marine fauna at varying temporal and spatial scales. Single-frequency upward-facing echosounders, mounted on the seabed and left *in-situ*, have been used to study the temporal change in both the density of pelagic fauna aggregations and depth of occurrence, revealing diel and seasonal trends (Urmy et al., 2012). They have been used in combination with additional sensors to explore the effect of down-welling lunar light on the extent of vertical migration (Benoit-Bird et al., 2009). Global acoustic transect data from hull-mounted echosounders have been used in combination with remotely sensed environmental data to predict global biomass of mesopelagic fish (Irigoien et al., 2014) and identify global mesopelagic bioregions (Proud et al., 2017). Such data have also been used to study global patterns of diel vertical migration behaviour, and predict the extent of shoaling of mesopelagic fauna in light of predicted rises in sea temperatures (Proud et al., 2018a).

There has been a recent expansion in methodologies for characterising deep scattering layers and examining patterns in acoustic data. By taking a single-frequency approach, it is possible to characterise deep layers by key metrics, such as depth, density, centre of mass (Urmy et al., 2012, Proud et al., 2015). While such methods can give valuable information

regarding the heterogeneous nature of biological components in space and time, by itself a single frequency cannot be used to discriminate the scattering components to species level or determine community structure. Echograms made using a single frequency can only provide limited information, as they cannot distinguish between changes in abundance or changes in scatterer type.

Data from multiple frequencies has been used to differentiate between species (Kloser et al., 2002). In zooplankton and micronekton there is marked heterogeneity in morphology leading to varying frequency responses (Figure 1.7), and multi-frequency methods have the potential to discriminate between different types of scattering organism, e.g. pteropods, euphausiids and organisms with gas-bearing organs (Korneliussen, 2003, Stanton et al., 2010). Jech and Michaels (2006), utilised multi-frequency data on herring schools to generate single composite echograms, enabling them to readily distinguish between gas and non-gas bearing species. However, multi-frequency methods are limited by the range of the highest frequency, as higher frequencies with shorter wavelengths are subject to higher rates of sound absorption in water (Simmonds and MacLennan, 2005). As such, mesopelagic studies using hull-mounted echosounders are commonly restricted to the use of frequencies of 38 kHz or lower that have observational ranges that extend to the deepest regions of the mesopelagic zone.

1.6 Thesis outline

The principal aim of this thesis is to refine the use of active acoustic methods to study mesopelagic fish, in particular myctophids, within the highly productive Scotia Sea and Southern Ocean. The research reported assesses the importance of environmental drivers of the distribution of mesopelagic fish, and contributes to our understanding of their behaviour while refining estimates of their biomass.

Chapter 2 assesses the swimbladder 'gas' condition of key mesopelagic fish within the Scotia Sea and Southern Ocean, and considers the implications for interpretation of acoustic data at the ocean basin scale. I use a combination of x-ray, computed tomography scanning and dissection to assess the gas-bearing status of the most prevalent myctophid species in the Scotia Sea and combine this with net sample abundance and biomass data to demonstrate community-wide changes in swimbladder phenotypes with latitude. I then compare this with latitudinal trends in integrated surface to 1000 m 38 kHz acoustic backscatter data and

Chapter 1

discuss how swimbladder morphology of myctophids influences our ability to resolve myctophid biomass using acoustic data in the Scotia Sea and Southern Ocean.

In Chapter 3 I focus on i) the acoustic evidence for diel vertical migration behaviour in relation to latitude, and ii) the environmental drivers of mesopelagic species distribution within the Scotia Sea. I use a combination of Generalised Linear Mixed Modelling and post hoc testing to test the hypothesis that there is no change in vertical migration behaviour with latitude. I then use a Generalised Additive Mixed Modelling (GAMM) approach to assess the main environmental drivers of changing acoustic backscatter as a proxy for mesopelagic fish in the Scotia Sea, and to generate a predictive model of acoustic backscatter for the Southern Ocean.

Building on data from the previous chapters, in Chapter 4 I derive acoustic estimates of abundance and biomass for mesopelagic fish in the Scotia Sea and Southern Ocean. I first combine my knowledge of swimbladder condition from Chapter 2, with empirically derived tissue density estimates and CTD oceanographic data, to parameterise two simple acoustic backscattering models (prolate spheroid for gas and finite cylinder for non-gas bearing fish) to derive species-specific estimates of Target Strength (TS) for eleven of the most prevalent mesopelagic fish species in the Scotia Sea. I then use the GAMM from Chapter 3 to predict acoustic backscatter from environmental climatologies for the Southern Ocean. Using species-specific proportions from net sample data and TS values, I then calculate species abundance and biomass from predicted acoustic backscatter. Finally, I discuss my acoustically derived biomass estimate in relation to previous net estimates locally and acoustic estimates globally.

I then conclude the thesis in Chapter 5 by drawing together the themes of previous chapters, the implications of using acoustic methods for studying mesopelagic fish, and discuss future research directions.

Chapter 2

Swimbladder morphology masks Southern Ocean mesopelagic fish biomass

An adapted version of this chapter has been published in:

DORNAN, T., FIELDING, S., SAUNDERS, R. A. & GENNER, M. J. 2019. Swimbladder morphology masks Southern Ocean mesopelagic fish biomass. *Proceedings of the Royal Society B: Biological Sciences*, 286, 20190353. (Appendix I)

Author contributions

TD participated in study design, fish sampling and x-ray, carried out dissection, computed tomography, acoustic data processing, statistical analysis, and drafted the manuscript. SF coordinated the study, collected acoustic data, guided acoustic data processing, participated in fish sampling and x-ray, and helped draft the manuscript. RAS coordinated and participated in fish sampling, fish id and length measurements, and critically revised the manuscript. MG participated in the design of the study, advised on statistical analysis and helped draft the manuscript.

2.1 Abstract

Within the twilight of the oceanic mesopelagic realm, 200-1000 m below sea level, are potentially vast resources of fish. Collectively, these mesopelagic fishes are the most abundant vertebrates on Earth, and this global fish community plays a vital role in the function of oceanic ecosystems. The biomass of these fishes has recently been estimated using acoustic survey methods, which rely on echosounder-generated signals being reflected from gas-filled swimbladders and detected by transducers on vessels. Here I use x-ray computed tomography scans to demonstrate that several of the most abundant species of mesopelagic fish in the Southern Ocean lack gas-filled swimbladders. I also show using catch data from survey trawls that the fish community switches from fish possessing gas-filled swimbladders to those lacking swimbladders as latitude increases towards the Antarctic continent. Thus, the acoustic surveys that repeatedly show a decrease in mesopelagic fish biomass towards polar environments systematically overlook a large proportion of fish species that dominate polar seas. Importantly, this includes lanternfish species that are key prey items for top predators in the region, including king penguins and elephant seals. This latitudinal community switch, from gas to non-gas dominance, has considerable implications for acoustic biomass estimation, ecosystem modelling and long-term monitoring of species at risk from climate change and potential exploitation.

2.2 Introduction

Mesopelagic fish inhabit the twilight zone of the world's oceans, 200 m to 1000 m below sea level. This global community of typically small (<20 cm) fish is often dominated by myctophids, commonly known as lanternfishes (Family Myctophidae) by both abundance and biomass (Gjøsaeter and Kawaguchi, 1980). Debate surrounds the magnitude of mesopelagic fish biomass, with global estimates ranging from 1 to 19.5 gigatonnes (Gjøsaeter and Kawaguchi, 1980, Irigoien et al., 2014, Proud et al., 2018b). A key issue underlying this uncertainty is that many mesopelagic fish, including lanternfishes exhibit net avoidance behaviour, potentially resulting in an underestimation of biomass (Kaartvedt et al., 2012).

Active acoustics provides a more informative method of studying these animals at the oceanic scale. Acoustic surveys are routinely used to estimate the biomass of commercially important fish stocks (Fernandes et al., 2002). The underlying principal of active acoustics is to transmit a pulse of sound of known frequency and duration into the water column from an

echosounder, when the soundwave encounters something of a different acoustic impedance, such as gas in the swimbladder of a fish, it is reflected or scattered back to the transducer. The quantity of reflected signal or 'echo' is then integrated throughout the water column, and is commonly used as a proxy for biomass (Irigoiien et al., 2014, Simmonds and MacLennan, 2005). However, the interpretation of acoustic data into meaningful biology is complex and requires ancillary information on species distribution, behaviour and fish morphology (Davison et al., 2015), as well as knowledge of how a specific target organism backscatters the acoustic signal at a given acoustic frequency (Simmonds and MacLennan, 2005).

Gas in the swimbladders of fish can account for up to 95% of reflected acoustic "backscatter" signal (Foote, 1980b), thus the swimbladder morphology of fish is critical for determining the effectiveness of active acoustics for estimating fish biomass. It has been known for over 50 years that mesopelagic fishes can differ in swimbladder morphology (Marshall, 1960), with species showing both intra- and interspecific variability. For example, some species can maintain a gas-filled swimbladder throughout their lifespan, while some species may never have a gas-filled swimbladder, and others lose the gas component in adulthood (Marshall, 1960). Net sampling is regularly used to ground-truth acoustic data, providing knowledge of the species present and their morphological characteristics (Benoit-Bird and Lawson, 2016). However, this is challenging to undertake comprehensively at the ocean basin scale (Kloser et al., 2009) and adequate net sampling has generally focused on commercially harvested species at smaller regional scales.

In the Southern Ocean, 35 species of myctophids are known to occur (Hulley, 1990) where they form a key component of the Antarctic ecosystem, acting as both predators of zooplankton (Pakhomov et al., 1996, Shreeve et al., 2009, Saunders et al., 2018) and prey for higher predators, including seabirds and seals (Duhamel, 1998, Lea et al., 2002, Connan et al., 2007, Guinet et al., 2014). In this food web that is typically dominated by krill (*Euphausia superba*), myctophids have elevated importance for higher trophic level species during the years when krill are scarce (Murphy et al., 2007). Additionally, these myctophid species play a key role in carbon transport through the water column during diel vertical migration (DVM), which may contribute up to 17% of total carbon export from the system (Davison et al., 2013). Assessment of the biomass of these species is important for our understanding of ecosystem function and carbon sequestration, both regionally and globally. However, the utility of active acoustics for this assessment has been hampered by limited data on swimbladder morphology both within and among key myctophid species. Specifically, it has been unclear if the reported

latitudinal decline in backscatter towards the Antarctic continent (Proud et al., 2017, Escobar-Flores et al., 2018b) is a consequence of a decrease in fish biomass, or instead a consequence of the coincidental change in mesopelagic fish community composition (Escobar-Flores et al., 2018b).

Here I report a detailed exploration of the potential influence of swimbladder morphology on estimates of mesopelagic fish biomass in the Southern Ocean, which for the purposes of this study I define as the region south of 50° S. I first use multiple acoustic transects to confirm a pattern of declining acoustic backscatter towards the Antarctic landmass in the South Atlantic, in agreement with observations from the South Pacific sector (Escobar-Flores et al., 2018b). I then analyse the swimbladder condition of the common myctophid species in the region using x-ray imaging of fresh specimens, dissection of fresh specimens, and x-ray micro-computed tomography of preserved specimens. Finally, I use net data to describe the change in the mesopelagic community towards higher latitudes. I conclude that the reduction in backscatter with latitude towards Antarctica is strongly influenced by a shift in community structure from gas-bladdered to non-gas bladdered species. I consider this result from the perspective of acoustic biomass assessment, and discuss the potential underlying ecological and evolutionary drivers of the observed shift in myctophid community composition and morphology.

2.3 Methods

2.3.1 Acoustic surveys

Nautical Area Scattering Coefficient (NASC, $\text{m}^2 \text{nmi}^{-2}$), a measure of mean water column acoustic backscatter and a proxy for biomass, was quantified in relation to latitude. Six acoustic transects from five individual cruises between the Falkland Islands and the South Orkneys were conducted aboard the RRS James Clark Ross, covering Austral spring to autumn (Figure 2.1). An EK60 split-beam hull-mounted transducer was used to collect 38 kHz data to depths of 1000 m on all cruises with the exception of JR161 and JR200 where data was collected to 800 m and 990 m respectively. All data were calibrated, processed and integrated in 1 km distance by 10 m depth bins in Echoview® (Version 8.0.95, Echoview Software Pty Ltd, Hobart, Australia). Prior to integration, bad or unwanted data such as false bottom echoes, seabed, surface near-field, intermittent noise and attenuated signal were set to “no-data” and excluded from analysis. Non-transit data, where vessel speed slowed below 4 knots to

undertake alternative science operations, were not included in the analysis. After integration, data collected in water shallower than 1000 m were excluded from analysis to constrain the study to mesopelagic waters. Total water column NASC was calculated in R (Version 3.5.1) (R Core Team, 2018) and \log_e transformed prior to fitting a linear regression model using latitude as a predictor variable. To verify that high NASC values were valid and not noise, the top 1% of NASC values were visually scrutinised on echograms. Less than 10% of these were suspected to be noise-biased, and the biased NASC values were removed from further analysis. Both day and night collected acoustic data were used in the analysis. To confirm that DVM did not introduce bias, linear regressions were also carried out on separate day and night data, and all reported trends remained consistent (see Supplement S.1).

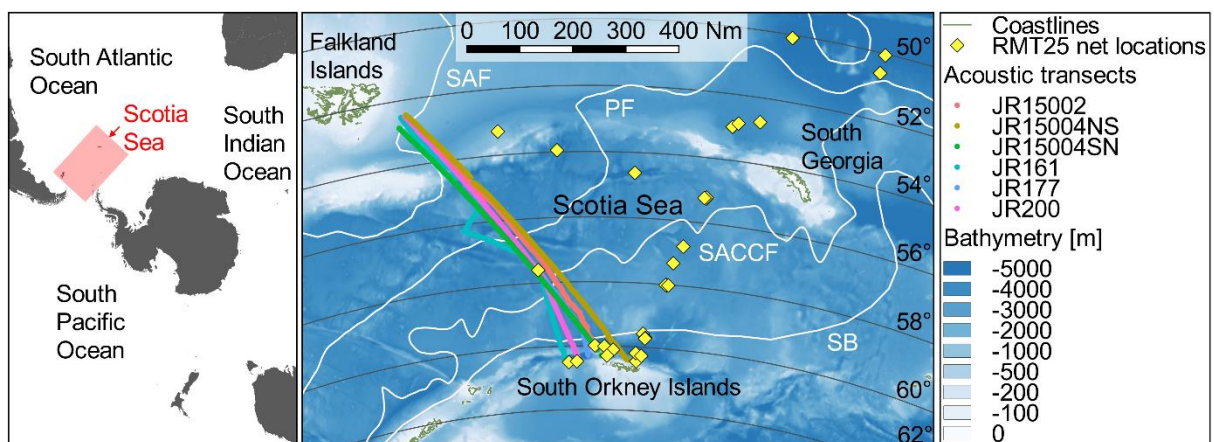


Figure 2.1 Study location in the Scotia Sea, Atlantic sector of the Southern Ocean. RMT25 surface to 1000 m depth net sample locations (yellow diamond). Acoustic transects between the Falkland Islands and the South Orkney Islands (coloured lines), Spring cruises: JR161 (Oct 2006), JR15002 (Nov 2015), Summer cruises JR177 (Jan 2008), JR15004 (Jan & Feb 2016), and Autumn cruise JR200 (Mar 2009). Mean frontal positions are represented in white, SAF (Sub Antarctic Front), PF (Polar Front), SACCF (Southern Antarctic Circumpolar Current Front) and SB (Southern Boundary of the Antarctic Circumpolar Current) (Orsi et al., 1995, Moore et al., 1999, Thorpe et al., 2002). Also shown are the 2° latitudinal bands used in analysis. Map generated in Quantum GIS ver 2.18 (www.qgis.org).

2.3.2 Net sampling

Stratified net sampling was undertaken on six cruises, between 2006 and 2017, at locations spanning the major frontal positions and water masses of the Scotia Sea (Figure 2.1). Nets were deployed day and night during early cruises (JR161 and JR177). These were later restricted to night only sampling (JR200, JR15004 and JR16003) due to comparatively low fish abundance within daylight catches presumably due to net avoidance behaviour.

Samples were collected using an opening and closing rectangular mid-water trawl RMT25 system (Baker et al., 1973). The RMT25 is equipped with two nets, with an aperture of 25 m², and cod-end mesh of 5 mm. To sample the mesopelagic and epipelagic regions, each haul was stratified into four depth zones: 1000 – 700 m, 700 – 400 m, 400 – 200 m and 200 m – surface. Nets were towed obliquely in each zone at a towing speed of approximately 2.5 knots, for a duration of 30 – 60 minutes. All nets were closed during deployment and recovery, to minimise contamination from different depth zones. Once on deck, cod-end samples were transferred to fresh seawater. The total catch weight of all fauna by species was recorded whenever possible. Fish were then placed on ice for identification, and the standard length (SL) measured, before either further morphological analysis on board the research vessel or preservation by freezing at -20°C.

Fish from these surveys were used for soft tissue x-ray and/or dissection (freshly caught specimens), or x-ray computed tomography (frozen specimens). Additional fish for morphological analysis were sampled opportunistically from RMT8 and MOCNESS nets deployed during the same cruises (Supplement S.2).

2.3.3 Swimbladder gas assessment

The swimbladders of seven of the eight most common species of myctophid (based on the net data) were assessed for the presence or absence of gas; *Electrona antarctica* (n=56), *Electrona carlsbergi* (n=28), *Gymnoscopelus braueri* (n=21), *Gymnoscopelus fraseri* (n=12), *Gymnoscopelus nicholsi* (n=14), *Krefflichthys anderssoni* (n=39), and *Protomyctophum bolini* (n=32). Assessment of individual fish was conducted using one of three methods, a) visual inspection following dissection, b) soft tissue x-ray scanning and c) x-ray computed tomography (CT) scans.

For visual inspection following dissection, freshly captured samples were dissected and swimbladder punctured under water to record presence or absence of swimbladder gas. All dissections occurred within 8 hours of capture with fish stored in individual sealed bags at ~4°C prior to dissection.

All soft tissue x-ray images were captured using an Ultrapower 100 veterinary x-ray unit. Lateral and dorsal x-rays were taken with the film cassette positioned 0.88 m from the radiography unit. Exposure time and peak voltage (kVp) were set depending on the size and

thickness of the animals being imaged, from small species being exposed for 0.08 seconds at 44 kVp, to larger species exposed for 0.09 seconds at 50 kVp.

Fish subjected to x-ray CT were scanned using one of two methods. 1) Fish were freshly defrosted, held on ice in the CT facility, and mounted in polyethylene and foam to minimise movement in the scanner; 2) Fish were fixed in 5% formalin, stained with Potassium Iodide IKI, rinsed and scanned in distilled water; using a Nikon XTH225ST CT scanner. Fish were scanned in batches or individually depending on the size of the fish; and settings were adjusted between scans to capture the maximum detail whilst retaining all of the fish in view.

Swimbladders were considered to be gas-filled if they were found to contain gas or if the swimbladder was visibly ruptured on x-ray computed tomography images, soft tissue x-ray images or during dissection. Fish were classed as non-gas-filled if they did not contain gas, or when gas was only present in the oesophagus/gut, indicative of ingestion of gas on hauling. Damaged fish, or those for which computed tomography images were inconclusive, were excluded from analysis. Supplement S.3 has detailed information on how gas presence or absence was determined from x-ray computed tomography images.

Species not assessed for gas component as part of this study were assigned swimbladder status from literature. *Protomyctophum tenisoni* was assigned as gas bearing, based on previously published analyses (Marshall, 1960). Non-myctophid Bathylagidae (Marshall, 1950), and *Notolepis* spp. (Post, 1990) do not possess swimbladders and so were not assessed for gas. As *Cyclothone* species were only identified to genus level, all were treated as 'fat invested' (for justification see Supplement S.4).

2.3.4 Statistical analysis

Community composition was determined from only the night-sampled, surface – 1000 m depth stratified, RMT25 net samples, which were standardised for tow speed and duration. Analyses focussed on 11 of the most dominant Scotia Sea fishes, which accounted for >94% of all fish captured by abundance in RMT25 net data (Supplement S.4). A depth-integrated abundance of each species was assessed for each sampling event, by calculating the average abundance across the four depth zones. Latitudinal community change was assessed by calculating mean species abundance in 2° latitudinal bands. Fish biomass for each of the 11 fish species was derived directly from the same net samples as the abundance data. Where catch weights were missing, abundance of each species was multiplied by a mean weight for

each species (calculated from combined JR161, JR177 and JR200 data). Swimbladder gas status was assigned from either this study or literature as described above, to each individual in the net based on species, and standard length where relevant. All statistical analysis were conducted in R (Version 3.5.1) (R Core Team, 2018).

2.4 Results

2.4.1 Acoustic backscatter declines with latitude

Significant declines in \log_e NASC with increasing latitudes were evident in all six acoustic transects (Figure 2.1 & Figure 2.2). The transect with the greatest variability along the linearly decreasing trend was undertaken during the late Austral spring cruise JR15002 (Figure 2.2), where visual inspection of echograms revealed high, patchy levels of backscatter in the upper water column. To confirm that the declining trend in NASC was not associated with a decreasing biomass in general, the total biomass of all fauna (both fish and invertebrates), and fish (study species only), captured in each stratified net sample, standardised for tow speed and duration, were plotted against latitude. This revealed that there was no decrease in biomass with increasing latitude (see Supplement S.5).

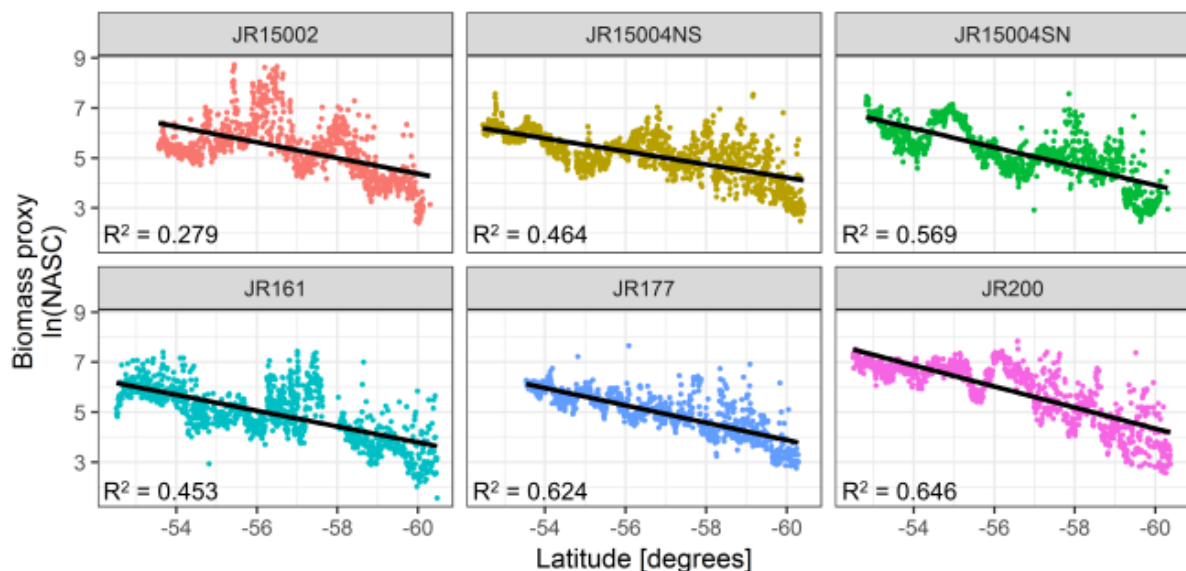


Figure 2.2 Relationship between the Nautical Area Scattering Coefficient (NASC, $\text{m}^2 \text{nmi}^{-2}$), a proxy for biomass, and increasing latitude by cruise number. JR15004 had both North to South (NS) and South to North (SN) transits, all others are one way only. All data shown were collected in water >1000 m depth. Linear regressions (black lines) are statistically significant ($p < 0.001$).

2.4.2 Gas presence and absence of key mesopelagic fish species

Electrona carlsbergi (SL 70 mm – 86 mm, n = 28), *K. anderssoni* (SL 30 mm – 70 mm, n = 39) and *P. bolini* (SL 29 mm – 62 mm, n = 32) all showed evidence of gas filled swimbladders across all lengths assessed, indicative of gas presence throughout their lifespans.

Gymnoscopelus braueri (SL 68 mm – 123 mm, n = 21), *G. nicholsi* (SL 124 mm – 153 mm, n = 14) and *G. fraseri* (SL 55 mm – 84 mm, n = 12), showed no evidence of swimbladder gas.

There was an apparent ontogenetic loss of swimbladder gas in *E. antarctica* (SL 27 mm – 103 mm, n = 56), with standard length a highly significant predictor of the presence of gas ($p < 0.001$), and the modelled shift in probability of gas presence to absence estimated at SL 51.4 mm (Supplement S.6). Both dissection and x-ray computed tomography images (Figure 2.3a) revealed the swimbladder tissue to be thickened in larger specimens with no gas retained.

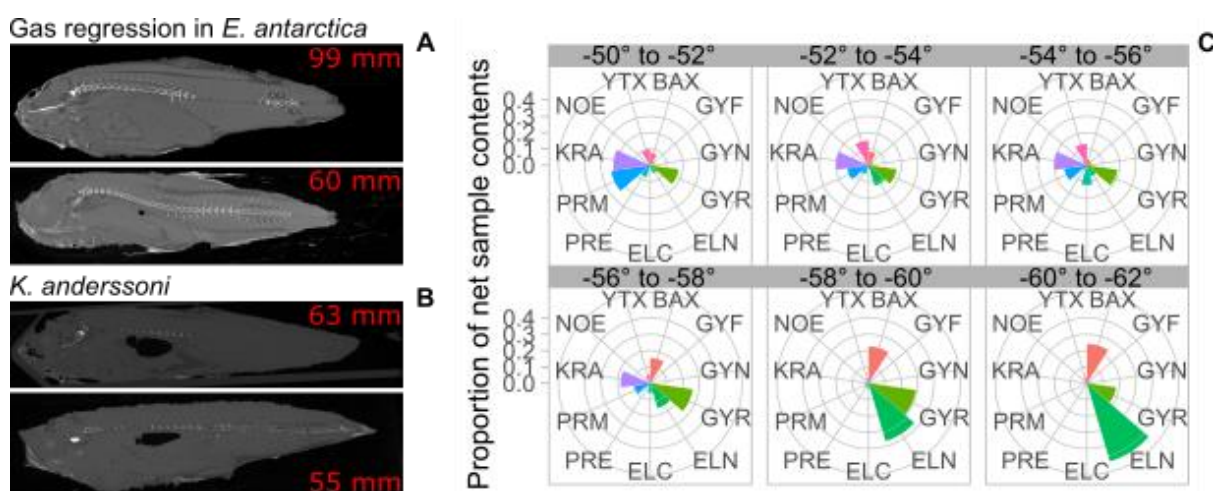


Figure 2.3 Single slice Computed Tomography scans of (a) *Electrona antarctica* showing loss of swimbladder gas and (b) *Kreftlichthys anderssoni* showing gas presence (dark regions in tissue). (c) Polar plots of standardised proportions of species captured in 2° latitude bins, each colour segment proportionally corresponds to the abundance of individual species.

The swimbladder of *K. anderssoni* was thick walled and possessed a fine transparent membraned oval structure at the anterior side, which was commonly inflated with a bubble-like appearance on dissected and CT-scanned specimens (Figure 2.3b). Swimbladders of *E. carlsbergi* and *P. bolini* were apparently thin walled as they were commonly ruptured on hauling with gas filling abdominal cavity.

2.4.3 Changing community structure

The mesopelagic fish community was dominated by Myctophidae by abundance, accounting for 75.07% of fishes captured with the RMT25, with Bathylagidae and Gonostomatidae accounting for 14.41% and 6.30% respectively. The eleven most commonly occurring mesopelagic taxa were selected for community assessment accounted for >94% of individuals captured (Supplement S.4). There was an overall reduction in species richness of mesopelagic fishes with increasing latitude, and a switch in the dominant species from the gas-bearing *P. bolini* and *K. anderssoni* at lower latitudes, to the regressed and non-gas-bearing swimbladder *E. antarctica* and *G. braueri* at higher latitudes (Figure 2.3c).

2.4.4 Effects of changing community on acoustic signal – less backscatter, not fewer fish

Mean fish abundance (mean 0.867 individuals 1000 m⁻³, range 0.751 – 0.920 individuals 1000 m⁻³) and biomass (median 3.993 g 1000 m⁻³, range 1.520 – 5.922 g 1000 m⁻³) as estimated using RMT25 trawl samples were consistent across the latitudinal gradient of the Scotia Sea (Figure 2.4a & Figure 2.4b). To examine change in morphology with latitude all *Gymnoscopelus* species, *E. antarctica* > 51.4 mm, Bathylagidae (Marshall, 1950), and *Notolepis* spp. (Post, 1990), were assigned 'No gas' status. *Electrona carlsbergi*, *P. bolini*, *K. anderssoni*, *E. antarctica* < 51.4 mm, and *P. tenisoni* (Marshall, 1960) were assigned as 'Gas'. Cyclothone were assigned as 'fat invested'. This categorisation revealed a clear latitudinal shift in the community from strongly scattering gas-bladdered species in the north of the sampled area, to acoustically cryptic non-gas bearing fish southwards towards the Antarctic continent (Figure 2.4c).

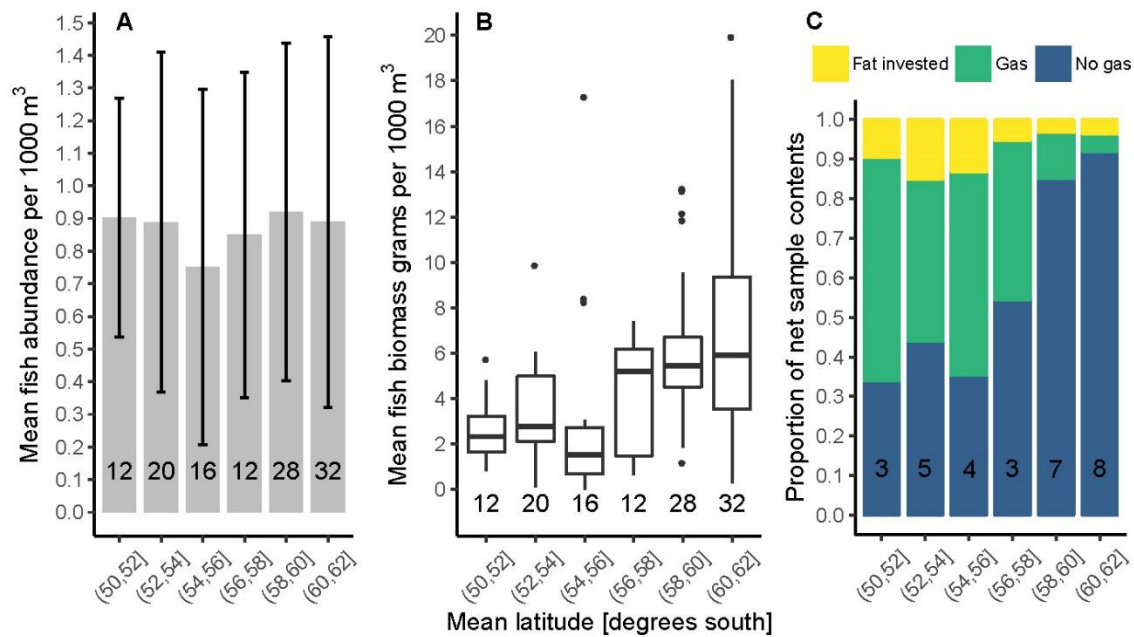


Figure 2.4 (a) Mean abundance of fish (individuals per 1000 m³) in RMT25 net samples by latitude. Bars indicate standard deviation between net samples and numbers in columns indicate numbers of individual net strata samples included. (b) Mean biomass of fish (grams per 1000m³) in RMT25 net samples by latitude, box spans interquartile range (IQR), horizontal line is the median, whiskers include values up to 1.5 x IQR, outlying values plotted individually. (c) Relative proportions of fish by swimbladder contents in net samples at latitude. Numbers in columns are the individual number of total water column samples (each comprising of four depth strata) used in analysis.

2.5 Discussion

Active acoustics can be an invaluable method for monitoring and understanding ecosystems (Benoit-Bird and Lawson, 2016). Since acoustic data are commonly used as a proxy for biomass, a change in the acoustic community structure, where strong scattering fish are replaced by weak scattering, could have considerable implications for ecosystem assessment and modelling of trophic interactions. It has previously been reported that there is a north to south shift in fish community composition in the Scotia Sea (Collins et al., 2012, Saunders and Tarling, 2018). This study has confirmed this poleward shift in mesopelagic community structure that parallels a decline in acoustic backscatter. I suggest that the decline is most likely to reflect a shift in the morphological and physiological properties of the fish community present towards the Antarctic continent, rather than a systematic change in total fish biomass.

2.5.1 Poleward loss of gas-filled swim bladders.

The apparent loss of gas-filled swimbladders in fish species with increasing latitude raises interesting questions about the ecology of the system, and the evolutionary drivers of shifts in swimbladder properties. Typically, mesopelagic fishes undertake large-scale DVM (mean ~590 m per cycle) (Klevjer et al., 2016), to enable them to forage on abundant near-surface zooplankton at night, while avoiding shallow-water predators during daytime (Pearre, 2003). However, at extreme polar latitudes DVM is apparently reduced relative to lower latitude habitats (Proud et al., 2018a). A key underlying factor could be a poleward shift in the light environment, which is known to be an important stimulus of DVM behaviour (Brierley, 2014). It is therefore plausible that the observed shift in swimbladder morphology is associated with a change in physiological requirements to enable large-scale diurnal depth changes. Species occupying higher latitudes may have a reduced need to alter buoyancy dynamically using a gas-filled swimbladder, instead relying upon buoyancy provided by lipid, and avoiding the physiological costs of rapid secretion and resorption of gas. Testing this hypothesis would require modelling of energetic costs of DVM using alternative gas and lipid buoyancy strategies across the depth ranges, temperatures, water densities and behaviours where diurnal migration takes place in the Southern Ocean (Strand et al., 2005).

2.5.2 Ontogenetic shifts in distribution and swimbladder morphology.

Data on the presence or absence of gas in swimbladders was restricted to larger size classes of myctophids captured, because small (<40 mm) individuals of most species are rarely taken in the Scotia Sea. Saunders et al. (2017) discussed the absence of larval myctophids in wider Scotia Sea net samples and suggested that many myctophid species of the Scotia Sea could be expatriates from sub-Antarctic, or temperate latitudes that migrate southwards during ontogeny, possibly in search of food hotspots. The main exceptions are *K. anderssoni*, which appears to produce larvae in the coastal waters around South Georgia (Cumberland Bay) (Belchier and Lawson, 2013), and *E. antarctica* the larvae of which are present in waters towards the Antarctic continental shelf in other regions of the Southern Ocean (Indian Ocean sector) (Moteki et al., 2017). Whether expatriated myctophids return to waters further north to reproduce remains unclear and requires further investigation.

Unlike the other Southern Ocean myctophids, *E. antarctica* is regarded as a polar specialist that is confined to waters south of the Antarctic Polar Front. This species appears to have a close association with sea ice in some regions of the Southern Ocean (Indian Ocean

sector), with the marginal sea ice zone seemingly important for larval development (Moteki et al., 2017). At present, it is unclear if an ontogenetic habitat shift from sea ice margin to open ocean of *E. antarctica* has favoured the loss of gas filled swimbladders with increasing body size, but it is plausible that loss of gas represents an adaptation to changing habitat occupancy and DVM behaviour during ontogeny. The observed ontogenetic shift could have importance for interpretation for acoustic data, as any seasonal increase in larval *E. antarctica* with small gas-bearing swimbladders could lead to increased resonance on echograms. Further sampling of smaller individuals of the species in this assemblage, coupled with analyses of their morphology and buoyancy strategies, would clarify if the ontogenetic regression of the swimbladder I observed in *E. antarctica* is unique to that species, or instead more widespread across myctophid species of the region, particularly in abundant *Gymnoscopelus* species as I could not rule out gas presence in earlier life stages. It would be advisable to chemically fix larvae and juveniles immediately on capture for later staining and CT scanning, as freezing of such small specimens can lead to tissue damage.

2.5.3 Challenges for acoustic studies of mesopelagic fish

As in other large-scale surveys of mesopelagic fish biomass (Irigoién et al., 2014), I used 38 kHz acoustic data as it generally has sufficient depth resolution to sample the mesopelagic zone. However, the Scotia Sea supports a diverse community of mesopelagic species (Piatkowski et al., 1994) and single-frequency acoustic data lack the detailed information to distinguish between taxa, presenting two main sources of bias. Firstly, fluid-like Antarctic krill *Euphausia superba* would be undetectable individually, but collectively the extensive dense aggregations would be readily detected by echosounders. Secondly, colonial siphonophores, many species of which bear a gas-filled pneumatophore, have been shown to be strong acoustic targets with the potential to resonate (Warren, 2001, Kloser et al., 2016, Proud et al., 2018b). Of 18 siphonophore species known to occur south of 50° S only five are physonect (gas-bearing) (Mapstone, 2014). While only limited data exists on the abundance of siphonophores in the region, there is evidence that both siphonophores and krill are more prevalent in the south of the Scotia Sea (Fielding et al., 2012, Ward et al., 2012, Atkinson et al., 2019). Thus, it seems unlikely that the pattern of a southward reduction in NASC in this study is driven by shifts in the abundance of either krill or physonect siphonophores, but there is a clear need for focussed research on the distribution and abundance patterns of siphonophores in the Southern Ocean (Proud et al., 2018b).

My study shows that reliable interpretation of acoustic biomass survey data requires additional biological information that can be derived by net sampling (Davison et al., 2015). Ideally net sampling and acoustic data collection would occur concurrently. However limited ship time requires a balance is achieved between obtaining consistent acoustic transects and acquiring sufficient net data. While much of the acoustic and net sample data used in this study are from longitudinally offset locations and a relatively small regional scale, both data sets span the same major Southern Ocean fronts and water masses (identified in Figure 2.1). This study reveals latitudinal trends in both the acoustics and community structure, which are consistent with other Southern Ocean regions (Escobar-Flores et al., 2018b). From an ecological perspective this is unsurprising as the most common mesopelagic fish typically have circumpolar distributions (Hulley, 1990), resulting from broadly analogous latitudinal water masses and habitats (Orsi et al., 1995). I therefore suggest that the trends revealed in this study may be broadly applicable to the wider Southern Ocean ecosystem. Further net sample and acoustic data would enable tests of the generality of my findings, particularly in the South West Atlantic, South Indian Ocean and South West Pacific Sectors.

It has been noted that there is a markedly greater acoustic backscatter in low latitude mesopelagic habitats relative to those at higher latitudes (Proud et al., 2017). A comparison between the Southern Ocean and what are known to be highly productive low latitude subtropical regions was not the focus of the current study. Nevertheless, it would be interesting to determine how the morphology of species contrasts between these latitudinal realms, and if fish scattering properties more generally are able to influence patterns of acoustic backscatter across larger global spatial scales.

2.5.4 Implications for monitoring and modelling

Recent modelling based on acoustic data predicts an increase in mesopelagic biomass under future warming scenarios (Proud et al., 2017). My results indicate that a proportion of the Southern Ocean mesopelagic community is dominated by acoustically cryptic species and therefore polar biomass may be underestimated. It is therefore important that complementary methods of accounting for potential 'missing' biomass are employed, including ground-truthing through net validation. However, such net sampling requires extensive investment in sampling resources, and would be challenging for larger basin and global scale surveys (Kloser et al., 2009). It is possible that the need for such extensive surveys could be partially mitigated by knowledge of basin scale trends in community composition, as well as backscatter

properties of species present, that would enable the development of geographical correction factors that can be applied to acoustics-based estimates. Future solutions may also lie in the development and refinement of environmental DNA techniques, where acoustic data may be validated and adjusted for through assessment of community composition within water samples (Stat et al., 2017). In the meantime, active acoustics in combination with net sampling will remain a powerful combination of methods for the collection of temporal and spatial data for assessment of mesopelagic communities.

2.6 Conclusions

There has been recent interest in the potential exploitation of abundant mesopelagic fish to meet growing human needs, but to achieve this sustainably requires a solid understanding of the impacts on the wider ecosystem (St. John et al., 2016). An inability to detect key species during acoustic monitoring presents a particular risk to fished stocks, where species could be exploited beyond sustainable levels. In addition, many fish species have shifted poleward to maintain their optimum thermal tolerance (Perry et al., 2005, Poloczanska et al., 2013, Sunday et al., 2012), as sea temperatures warm, and further shifts are projected. Development of reliable sampling methods, including acoustics, can only enhance our ability to monitor changes in population dynamics of myctophids, informing long-term management of the wider Antarctic ecosystem.

Acknowledgements

I thank the crew and scientists of the RRS James Clark Ross for support in sample and acoustic data collection. Tom Davies (University of Bristol) and Ket Smithson (University of Cambridge) supported CT scanning. John Horne provided guidance and practical support with on-board X-ray capture.

Chapter 2

Supplementary material

S.1 Linear regressions on day night acoustic data.

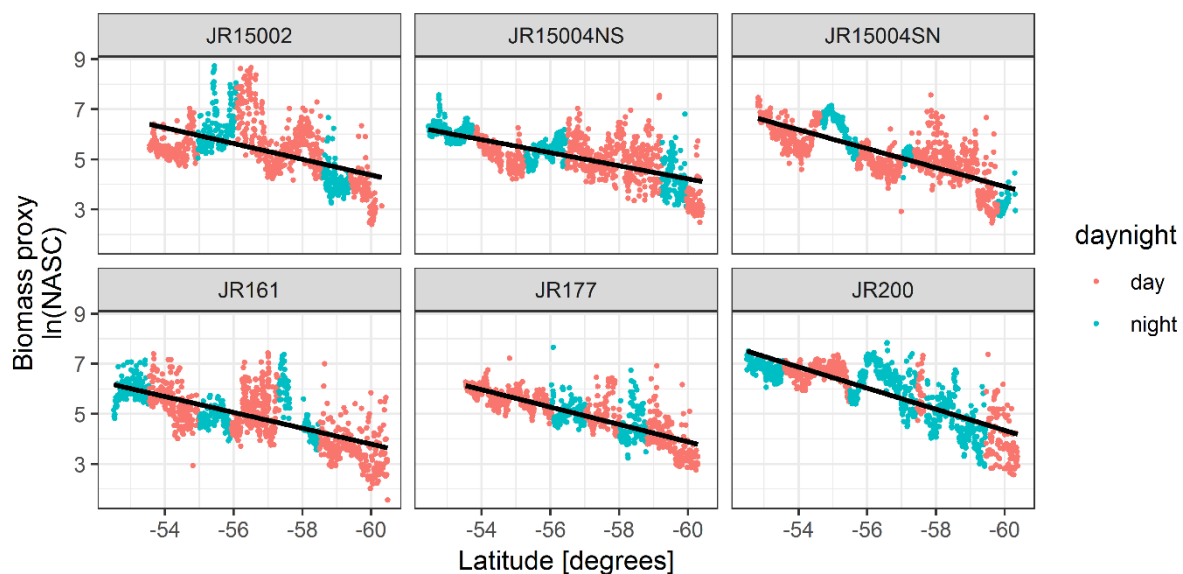


Figure S.1 Linear regression plots on day night acoustic data. To confirm that diel vertical migration behaviour did not introduce bias, linear regressions on day and night only data were also carried out. Linear regressions continue to reveal highly significant declines in NASC with an increase in latitude ($p < 0.0001$).

Table S.1 Linear regression coefficients of \log_e transformed NASC against latitude.

Data	Cruise	Slope	Standard Error	R ²
All data	JR15002	0.314709	0.016844	0.279
"	JR15004NS	0.261223	0.008407	0.464
"	JR15004SN	0.378643	0.010354	0.569
"	JR161	0.316616	0.010446	0.453
"	JR177	0.346625	0.009056	0.624
"	JR200	0.421575	0.009866	0.646
Day only	JR15002	0.235145	0.019766	0.184
"	JR15004NS	0.211170	0.015136	0.231
"	JR15004SN	0.312942	0.011233	0.497
"	JR161	0.345870	0.013167	0.473
"	JR177	0.357730	0.009004	0.708
"	JR200	0.470532	0.013512	0.760
Night only	JR15002	0.556826	0.027631	0.601
"	JR15004NS	0.293638	0.008841	0.703
"	JR15004SN	0.650096	0.013242	0.914
"	JR161	0.223463	0.019327	0.283
"	JR177	0.232736	0.039173	0.135
"	JR200	0.383161	0.013744	0.559

Chapter 2 Supplementary material

S.2 Swimbladder gas contents used in analysis. Swimbladder gas contents used in analysis.

Species: KRA – *Krefflichthys anderssoni*, ELN – *Electrona antarctica*, ELC – *E. carlsbergi*, GYR – *Gymnoscopelus braueri*, GYF – *G. fraseri*, GYN – *G. nicholsi*, PRM – *Protomyctophum bolini*.

Treatment details pre-treatment of fish prior to assessment of swimbladder condition, Frozen:

scanned from frozen, IKI: fixed and stained with Potassium Iodide, Fresh: untreated, freshly captured.

Gas: Y – Yes, R – Ruptured, N – No, Inc – Inconclusive exclude from analysis, D – Damaged exclude from analysis. Data source is method of assessment, CT – computed tomography, X-ray – Soft tissue x-ray, Dis – dissection of freshly captured fish. Net type indicates sample method of capture, either RMT25 or opportunistic samples from RMT8 or MOCNESS (MOC). Lat and Lon are the mean net sample latitude and longitude during oblique tows respectively.

Cruise	Event	Net	Species	Sex	SL mm	Treatment	Gas	Gas binary	Data source	Net type	Lat	Lon
JR16003	130	2	KRA	F	63	Frozen	Y	1	CT	RMT25	-54.576	-45.107
JR16003	130	2	KRA	M	63	Frozen	Y	1	CT	RMT25	-54.576	-45.107
JR16003	130	2	KRA	M	55	Frozen	Y	1	CT	RMT25	-54.576	-45.107
JR16003	171	1	KRA	F	55	Frozen	Y	1	CT	RMT25	-56.719	-56.858
JR16003	147	1	KRA	M	51	Frozen	Inc	NA	CT	RMT25	-53.951	-49.247
JR16003	171	1	KRA	M	46	Frozen	R	1	CT	RMT25	-56.719	-56.858
JR16003	130	2	KRA	J	36	Frozen	R	1	CT	RMT25	-54.576	-45.107
JR16003	171	1	KRA	U	38	Frozen	Inc	NA	CT	RMT25	-56.719	-56.858
JR16003	164	1	KRA	U	39	Frozen	R	1	CT	RMT25	-53.292	-52.200
JR16003	171	1	KRA	J	30	Frozen	Y	1	CT	RMT25	-56.719	-56.858
JR15004	60	2	ELN	F	99	Frozen	N	0	CT	RMT25	-59.997	-47.231
JR15004	60	2	ELN	M	96	Frozen	N	0	CT	RMT25	-59.997	-47.231
JR15004	60	2	ELN	F	76	Frozen	N	0	CT	RMT25	-59.997	-47.231
JR15004	60	2	ELN	F	77	Frozen	N	0	CT	RMT25	-59.997	-47.231
JR15004	60	2	ELN	M	68	Frozen	N	0	CT	RMT25	-59.997	-47.231
JR15004	91	1	ELN	F	64	Frozen	N	0	CT	RMT25	-60.257	-46.213
JR15004	96	2	ELN	F	61	Frozen	N	0	CT	RMT25	-60.340	-46.662
JR15004	91	1	ELN	F	60	Frozen	Y	1	CT	RMT25	-60.257	-46.213
JR15004	73	2	ELN	J	45	Frozen	Inc	NA	CT	RMT25	-60.119	-46.081
JR15004	72	2	ELN	J	45	Frozen	Y	1	CT	RMT25	-60.115	-46.078
JR177	165	2	ELN	U	45	IKI	Y	1	CT	RMT25	-59.684	-44.170
JR177	165	2	ELN	U	45	IKI	Y	1	CT	RMT25	-59.684	-44.170
JR177	165	2	ELN	U	51	IKI	N	0	CT	RMT25	-59.684	-44.170
JR177	165	2	ELN	U	47	IKI	Y	1	CT	RMT25	-59.684	-44.170
JR177	165	2	ELN	U	50	IKI	R	1	CT	RMT25	-59.684	-44.170
JR177	300	2	ELN	F	93	IKI	N	0	CT	RMT25	-52.879	-40.153
JR177	300	2	ELN	F	84	IKI	N	0	CT	RMT25	-52.879	-40.153
JR177	300	2	ELN	M	61	IKI	N	0	CT	RMT25	-52.879	-40.153
JR177	300	2	ELN	U	47	IKI	Inc	NA	CT	RMT25	-52.879	-40.153
JR177	300	2	ELN	F	59	IKI	N	0	CT	RMT25	-52.879	-40.153
JR177	300	2	ELN	F	70	IKI	N	0	CT	RMT25	-52.879	-40.153
JR177	379	1	ELN	M	73	IKI	N	0	CT	RMT25	-53.590	-37.659

Chapter 2 Supplementary material

JR177	379	1	ELN	M	67	IKI	D	NA	CT	RMT25	-53.590	-37.659
JR177	379	1	ELN	F	66	IKI	Inc	NA	CT	RMT25	-53.590	-37.659
JR177	379	1	ELN	F	44	IKI	Y	1	CT	RMT25	-53.590	-37.659
JR177	379	1	ELN	F	64	IKI	N	0	CT	RMT25	-53.590	-37.659
JR177	379	1	ELN	M	66	IKI	N	0	CT	RMT25	-53.590	-37.659
JR177	357	1	ELC	F	81	IKI	R	1	CT	RMT25	-50.520	-34.081
JR177	357	1	ELC	M	78	IKI	Y	1	CT	RMT25	-50.520	-34.081
JR177	357	1	ELC	F	76	IKI	R	1	CT	RMT25	-50.520	-34.081
JR177	357	1	ELC	M	76	IKI	R	1	CT	RMT25	-50.520	-34.081
JR177	357	1	ELC	F	82	IKI	R	1	CT	RMT25	-50.520	-34.081
JR177	357	1	ELC	F	71	IKI	R	1	CT	RMT25	-50.520	-34.081
JR177	357	1	ELC	M	74	IKI	Y	1	CT	RMT25	-50.520	-34.081
JR177	379	1	GYR		98	Frozen	N	0	X-ray	RMT25	-53.590	-37.659
JR177	379	1	GYR		110	Frozen	N	0	X-ray	RMT25	-53.590	-37.659
JR177	379	1	GYR		99	Frozen	N	0	X-ray	RMT25	-53.590	-37.659
JR177	379	1	GYR		77	Frozen	N	0	X-ray	RMT25	-53.590	-37.659
JR177	379	1	GYR		107	Frozen	N	0	X-ray	RMT25	-53.590	-37.659
JR15004	73	2	GYR		68	Frozen	N	0	X-ray	RMT25	-60.119	-46.081
JR15004	73	2	GYR		69	Frozen	N	0	X-ray	RMT25	-60.119	-46.081
JR15004	73	2	GYR		74	Frozen	N	0	X-ray	RMT25	-60.119	-46.081
JR15004	73	2	GYR		96	Frozen	N	0	X-ray	RMT25	-60.119	-46.081
JR15004	73	2	GYR		70	Frozen	N	0	X-ray	RMT25	-60.119	-46.081
JR15004	61	1	GYR		112	Frozen	N	0	X-ray	RMT25	-59.975	-47.202
JR15004	61	1	GYR		113	Frozen	N	0	X-ray	RMT25	-59.975	-47.202
JR15004	61	1	GYR		101	Frozen	N	0	X-ray	RMT25	-59.975	-47.202
JR15004	61	1	GYR		115	Frozen	N	0	X-ray	RMT25	-59.975	-47.202
JR15004	61	1	GYR		123	Frozen	N	0	X-ray	RMT25	-59.975	-47.202
JR177	305	2	GYF	F	37	Frozen	Inc	NA	X-ray	RMT25	-52.870	-40.085
JR177	305	2	GYF	F	55	Frozen	N	0	X-ray	RMT25	-52.870	-40.085
JR177	305	2	GYF	F	37	Frozen	D	NA	X-ray	RMT25	-52.870	-40.085
JR177	305	2	GYF	M	63	Frozen	N	0	X-ray	RMT25	-52.870	-40.085
JR177	305	2	GYF	F	40	Frozen	Inc	NA	X-ray	RMT25	-52.870	-40.085
JR16003	164	2	GYF		75	Frozen	N	0	X-ray	RMT25	-53.301	-52.207
JR16003	164	2	GYF	F	73	Frozen	N	0	X-ray	RMT25	-53.301	-52.207
JR16003	164	2	GYF		82	Frozen	N	0	X-ray	RMT25	-53.301	-52.207
JR177	378	1	GYN		146	Frozen	N	0	X-ray	RMT25	-53.587	-37.662
JR177	378	1	GYN		131	Frozen	N	0	CT	RMT25	-53.587	-37.662
JR177	378	1	GYN		133	Frozen	N	0	X-ray	RMT25	-53.587	-37.662
JR177	378	1	GYN		126	Frozen	N	0	X-ray	RMT25	-53.587	-37.662
JR177	378	1	GYN		141	Frozen	N	0	X-ray	RMT25	-53.587	-37.662
JR15004	104	1	PRM		41	IKI	Y	1	CT	RMT8	-57.027	-51.601
JR15004	104	1	PRM		37	IKI	Y	1	CT	RMT8	-57.027	-51.601
JR15004	104	1	PRM		43	IKI	Y	1	CT	RMT8	-57.027	-51.601
JR15004	104	1	PRM		42	IKI	Y	1	CT	RMT8	-57.027	-51.601
JR15004	104	1	PRM		43	IKI	Y	1	CT	RMT8	-57.027	-51.601
JR15004	104	1	PRM		42	IKI	R	1	CT	RMT8	-57.027	-51.601
JR15004	104	1	PRM		51	IKI	R	1	CT	RMT8	-57.027	-51.601

Chapter 2 Supplementary material

JR15004	104	1	PRM		43	IKI	R	1	CT	RMT8	-57.027	-51.601
JR15004	104	1	PRM		44	IKI	R	1	CT	RMT8	-57.027	-51.601
JR15004	104	1	PRM		42	IKI	R	1	CT	RMT8	-57.027	-51.601
JR15004	104	1	PRM		45	IKI	R	1	CT	RMT8	-57.027	-51.601
JR15004	60	2	ELN	F	79	Fresh	N	0	X-ray	RMT25	-59.997	-47.231
JR15004	60	2	ELN	M	77	Fresh	N	0	X-ray	RMT25	-59.997	-47.231
JR15004	60	2	ELN		70	Fresh	N	0	X-ray	RMT25	-59.997	-47.231
JR15004	60	2	ELN		103	Fresh	N	0	X-ray	RMT25	-59.997	-47.231
JR15004	60	2	ELN		92	Fresh	N	0	X-ray	RMT25	-59.997	-47.231
JR15004	60	2	GYR		81	Fresh	N	0	X-ray	RMT25	-59.997	-47.231
JR15004	60	2	GYR		108	Fresh	N	0	X-ray	RMT25	-59.997	-47.231
JR15004	60	2	GYR		115	Fresh	N	0	X-ray	RMT25	-59.997	-47.231
JR15004	60	2	GYR		104	Fresh	N	0	X-ray	RMT25	-59.997	-47.231
JR15004	60	2	GYR		80	Fresh	N	0	X-ray	RMT25	-59.997	-47.231
JR15004	65	1	ELN	M	66	Fresh	N	0	X-ray	RMT25	-60.014	-46.614
JR15004	65	1	ELN	F	88	Fresh	N	0	X-ray	RMT25	-60.014	-46.614
JR15004	65	1	ELN	F	88	Fresh	N	0	X-ray	RMT25	-60.014	-46.614
JR15004	65	1	ELN	F	82	Fresh	N	0	X-ray	RMT25	-60.014	-46.614
JR15004	65	1	ELN	F	66	Fresh	N	0	X-ray	RMT25	-60.014	-46.614
JR15004	65	1	ELN	F	78	Fresh	N	0	X-ray	RMT25	-60.014	-46.614
JR15004	65	1	ELN	F	81	Fresh	N	0	X-ray	RMT25	-60.014	-46.614
JR15004	65	1	ELN	F	88	Fresh	N	0	X-ray	RMT25	-60.014	-46.614
JR15004	65	1	ELN	F	71	Fresh	N	0	X-ray	RMT25	-60.014	-46.614
JR15004	65	1	ELN	F	66	Fresh	N	0	X-ray	RMT25	-60.014	-46.614
JR15004	72	2	ELN	J	49	Fresh	Y	1	X-ray	RMT25	-60.115	-46.078
JR15004	72	2	ELN	M	63	Fresh	N	0	X-ray	RMT25	-60.115	-46.078
JR15004	72	2	ELN	F	69	Fresh	N	0	X-ray	RMT25	-60.115	-46.078
JR15004	72	2	ELN	M	62	Fresh	N	0	X-ray	RMT25	-60.115	-46.078
JR15004	73	2	PRM	M	40	Fresh	R	1	X-ray	RMT25	-60.115	-46.078
JR15004	73	2	ELN	M	70	Fresh	N	0	X-ray	RMT25	-60.115	-46.078
JR15004	91	1	ELN	F	59	Fresh	N	0	X-ray	RMT25	-60.257	-46.213
JR15004	91	1	ELN	F	66	Fresh	N	0	X-ray	RMT25	-60.257	-46.213
JR15004	91	1	ELN	F	64	Fresh	N	0	X-ray	RMT25	-60.257	-46.213
JR15004	96	2	GYN		139	Fresh	N	0	X-ray	RMT25	-60.340	-46.662
JR15004	96	2	GYN		141	Fresh	N	0	X-ray	RMT25	-60.340	-46.662
JR15004	96	2	GYN		135	Fresh	N	0	X-ray	RMT25	-60.340	-46.662
JR15004	96	2	GYN		153	Fresh	N	0	X-ray	RMT25	-60.340	-46.662
JR15004	96	2	GYN		150	Fresh	N	0	X-ray	RMT25	-60.340	-46.662
JR15004	96	2	GYN		144	Fresh	N	0	X-ray	RMT25	-60.340	-46.662
JR15004	96	2	GYN		124	Fresh	N	0	X-ray	RMT25	-60.340	-46.662
JR15004	96	2	GYN		141	Fresh	N	0	X-ray	RMT25	-60.340	-46.662
JR15004	96	2	GYN		129	Fresh	N	0	X-ray	RMT25	-60.340	-46.662
JR15004	96	2	ELN	F	60	Fresh	N	0	X-ray	RMT25	-60.340	-46.662
JR15004	96	2	ELN	M	65	Fresh	N	0	X-ray	RMT25	-60.340	-46.662
JR15004	104	1	ELC	F	74	Fresh	R	1	X-ray	RMT8	-57.027	-51.601
JR15004	104	1	ELC	F	77	Fresh	R	1	X-ray	RMT8	-57.027	-51.601
JR15004	105	2	ELC		83	Fresh	R	1	X-ray	RMT8	-57.026	-51.553

Chapter 2 Supplementary material

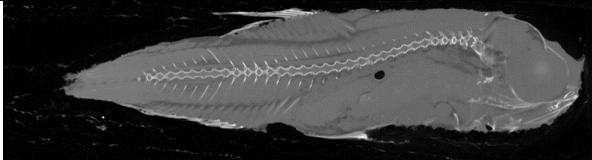
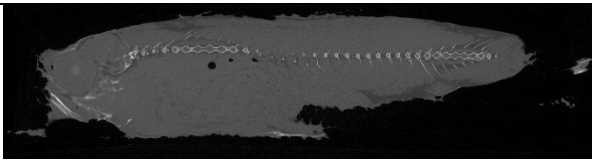
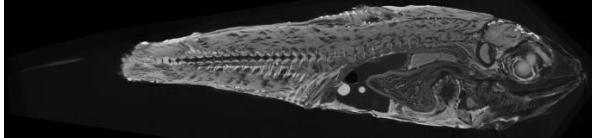
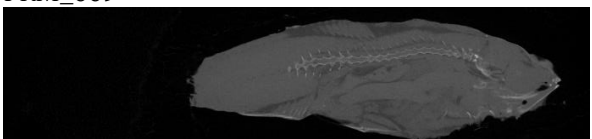
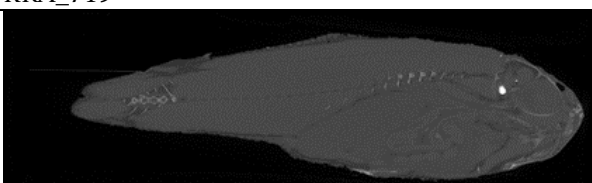
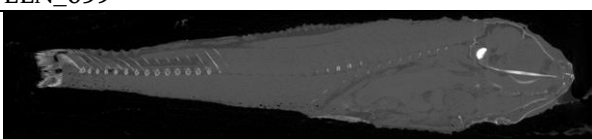
JR15004	105	2	ELC		86	Fresh	R	1	X-ray	RMT8	-57.026	-51.553
JR15004	105	2	ELC		85	Fresh	R	1	X-ray	RMT8	-57.026	-51.553
JR15004	105	1	ELC	F	75	Fresh	R	1	X-ray	RMT8	-57.041	-51.519
JR15004	105	1	ELC		73	Fresh	R	1	X-ray	RMT8	-57.041	-51.519
JR15004	105	1	PRM	M	43	Fresh	Y	1	X-ray	RMT8	-57.041	-51.519
JR15004	105	1	PRM	M	47	Fresh	Y	1	X-ray	RMT8	-57.041	-51.519
JR15004	105	1	PRM	F	48	Fresh	R	1	X-ray	RMT8	-57.041	-51.519
JR15004	106	2	ELC		76	Fresh	R	1	X-ray	RMT8	-57.024	-51.545
JR15004	106	2	ELC		84	Fresh	R	1	X-ray	RMT8	-57.024	-51.545
JR15004	106	2	ELC		77	Fresh	R	1	X-ray	RMT8	-57.024	-51.545
JR15004	106	2	ELC		76	Fresh	R	1	X-ray	RMT8	-57.024	-51.545
JR15004	106	2	ELC		86	Fresh	R	1	X-ray	RMT8	-57.024	-51.545
JR15004	106	2	ELC		70	Fresh	R	1	X-ray	RMT8	-57.024	-51.545
JR15004	106	2	ELC		80	Fresh	R	1	X-ray	RMT8	-57.024	-51.545
JR15004	106	2	ELN	J	43	Fresh	N	0	X-ray	RMT8	-57.024	-51.545
JR15004	106	2	ELN	J	32	Fresh	Y	1	X-ray	RMT8	-57.024	-51.545
JR15004	106	2	PRM		51	Fresh	Y	1	X-ray	RMT8	-57.024	-51.545
JR16003	39	2	ELN	F	44	Fresh	Y	1	Dis	RMT8	-53.540	-39.250
JR16003	39	2	PRM	F	51	Fresh	Y	1	Dis	RMT8	-53.540	-39.250
JR16003	89	1	PRM		29	Fresh	Y	1	Dis	MOC	-52.840	-40.211
JR16003	129	2	ELC		79	Fresh	Y	1	Dis	RMT25	-54.653	-45.188
JR16003	129	2	ELC		76	Fresh	Y	1	Dis	RMT25	-54.653	-45.188
JR16003	129	2	ELC		79	Fresh	Y	1	Dis	RMT25	-54.653	-45.188
JR16003	129	2	ELC		80	Fresh	Y	1	Dis	RMT25	-54.653	-45.188
JR16003	129	2	ELC		72	Fresh	Y	1	Dis	RMT25	-54.653	-45.188
JR16003	129	2	ELC		78	Fresh	Y	1	Dis	RMT25	-54.653	-45.188
JR16003	129	2	ELC		77	Fresh	Y	1	Dis	RMT25	-54.653	-45.188
JR16003	129	2	ELN		65	Fresh	Y	1	Dis	RMT25	-54.653	-45.188
JR16003	129	2	ELN		95	Fresh	N	0	Dis	RMT25	-54.653	-45.188
JR16003	129	2	PRM	M	62	Fresh	Y	1	Dis	RMT25	-54.653	-45.188
JR16003	129	2	PRM	M	61	Fresh	Y	1	Dis	RMT25	-54.653	-45.188
JR16003	129	2	PRM	F	53	Fresh	Y	1	Dis	RMT25	-54.653	-45.188
JR16003	129	2	PRM	F	60	Fresh	Y	1	Dis	RMT25	-54.653	-45.188
JR16003	129	2	PRM	F	57	Fresh	Y	1	Dis	RMT25	-54.653	-45.188
JR16003	143	2	KRA		42	Fresh	Y	1	Dis	MOC	-53.930	-49.164
JR16003	143	1	ELN		27	Fresh	Y	1	Dis	MOC	-53.932	-49.112
JR16003	146	2	KRA	F	51	Fresh	Y	1	Dis	RMT25	-53.958	-49.197
JR16003	146	2	KRA	M	45	Fresh	Y	1	Dis	RMT25	-53.958	-49.197
JR16003	146	2	KRA	M	40	Fresh	Y	1	Dis	RMT25	-53.958	-49.197
JR16003	146	2	KRA	M	45	Fresh	Y	1	Dis	RMT25	-53.958	-49.197
JR16003	146	2	KRA	M	52	Fresh	Y	1	Dis	RMT25	-53.958	-49.197
JR16003	146	2	GYR		105	Fresh	N	0	Dis	RMT25	-53.958	-49.197
JR16003	146	1	KRA	F	68	Fresh	Y	1	Dis	RMT25	-53.948	-49.180
JR16003	146	1	KRA	F	62	Fresh	Y	1	Dis	RMT25	-53.948	-49.180
JR16003	146	1	KRA	M	64	Fresh	Y	1	Dis	RMT25	-53.948	-49.180
JR16003	147	1	KRA	F	48	Fresh	Y	1	Dis	RMT25	-53.951	-49.247
JR16003	147	1	KRA	F	48	Fresh	Y	1	Dis	RMT25	-53.951	-49.247

Chapter 2 Supplementary material

JR16003	147	1	KRA	F	49	Fresh	N	0	Dis	RMT25	-53.951	-49.247
JR16003	147	1	KRA	F	48	Fresh	Y	1	Dis	RMT25	-53.951	-49.247
JR16003	147	2	PRM	F	59	Fresh	Y	1	Dis	RMT25	-53.929	-49.262
JR16003	147	2	PRM	F	56	Fresh	Y	1	Dis	RMT25	-53.929	-49.262
JR16003	147	2	PRM	M	57	Fresh	Y	1	Dis	RMT25	-53.929	-49.262
JR16003	147	2	PRM	F	60	Fresh	Y	1	Dis	RMT25	-53.929	-49.262
JR16003	164	2	GYF		76	Fresh	N	0	Dis	RMT25	-53.301	-52.207
JR16003	164	2	PRM	M	54	Fresh	Y	1	Dis	RMT25	-53.301	-52.207
JR16003	164	2	PRM	M	51	Fresh	Y	1	Dis	RMT25	-53.301	-52.207
JR16003	164	2	PRM	J	32	Fresh	Y	1	Dis	RMT25	-53.301	-52.207
JR16003	164	2	PRM	M	37	Fresh	Y	1	Dis	RMT25	-53.301	-52.207
JR16003	164	2	PRM	F	50	Fresh	Y	1	Dis	RMT25	-53.301	-52.207
JR16003	164	2	KRA	M	48	Fresh	N	0	Dis	RMT25	-53.301	-52.207
JR16003	171	1	ELN	J	42	Fresh	Y	1	Dis	RMT25	-56.719	-56.858
JR16003	171	1	KRA	M	65	Fresh	Y	1	Dis	RMT25	-56.719	-56.858
JR16003	171	1	KRA	M	58	Fresh	Y	1	Dis	RMT25	-56.719	-56.858
JR16003	171	1	KRA	F	64	Fresh	Y	1	Dis	RMT25	-56.719	-56.858
JR16003	171	1	KRA	M	67	Fresh	Y	1	Dis	RMT25	-56.719	-56.858
JR16003	171	1	ELN	J	41	Fresh	N	0	Dis	RMT25	-56.719	-56.858
JR16003	171	1	KRA	F	37	Frozen	N	0	CT	RMT25	-56.719	-56.858
JR16003	171	1	KRA	J	33	Frozen	R	1	CT	RMT25	-56.719	-56.858
JR16003	171	2	KRA	M	31	Frozen	Y	1	CT	RMT25	-56.731	-56.866
JR16003	130	1	KRA	J	39	Frozen	Inc	NA	CT	RMT25	-54.594	-45.118
JR16003	171	1	KRA	F	38	Frozen	Y	1	CT	RMT25	-56.719	-56.858
JR16003	171	1	KRA	F	47	Frozen	R	1	CT	RMT25	-56.719	-56.858
JR16003	171	1	KRA	M	49	Frozen	N	0	CT	RMT25	-56.719	-56.858
JR16003	171	1	KRA	F	43	Frozen	Y	1	CT	RMT25	-56.719	-56.858
JR16003	147	1	KRA	F	45	Frozen	Inc	NA	CT	RMT25	-53.951	-49.247
JR16003	171	1	KRA	M	50	Frozen	Inc	NA	X-ray	RMT25	-56.719	-56.858
JR16003	164	2	KRA	F	52	Frozen	D	NA	CT	RMT25	-53.301	-52.207
JR16003	171	1	KRA	F	53	Frozen	N	0	X-ray	RMT25	-56.719	-56.858
JR16003	163	2	KRA	F	54	Frozen	N	0	CT	RMT25	-53.267	-52.174
JR16003	163	2	KRA	F	57	Frozen	R	1	X-ray	RMT25	-53.267	-52.174
JR16003	171	1	KRA	M	55	Frozen	D	NA	X-ray	RMT25	-56.719	-56.858
JR16003	130	2	KRA	F	70	Frozen	R	1	X-ray	RMT25	-54.576	-45.107
JR16003	130	2	KRA	F	70	Frozen	R	1	CT	RMT25	-54.576	-45.107
JR16003	130	2	KRA	F	62	Frozen	Y	1	CT	RMT25	-54.576	-45.107
JR16003	130	2	KRA	M	71	Frozen	Inc	NA	X-ray	RMT25	-54.576	-45.107
JR16003	130	2	GYF	M	70	Frozen	N	0	CT	RMT25	-54.576	-45.107
JR16003	147	2	GYF	M	69	Frozen	N	0	CT	RMT25	-53.929	-49.262
JR16003	147	2	GYF	M	70	Frozen	N	0	CT	RMT25	-53.929	-49.262
JR16003	147	2	GYF		74	Frozen	N	0	CT	RMT25	-53.929	-49.262
JR16003	147	2	GYF		84	Frozen	N	0	CT	RMT25	-53.929	-49.262
JR200	115	1	GYF		79	Frozen	D	NA	CT	RMT25	-56.803	-42.247
JR200	141	1	GYF		80	Frozen	N	0	CT	RMT25	-55.256	-41.356
JR200	185	2	GYF		67	Frozen	D	NA	CT	RMT25	-52.826	-39.877

S.3 Gas presence absence description and summary

Table S.3.1 Decision tree for classifying presence / absence of gas in species, based on condition. All scans deemed damaged or inconclusive were excluded from further analysis. Images here are representative 2D slices of CT scans. All CT were checked for gas as 3D reconstructions. Other data used to ascertain presence/absence of gas were soft tissue x-ray and dissection.

Fish condition	Gas bearing bladder	Gas binary	Example image
Gas contained in un-ruptured bladder. All other tissue good.	Yes	1	 ELN_030
Gas in swimbladder region and /or abdomen due to apparent rupturing. Surrounding tissue good.	Yes (ruptured)	1	 KRA_315  PRM_009  KRA_719
No gas in swimbladder. No gas in abdomen. All surrounding tissue good.	No	0	 ELN_059
No gas visible in swimbladder region. Gas entrainment along skeletal tissues to upper body and extremities (muscle tissue striation).	No	0	 ELN_060

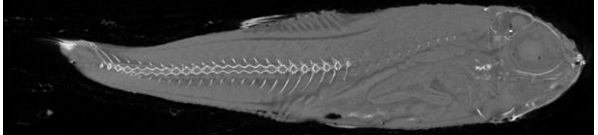
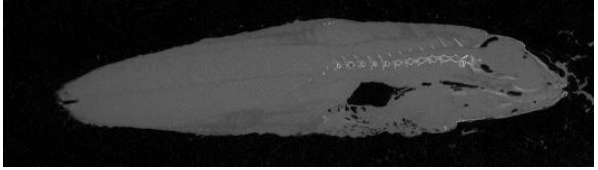
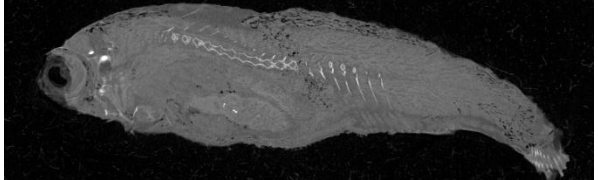
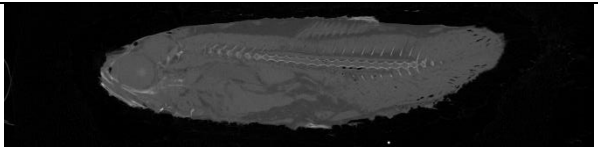











No gas visible in swimbladder region. Gas entrainment via orifices.	No	0	 ELN_063  GYF_Cam049
Gas entrainment throughout fish tissues OR damage to abdomen likely to have resulted in gas entrainment.	Damaged	NA	 KRA_Cam711
Scan inconclusive / lack of tissue or cavity definition	Inconclusive	NA	 KRA_569

Table S.3.2 Summary of swimbladder condition of myctophid species and data type. Species: ELN – *Electrona antarctica*, ELC – *Electrona carlsbergi*, GYR – *Gymnoscopelus braueri*, GYF – *Gymnoscopelus fraseri*, GYN – *Gymnoscopelus nicholsi*, KRA – *Krefftichthys anderssoni*, PRM – *Protomyctophum bolini*. Gas (+), Non-gas (-), Damaged sample excluded from analysis (D), inconclusive scan excluded from analysis (Inc.).

Species	CT				X-ray				Dissection				Total		
	+	-	D	Inc.	+	-	D	Inc.	+	-	D	Inc.	+	-	Excluded
ELN	7	16	1	3	2	25			4	2			13	43	4
ELC	7				14				7				28	0	0
GYR						20				1			0	21	0
GYF		6	2		5	1	2		1				0	12	5
GYN		1				13							0	14	0
KRA	15	3	1	4	2	1	1	2	16	2			33	6	8
PRM	11				5				16				32	0	0
Total	40	26	4	7	23	64	2	4	43	6	0	0	106	96	17

Chapter 2 Supplementary material

S.4 Species used in community assessment and gas bladder condition applied. The most abundant mesopelagic fish species were identified for latitudinal community analysis based on Scotia Sea RMT25 nets data from cruises JR161, JR177, JR200, JR15004 and JR16003. The percentage community contribution (%) is based on the percentage of individuals sampled from all available data, where n is the total number of individuals. Species included account for 94.6% (n = 10674) of individuals, the remaining 5.4% of individuals (n = 609) was comprised of 41 species of mesopelagic fish. Of the potential *Cyclothone* species in the Scotia Sea, the fat-invested *Cyclothone microdon* is most prevalent in the region (Ainley et al., 1986, Donnelly et al., 1990). Since *Cyclothone* species were not identified to species, I base my analyses on an assumption that the dominant species in catches is *C. microdon* and therefore *Cyclothone* individuals in the RMT25 catches are predominantly fat-invested.

Species	Family	Swimbladder	Source	n	%	
<i>Electrona antarctica</i>	Myctophidae	Gas to None	Current study	2728	24.18	
<i>Electrona carlsbergi</i>		Gas	Current study	704	6.24	
<i>Gymnoscopelus braueri</i>		Regressed	Current study	1890	16.75	
<i>Gymnoscopelus fraseri</i>		Regressed	Current study	187	1.66	
<i>Gymnoscopelus nicholsi</i>		Regressed	Current study	118	1.05	
<i>Protomyctophum bolini</i>		Gas	Current study	876	7.76	
<i>Protomyctophum tenisoni</i>		Gas	Marshall (1960)	324	2.87	
<i>Krefflichthys anderssoni</i>		Gas	Current study	1307	11.58	
Bathylagus spp.	Bathylagidae	No swimbladder	Marshall (1960)	1626	14.41	
Cyclothone spp.	Gonostomatidae	Fat invested	Marshall (1960)	711	6.30	
Notolepis spp.	Paralepididae	No swimbladder	Froese & Pauly. eds. (2018)	203	1.80	

S.5 RMT25 total biomass plots

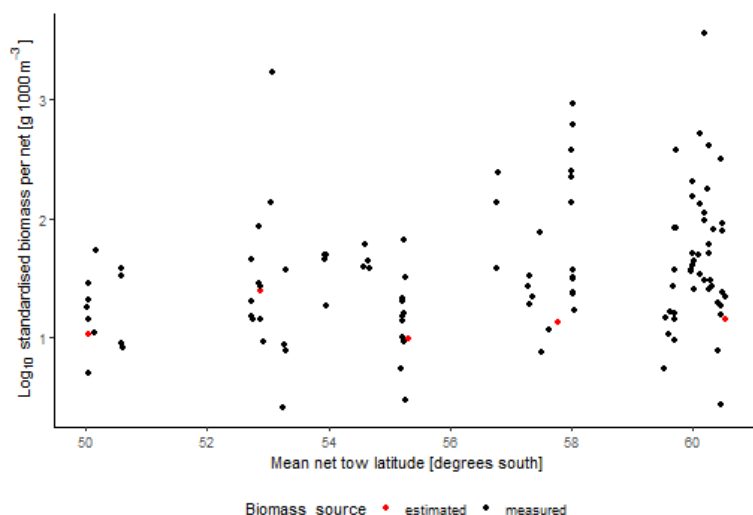


Figure S5.1 Log₁₀ total net biomass of all fauna (both fish and invertebrate) captured in the night RMT25 nets used in the current study, plotted against mean net tow latitude. All nets were standardised for tow speed and duration.

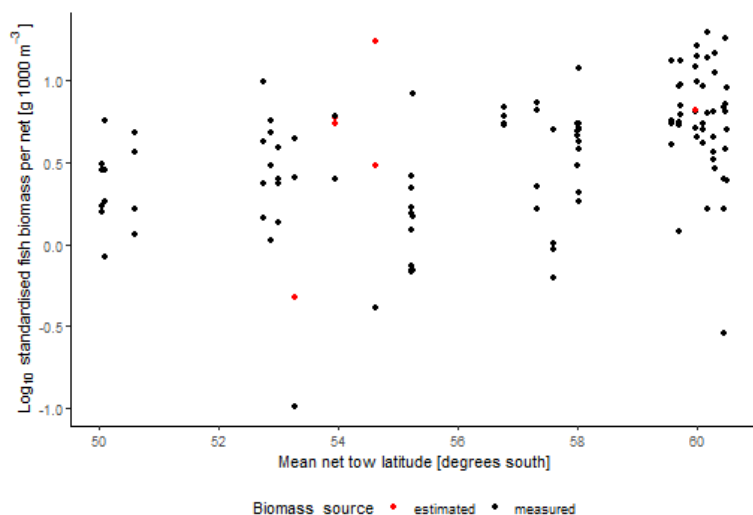


Figure S5.2 Log₁₀ total fish biomass captured in the night RMT25 nets used in the current study, plotted against mean net tow latitude. Fish species included in fish biomass assessment are those listed in supplementary Table S.4 only. All nets were standardised for tow speed and duration.

Where catch biomass weights were missing, a mean weight for an individual from each species was calculated from combined JR161, JR177 and JR200 RMT25 catch biomass data. Abundances were then multiplied by mean weight to estimate biomass. Net samples containing some estimated values are coloured red. Ships scale precision is to the nearest gram. Where species weights were recorded as < 1 g these were set to 0.5 g for the purposes of calculation.

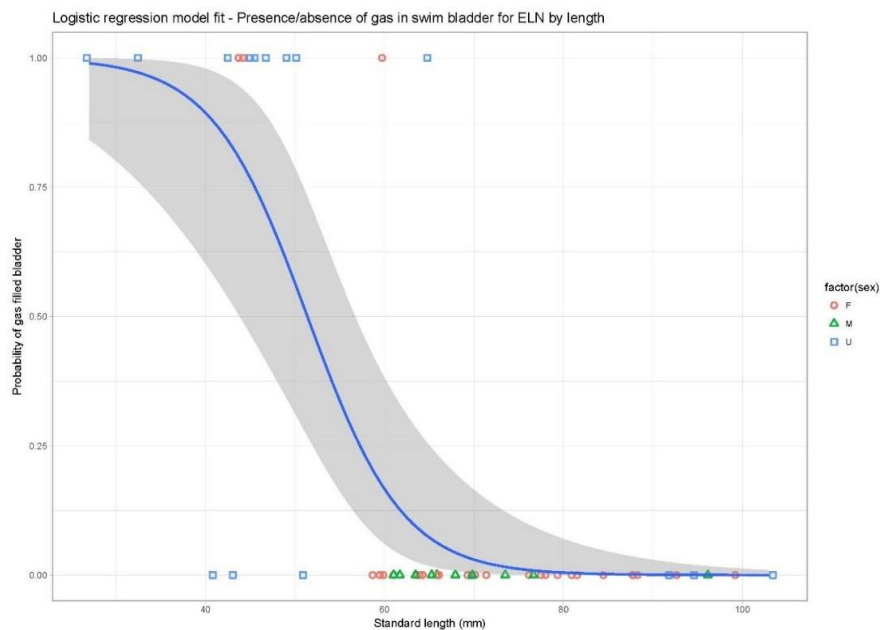
S.6 *Electrona antarctica* gas presence / absence logistic regression

Figure S.6.1 Logistic regression model fit predicting the probability of presence of gas in *Electrona antarctica* swim bladders, by standard length (mm). Shading indicates 95% confidence intervals. Jitter added to data points (width 0.5) for visualisation. Sex indicated by points, red circle: female, green triangle: male, blue square: unclassified.

Standard length was a highly significant predictor of the presence of gas, p -value <0.0001 , null deviance 60.687 on 55 df, residual deviance 27.866 on 54 df. Using values of intercept (a) and slope (b) defined by the model, the estimated standard length of *E. antarctica*, where probability (p) of presence of gas was 0.5 ($SL_{0.5}$) was calculated as follows:

$$SL_{0.5} = \frac{\log\left(\frac{p}{1-p}\right) - a}{b} = \frac{\log\left(\frac{0.5}{1-0.5}\right) - 9.614876}{-0.18714} = 51.378 \text{ mm}$$

Prediction of standard length with gas presence probability of 0.5 was 51.378 mm, which was subsequently used to assess the proportion of the *E. antarctica* community likely to be gas bearing.

Binomial glm coefficients based on logit link function

Model	term	estimate	std.error	statistic	p.value	link
1	(Intercept)	9.614876	2.813797	3.417047	0.000633	logit
1	standard_length_mm	-0.18714	0.051166	-3.65747	0.000255	logit

Binomial glm outputs based on logit link function

Model	null.deviance	df.null	logLik	AIC	BIC	deviance	df.residual	link
1	60.6875	55	-13.9332	31.86647	35.91717	27.86647	54	logit

Chapter 3

Vertical migration behaviour and environmental drivers of mesopelagic fish distribution

3.1 Abstract

Active acoustics are routinely used to monitor commercial fish stocks and gain insight into the behaviour of pelagic organisms, such as diel vertical migration (DVM). In the Southern Ocean mesopelagic fish occupy a key position in the Antarctic food web, and promote biogeochemical cycling through DVM. However, it remains unclear to what extent DVM behaviour is occurring across the region. Moreover, the environmental drivers of mesopelagic fish distribution at the ocean basin scale are also unclear. This study uses depth integrated (surface to 800 m, in 10 m depth increments) 38 kHz acoustic data as a proxy for mesopelagic fish abundance and aims to quantify latitudinal variation in DVM behaviour in the Scotia Sea region of the Southern Ocean. Additionally, generalised additive mixed modelling (GAMM) is used to assess the importance of key environmental drivers for explaining spatial patterns of acoustic backscatter (integrated surface to 1000 m). The results show that DVM between the mesopelagic and epipelagic zone is evident in the Scotia Sea in regions north of 57° S, the approximate location of the Antarctic Polar Front, but further south DVM is suppressed with no significant migration from the mesopelagic zone (>230 m to 800 m) into the epipelagic zone (≤230 m) at night. In addition, GAMM modelling revealed that sea surface temperature, hours of daylight, and sea ice concentration were significant drivers of acoustic backscatter, with acoustic backscatter positively correlated to SST and negatively correlated with daylight hours and sea ice concentration, with backscatter consequently declining towards the pole. These results are discussed from the perspective of the underlying environmental drivers of both vertical and latitudinal patterns of backscatter, and their implications for modelling ecological processes.

3.2 Introduction

Active acoustics enables us to “see” into the depths of the open ocean and acquire unique understanding of its ecology, at unrivalled spatial and temporal scales (Benoit-Bird and Lawson, 2016). By transmitting pulses of sound into the water column and then echo integrating the reflected (or backscattered) signal from ensonified organisms, we can build up a snapshot picture of the oceans biological community at an unparalleled resolution. From their routine use in fisheries stock assessments (Fernandes et al., 2002), to understanding spatio-temporal trends in pelagic community ecology (Urmy et al., 2012, Escobar-Flores et al., 2018b), active acoustics methods have become an invaluable component in the aquatic ecologist’s toolkit. Used in combination with underlying environmental data we can start to

elucidate the drivers of faunal distribution patterns and habitat occupation, thus mapping the biogeography of our oceans (Irigoiien et al., 2014, Proud et al., 2017). In the Southern Ocean, active acoustics are used to monitor stocks of Antarctic krill (*Euphausia superba*), a species that is both keystone in the operation of this ecosystem and commercially important (Fielding et al., 2014). As we shift our focus towards a more holistic approach to ecosystem management (Demer et al., 2009, Godø et al., 2014, European Commission, 2018), attention has turned increasingly to the use of active acoustics to study non-commercial species in the Southern Ocean, including mesopelagic fish (Fielding et al., 2012, Escobar-Flores et al., 2013, Saunders et al., 2013). However, little is known of the environmental drivers of mesopelagic fish distribution and behavioural patterns at the ocean basin scale, which has implications for ecosystem assessment and management.

Acoustic backscatter within the mesopelagic realm (200 – 1000 m) is commonly used as a proxy for mesopelagic fish biomass (Irigoiien et al., 2014), and while the previous chapter (Dornan et al., 2019) has shown that acoustic backscatter is also likely to reflect a change in the community, the relationships between patterns in acoustic backscatter and environmental variables can be used to explore the environmental drivers of mesopelagic fish distribution, and potentially predict future distributions (Guisan et al., 2002). The previous chapter's analysis of night-time surface to 1000 m net sample data highlighted a latitudinal change in the mesopelagic fish community in the Scotia Sea (Atlantic sector of the Southern Ocean), with a decrease in diversity (but not abundance) towards higher latitudes, which has yet to be explored in relation to environmental variables at the basin scale. Mesopelagic fish distribution has been linked to oceanographic and biogeochemical properties, including sea temperature, primary production, oxygen minimum zones and water mass boundaries e.g. fronts, eddies and upwelling regions (Cade and Benoit-Bird, 2015, Bianchi et al., 2013, Fielding et al., 2012, Opdal et al., 2008). In addition, some species are known to be polar specialists, with evidence suggesting that the sea-ice sector of the Southern Ocean is important for the larval stage of the myctophid *Electrona antarctica* (Moteki et al., 2017). Other biomass-dominant species are thought to exist only as sink populations in the region, highlighting the importance of behavioural migrations and oceanic processes in maintaining connections between temperate/sub-Antarctic and Antarctic waters (Saunders et al., 2017). Alongside oceanographic properties, patterns in distribution are also likely to be influenced by prey distribution and predation pressure, as mesopelagic fauna undertake strategies for feeding on the abundant food resources in the upper water column whilst evading sight-

driven predators. Therefore, species distribution, aggregation and patchiness are all likely to be affected by both small- and large-scale temporal and spatial processes (Atkinson et al., 2012a).

A distinctive behaviour that can commonly be tracked by active acoustics is that of diel vertical migration (DVM). DVM is a daily phenomenon of both fresh and marine water habitats, where fauna from tiny zooplankton to predatory fish, typically migrate up into nutrient rich surface waters to feed under the cover of darkness before retreating to the relative safety of deeper darker waters at dawn (Brierley, 2014). In terms of biomass, this is potentially the largest animal migration on earth (Hays, 2003). This vast migration plays a key role in the active transportation of carbon known as the biological carbon pump. In the Southern Ocean, respiratory carbon transport driven by the mesopelagic fish family Myctophidae is equivalent to up to 47% of the gravitational flux (passive sinking) of carbon in the Scotia Sea (Belcher et al., 2019). However, there is evidence that the signal of DVM weakens at high latitudes (Proud et al., 2018a), which has implications for survey design, interpretation of existing ecological data, and future biogeochemical modelling. Mesopelagic fish in the Scotia Sea have also been shown to exhibit seasonally different depth distributions, suggesting that DVM behaviour may also be temporally variable within species (Saunders et al., 2014a, Saunders et al., 2018). Given that mesopelagic fish, particularly Myctophidae, are food for many air-breathing higher predators in the Southern Ocean (Connan et al., 2007, Scheffer et al., 2012, Guinet et al., 2014), their DVM behavioural patterns are likely to have important implications for food web dynamics.

This study examines 38 kHz acoustic data collected across the Scotia Sea over a period of 6 years. There are two main aims: 1) to quantify patterns of DVM in acoustic backscatter, and 2) investigate the key environmental drivers that control spatial variations in acoustic backscatter. Firstly, I explore the possibility of broad-scale variations in DVM within the Scotia Sea by examining latitudinal changes in the relative difference between day and night backscatter in epipelagic and mesopelagic water masses. Secondly, the ability of key environmental drivers such as surface chlorophyll, temperature and sea ice cover to predict surface to 1000 m integrated acoustic backscatter is assessed using Generalised Additive Mixed Modelling (GAMM). The possible causal mechanisms and broader implications of spatial variations in mesopelagic fish DVM behaviour in the region are then discussed, together with the modelling and biological implications for predicting mesopelagic fish backscatter from environmental data at the ocean-basin scale.

3.3 Methods

3.3.1 Acoustic data collection

Acoustic data were collected using an EK60 echosounder operating at 38 kHz during six research cruises (13 transits) on-board RRS James Clark Ross in the Scotia Sea between the Falkland Islands, the South Orkney Islands and South Georgia. The cruises were undertaken between austral spring and autumn of 2006-2017 (see Table 3.1 and Figure 3.1). The echosounder was calibrated at least once per field season using standard calibration spheres and methods (Foote et al., 1987, Demer et al., 2015).

Table 3.1 Spatio-temporal summary of acoustic transect data used in DVM and GAMM analysis. All data sets were used in GAMM, data sets used in DVM analysis are shaded. Transect date format year-month-day, and time is hours:minutes:seconds in GMT. Latitude (lat) and longitude (lon) both in decimal degrees South.

Cruise leg ID	Start date	Start time (GMT)	End date	End time (GMT)	Start lat ° S	Start lon ° S	End lat ° S	End lon ° S
JR15002_001	2015-11-13	13:38:50	2015-11-15	12:33:18	53.55	55.33	60.30	46.82
JR15002_007	2015-12-11	00:04:19	2015-12-14	00:09:42	52.63	39.12	51.74	56.11
JR15004_001	2016-01-22	00:17:06	2016-01-24	11:05:19	52.45	56.65	60.42	45.17
JR15004_002	2016-02-18	03:53:12	2016-02-20	22:20:25	60.31	46.78	52.81	57.09
JR16003_PF	2017-01-01	09:22:50	2017-01-08	23:59:58	55.30	41.36	60.36	60.67
JR161_001	2006-10-25	01:52:41	2006-10-27	00:19:08	52.58	56.86	57.62	50.49
JR161_002	2006-10-31	04:30:56	2006-10-31	18:56:32	58.02	50.25	60.47	49.10
JR161_009	2006-11-30	16:44:51	2006-12-03	03:46:37	49.99	38.53	51.37	55.77
JR177_001	2008-01-01	07:22:46	2008-01-03	17:38:28	53.53	55.55	60.29	47.65
JR177_011	2008-02-14	07:26:11	2008-02-17	00:50:06	53.67	38.52	51.82	56.16
JR200_001	2009-03-12	02:22:40	2009-03-13	10:17:04	52.49	56.72	57.64	50.50
JR200_002	2009-03-13	22:20:14	2009-03-14	18:01:57	57.72	50.36	60.37	48.29
JR200_012	2009-04-15	23:49:39	2009-04-18	10:37:05	53.69	38.81	51.83	56.12

Temperature and salinity from the water column were measured using a Sea-Bird SBE911Plus Conductivity Temperature Depth (CTD) unit during each cruise. Mean temperature and salinity values were used to calculate the sound speed constant (c) and absorption coefficient (α), using 20-1000 m depth samples obtained from the nearest consistently sampled CTD stations. R (version 3.5.1) package ‘sonar’ (Gama, 2016, R Core

Team, 2018) was used to calculate values for c and α for each measurement based on algorithms by Mackenzie (1981) and Francois and Garrison (1982) respectively, using an average pH of 8.0 (Simmonds and MacLennan, 2005). See Supplement S.1 for CTD files used.

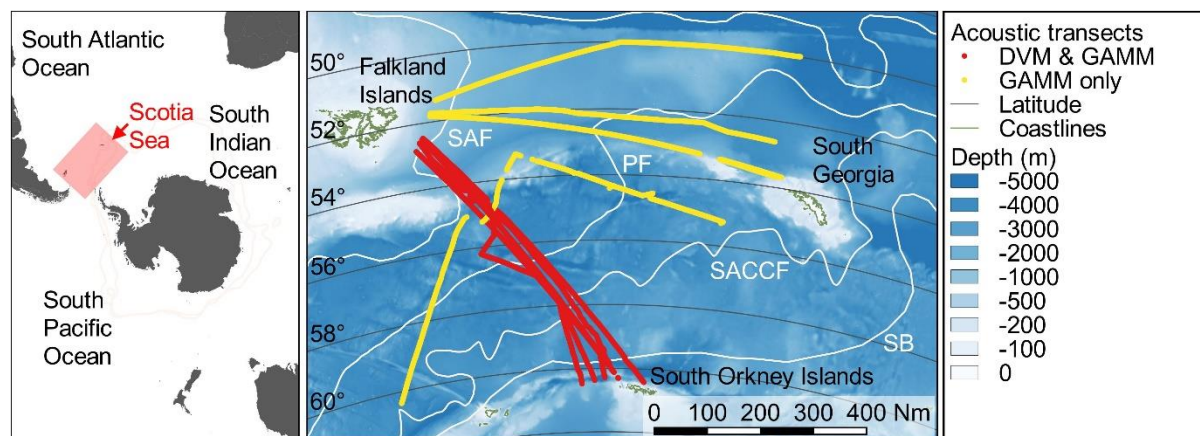


Figure 3.1 Acoustic transects used as part of the current study. All transects (red and yellow lines) were used in GAMM assessment of environmental drivers of acoustic backscatter. Latitudinal patterns in DVM only used transits between Falkland and South Orkney Islands (red lines). Mean frontal positions are represented in white, SAF (Sub Antarctic Front), PF (Polar Front), SACCF (Southern Antarctic Circumpolar Current Front) and SB (Southern ACC Boundary). Also shown are 2° latitudinal graticules. Map generated in Quantum GIS ver 2.18 (www.qgis.org), projection EPSG:3031.

3.3.2 Acoustic data processing

Calibrated acoustic data was processed in Echoview® (Version 8.0.95, Echoview Software Pty Ltd, Hobart, Australia). Bad and unwanted data regions were identified and removed (set to 'No data'), including below seabed (with a back step of 10 m), surface water (0-17 m to eliminate nearfield and account for transducer depth and bubbles), and data deeper than 1000 m. False bottom echoes were masked manually and set to 'No data'. Background noise (BN) was removed following a modified De Robertis and Higginbottom (2007) method, which estimates BN from the data, by assuming that a portion of the acoustic backscatter will be dominated by noise when there is little in the water column to reflect the acoustic sound wave. The BN filter was modified to calculate noise on the 90th percentile (minus time varied gain) of the averaged data similar to that implemented by Korneliussen (2000), rather than the mean. This modification was undertaken because background noise remained amplified at depth after applying the method of De Robertis and Higginbottom (2007), when using the mean of the cell (Figure 3.2a-c). Notably the original BN algorithm was developed using data

collected in water depths of less than 200 m and therefore would not have been an issue in that study.

Data were cleaned of Impulse Noise (IN) by averaging vertically in 10 m depth bins and rejecting any data more than 10 dB higher than both the preceding and following pings (Anderson et al., 2005, Ryan et al., 2015). Attenuated signal (AS), the signal blocked from returning to transducer as a result of bubble sweep down on the hull, was removed following Ryan et al. (Ryan et al., 2015). Signal was marked as attenuated if the data in a single ping within a manually defined scattering layer was 6 dB less than the mean of the surrounding 300 pings based on sensitivity analysis. Once data was cleaned of IN and AS, a signal to noise ratio (SNR) was calculated following De Robertis and Higginbottom (2007), all data below SNR threshold of 6 dB was set to -999 dB. The effect of data cleaning is shown in Figure 3.2d.

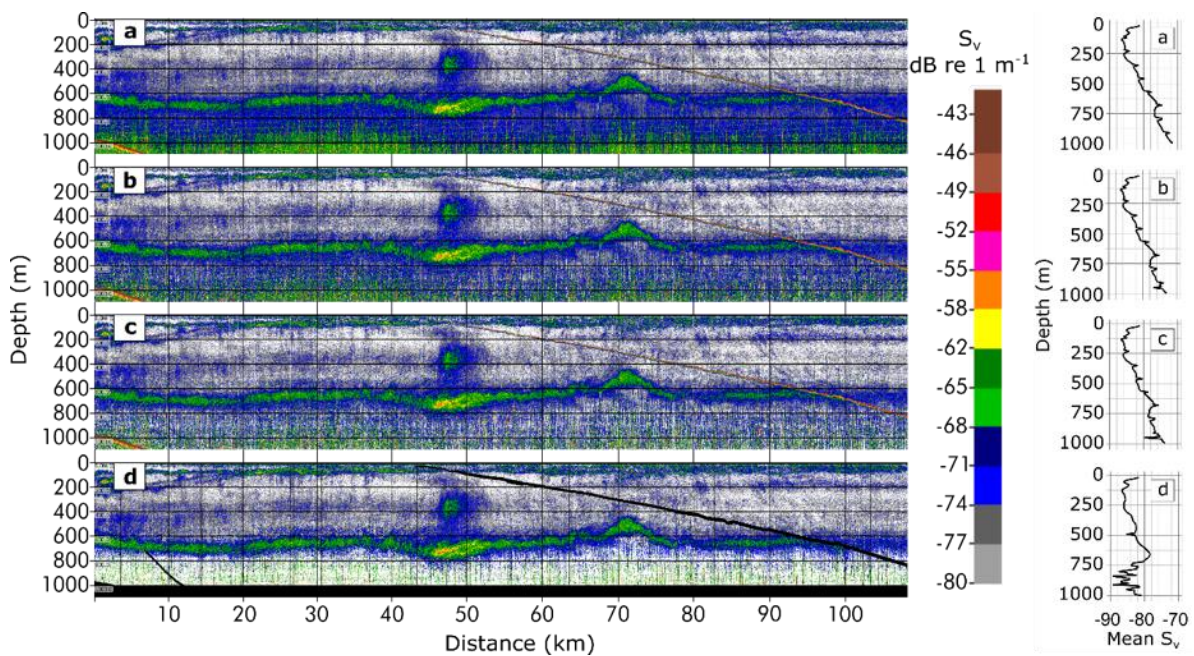


Figure 3.2 (a) Example echogram of raw calibrated data. (b) Background Noise Removal following De Robertis & Higginbottom (2007), using mean noise (calculated as mean S_v in 20 ping wide by 10 m depth cell minus Time Varied Gain) leaves considerable amount of noise visible at depth. (c) Calculating noise in cell based on 90th percentile (Korneliussen, 2000) results in cleaner data whilst retaining signal. (d) Echogram post-cleaning, black regions are excluded data (e.g. surface near-field, depths >1000 m and false bottom echoes). Colour scale is in dB, visible threshold set to -80 dB. Panel on the right shows effect of data cleaning steps on mean S_v .

A maximum S_v threshold of -35 dB was applied to minimise the impact of traces of noise remaining after data cleaning, as these were found to introduce a disproportionately high bias on integrated Nautical Area Scattering Coefficient (NASC or S_A , $m^2 nmi^{-2}$), all data values

exceeding the -35 dB threshold were set to No Data. The maximum threshold of -35 dB was a compromise between dampening noise and retaining signal based on a sensitivity analysis (Supplement S.2). The processing data flow is shown in Supplement S.3. The calibrated and cleaned 38 kHz data was integrated and exported from Echoview®, in 1 km distance by 10 m depth bins. Further analysis was completed in R 3.5.1 (R Core Team, 2018) and high values of NASC visually inspected for potential noise bias, see Chapter 2 (Dornan et al., 2019) for further details.

3.3.3 Diel Vertical Migration

To explore the effect of latitude on DVM, six transects from five cruises, which ran broadly north-south, were analysed (Figure 3.1). First, each 1 km distance sampling unit was assigned a 'day', 'night', 'dawn' or 'dusk' category using a modified version of sun-methods functions in R package 'maptools' (Bivand and Lewin-Koh, 2018). Dusk and dawn were assigned when sun was up to 6° below horizon (civil twilight). As all ship data were collected in GMT, which resulted in some sunset and dusk times occurring after midnight the following day, only 24 hour day fractions of were used to assign categories. This is likely to have minimal impact, as the greatest time difference between sunset on consecutive days for a high latitude of 65° S during spring equinox is <4 minutes. Crepuscular periods (dawn and dusk) were excluded from analysis to remove 'noise' introduced as an effect of active diurnal migration. As a portion of data in JR161 was only collected to 800 m, all data collected below 800 m from all surveys was also excluded from DVM analysis.

To explore evidence for DVM behaviour, where animals migrate into shallower water under the cover of darkness, acoustic data were separated into different water depth zones. Depth zones were assigned as Epipelagic (depth \leq 230 m), Mesopelagic (depth $>$ 230 m), Upper-mesopelagic (depth $>$ 230 m \leq 580 m) and Deep-mesopelagic (depth $>$ 580 m), see Figure 3.3. These were objectively defined based on the inflection-points in median standardised NASC values plotted against depth using daytime data (see Supplement S.4). A vertical distribution index was calculated as the ratio of backscatter between the upper and lower depth zones in each 1 km distance sampling unit, \log_e transformed to downweight extreme values.

$$\text{Vertical distribution index} = \frac{\log_e((\sum \text{NASC}_{\text{upper}})+1)}{\log_e((\sum \text{NASC}_{\text{lower}})+1)} \quad 3.1$$

Three DVM scenarios were explored, migration between (1) Epipelagic and Mesopelagic, (2) Epipelagic and Upper-mesopelagic, and (3) Upper-mesopelagic and Deep-mesopelagic (Figure 3.3). If DVM behaviour from deep to shallow was occurring, we would expect to see a lower vertical distribution index value during the day than in the night, and this would manifest in a statistical model as a significant effect of the binomial variable “day-night”. If DVM behaviour was strongly suppressed at higher latitudes towards the pole, we may expect to find a significant interaction between the binomial variable “day-night” and latitude, with a reduction in the difference between day and night indices would be expected.

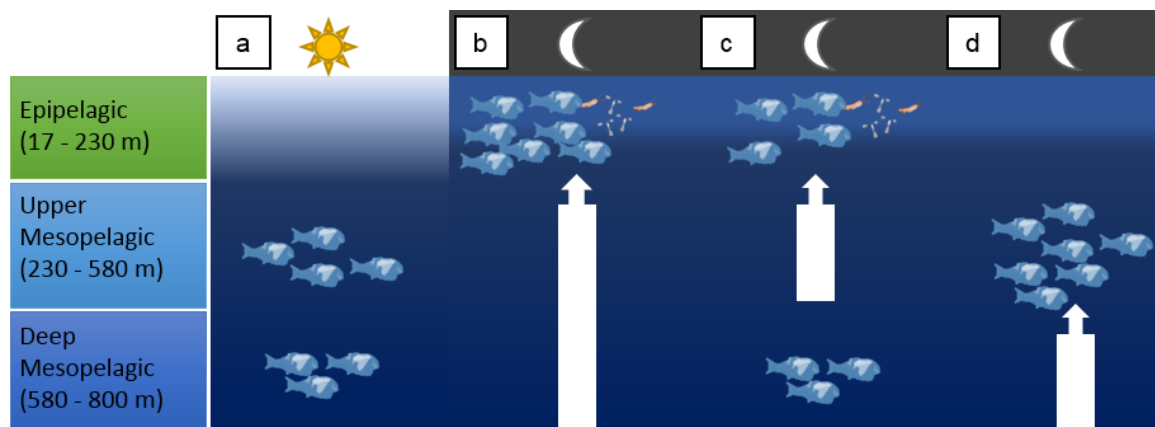


Figure 3.3 Schematic of diel vertical migration behaviour under consideration, (a) daytime occupation by mesopelagic fish of upper and deep mesopelagic water, (b) synchronous migration during night from mesopelagic to epipelagic, (c) migration during night from only the upper-mesopelagic into epipelagic, d) migration during the night from the deep mesopelagic to upper mesopelagic.

To explore the relationship between changing latitude and DVM behaviour, post-hoc comparisons were carried out on the GLMM using R package ‘emmeans’ (Lenth, 2019), where contrasts and significant difference between day and night were calculated from estimated marginal means of the vertical distribution index within each 1° latitudinal band. See Supplement S.5 for model specification.

To test these three scenarios, a generalised linear mixed effects model (GLMM) was implemented in R package ‘lme4’ (Bates et al., 2015). The fixed factors were “day-night” and 1° latitudinal band. Additionally, two random factors were specified in the model, (i) the cruise transect, and (ii) latitude sub-bands of 0.05°. The latter effectively served to aggregate acoustic

data points that were sampled each kilometre into a single data point for each 0.05° unit within a cruise transect, limiting the effects of pseudoreplication. Analysis of variance was used to test for significant differences in the mean vertical distribution index between day and night for all data, and between day and night within each 1° latitudinal band for all three DVM scenarios.

3.3.3.1 Day night total water column backscatter

In addition to looking for diel changes within the epi- and mesopelagic depth zones, differences in total water column backscatter were assessed to check for potential bias caused by fauna consistently migrating into or out of the surface-800 m depth range by day-night. The total water column NASC values were obtained by summing each of the 10 m depth cell NASC values for each 1 km distance-sampling unit, and \log_e transformed to downweight extreme values. Contrasts between day-night estimated marginal means of total water column NASC in 1° latitude bands, were used to check for consistent day-night trend for higher or lower backscatter, as this would need to be accounted for in analysis of environmental drivers.

3.3.4 Environmental drivers of backscatter

Environmental drivers of acoustic backscatter initially considered were sea surface temperature (SST), sea temperature at 200 m (ST_{200}), geopotential height as a proxy for the location of fronts and water masses, geostrophic current speed, maximum sea ice cover (percentage) preceding the acoustic sample date, water depth (bathymetry), daylight hours (the hours between sunrise and sunset), and distance to coast as a proxy for predation pressure from land or coastal-based predators. Monthly means of surface chlorophyll (a proxy for net primary productivity) were assessed with a) no time lag, b) lagged by one month from acoustic sample month and c) lagged by one month where acoustic sample date was before the 15th day of the month. All other environmental data was extracted corresponding to the same date that the acoustic sample was collected or the nearest prior date (for weekly or monthly climatologies), by latitude and longitude (see Table 3.2). Binomial factors included 'day' or 'night', and 'sea ice zone', which was classified as 'sea ice' when the maximum percentage sea ice concentration $\geq 15\%$.

All environmental raster data was in the WGS84 projection with the exception of sea ice data, which was re-projected from Antarctic Polar Stereographic to WGS84 using the R 'raster' package (Hijmans, 2018). Based on exploratory density plots, surface chlorophyll and

Chapter 3

response variable NASC were both \log_e transformed, and geostrophic current was square root transformed prior to GAMM fitting, to downweight extreme values. Datasets and their origin are summarised in Table 3.2.

Table 3.2 Environmental variables considered for inclusion in assessment of environmental drivers of acoustic backscatter.

Variable	Abbreviation	Units	Resolution	Product
Sea surface temperature	SST	°C	0.01° grid Daily	GHRSSST Level 4 MUR Global Foundation Sea Surface Temperature Analysis (v4.1) (JPL MUR MEaSURES Project, 2015)
Sea temperature at 200m	ST ₂₀₀	°C		
Geopotential height (proxy for frontal positions)	GeoHeight	m	0.25° grid Weekly	Copernicus Marine and Environment Monitoring Service (CMEMS) Products MULTIOBS_GLO_PHY_REP_015_002 (Guinehut et al., 2004, Guinehut et al., 2012, Mulet et al., 2012)
Geostrophic current speed	CurrSpeed	m s ⁻¹		
Surface chlorophyll (proxy for primary productivity)	Chl	mg m ⁻³	1/24° grid (~4 km) Monthly mean	Copernicus Marine and Environment Monitoring Service (CMEMS) Products OCEANCOLOUR_GLO_CHL_L4_REP_OBSERVATIONS_009_082 (Gohin et al., 2002, Hu et al., 2012)
Water depth (bathymetry)	Depth	m	30 arc-second grid intervals	GEBCO_2014 grid (GEBCO, 2014)
Distance to coast (proxy for land and coastal predation pressure)	DistToCoast	km	-	Natural Earth Data - ne_10m_coastline (Version 4.1) Distance calculated using R package 'rgeos' gDistance (Bivand and Rundel, 2018)
Maximum sea ice percentage cover	SIP	%	25 km grid Daily	National Snow and Ice Data Centre - Sea Ice Index, Version 3 (Fetterer et al., 2017)
Sea ice zone (ice conc. ≥15%)	SIZ	Presence /Absence		
Daylight hours	DHr	Hours	-	Calculated using R package 'maptools' (Bivand and Lewin-Koh, 2018)
Day or Night	DN	Day /Night	-	Calculated using R package 'maptools' (Bivand and Lewin-Koh, 2018)

3.3.5 Modelling environmental drivers of water column backscatter

Prior to fitting a Generalised Additive Mixed Model (GAMM), environmental predictor variables were assessed for collinearity using pairwise plots, Pearson correlation coefficients and Variance Inflation Factors (VIF). Where collinearity was identified variables were eliminated to reduce the possibility of Type II errors (Zuur et al., 2009). As geopotential height, ST_{200} and SST were all highly correlated to each other, only SST was retained for modelling, as it was the most highly correlated with NASC (see Supplement S.6). As all three chlorophyll lag options assessed using pairwise and correlation coefficients were correlated with each other, only surface chlorophyll lagged by one month where acoustic sample date was < 15th day of the month was retained, as this had the highest correlation coefficient with NASC. Of 12,318 total water column 1 km distance NASC values, 85 were excluded from analysis, as no surface chlorophyll data was available for those locations. Variance inflation factors (VIF) were used to identify variables of with a $VIF > 3$ (Zuur et al., 2009) resulting in the removal of binomial variable sea ice zone. The final model selection included smoothing terms for SST (sea surface temperature °C), Depth (water depth m), DistToCoast (distance to coast km), Chl (\log_e surface chlorophyll concentration mg m^3), CurrSpeed (square root of geostrophic current speed ms^{-1}), DHr (Daylight hours), SIP (maximum percentage sea ice cover %); and binomial term DN (Day or Night). See Figure 3.4 for representative climatologies of final model variables. Using R package ‘mgcv’ (Wood, 2019) scaled t family GAMMs were fitted using a Restricted Maximum Likelihood (REML), and penalised thin plate regression splines used on all smooth terms with a conservative value of $k = 3$ to constrain overfitting.

The full model specification was:

$$\log_e \text{NASC} \sim s(\text{Chl}, k = 3) + s(\text{CurrSpeed}, k = 3) + s(\text{SST}, k = 3) + s(\text{Depth}, k = 3) \\ + s(\text{DistToCoast_km}, k = 3) + s(\text{DHr}, k = 3) + s(\text{SIP}, k = 3) + \text{DN}$$

Regularly spaced acoustic data is likely to exhibit a degree of spatial autocorrelation, resulting in a violation of the assumption of independence between samples (Legendre, 1993, Zuur et al., 2009). To test for spatial autocorrelation Moran’s I was calculated on model residuals using R package ‘ape’ (Paradis and Schliep, 2018), and an autoregressive correlation structure of order 1 (corAR1) was subsequently specified in GAMMs (Pinheiro and Bates, 2000). Once the model was built variables were dropped sequentially from the full model to evaluate their relative importance for explaining deviance in acoustic backscatter. Adjusted R^2 values and F-statistics were used to identify the most parsimonious model.

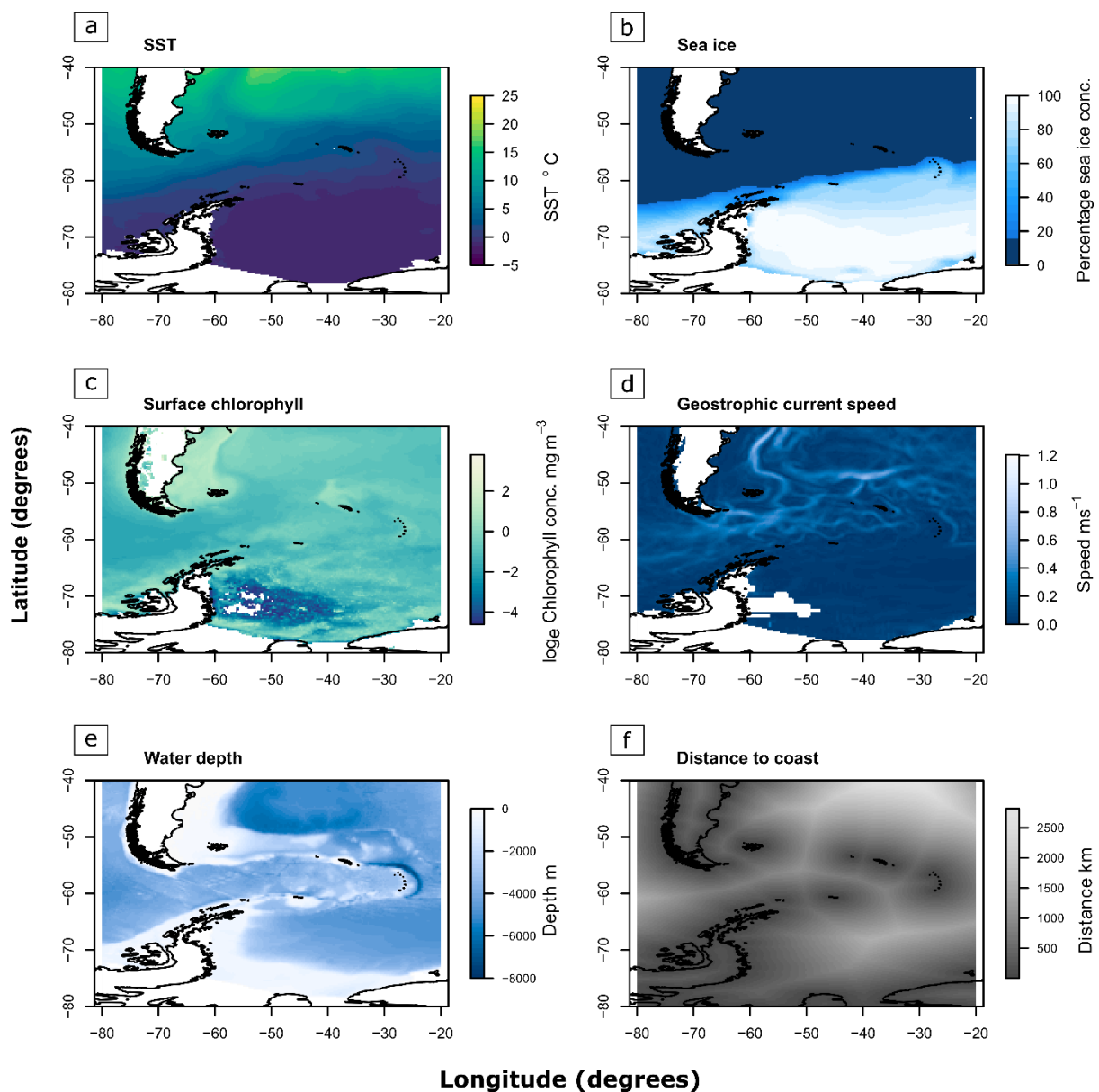


Figure 3.4 Representative climatologies of environmental variables used in generalised additive mixed model (GAMM). Actual data used in GAMM were from finer temporal resolution (see Table 3.2 for GAMM data sources). (a) SST climatology for months Oct-Apr 2005-2017, (b) mean sea ice concentration climatology for month of September (2005-2017), (c) \log_e surface chlorophyll concentration (mg m^{-3}) Oct-Apr 2005-2017, (d) mean geostrophic current speed (m s^{-1}), (e) water depth (m) and (f) distance to coast (km) a proxy for predation pressure. See Supplement S.7 for details of the climatology source data.

3.4 Results

3.4.1 Diel Vertical Migration

Echograms of 1 km by 10 m depth, Mean Volume Backscattering Strength (S_v dB re 1 m^{-1}) were plotted to enable visualisation of DVM pattern change with latitude (Figure 3.5). These indicate a clear pattern of DVM at lower latitudes in all cruises, which becomes weaker, as signal decreases, further south.

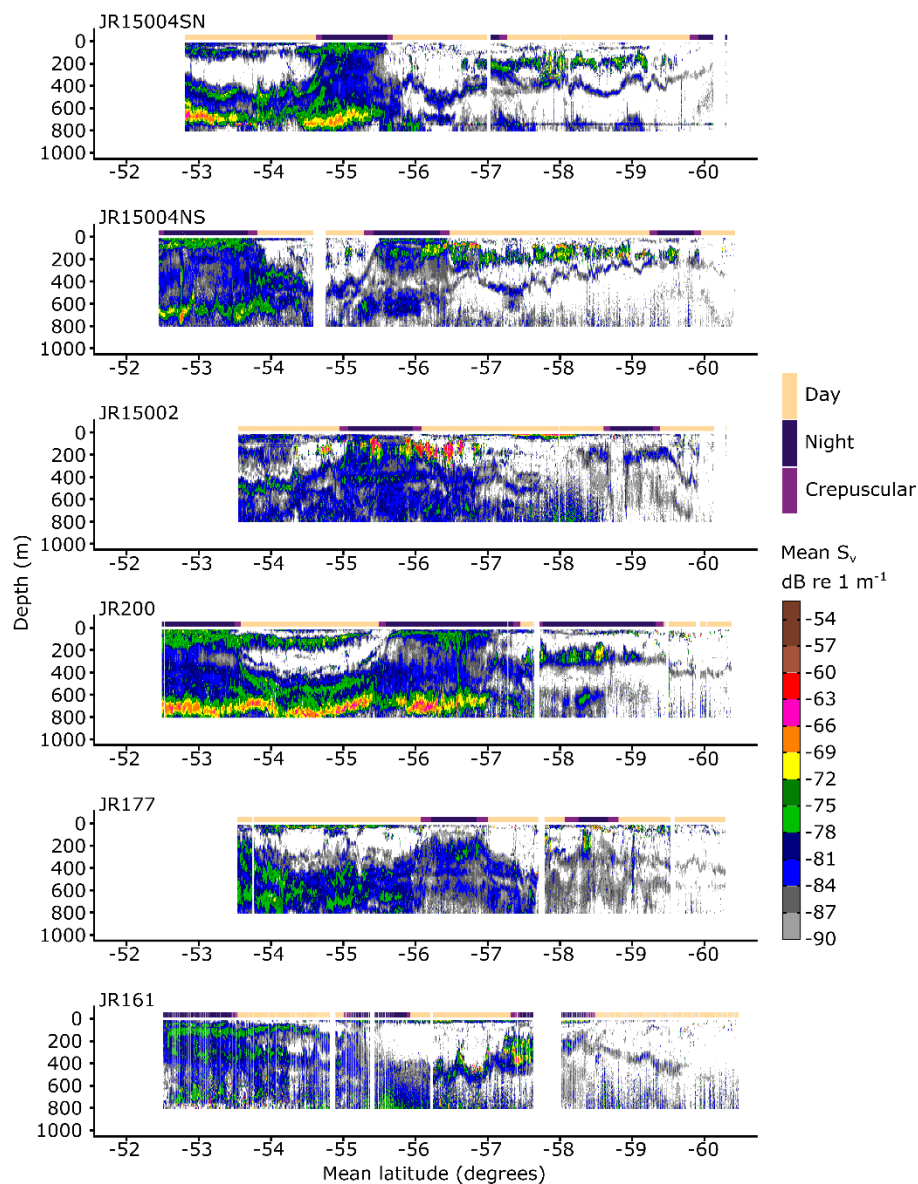


Figure 3.5 Echograms of mean volume backscattering strength ($\text{Mean } S_v \text{ dB re } 1 \text{ m}^{-1}$) of 1 km distance by 10 m depth integrated 38 kHz acoustic data for cruises used in latitudinal DVM assessment. Missing data and data less than -90 dB in white. Day, night and crepuscular periods indicated in top strip. Data processed in Echoview® 8.0.95, plots made in R 3.5.1, package cowplot (Wilke, 2018), ggplot2 (Wickham, 2016), and data.table (Dowle and Srinivasan, 2018).

Analysis of variance of fitted GLMMs revealed statistically significant differences between day and night vertical distribution index across the full latitude range (52°–61° S), and a statistically significant interaction between day-night and latitude, along the 1° latitudinal gradient, for all three DVM scenarios (Table 3.3). This suggests that there are day-night differences in water column occupation conducive with DVM, but that this varies with latitude.

Table 3.3 Summary of analysis of variance for GLMMs used to investigate effect of day-night and latitude on vertical distribution index.

DVM scenario	Predictor variable / Interaction	F value	P value
1. Epipelagic and full mesopelagic	DN	6.8141	<0.01
	DN : 1° Latitude	15.4325	< 0.001
2. Epipelagic and upper mesopelagic	DN	4.1562	<0.05
	DN : 1° Latitude	18.4618	< 0.001
3. Upper mesopelagic and deep mesopelagic	DN	5.2355	<0.05
	DN : 1° Latitude	34.3182	< 0.001

Post-hoc comparisons of day-night difference with latitude revealed distinct Northern and Southern DVM regimes in the Scotia Sea (see Table 3.4 for summary statistics).

The Northern regime (52°–57° S), consistently had a statistically significant higher vertical distribution index at night (negative day-night contrast), conducive with typical DVM behaviour where fauna migrate into the epipelagic zone from the mesopelagic zone. This migration from mesopelagic to epipelagic at night was consistent when comparing migration from the full mesopelagic zone to epipelagic (scenario 1, Figure 3.6a) and the upper mesopelagic to epipelagic (scenario 2, Figure 3.6). Within the northern regime, there also appeared to be a non-migrating portion of the mesopelagic community occupying the deep-mesopelagic zone (>580 m), as evidenced by a lower night-time vertical distribution index (positive day-night contrast) within the upper-mesopelagic and deep-mesopelagic zones (scenario 3, Figure 3.6c) at latitudes 54° - 55° S and 56° - 57° S.

The Southern regime (57°–60° S) showed no evidence of fauna migrating from the mesopelagic to epipelagic at night, but there was evidence of suppressed DVM occurring between the deep- and upper-mesopelagic zones. Non-migration into the epipelagic is clearest in scenario 1 (epipelagic and full mesopelagic), where there was generally no significant

difference between day and night vertical distribution index (Table 3.4). However, within the upper-mesopelagic and deep-mesopelagic zones (scenario 3), there is a consistently significant higher vertical distribution index at night, conducive with DVM behaviour within the mesopelagic zone. This night-time shift from deep to upper-mesopelagic zone in the south, likely drives the relative decrease in scenario 2's night-time vertical distribution index (which at first glance may seem indicative of reverse DVM, a phenomenon where fauna migrate into deeper water at night).

Latitude band 60°-61° S, showed no statistical difference between day and night vertical distribution index in any scenario, though this region had limited night-time data for comparison (see Figure 3.5).

Table 3.4 Summary statistics of day-night mean vertical distribution index, and contrasts within 1° latitude bands, for three DVM scenarios. D - day, N – night, EMM VDI – estimated marginal mean vertical distribution index, SE – standard error, df – degrees of freedom, CL – comparison level, CI – confidence interval. Significance codes: '****' <0.001, '***' <0.01, '**' <0.05, 'NS'≥0.1. Negative contrast (green) consistent with typical DVM, positive (red) inconsistent with typical DVM.

DVM	Latitude	(52,53]		(53,54]		(54,55]		(55,56]		(56,57]		(57,58]		(58,59]		(59,60]		(60,61]	
		D	N	D	N	D	N	D	N	D	N	D	N	D	N	D	N	D	N
1. Epipelagic and full mesopelagic	EMM VDI	0.675	0.841	0.717	0.811	0.704	0.815	0.575	0.794	0.780	0.833	0.812	0.829	1.007	0.958	0.866	0.818	0.613	0.648
	SE	0.085	0.063	0.059	0.061	0.057	0.074	0.059	0.058	0.058	0.059	0.058	0.063	0.058	0.059	0.058	0.061	0.063	0.090
	df	30.868	9.447	7.363	8.241	6.638	18.038	7.419	6.997	6.839	7.575	6.785	9.589	6.960	7.570	6.849	8.515	9.730	39.853
	Lower CL	0.612	0.779	0.686	0.780	0.656	0.767	0.554	0.771	0.758	0.810	0.782	0.799	0.985	0.935	0.840	0.792	0.554	0.580
	Upper CL	0.737	0.904	0.747	0.841	0.752	0.863	0.598	0.816	0.803	0.855	0.842	0.859	1.029	0.981	0.892	0.844	0.681	0.716
	Contrast	-0.166 **	-0.094 **	-0.111 *	-0.218 ***	-0.052 *	-0.017 NS	0.049 *	0.048 NS	-0.035 NS									
	SE	0.064	0.031	0.049	0.023	0.023	0.031	0.023	0.027	0.069									
	Lower CI	-0.291	-0.155	-0.207	-0.263	-0.097	-0.077	0.004	-0.005	-0.171									
	Upper CI	-0.041	-0.033	-0.015	-0.173	-0.007	0.042	0.095	0.100	0.101									
	2. Epipelagic and upper mesopelagic	EMM VDI	0.904	1.062	0.872	1.001	0.851	1.054	0.707	0.940	0.893	1.028	0.973	0.873	1.235	1.048	1.040	0.946	0.840
SE		0.100	0.072	0.068	0.070	0.066	0.086	0.068	0.067	0.066	0.068	0.066	0.073	0.066	0.068	0.066	0.070	0.073	0.107
df		36.452	10.153	7.717	8.754	6.869	20.634	7.786	7.290	7.105	7.971	7.041	10.365	7.247	7.965	7.117	9.085	10.479	47.701
Lower CL		0.829	0.986	0.835	0.964	0.792	0.996	0.681	0.912	0.865	1.001	0.937	0.837	1.207	1.021	1.008	0.914	0.757	0.681
Upper CL		0.980	1.138	0.909	1.038	0.909	1.112	0.735	0.967	0.920	1.055	1.010	0.910	1.261	1.076	1.072	0.978	0.922	0.868
Contrast		-0.158 *	-0.129 ***	-0.203 ***	-0.232 ***	-0.135 ***	0.100 **	0.187 ***	0.094 **	0.054 NS									
SE		0.077	0.038	0.060	0.028	0.028	0.037	0.028	0.032	0.084									
Lower CI		-0.309	-0.203	-0.320	-0.287	-0.190	0.027	0.131	0.030	-0.111									
Upper CI		-0.006	-0.055	-0.086	-0.178	-0.081	0.172	0.242	0.158	0.219									
3. Upper mesopelagic and deep mesopelagic		EMM VDI	0.742	0.903	0.945	0.916	1.010	0.772	0.932	0.977	1.185	1.061	1.229	1.491	1.120	1.408	1.243	1.359	1.047
	SE	0.079	0.048	0.042	0.045	0.039	0.065	0.042	0.041	0.040	0.043	0.040	0.049	0.041	0.043	0.040	0.046	0.048	0.086
	df	156.671	22.173	13.394	17.366	10.419	74.217	13.741	11.915	11.249	14.440	11.028	24.201	11.762	14.428	11.298	18.850	23.236	220.541
	Lower CL	0.704	0.834	0.912	0.883	0.957	0.704	0.907	0.952	1.160	1.036	1.196	1.458	1.095	1.383	1.214	1.330	0.972	1.102
	Upper CL	0.811	0.972	0.979	0.949	1.063	0.825	0.957	1.002	1.210	1.086	1.262	1.529	1.145	1.433	1.272	1.388	1.122	1.252
	Contrast	-0.161 *	0.030 NS	0.238 ***	-0.045 NS	0.124 ***	-0.262 ***	-0.288 ***	-0.116 ***	-0.130 NS									
	SE	0.070	0.034	0.054	0.025	0.025	0.034	0.026	0.030	0.077									
	Lower CI	-0.299	-0.037	0.132	-0.095	0.075	-0.329	-0.338	-0.174	-0.281									
	Upper CI	-0.023	0.096	0.345	0.005	0.174	-0.196	-0.237	-0.058	0.020									

Chapter 3

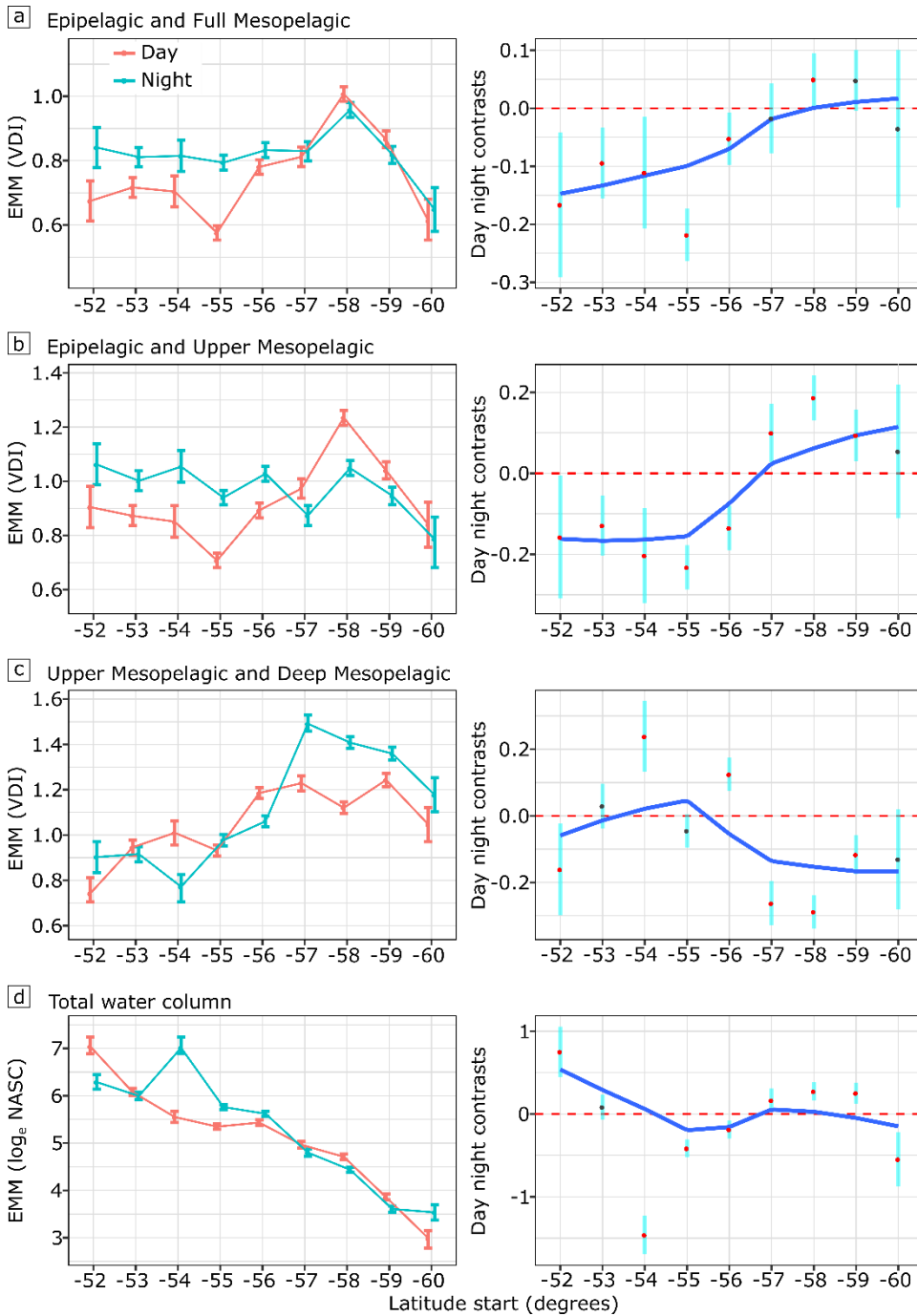


Figure 3.6 Left panel (a-c): Day-night difference of Estimated Marginal Means (EMM) of vertical distribution index (VDI) in 1° latitude bands. A higher index at night is conducive with a shallowing of backscatter, typical of DVM. Bars indicate comparison levels, adjusted for multiplicity (Lenth, 2019). Right panel: Contrasts between day night EMM, cyan bars are 95% confidence intervals, red points indicative of significance at <0.05 level. Blue lowess-smoothing line indicative of trend. Points approaching 0 line indicate less difference between day and night. (a) Ratio between Epipelagic (0-230 m) and Mesopelagic (>230 m) backscatter, (b) Epipelagic and Upper-mesopelagic (>230 m ≤580 m), and (c) Upper-mesopelagic and Deep-mesopelagic (>580 m). (d) Day-night difference in total water column backscatter \log_e Nautical Area Scattering Coefficient. Note difference in y-axis scales.

Chapter 3

Table 3.5 Summary statistics of day-night mean total water column log_e Nautical Scattering Area Coefficient (acoustic backscatter), and contrasts within 1° latitude bands. EMM NASC – estimated marginal mean of total water column log_e Nautical Scattering Area Coefficient, SE – standard error, df – degrees of freedom, CL – comparison level, CI – confidence interval. Significance codes: ‘***’ <0.001, ‘**’ <0.01, ‘*’ <0.05, ‘NS’ ≥0.1. Negative contrast indicates higher total water column backscatter at night (green), positive contrast indicates lower total water column backscatter at night (red).

DVM	Latitude	(52,53]		(53,54]		(54,55]		(55,56]		(56,57]		(57,58]		(58,59]		(59,60]		(60,61]	
		D	N	D	N	D	N	D	N	D	N	D	N	D	N	D	N	D	N
4. TWC day night comparison	EMM NASC	7.042	6.290	6.080	5.995	5.550	7.012	5.347	5.762	5.433	5.619	4.963	4.798	4.710	4.436	3.859	3.606	2.989	3.536
	SE	0.206	0.153	0.142	0.146	0.138	0.178	0.142	0.140	0.139	0.143	0.139	0.151	0.140	0.143	0.139	0.147	0.155	0.219
	df	35.512	10.922	8.100	9.086	7.252	19.991	8.117	7.650	7.475	8.288	7.414	10.527	7.608	8.281	7.486	9.330	11.374	45.798
	Lower CL	6.891	6.138	6.005	5.920	5.434	6.895	5.292	5.707	5.378	5.565	4.891	4.726	4.655	4.381	3.796	3.543	2.786	3.371
	Upper CL	7.245	6.441	6.156	6.070	5.667	7.245	5.401	5.816	5.487	5.674	5.036	4.871	4.765	4.491	3.922	3.670	3.154	3.701
	Contrast	0.752 ***		0.085 NS		-1.462 ***		-0.415 ***		-0.186 ***		0.165 *		0.274 ***		0.253 ***		-0.547 **	
	SE	0.155		0.077		0.119		0.056		0.056		0.074		0.056		0.065		0.168	
	Lower CI	0.449		-0.065		-1.695		-0.524		-0.295		0.020		0.163		0.126		-0.876	
	Upper CI	1.056		0.236		-1.228		-0.306		-0.078		0.310		0.384		0.379		-0.218	

3.4.2 Environmental drivers of acoustic backscatter

The full GAMM explained 57.7% of the variance in Scotia Sea acoustic backscatter data. F statistics clearly reveal that the major contributors to explaining NASC variability were sea surface temperature ($F = 283.57$), followed by daylight hours ($F = 168.66$) and maximum percentage sea ice ($F = 97.39$), see summary Table 3.6. Sequentially dropping environmental predictors from the GAMM confirm the degree to which SST, daylight hours and sea ice percentage contribute to backscatter variability (Figure 3.7). The SST smoothing term alone accounted for 43.7% of variation and reducing the GAMM to SST, daylight hours and maximum percentage sea ice only, explained 55.6% of variance, resulting in a parsimonious model with limited reduction in predictive capability (Table 3.6). Estimated smoothing curves indicate that NASC is positively correlated with SST, negatively correlated with sea ice concentration, and negatively correlated with daylight hours up ~15 hours of daylight (Figure 3.8).

On checking the GAMM fit, model residuals broadly conformed to normality (see GAMM results in Supplement S.8), with a small number of outlying points. While the vast majority of residuals were normally distributed and NASC values reasonably predicted by the model, a limited number are likely to be overestimated.

Table 3.6 Summary of GAMM results. DN – Day night, Chl – \log_e surface chlorophyll (mg m^{-3}), GeoCurr – square root geostrophic current speed (ms^{-1}), SST – sea surface temperature ($^{\circ}\text{C}$), Depth – water depth (m), DistToCoast – distance to coast (km), DHr – Daylight hours, SIP – max percentage sea ice (%). All GAMMs were specified as ‘scaled t’ family, with identity link function. Response variable \log_e NASC. All explanatory variables were treated as smoothing terms ($k=3$) with the exception of binomial term DN.

Model	AIC	BIC	R ² adj.	Test statistics of explanatory variables							
				t	F						
				DN	Chl	GeoCurr	SST	Depth	DistTo Coast	DHr	SIP
Full GAMM	16008.49	16141.90	0.577	1.84	9.29	10.31	283.57	3.77	50.99	168.66	97.39
Full GAMM - Chl	16022.41	16141.00	0.573	1.83	NA	8.98	269.57	2.74	39.66	166.33	98.47
Full GAMM - GeoCurr	16021.52	16140.10	0.571	1.53	8.01	NA	279.77	4.33	51.47	161.76	156.94
Full GAMM - SST	16461.58	16580.17	0.455	2.92	2.16	7.28	NA	88.99	48.01	132.29	90.58
Full GAMM - Depth	16008.25	16126.83	0.577	1.81	8.81	10.27	414.04	NA	48.10	166.85	95.46
Full GAMM -DistToCoast	16053.30	16171.88	0.569	2.48	10.39	10.42	298.96	1.93	NA	138.47	96.25
Full GAMM - DHr	16144.20	16262.78	0.545	5.36	9.65	3.08	231.61	1.07	2.57	NA	68.52
Full GAMM - SIP	16302.37	16420.95	0.505	1.64	10.54	11.48	311.85	7.78	43.51	176.48	NA
Full GAMM - DayNight	16009.78	16135.77	0.577	NA	9.27	9.52	288.19	3.70	54.09	187.86	127.57
SST only	16457.11	16494.16	0.437	NA	NA	NA	1156.00	NA	NA	NA	NA
DHr only	16879.02	16916.08	0.211	NA	NA	NA	NA	NA	NA	281.40	NA
SIP only	16846.36	16883.41	0.242	NA	NA	NA	NA	NA	NA	NA	188.20
SST, DHr and SIP	16077.38	16144.09	0.556	NA	NA	NA	364.90	NA	NA	150.50	127.90

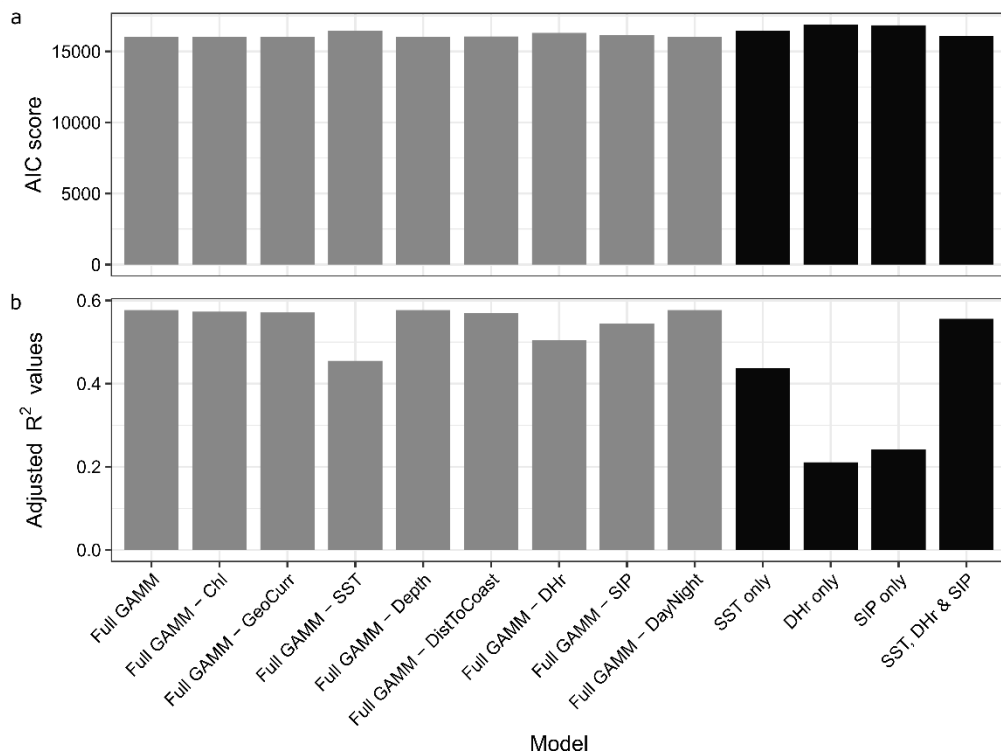


Figure 3.7 Effects of sequentially dropping variables from GAMM on model performance (a) Akaike's Information Criterion (AIC) and (b) R² values adjusted for degrees of freedom. Full GAMM contains all modelled variables. Four black bars are reduced variable models for the three most influential variables, sea surface temperature (SST), daylight hours (Dhr), sea ice percentage (SIP), and final model selection SST, Dhr and SIP.

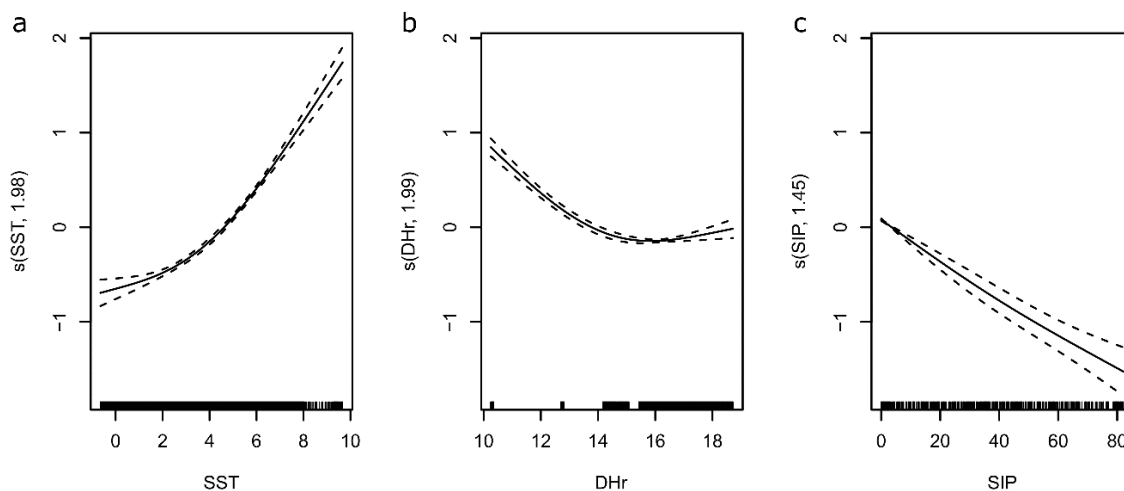


Figure 3.8 Estimated smoothing curves for the GAMM fitted to log_e Nautical Area Scattering Coefficient (NASC m² nmi⁻²) (a) sea surface temperature (b) daylight hours and (c) maximum percentage of sea ice. Centred smoothing curves indicate that response variable NASC increases with SST, initially decreases up to 15 hours of Dhr, and decreases with SIP. Dotted lines are ± 2 standard errors. Degrees of freedom in parenthesis. Rug plots on x-axis indicate number and distribution of observations.

3.5 Discussion

Mesopelagic fish play a vital role in biogeochemical cycling and the Antarctic food web, but knowledge of their vertical migration behaviour and the environmental drivers of their distribution within the Scotia Sea has been lacking. Previous studies have reported a lack of clear DVM behaviour detectable in acoustic scattering layers (Proud et al., 2018a), which has implications for active carbon sequestration and food web dynamics. This study has identified a clear DVM signal between epipelagic and mesopelagic organisms using acoustic data north of 57° S, which changes in magnitude and diminishes further south alongside a decrease in backscatter. Night-time migration into epipelagic water disappeared south of 57° S, although there was evidence of DVM within the mesopelagic layer.

3.5.1 Drivers of DVM change with latitude

While there is strong evidence from acoustic observations for typical DVM behaviour at lower latitudes in the Scotia Sea, where mesopelagic fauna migrate into epipelagic surface waters at night, the absence of conventional DVM south of 57° S, the approximate location of the Antarctic Polar Front during transits from the Falkland Islands to the South Orkney Islands (Moore et al., 1999), has a number of potential contributing factors. Changes in behaviour at high latitudes in response to extreme light regimes (Norheim et al., 2016), changes in temperature as animals seek their optimal thermal preference (Gjøsæter et al., 2017), food availability (Pearre, 2003), and a decrease in detectability of some species because of changes in their swimbladder morphology (Dornan et al., 2019), may all contribute to altered DVM signal. These factors are discussed below.

3.5.1.1 *Light*

The DVM pattern in the acoustic data north of 57° S is typical of that found near ubiquitously around the globe. My results indicate clear DVM patterns from the mesopelagic to the epipelagic zone, with apparent non-migrating portions of the mesopelagic community present within the deep mesopelagic water (>580 m). Partial and non-migration is common in mesopelagic fauna globally (Dypvik et al., 2012, Flynn and Kloser, 2012, Proud et al., 2018a). One of the primary explanations for DVM behaviour is that of avoiding visual predators by spending the day in the relative safety of the ocean's twilight (Pearre, 2003). Under extreme light conditions towards the pole, where hours of daylight far outweigh hours of darkness in summer and darkness prevails in winter, DVM may be suppressed, with the minimum depth

of occupation occurring deeper in summer to evade predation (Norheim et al., 2016). My study found that south of 57° S there was general tendency for a shallowing of mesopelagic acoustic backscatter at night, which did not encroach into the epipelagic zone. Gjørseter et al. (2017) found a similar pattern in DVM in Arctic acoustic data (latitude 79-82° N), where DVM was visible but predominantly constrained to mesopelagic depths even under low-light conditions during the Arctic summer. Furthermore, modelling by Longbehn et al. (2019) revealed that light levels were the major driver of vertical mesopelagic fish distribution, with increases in light intensity predicted to be responsible for suppressing depth of occupation below 300 m at night at high latitude in the acoustic patterns described by Norheim et al. (2016). My study therefore demonstrates that suppression in DVM may be ubiquitous at both poles.

3.5.1.2 Temperature

In addition to a limited contrast between day and night light levels, Gjørseter et al. (2017) proposed that suppressed DVM might be the result of surface water freshening, cooling and brine intrusions from the ice shelf, which may cause both water masses and organisms to deepen. While conventional DVM between mesopelagic and epipelagic was not evident in my high latitude data (> 57° S), DVM between the deep and upper mesopelagic zones was significant. A possible contributor to suppressing DVM within the Scotia Sea may be the considerable drop in surface water temperature south of the Antarctic Polar Front. Antarctic surface water or “Winter Water” masses, are characterised by a below 0° C temperature minima within the epipelagic zone (Garabato et al., 2004, Firing et al., 2017). As the abundant mesopelagic fish fauna of the Scotia Sea lack antifreeze glycoproteins (Cullins et al., 2011), cold water intrusion could drive a change in DVM behaviour within the Scotia Sea by forming a temperature barrier to vertically migrating fauna or restricting migration to cold adapted species (Collins et al., 2012).

3.5.1.3 Food availability

While DVM enables fish to feed in nutrient rich surface waters under the cover of darkness, different species can employ a range of strategies depending on their need to feed and the available food resources (Pearre, 2003). The dominant myctophid species' in the south of the Scotia Sea, where the acoustic DVM signal was suppressed, are *Electrona antarctica* and *Gymnoscopelus braueri* (Chapter 2, Dornan et al., 2019). However it is not yet clear what

DVM-related feeding strategies these species employ. *Electrona antarctica* primarily prey on euphausiids (mainly *Euphausia superba*), copepods (mainly *Metridia* spp.) and amphipods (mainly *Themisto gaudichaudii*) (Saunders et al., 2014a). *Gymnoscopelus braueri* primarily feed on copepods (mainly *Metridia* spp.) and euphausiids (mainly *Thysanoessa* spp.) (Saunders et al., 2014b). While there is considerable variability in the depths these prey items occupy, with many focussed in epipelagic waters, *Metridia* spp. are commonly found in deeper mesopelagic waters, potentially providing feeding opportunities at depth (Ward et al., 1995, Taki et al., 2008, Atkinson et al., 2012b, Tarling and Fielding, 2016, Saunders et al., 2018). It may be that the reduction in DVM signal is partially driven by some members of the mesopelagic fish community feeding opportunistically at depth or conducting brief asynchronous forays to capture prey in surface waters (Pearre, 2003, Dypvik et al., 2012, Saunders et al., 2018). However, much remains unclear about the DVM behaviour of prey species at the basin scale of the Scotia Sea, which requires further research.

3.5.1.4 Non-identification – detectability and behaviour issues

A potentially large contributing factor to the absence of DVM signal in the southern Scotia Sea is the marked latitudinal change in mesopelagic fish community composition, which changes from a community dominated gas-bearing swimbladdered species to one that is dominated by non-gas-bearing species (Dornan et al., 2019). As a gas-filled swimbladder can account for up to 95% of the acoustic signal from a fish (Foote, 1980b), the loss of a gas-bearing swimbladder in mesopelagic fish species makes them weak acoustic targets, such that pronounced changes in morphology at high latitudes potentially limits our ability to detect or track the movements of these species. It may be that mesopelagic fish are performing DVM in these regions, but we are simply not able to detect this movement using acoustic methods alone. Day-night comparisons of depth stratified net samples provide evidence that species within the sea-ice sector of the Scotia Sea at higher latitudes, including the biomass-dominant *Electrona antarctica*, do perform DVM (Torres and Somero, 1988, Lancraft et al., 1989, Robison, 2003, Collins et al., 2012). However, given that mesopelagic fishes have been shown to exhibit net avoidance behaviour (Collins et al., 2012, Kaartvedt et al., 2012) the extent to which day-night differences in net sampled biomass are indicative of DVM should be treated with caution.

3.5.1.5 *Additional factors*

It is important to bear in mind that single-frequency acoustic data lacks the capacity to distinguish between species in a mixed community assemblage and fauna other than fish may be responsible for part of the acoustic signal. Antarctic krill (*Euphausia superba*) are highly abundant in the Scotia Sea (Atkinson et al., 2004), visible when swarming in 38 kHz acoustic data (Watkins and Brierley, 2002), and undertake DVM (Demer and Hewitt, 1995). However, Antarctic krill are predominantly thought to swarm and migrate in the surface 100 m of the water column (Tarling et al., 2018), they would therefore be unlikely to be responsible for the DVM signal observed north of 57° S. In addition, if Antarctic krill were dominating the acoustic signal, then NASC would not decrease towards the pole and DVM signal would not disappear.

Whilst this study reveals DVM trends in the Scotia Sea, it is acknowledged that the acoustic data used in this study spans multiple years and seasons, and there are likely to be temporal and seasonal trends confounding DVM signals, particularly in the low backscatter high latitude region. To gain an in-depth understanding of DVM behaviour, it is recommended that longer-term directed acoustic sampling be undertaken in high latitude areas to examine diel, seasonal and inter-annual trends in acoustic backscatter and behaviour. The use of upward facing echosounders on fixed moorings and dedicated acoustic transects deployed throughout a field season, would also help to address potential temporal and spatial bias.

3.5.2 **Environmental drivers of acoustic backscatter in the Scotia Sea**

3.5.2.1 *Drivers of backscatter in the Scotia Sea, Southern Ocean and globally*

Modelling NASC as a function of environmental variables reveals that sea surface temperature, daylight hours and sea ice concentration are the major environmental drivers of acoustic backscatter in the Scotia Sea. Previous research in polar waters has also found that sea surface temperature is a key environmental driver of both acoustic backscatter (Fielding et al., 2012) and myctophid species distribution (Freer et al., 2019) and when combined with time of day can be used to predict backscatter at depth (Boersch-Supan et al., 2017, Escobar-Flores et al., 2018a).

At a global level, primary production becomes the key environmental driver, both for predicting backscatter for the mesopelagic water column (Irigoien et al., 2014), and predicting the backscatter of deep scattering layers, when combined with temperature at the layer's depth (Proud et al., 2017). There are also multiple reports of shoaling (or shallowing) of mesopelagic fauna maximum depth of occupation in response to Oxygen Minimum Zones (OMZ) (Bianchi et al., 2013a, Netburn and Anthony Koslow, 2015, Klevjer et al., 2016), which are predicted to reduce the habitable space above the OMZ under future ocean warming scenarios, as temperature inhibits oxygen solubility (Gilly et al., 2013). While there are no defined values for oxygen minimum zones, Gilly (2013) notes that oxygen concentrations of up to $120 \mu\text{mol kg}^{-1}$ can be hypoxic to many marine organisms, however polar waters tend to be well-oxygenated with minimum oxygen concentrations within the Antarctic circumpolar current, far exceeding this limit (Orsi et al., 1995), and were therefore not considered as part of this study.

As a result of collinearity between environmental candidate variables, the extent to which ST_{200} had to play in explaining acoustic backscatter has not been explored in this study, though it has been demonstrated that it is highly likely to be a considerable driver for at least portions of the backscattering community (Freer et al., 2019). SST and dynamic height are both defining properties of Southern Ocean frontal positions and water masses (Orsi et al., 1995, Venables et al., 2012). It is therefore likely that specific water masses are the underlying environmental conditions driving the variability explained by SST on acoustic backscatter. Silk et al. (2016), identified that sea level anomaly (dynamic height) and velocity, both variables which were dropped from the current model, were highly predictive of krill distribution in the Scotia Sea. Moreover, whereas SST was the strongest predictor of NASC values in this study, and increased temperatures are understood to be driving changes in krill distribution and community structure (Atkinson et al., 2019), SST was not revealed as a significant driver of krill distribution in Silk et al. (2016). A plausible explanation for this pattern is that Silk et al. (2016), subdivide their study area into smaller sub-regions over which SST may be more stable. It is possible that at a finer spatial scale the predictive ability of SST may be more limited.

3.5.2.2 *Biological implications*

The link between acoustic backscatter, SST and sea ice, coincides with a community shift to polar specialist myctophid species further south, which have consistently adapted to lose the

gas component in their swimbladders in adulthood, making them weaker acoustic targets (see Chapter 2, Dornan et al., 2019). This link between colder, sea ice covered waters and the loss of swimbladder gas has implications for future ecosystem function and modelling mesopelagic fish population changes within the Scotia Sea. Research has predicted a poleward shift of mesopelagic fish species under future warming scenarios, with a corresponding reduction in suitable habitat for polar specialists (Freer et al., 2019). The current findings suggest that as sea temperatures rise it seems likely that we will see a corresponding increase in acoustic backscatter towards the pole, which is likely to reflect a change in community composition, with gas-bearing species displacing non-gas-bearing polar specialists. As Southern Ocean mesopelagic fish appear to follow Bergmann's rule, where larger animals are found in colder environments (Meiri, 2011, Saunders and Tarling, 2018), there is also the potential for a southward shift in community size-spectra under a scenario of ocean warming, as predominantly small, warmer water species (and intra-specific sizes) migrate increasingly to higher latitudes, potentially displacing the larger species normally found in these regions. So, whilst in the future we may see an increase in acoustic backscatter, it may not result in an increase in mesopelagic fish biomass. It is also unclear how well these smaller gas-bearing species will be adapted to the extreme light regime further south, how it may interfere with their foraging opportunities or patterns in diel vertical migration. Future acoustic data should enable us to rapidly track southward migration of gas-bearing species and consequent community changes, but it is imperative that the acoustic data are periodically validated with up to date knowledge on species present and their backscattering properties.

3.6 Conclusions

The use of active acoustics in this study has revealed a complex pattern in DVM behaviour in the Scotia Sea, where the DVM signal in acoustic data becomes weakened with increased latitude. While it should not be overlooked that this may be the result of an inability to detect species (Dornan et al., 2019), it is also likely to be a result of reduced vertical migration in response to epipelagic cold-water intrusion and an extreme light regime. In a warming world, where community structure is predicted to change (Proud et al., 2017, Freer et al., 2019), understanding how biomass-dominant pelagic organisms migrate vertically through the water column at high latitudes is a necessary pre-requisite for modelling carbon sequestration and food web dynamics at both a regional and global level.

Chapter 3

Supplementary material

Chapter 3 Supplementary material

S.1 File list of Conductivity Temperature Depth (CTD) profiler

Cruise	CTD filename	Station	Latitude (°)	Longitude (°)
JR16003PF	jr16003_021svp	PF	-53.2943	-52.1852
	jr16003_020svp	PF	-53.9049	-49.2740
	jr16003_019svp	PF	-54.1331	-48.1662
	jr16003_018svp	PF	-54.3390	-47.2022
	jr16003_017svp	PF	-54.5179	-46.2236
	jr16003_016svp	PF	-54.5380	-45.0937
	jr16003_015svp	PF	-54.8388	-44.2625
	jr16003_014svp	PF	-55.1194	-42.2662
	jr16003_011svp	P2	-55.2444	-41.2740
	jr16003_012svp	P2	-55.2486	-41.2621
JR15004	JR15004_059svp	MSS-Oceanic	-59.9996	-47.2503
	JR15004_064svp	MSS-Oceanic	-59.9999	-46.6492
	JR15004_071svp	MSS-Oceanic	-60.1244	-46.0772
	JR15004_108svp	Along Track station	-56.9944	-51.5990
JR15002	jr15002_021svp	P2	-55.2426	-41.2576
	jr15002_040svp	P2	-55.2428	-41.2575
	jr15002_031svp	P3	-52.8052	-40.0862
	JR15002_114svp	P3	-52.8117	-40.1116
JR15002	jr15002_010svp	C2	-60.2082	-44.4077
	jr15002_011svp	C3	-59.6887	-44.0543
JR200	jr200ctd032_139_2db	P2	-55.2590	-41.3581
	jr200ctd034_148_2db	P2	-55.2588	-41.3576
	jr200ctd041_168_2db	P3	-52.8084	-40.1156
	jr200ctd043_173_2db	P3	-52.8080	-40.1145
JR200	jr200ctd008_33_2db	C2	-60.2085	-44.4081
	jr200ctd010_37_2db	C2	-60.2086	-44.4085
	jr200ctd012_66_2db	C3	-59.6887	-44.0550
	jr200ctd013_73_2db	C3	-59.6887	-44.0540
JR177	jr177ctd037_2db	P2	-55.2090	-41.2447
	jr177ctd039_2db	P2	-55.2069	-41.1567
	jr177ctd048_2db	P3	-52.8589	-40.0969
	jr177ctd050_2db	P3	-52.8582	-40.0974
JR177	jr177ctd001_2db	Mid Test station	-57.6789	-50.4296
	jr177ctd007_2db	C2	-60.2092	-44.4089
	jr177ctd017_2db	C3	-59.6887	-44.0543
	jr177ctd019_2db	C3	-59.6801	-44.0571
JR161	jr161ctd033_2db	P2	-55.2059	-41.2462
	jr161ctd037_2db	P2	-55.2061	-41.2460
	jr161ctd038_2db	P2	-55.2141	-41.2174
	jr161ctd042_2db	P2	-55.2067	-41.2467
	jr161ctd043_2db	P2	-55.2131	-41.2364
	jr161ctd048_2db	P3	-52.8589	-40.0971
	jr161ctd051_2db	P3	-52.8757	-40.0911
	jr161ctd052_2db	P3	-52.8703	-40.1392
	jr161ctd056_2db	P3	-52.8702	-40.1388
	jr161ctd059_2db	P3	-53.0008	-39.8622
JR161	jr161ctd001_2db	PS1 (Test station)	-57.7420	-50.4383
	jr161ctd004_2db	PS1 (Test station)	-57.7430	-50.4196
	jr161ctd007_2db	PS1 (Test station)	-57.7429	-50.4218
	jr161ctd010_2db	PS1 (Test station)	-57.7422	-50.4385
	jr161ctd013_2db	PS1 (Test station)	-57.7455	-50.3995
	jr161ctd018_2db	C2	-60.4190	-44.6793
	jr161ctd024_2db	C3	-59.6801	-44.0599

S.2 Sensitivity analysis for setting Max S_v integration threshold

Rationale: Upon plotting NASC in relation to latitude for acoustic transect JR15004_002.20160220, some unexpectedly high values for NASC were visible in 1 km by Total Water Column grid cell integrated data (see Figure S.2.1). Manually scrutinising echograms for these data points, reveals that these echogram cells were dominated by transient noise, or a small fleck of intermittent noise with a high S_v (left behind from intermittent noise removal filter). These small number of high S_v values can drive artificially high NASC values over the entire water column. This was confirmed by manually assigning the small-flecked region as no data and integrating again.

One method of reducing bias from noise whilst retaining signal is the implementation of a maximum S_v data threshold. A sensitivity analysis of maximum integration thresholds was undertaken to assess viability of applying a Max S_v value across all data sets.

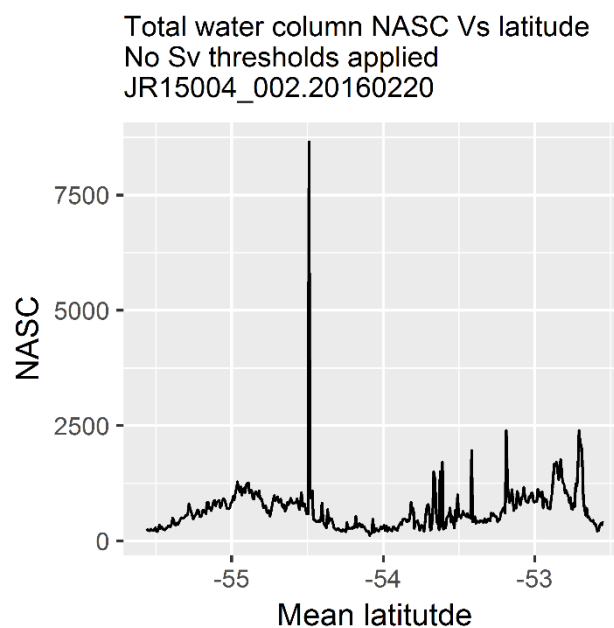


Figure S.2.1. Elevated NASC values in acoustic transect JR15004_002.20160220, driven by transient and Impulse Noise flecks.

Protocol: JR15004_002.20160220 transect data plus five additional transects, were selected at random to assess sensitivity of median NASC values to adjustment of maximum integration threshold.

Using COM scripting, echo integration data was exported from Echoview, with varying maximum S_v thresholds applied plus a control of 'No Threshold'. Two approaches were considered in the potential to identify the most appropriate Max S_v threshold to apply:

1. S_v threshold induced break points in median NASC.
2. Removal based on top 5% max S_v in a cell.

Table S.2.1 gives an overview of results on the effects of applying a maximum S_v threshold on integrated data. Figures S.2.2-7 show effect of applying maximum S_v thresholds on median NASC along the transect data (left) and break points of transect median NASC (right).

Table S.2.1 Summary of integration data output at a range of maximum integration thresholds for six 24-hour cruise transects. Values relate to data integrated and exported in 1 km by total water column depth cells. S_v max is the maximum value of S_v recorded anywhere in the transect. S_v max 0.95 is the lower boundary of the 95th percentile for maximum S_v values recorded. For clarity, bold text is unthresholded data, yellow highlighted text is indicative of last value of median NASC unaffected by maximum S_v thresholding.

Cruise ID CruiseNo_ Leg.Date (yyyymmdd)	Max. S_v integration threshold (dB)	NASC max	NASC median	NASC mean	S_v min (dB)	S_v max (dB)	S_v max 0.95 (dB)
JR15002_007.20151212	None	6341.5	240.6	395.4	-132.6	-28.0	-35.6
JR15002_007.20151212	-20	6341.5	240.6	395.4	-132.6	-28.0	-35.6
JR15002_007.20151212	-30	6341.5	240.6	394.5	-132.6	-32.1	-35.7
JR15002_007.20151212	-32	6341.5	240.6	394.5	-132.6	-32.1	-35.7
JR15002_007.20151212	-34	6341.5	240.6	393.6	-132.6	-34.3	-35.9
JR15002_007.20151212	-36	6341.5	240.6	391.8	-132.6	-36.0	-37.1
JR15002_007.20151212	-38	6341.5	240.6	389.3	-132.6	-38.0	-38.5
JR15002_007.20151212	-40	6341.5	238.2	385.6	-132.6	-40.0	-40.3
JR15002_007.20151212	-42	6254.5	238.2	380.7	-132.6	-42.0	-42.2
JR15002_007.20151212	-44	6011.9	235.8	375.3	-132.6	-44.0	-44.1
JR15002_007.20151212	-46	5446.1	235.8	367.8	-132.6	-46.0	-46.0
JR15002_007.20151212	-48	4571.5	232.4	357.5	-132.6	-48.0	-48.0
JR15002_007.20151212	-50	3597.6	229.8	344.8	-132.6	-50.0	-50.0
JR15004_002.20160220	None	8396.5	573.9	669.7	-134.7	-18.1	-36.0
JR15004_002.20160220	-20	6579.2	573.9	665.4	-134.7	-21.0	-36.0
JR15004_002.20160220	-30	2686.9	573.9	653.8	-134.7	-30.1	-36.0
JR15004_002.20160220	-32	2576.5	573.9	650.6	-134.7	-32.0	-36.0
JR15004_002.20160220	-34	2472.6	573.9	645.3	-134.7	-34.0	-36.2
JR15004_002.20160220	-36	2392.9	566.7	640.5	-134.7	-36.0	-37.6
JR15004_002.20160220	-38	2392.9	553.0	635.4	-134.7	-38.1	-38.5

Chapter 3 Supplementary material

Cruise ID	Max. Sv integration threshold (dB)	NASC max	NASC median	NASC mean	Sv min (dB)	Sv max (dB)	Sv max 0.95 (dB)
CruiseNo_Leg.Date (yyyymmdd)							
JR15004_002.20160220	-40	2392.9	549.7	629.7	-134.7	-40.0	-40.4
JR15004_002.20160220	-42	2392.9	547.8	625.1	-134.7	-42.0	-42.1
JR15004_002.20160220	-44	2392.9	542.5	620.1	-134.7	-44.0	-44.1
JR15004_002.20160220	-46	2392.9	536.9	616.1	-134.7	-46.0	-46.1
JR15004_002.20160220	-48	2392.9	532.2	612.9	-134.7	-48.0	-48.0
JR15004_002.20160220	-50	2382.5	532.2	609.9	-134.7	-50.0	-50.0
JR177_011.20080215	None	2862.7	279.0	437.6	-132.5	-28.2	-38.2
JR177_011.20080215	-20	2862.7	279.0	437.6	-132.5	-28.2	-38.2
JR177_011.20080215	-30	2654.4	279.0	436.9	-132.5	-30.1	-38.2
JR177_011.20080215	-32	2272.3	279.0	433.8	-132.5	-32.1	-38.2
JR177_011.20080215	-34	2272.3	279.0	431.4	-132.5	-34.0	-38.3
JR177_011.20080215	-36	2272.3	278.8	429.2	-132.5	-36.1	-39.0
JR177_011.20080215	-38	2265.3	277.3	427.2	-132.5	-38.1	-39.6
JR177_011.20080215	-40	2265.3	275.9	425.1	-132.5	-40.0	-41.0
JR177_011.20080215	-42	2265.3	275.9	423.2	-132.5	-42.0	-42.4
JR177_011.20080215	-44	2265.3	275.9	420.6	-132.5	-44.0	-44.3
JR177_011.20080215	-46	2265.3	275.9	418.0	-132.5	-46.0	-46.2
JR177_011.20080215	-48	2265.3	274.5	415.1	-132.5	-48.0	-48.1
JR177_011.20080215	-50	2265.3	274.3	411.7	-132.5	-50.0	-50.0
JR200_001.20090313	None	8291.3	715.3	895.5	-129.1	-25.3	-30.9
JR200_001.20090313	-20	8291.3	715.3	895.5	-129.1	-25.3	-30.9
JR200_001.20090313	-30	7406.5	715.3	877.1	-129.1	-30.0	-31.9
JR200_001.20090313	-32	6775.7	715.3	863.0	-129.1	-32.0	-33.2
JR200_001.20090313	-34	6134.3	713.8	849.8	-129.1	-34.0	-34.6
JR200_001.20090313	-36	5629.5	712.5	832.0	-129.1	-36.0	-36.2
JR200_001.20090313	-38	4763.1	710.3	812.1	-129.1	-38.0	-38.1
JR200_001.20090313	-40	4219.1	698.2	791.6	-129.1	-40.0	-40.1
JR200_001.20090313	-42	3500.6	678.7	772.5	-129.1	-42.0	-42.1
JR200_001.20090313	-44	2873.9	678.6	754.8	-129.1	-44.0	-44.0
JR200_001.20090313	-46	2750.4	670.9	737.9	-129.1	-46.0	-46.0
JR200_001.20090313	-48	2750.4	659.4	722.6	-129.1	-48.0	-48.0
JR200_001.20090313	-50	2744.9	623.3	707.8	-129.1	-50.0	-50.0
JR200_012.20090417	None	2211.4	1225.4	1268.2	-133.9	-31.4	-50.5
JR200_012.20090417	-20	2211.4	1225.4	1268.2	-133.9	-31.4	-50.5
JR200_012.20090417	-30	2211.4	1225.4	1268.2	-133.9	-31.4	-50.5
JR200_012.20090417	-32	2211.4	1225.4	1268.2	-133.9	-34.1	-50.5
JR200_012.20090417	-34	2211.4	1225.4	1268.2	-133.9	-34.1	-50.5
JR200_012.20090417	-36	2211.4	1225.4	1268.2	-133.9	-39.4	-50.5

Cruise ID	Max. Sv integration threshold (dB)	NASC max	NASC median	NASC mean	Sv min (dB)	Sv max (dB)	Sv max 0.95 (dB)
CruiseNo_Leg.Date (yyyymmdd)							
JR200_012.20090417	-38	2211.4	1225.4	1268.2	-133.9	-39.4	-50.5
JR200_012.20090417	-40	2211.4	1225.4	1268.2	-133.9	-40.1	-50.5
JR200_012.20090417	-42	2211.4	1225.4	1268.1	-133.9	-42.2	-50.5
JR200_012.20090417	-44	2211.4	1225.4	1268.1	-133.9	-44.1	-50.5
JR200_012.20090417	-46	2211.4	1225.4	1268.0	-133.9	-46.0	-50.5
JR200_012.20090417	-48	2211.4	1225.4	1268.0	-133.9	-48.0	-50.7
JR200_012.20090417	-50	2209.0	1225.4	1267.9	-133.9	-50.0	-51.2
JR291_001.20131116	None	4648.2	308.8	475.8	-134.4	-29.1	-35.8
JR291_001.20131116	-20	4648.2	308.8	475.8	-134.4	-29.1	-35.8
JR291_001.20131116	-30	4648.2	308.8	474.8	-134.4	-30.2	-35.8
JR291_001.20131116	-32	4648.2	308.8	472.4	-134.4	-32.2	-36.1
JR291_001.20131116	-34	4648.2	308.5	470.5	-134.4	-34.0	-36.5
JR291_001.20131116	-36	4648.2	305.8	466.5	-134.4	-36.0	-37.4
JR291_001.20131116	-38	4648.2	302.6	461.3	-134.4	-38.0	-38.6
JR291_001.20131116	-40	4648.2	301.7	455.9	-134.4	-40.0	-40.3
JR291_001.20131116	-42	4547.1	297.2	448.8	-134.4	-42.0	-42.1
JR291_001.20131116	-44	4180.9	294.1	439.4	-134.4	-44.0	-44.1
JR291_001.20131116	-46	3704.5	291.3	427.8	-134.4	-46.0	-46.0
JR291_001.20131116	-48	3219.7	285.2	412.8	-134.4	-48.0	-48.0
JR291_001.20131116	-50	3145.9	280.2	394.1	-134.4	-50.0	-50.0

Results:

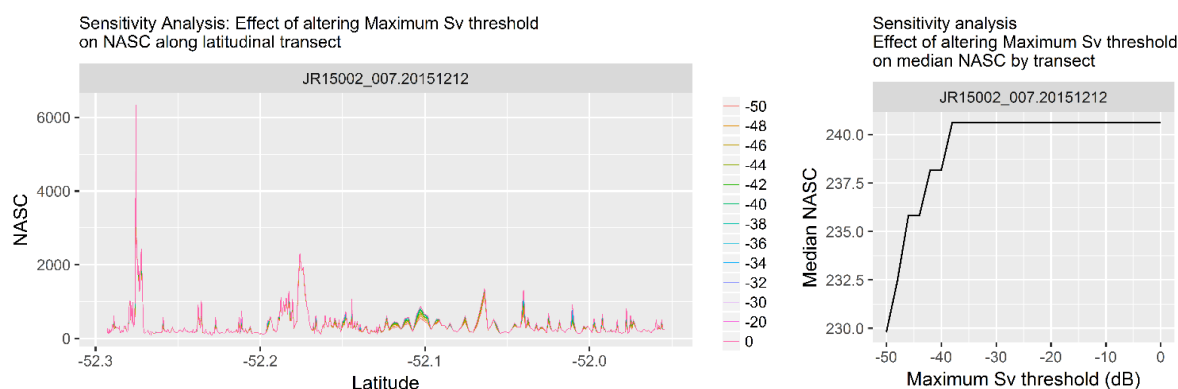


Figure S.2.2 JR15002_007.20151212 Peak visible at latitude -52.28 is not affected by thresholding and on echogram inspection this region has a high quantity of backscatter in upper water column.

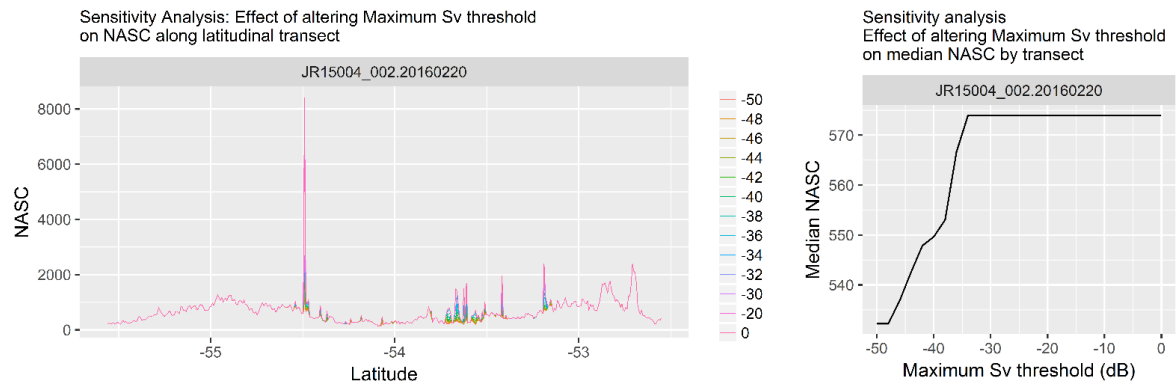


Figure S.2.3 JR15004_002.20160220 Peaks visible are the result of transient noise and application of max S_v threshold dampens the effect of this artificially elevated signal.

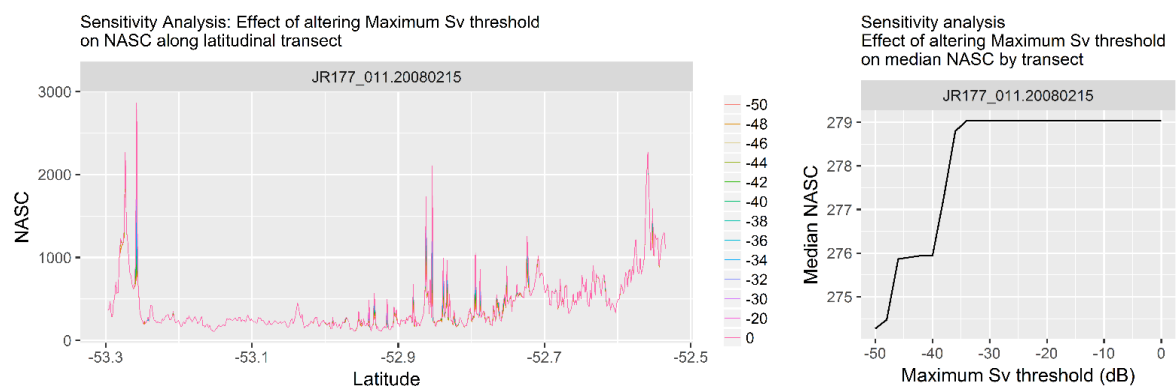


Figure S.2.4 JR177_011.20080215 Peaks visible are the result of a mix of high signal and transient or impulse noise. However, inspection of individual peaks on echogram indicates that the max S_v threshold is dampening just the noise whilst leaving genuine signal untouched.

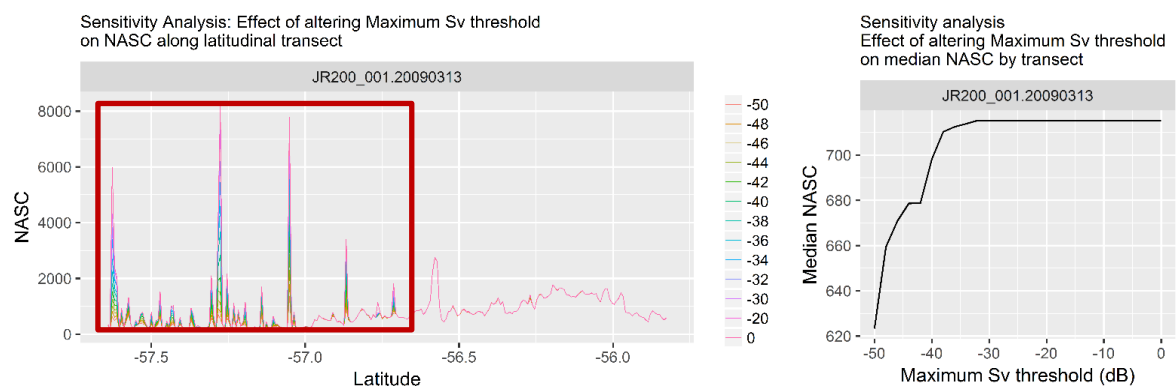


Figure S.2.5 JR200_001.20090313 A high degree of transient noise is visible on echograms corresponding to NASC spikes at higher latitudes (highlighted by red bounding box) in what was otherwise an area with low signal. Manually excluding TN in Echoview® 8.0.95, revealed that applying a filter close to the median NASC break point of -32 to -34 dB does not effectively remove the noise or reduce NASC values sufficiently.

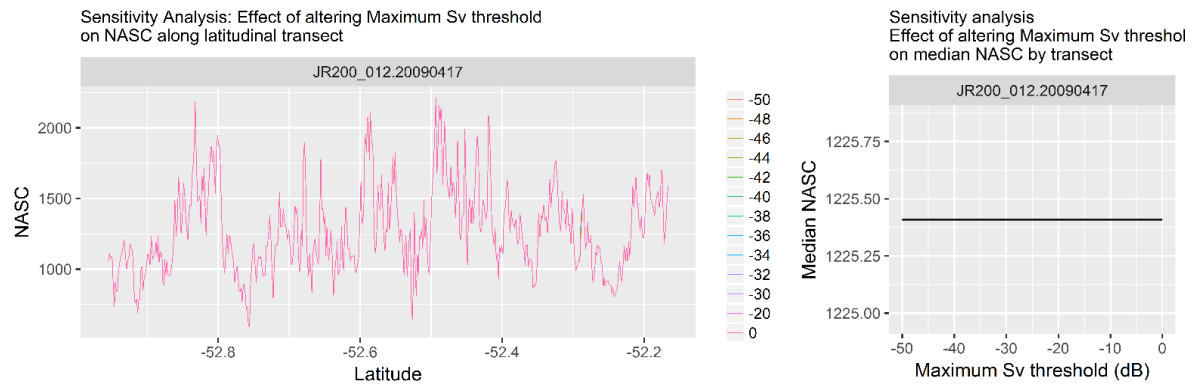


Figure S.2.6 JR200_012.20090417 Thresholding has no effect on this clean dataset.

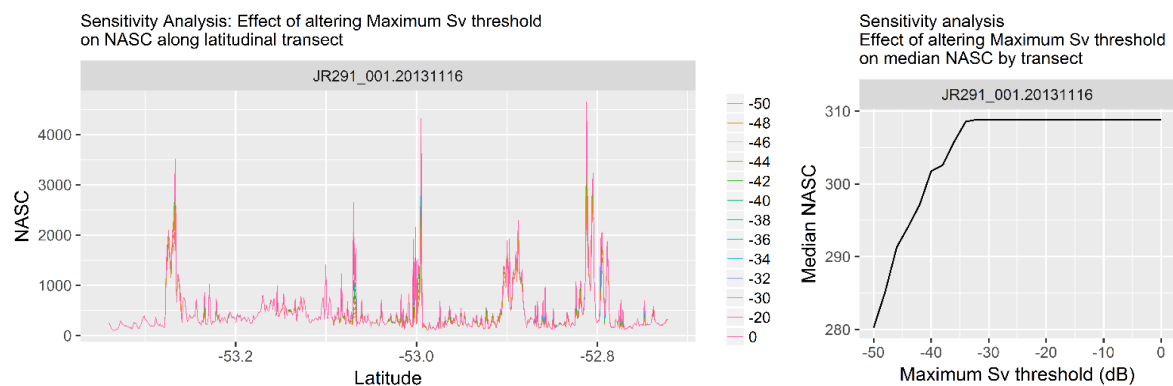


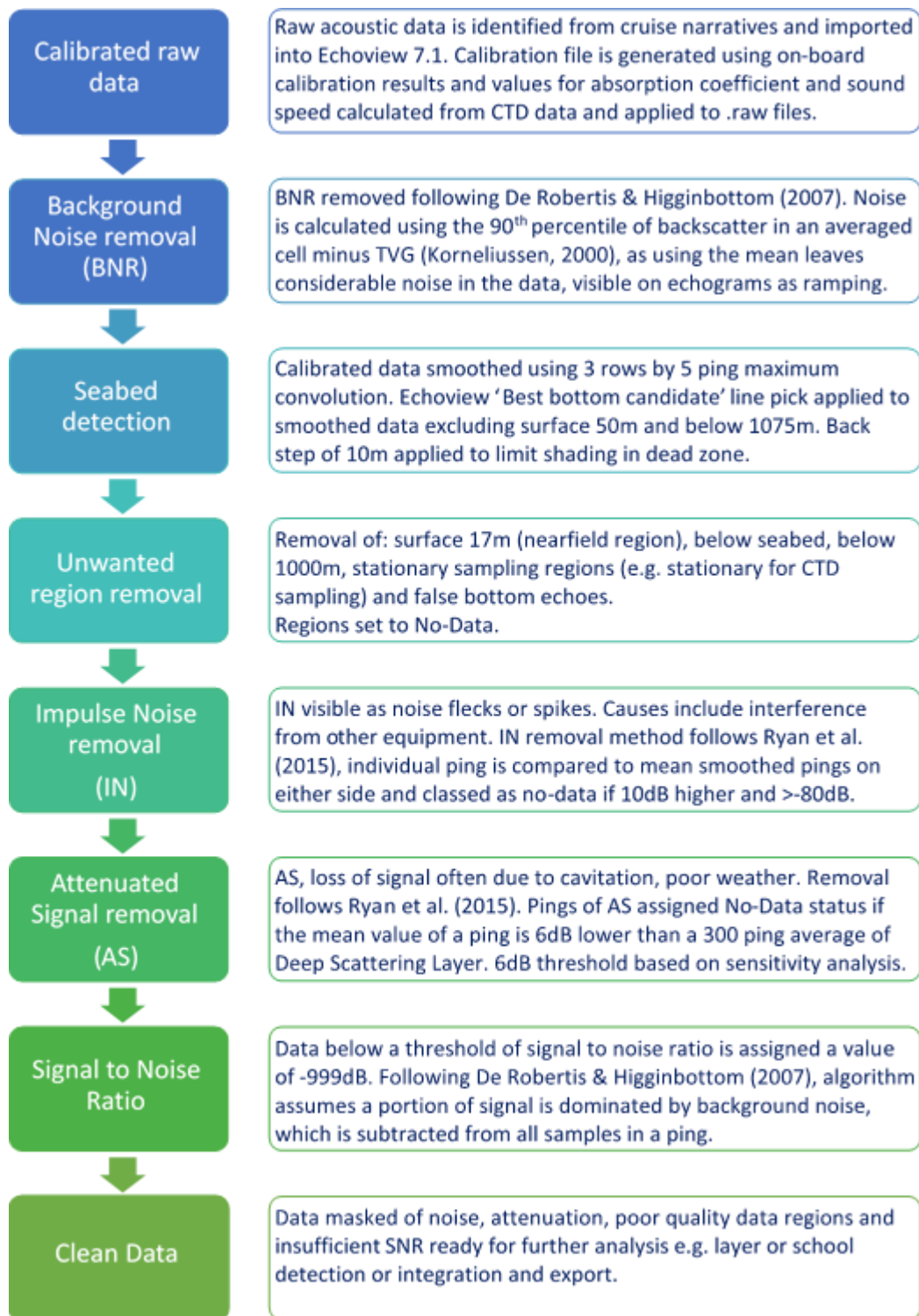
Figure S.2.7 JR291_001.20131116 Transit has patches of TN visible however many of the peaks in this transect are congruent with small dense swarms and elevated signal in general. Thresholding may marginally dampen a portion of the densest concentrations of biota.

Conclusions

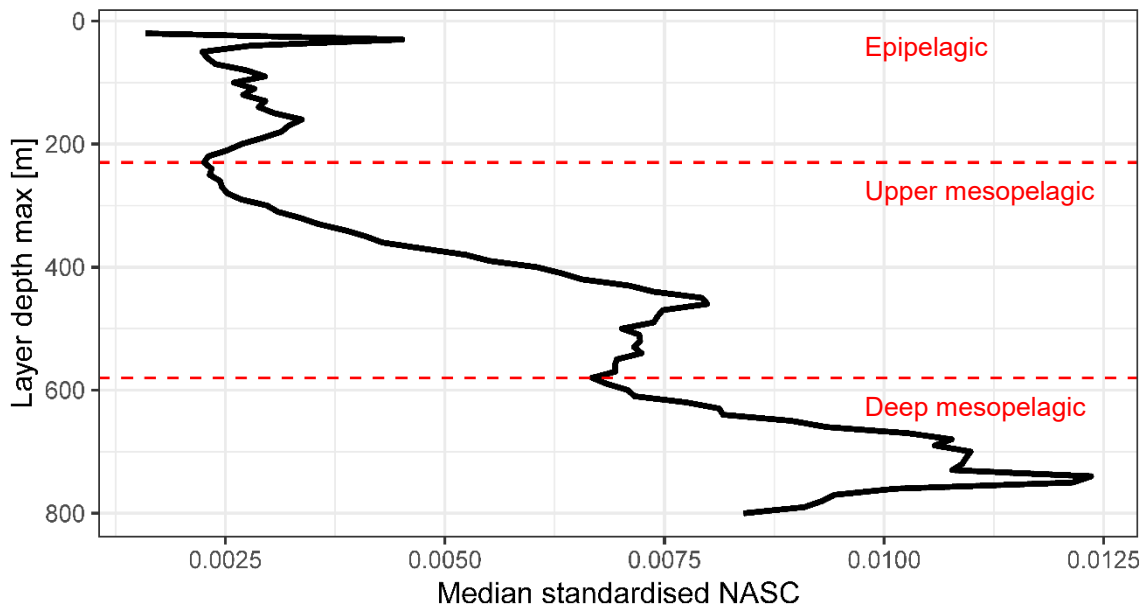
Applying a maximum S_v threshold for integration appears to be sufficient to dampen the effects of noise in all but the noisiest data sets, whilst leaving the majority signal unaffected. By applying a blanket max S_v threshold at a level of -35 dB, that is the mean S_v threshold for those data sets not skewed by excessive noise (or the absence of noise), the effects of noise on NASC could be dampened across all datasets (setting all S_v data points above this threshold to No Data).

The application of a max S_v threshold of -36.5 dB, relating to the mean of the top 5% of maximum S_v values along transects, would be more conservative still. However, it is considered that where median NASC is being affected this is in fact no longer removing outlying noise values but rather it is affecting a degree of signal.

Datasets that required an excessive degree of thresholding to reduce the effect of transient noise on NASC levels (e.g. transect. JR200_001.20090313) are potentially too compromised by noise to effectively distinguish meaningful signal by thresholding alone. Integrated NASC data was subsequently imported to R and the top 1% of high NASC values were visually inspected and rejected from analysis if found to be noise biased.



S.3 Overview of acoustic pre-processing required to clean data prior to aggregation detection, echo integration or statistical analysis.



S.4 Median NASC by depth of all cruise day-time data (standardised throughout full total water column depth for each distance sampling unit), reveal low NASC inflection points at 230 m and 580 m, which were used to partition data into epipelagic (depth ≤ 230 m), upper-mesopelagic (depth >230 m and ≤ 580 m) and deep-mesopelagic (depth >580 m) zones.

To categorise acoustic data as either epipelagic, upper-mesopelagic or deep-mesopelagic objectively, median values of standardised Nautical Scattering Area Coefficient (NASC, $\text{m}^2 \text{nmi}^{-2}$) a linear measure of acoustic backscatter were plotted against depth. NASC values were standardised within each 1 km sampling unit by dividing each 10 m depth cell NASC by sum of NASC throughout the water column. Median standardised NASC for all daytime only data from the entire data set was plotted against depth. Inflection points were identified at 230 m and 580 m, and were used as the break points between epipelagic, upper-mesopelagic and deep-mesopelagic zones to assess effect of latitude on Diel Vertical Migration in acoustic backscatter data.

S.5 Estimated marginal means model output – Example code

This example is from the comparison of vertical distribution index between the Epipelagic and Mesopelagic DVM scenario.

When uncorrected for pseudoreplication, a simple analysis of variance (aov) was used to estimate the variance in the vertical distribution index (ratio of epipelagic NASC to mesopelagic NASC) between day and night samples with an interaction between within 1° latitude bands, and variance of vertical distribution index with cruise.

Model specification format is:

```
aov (dependent var ~ predictor 1 interacting with (:) predictor 2 +
predictor 3, data=dtem)
```

Model:

```
aov.result_uncorrected <- aov (emindex ~ daynight:lat_bin1 + cruise,
data=dtem)
```

```
> summary(aov.result_uncorrected)
```

	Df	Sum Sq	Mean Sq	F value	Pr(>F)	
cruise	5	96.4	19.286	219.95	<2e-16	***
daynight:lat_bin1	17	60.7	3.569	40.71	<2e-16	***
Residuals	5584	489.6	0.088			

This reveals that there is a high amount of variance explained by the cruise, which we would expect as cruise transects occur in different years and seasons, which needs to be controlled for. There is also a significant interaction between daynight:latitude, which is what I am interested in.

Emmeans package from R is good for unbalanced messy data. It takes the aov model results and generates estimated marginal means (least-square means) for day and night vertical distribution index within latitude bins, so that we can explore differences between day and night within the latitude bins:

```
> aov.results.unc.s <- as.data.table(emmeans(aov.result_uncorrected, "dayn
ight", "lat_bin1"))
```

```
> aov.results.unc.s
```

	daynight	lat_bin1	emmean	SE	df	lower.CL	upper.CL
1:	day	(52,53]	0.6556194	0.05885061	5584	0.5402493	0.7709895
2:	night	(52,53]	0.8414300	0.02137615	5584	0.7995244	0.8833355
3:	day	(53,54]	0.7027774	0.01474329	5584	0.6738748	0.7316799
4:	night	(53,54]	0.8271482	0.02027792	5584	0.7873956	0.8669008
5:	day	(54,55]	0.7074977	0.01052606	5584	0.6868625	0.7281329
6:	night	(54,55]	0.8140923	0.04667634	5584	0.7225886	0.9055961

```

7:      day  (55,56] 0.5876394 0.01753698 5584 0.5532601 0.6220187
8:     night (55,56] 0.7795824 0.01427808 5584 0.7515918 0.8075730
9:      day  (56,57] 0.7835084 0.01291461 5584 0.7581907 0.8088260
10:    night (56,57] 0.8317844 0.01878582 5584 0.7949569 0.8686119
11:     day  (57,58] 0.8024287 0.01238541 5584 0.7781485 0.8267089
12:    night (57,58] 0.7977010 0.02821532 5584 0.7423880 0.8530140
13:     day  (58,59] 1.0037028 0.01416185 5584 0.9759401 1.0314656
14:    night (58,59] 0.9583617 0.01884610 5584 0.9214160 0.9953074
15:     day  (59,60] 0.8678129 0.01305472 5584 0.8422205 0.8934052
16:    night (59,60] 0.8302139 0.02395449 5584 0.7832538 0.8771741
17:     day  (60,61] 0.6150614 0.02048940 5584 0.5748942 0.6552286
18:    night (60,61] 0.6253285 0.06689624 5584 0.4941858 0.7564711

```

However, in this data set we have elevated degrees of freedom, because we sample every km, which effectively results in pseudoreplication.

To account for pseudoreplication, a generalised linear mixed effects model was fitted (R package lme4, Douglas Bates, Martin Maechler, Ben Bolker, Steve Walker (2015). Fitting Linear Mixed-Effects Models Using lme4. Journal of Statistical Software, 67(1), 1-48. doi:10.18637/jss.v067.i01.)

```

library(lme4) # fit linear fixed effects models
library(pbkrtest)
library(lmerTest)

> aov.result_corrected <- lmer (emindex ~ daynight:lat_bin1 + daynight +
(1|lat_bin0.05) + (1|cruise), data=dtem)

```

This above formula fits a linear mixed effects model, similar to the previous AOV, but with cruise and latitude bin of 0.05° specified as random effects. Carrying out an anova on the model to test for differences between day and night data and day and night within 1° latitude groups:

```

anova(aov.result_corrected)
Type III Analysis of Variance Table with Satterthwaite's method
              Sum Sq Mean Sq NumDF  DenDF F value    Pr(>F)
daynight           0.554 0.55401      1 5489.8  6.8141 0.009068 **
daynight:lat_bin1 20.075 1.25470     16  414.9 15.4325 < 2.2e-16 ***
---
Signif. codes:  0 '***' 0.001 '**' 0.01 '*' 0.05 '.' 0.1 ' ' 1

```

Having accounted for pseudoreplication by adding in 0.05° lat bins (i.e. reducing resolution by 1/20th of original resolution) roughly equivalent to ~5.55 km (1° latitude ≈ 111 km) though as transects were not directly north to south value will be higher than this) as a random factor there is still a significant interaction between daynight and latitude.

Recalculating the estimated marginal means the results are fairly similar:

```
aov.result_corrected.s <- as.data.table(emmeans(aov.result_corrected, "day
night", "lat_bin1", nesting=NULL))
```

```
> aov.result_corrected.s
  daynight lat_bin1   emmean      SE      df  lower.CL  upper.CL
1:    day  (52,53]  0.6746815 0.08452752 30.867802 0.5022565 0.8471064
2:   night (52,53]  0.8410199 0.06280064  9.447244 0.6999736 0.9820662
3:    day  (53,54]  0.7165869 0.05897981  7.362738 0.5785026 0.8546711
4:   night (53,54]  0.8108929 0.06066942  8.241061 0.6716981 0.9500877
5:    day  (54,55]  0.7039003 0.05745894  6.637654 0.5665134 0.8412872
6:   night (54,55]  0.8148141 0.07381580 18.038460 0.6597565 0.9698716
7:    day  (55,56]  0.5753795 0.05908202  7.418666 0.4372553 0.7135038
8:   night (55,56]  0.7937428 0.05822203  6.996884 0.6560571 0.9314284
9:    day  (56,57]  0.7803222 0.05789177  6.839385 0.6427755 0.9178689
10:  night (56,57]  0.8327212 0.05939220  7.575430 0.6944148 0.9710275
11:   day  (57,58]  0.8119732 0.05777522  6.785000 0.6744740 0.9494723
12:  night (57,58]  0.8294248 0.06300055  9.588791 0.6882306 0.9706191
13:   day  (58,59]  1.0073820 0.05814508  6.960170 0.8697310 1.1450329
14:  night (58,59]  0.9579110 0.05937976  7.569928 0.8196150 1.0962070
15:   day  (59,60]  0.8660556 0.05791168  6.849370 0.7285034 1.0036079
16:  night (59,60]  0.8182679 0.06115314  8.514980 0.6787194 0.9578165
17:   day  (60,61]  0.6127166 0.06327962  9.729797 0.4711883 0.7542449
18:  night (60,61]  0.6479693 0.09012296 39.852991 0.4658031 0.8301355
```

Contrasts and significance estimates for latitudinal day night pairs are then calculated using the pairs() function.

```
> pairs (aov.result_corrected.s)
lat_bin1 = (52,53]:
  contrast      estimate      SE      df t.ratio p.value
day - night -0.1663 0.0638 5491 -2.609 0.0091

lat_bin1 = (53,54]:
  contrast      estimate      SE      df t.ratio p.value
day - night -0.0943 0.0311 2237 -3.034 0.0024

lat_bin1 = (54,55]:
  contrast      estimate      SE      df t.ratio p.value
day - night -0.1109 0.0492 5540 -2.255 0.0241

lat_bin1 = (55,56]:
  contrast      estimate      SE      df t.ratio p.value
day - night -0.2184 0.0230 5587 -9.506 <.0001

lat_bin1 = (56,57]:
  contrast      estimate      SE      df t.ratio p.value
day - night -0.0524 0.0230 5529 -2.278 0.0228

lat_bin1 = (57,58]:
  contrast      estimate      SE      df t.ratio p.value
day - night -0.0175 0.0306 5551 -0.571 0.5681

lat_bin1 = (58,59]:
  contrast      estimate      SE      df t.ratio p.value
```

Chapter 3 Supplementary material

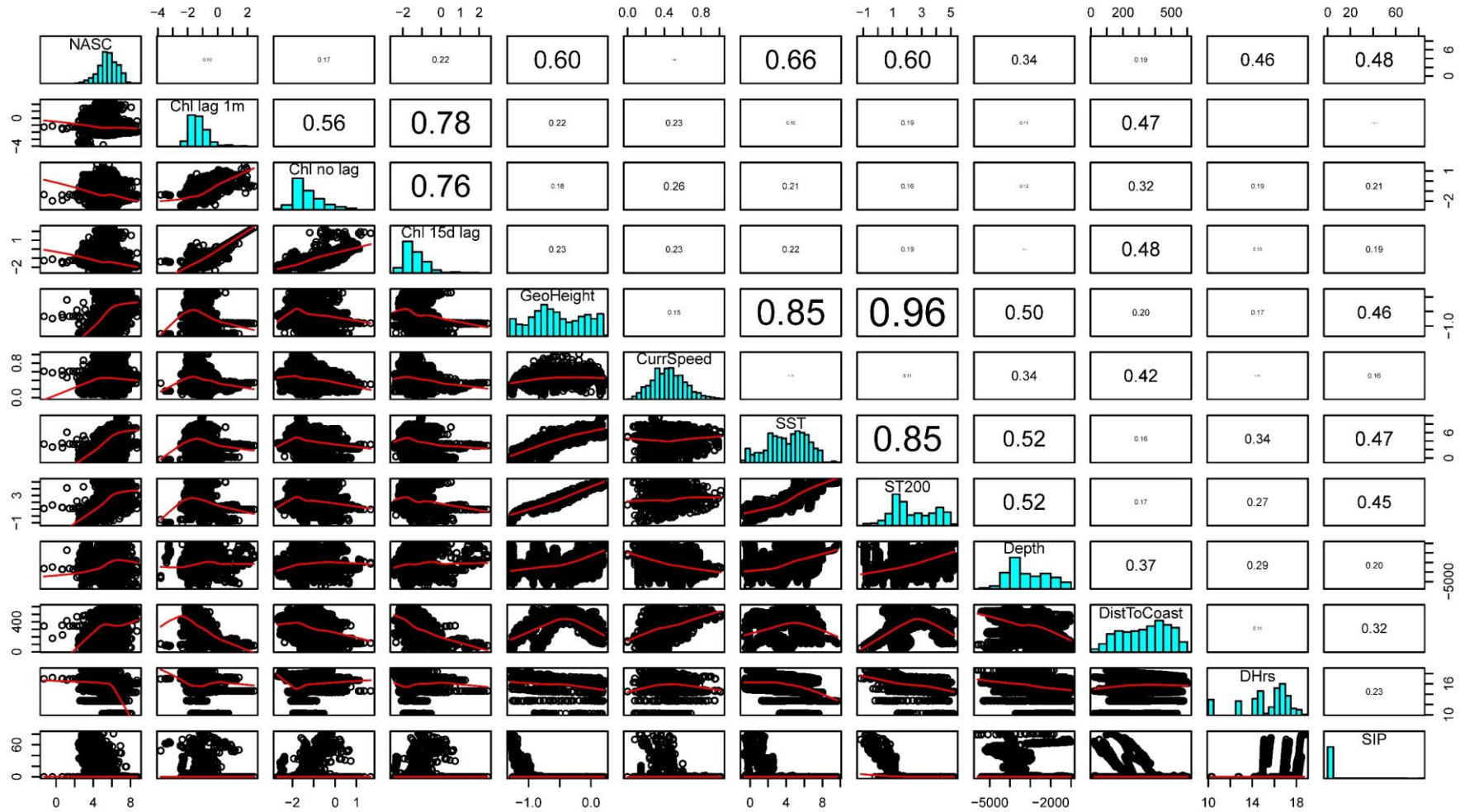
```
day - night    0.0495 0.0233 5480  2.123  0.0338
```

```
lat_bin1 = (59,60]:
```

```
contrast      estimate      SE    df t.ratio p.value  
day - night    0.0478 0.0268 5511  1.786  0.0741
```

```
lat_bin1 = (60,61]:
```

```
contrast      estimate      SE    df t.ratio p.value  
day - night   -0.0353 0.0695 5579 -0.507  0.6118
```



S.6 Pairplot of response variable \log_e NASC and candidate environmental variables to assess for collinearity. Upper panel contains estimated pairwise correlations, size of font is proportional to absolute value of estimated Pearson correlation coefficients. Lower panel contains scatter plots with LOESS smoother. Diagonal panel contains frequency histograms for data visualisation.

Chapter 3 Supplementary material

S.7 Data used to generate climatologies for backscatter prediction from GAMM

Variable	Units	Months	Years	Original resolution	Original projection	Transformation & processing	Source	Data type
SST	°C	Oct-Apr	2005-2017	0.25° grid	WGS84	No transform applied. Mean SST of all data sets calculated using R package 'data.table'.	World Ocean Atlas 2018, Volume 1 (Locarnini et al., 2018)	.csv
Surface chlorophyll conc.	mg m ⁻³	Oct-Apr	2005-2017	4 km grid	Equidistant Cylindrical	Stack rasters. Calculate mean. Resample to 0.25° WGS84 grid using bilinear interpolation.	Copernicus Marine and Environment Monitoring Service (CMEMS) Products OCEANCOLOUR_GLO_CHL_L4_REP_OBSERVATIONS_009_082 (Gohin et al., 2002, Hu et al., 2012)	.nc
Geostrophic current speed	ms ⁻¹	Oct-Apr	2005-2017	0.25° grid	WGS84	No transform applied. For each of UGO and VGO variables: Stack rasters. Calculate mean. Rotate through 180°. Current speed = sqrt(ugo ² + vgo ²)	Copernicus Marine and Environment Monitoring Service (CMEMS) Products MULTIOBS_GLO_PHY_REP_015_002 (Guinehut et al., 2004, Guinehut et al., 2012, Mulet et al., 2012)	.nc
Sea Ice Percentage	%	Sept	2005-2017	25 km grid	Mercator	Stack rasters. Calculate mean. Assign land and coast values as NA. Reproject to 0.25° WGS84 grid, using bilinear interpolation. Divide all values by 10 to get percentage.	National Snow and Ice Data Centre - Sea Ice Index, Version 3 (Fetterer et al., 2017)	
Daylight hours	hrs	Oct-Apr	NA	NA	WGS84	Calculated in R on a 0.25° WGS84 grid.	Daylight hours calculated using R package 'geosphere' daylength function (Hijmans, 2019)	.csv
Depth	m	NA	NA	0.004166'° grid	WGS84	Resample to 0.25° WGS84 grid using bilinear interpolation.	GEBCO_2019 15 arc-second grid (GEBCO Compilation Group, 2019)	.nc
Distance to coast	km	NA	NA	NA	WGS84	Align with Scotia Sea latitude +proj=eqdc +lat_1=-62.666666666666664 +lat_2=-49.333333333333336 +lon_0=-50	Natural Earth - ne_10m_coastline (Version 4.1). Distance calculated using R package 'rgeos' gDistance function (Bivand and Rundel, 2018)	.shp

S.8 GAMM Results

Full GAMM model with autoregressive correlation structure of order 1 (corAR1)

Family: scaled t

Link function: identity

Formula:

$$\log\text{NASC} \sim s(\log\text{ChlorA_m_14daylag}, k = 3) + s(\text{sqrt_current_ms}, k = 3) + s(\text{sst_centigrade}, k = 3) + s(\text{gebco_depth_m}, k = 3) + s(\text{dist_to_coast_km}, k = 3) + s(\text{hours_light}, k = 3) + s(\text{MaxSeaIce_Perc}, k = 3) + \text{daynight}$$

Parametric coefficients:

	Estimate	Std. Error	t value	Pr(> t)
(Intercept)	5.57007	0.01772	314.42	<2e-16 ***
daynight	0.05534	0.03008	1.84	0.0658 .

Approximate significance of smooth terms:

	edf	Ref.df	F	p-value
s(logChlorA_m_14daylag)	1.941	1.941	9.294	6.80e-05 ***
s(sqrt_current_ms)	1.954	1.954	10.311	4.96e-05 ***
s(sst_centigrade)	1.987	1.987	283.570	< 2e-16 ***
s(gebco_depth_m)	1.000	1.000	3.773	0.0521 .
s(dist_to_coast_km)	1.000	1.000	50.986	9.82e-13 ***
s(hours_light)	1.991	1.991	168.655	< 2e-16 ***
s(MaxSeaIce_Perc)	1.499	1.499	97.388	< 2e-16 ***

Signif. codes: 0 '***' 0.001 '**' 0.01 '*' 0.05 '.' 0.1 ' ' 1

R-sq.(adj) = 0.577 Scale est. = 1.1699 n = 12227

Final SST, Daylight Hours and Sea Ice percentage GAMM (with corAR1)

Family: scaled t

Link function: identity

Formula:

$$\log\text{NASC} \sim s(\text{sst_centigrade}, k = 3) + s(\text{hours_light}, k = 3) + s(\text{MaxSeaIce_Perc}, k = 3)$$

Parametric coefficients:

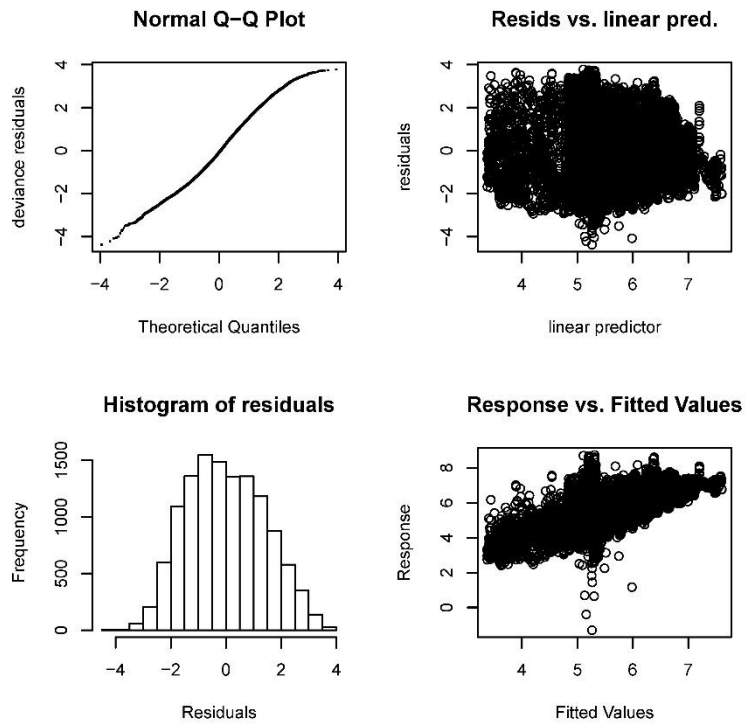
	Estimate	Std. Error	t value	Pr(> t)
(Intercept)	5.58776	0.01525	366.3	<2e-16 ***

Approximate significance of smooth terms:

	edf	Ref.df	F	p-value
s(sst_centigrade)	1.980	1.980	364.9	<2e-16 ***
s(hours_light)	1.988	1.988	150.5	<2e-16 ***
s(MaxSeaIce_Perc)	1.448	1.448	127.9	<2e-16 ***

Signif. codes: 0 '***' 0.001 '**' 0.01 '*' 0.05 '.' 0.1 ' ' 1

R-sq.(adj) = 0.556 Scale est. = 1.2332 n = 12227



S8.1 GAMM check results. Model checking plots of final GAMM, reveal some outlying residuals. However, the model is deemed acceptable, as whilst the model may occasionally over predict backscatter the vast majority of the residuals conform to normality.

Chapter 3 Supplementary material

All GAMMs were specified as ‘scaled t’ with identity link function and autoregressive correlation structure of order 1.

Significance codes: ‘***’ <0.001, ‘**’ <0.01, ‘*’ <0.05, ‘.’ <0.1, ‘NS’ ≥0.1

Full GAMM

Formula: $\log\text{NASC} \sim s(\log\text{ChlorA_m_14daylag}, k = 3) + s(\text{sqrt_current_ms}, k = 3) + s(\text{sst_centigrade}, k = 3) + s(\text{gebco_depth_m}, k = 3) + s(\text{dist_to_coast_km}, k = 3) + s(\text{hours_light}, k = 3) + s(\text{MaxSeaIce_Perc}, k = 3) + \text{daynight}$

Response variable	Explanatory variable	Parametric coefficient				Non-parametric smoothers		
		Estimate	S.E.	t	P	edf	F	P
Log NASC	Intercept	5.570	0.018	314.42	***			
	Daynight night	0.055	0.030	1.84	.			
	s(logChlorA_m_14daylag)					1.941	9.29	***
	s(sqrt_current_ms)					1.954	10.31	***
	s(sst_centigrade)					1.987	283.57	***
	s(gebco_depth_m)					1.000	3.77	.
	s(dist_to_coast_km)					1.000	50.99	***
	s(hours_light)					1.991	168.66	***

Full GAMM excluding day night

Formula: $\log\text{NASC} \sim s(\log\text{ChlorA_m_14daylag}, k = 3) + s(\text{sqrt_current_ms}, k = 3) + s(\text{sst_centigrade}, k = 3) + s(\text{gebco_depth_m}, k = 3) + s(\text{dist_to_coast_km}, k = 3) + s(\text{MaxSeaIce_Perc}, k = 3)$

Response variable	Explanatory variable	Parametric coefficient				Non-parametric smoothers		
		Estimate	S.E.	t	P	edf	F	P
Log NASC	Intercept	5.589	0.014	387.10	***			
	s(logChlorA_m_14daylag)					1.939	9.27	***
	s(sqrt_current_ms)					1.951	9.52	***
	s(sst_centigrade)					1.987	288.19	***
	s(gebco_depth_m)					1.000	3.70	.
	s(dist_to_coast_km)					1.000	54.09	***
	s(hours_light)					1.992	187.86	***
	s(MaxSeaIce_Perc)					1.175	127.57	***

Chapter 3 Supplementary material

Full GAMM excluding surface chlorophyll

Formula: $\log\text{NASC} \sim s(\text{sqrt_current_ms}, k = 3) + s(\text{sst_centigrade}, k = 3) + s(\text{gebco_depth_m}, k = 3) + s(\text{dist_to_coast_km}, k = 3) + s(\text{hours_light}, k = 3) + s(\text{MaxSealce_Perc}, k = 3) + \text{daynight}$

Response variable	Explanatory variable	Parametric coefficient				Non-parametric smoothers		
		Estimate	S.E.	t	P	edf	F	P
Log NASC	Intercept	5.570	0.018	310.34	***			
	Daynight night	0.056	0.030	1.83	.			
	s(sqrt_current_ms)					1.949	8.98	***
	s(sst_centigrade)					1.985	269.57	***
	s(gebco_depth_m)					1.000	2.74	.
	s(dist_to_coast_km)					1.327	39.66	***
	s(hours_light)					1.990	166.33	***
	s(MaxSealce_Perc)					1.504	98.47	***

Full GAMM excluding water depth

Formula: $\log\text{NASC} \sim s(\log\text{ChlorA_m_14daylag}, k = 3) + s(\text{sqrt_current_ms}, k = 3) + s(\text{sst_centigrade}, k = 3) + s(\text{dist_to_coast_km}, k = 3) + s(\text{hours_light}, k = 3) + s(\text{MaxSealce_Perc}, k = 3) + \text{daynight}$

Response variable	Explanatory variable	Parametric coefficient				Non-parametric smoothers		
		Estimate	S.E.	t	P	edf	F	P
Log NASC	Intercept	5.571	0.018	313.97	***			
	Daynight night	0.054	0.030	1.81	.			
	s(logChlorA_m_14daylag)					1.939	8.81	***
	s(sqrt_current_ms)					1.954	10.27	***
	s(sst_centigrade)					1.987	414.04	***
	s(dist_to_coast_km)					1.000	48.10	***
	s(hours_light)					1.991	166.85	***
	s(MaxSealce_Perc)					1.573	95.46	***

Chapter 3 Supplementary material

Full GAMM excluding distance to coast

Formula: $\log\text{NASC} \sim s(\log\text{ChlorA_m_14daylag}, k = 3) + s(\text{sqrt_current_ms}, k = 3) + s(\text{sst_centigrade}, k = 3) + s(\text{gebco_depth_m}, k = 3) + s(\text{hours_light}, k = 3) + s(\text{MaxSealce_Perc}, k = 3) + \text{daynight}$

Response variable	Explanatory variable	Parametric coefficient				Non-parametric smoothers		
		Estimate	S.E.	t	P	edf	F	P
Log NASC	Intercept	5.563	0.018	307.42	***			
	Daynight night	0.076	0.031	2.48	*			
	s(logChlorA_m_14daylag)					1.947	10.39	***
	s(sqrt_current_ms)					1.949	10.42	***
	s(sst_centigrade)					1.983	298.96	***
	s(gebco_depth_m)					1.600	1.93	NS
	s(hours_light)					1.989	138.47	***
	s(MaxSealce_Perc)					1.787	96.25	***

Full GAMM excluding geostrophic current speed

Formula: $\log\text{NASC} \sim s(\log\text{ChlorA_m_14daylag}, k = 3) + s(\text{sst_centigrade}, k = 3) + s(\text{gebco_depth_m}, k = 3) + s(\text{dist_to_coast_km}, k = 3) + s(\text{hours_light}, k = 3) + s(\text{MaxSealce_Perc}, k = 3) + \text{daynight}$

Response variable	Explanatory variable	Parametric coefficient				Non-parametric smoothers		
		Estimate	S.E.	t	P	edf	F	P
Log NASC	Intercept	5.573	0.018	311.11	***			
	Daynight night	0.046	0.030	1.53	NS			
	s(logChlorA_m_14daylag)					1.931	8.01	***
	s(sst_centigrade)					1.987	279.77	***
	s(gebco_depth_m)					1.000	4.33	*
	s(dist_to_coast_km)					1.000	51.47	***
	s(hours_light)					1.992	161.76	***
	s(MaxSealce_Perc)					1.000	156.94	***

Chapter 3 Supplementary material

Full GAMM excluding daylight hours

Formula: $\log\text{NASC} \sim s(\log\text{ChlorA_m_14daylag}, k = 3) + s(\text{sqrt_current_ms}, k = 3) + s(\text{sst_centigrade}, k = 3) + s(\text{gebco_depth_m}, k = 3) + s(\text{dist_to_coast_km}, k = 3) + s(\text{MaxSeaIce_Perc}, k = 3) + \text{daynight}$

Response variable	Explanatory variable	Parametric coefficient				Non-parametric smoothers		
		Estimate	S.E.	t	P	edf	F	P
Log NASC	Intercept	5.525	0.021	267.57	***			
	Daynight night	0.180	0.034	5.36	***			
	s(logChlorA_m_14daylag)					1.916	9.65	**
	s(sqrt_current_ms)					1.865	3.08	*
	s(sst_centigrade)					1.972	231.61	***
	s(gebco_depth_m)					1.694	1.07	NS
	s(dist_to_coast_km)					1.342	2.57	NS
	s(MaxSeaIce_Perc)					1.769	68.52	***

Full GAMM excluding sea ice percent

Formula: $\log\text{NASC} \sim s(\log\text{ChlorA_m_14daylag}, k = 3) + s(\text{sqrt_current_ms}, k = 3) + s(\text{sst_centigrade}, k = 3) + s(\text{gebco_depth_m}, k = 3) + s(\text{dist_to_coast_km}, k = 3) + s(\text{hours_light}, k = 3) + \text{daynight}$

Response variable	Explanatory variable	Parametric coefficient				Non-parametric smoothers		
		Estimate	S.E.	t	P	edf	F	P
Log NASC	Intercept	5.570	0.019	291.96	***			
	Daynight night	0.053	0.032	1.64	NS			
	s(logChlorA_m_14daylag)					1.950	10.54	***
	s(sqrt_current_ms)					1.955	11.48	***
	s(sst_centigrade)					1.889	311.85	***
	s(gebco_depth_m)					1.000	7.78	**
	s(dist_to_coast_km)					1.626	43.51	***
	s(hours_light)					1.983	176.48	***

Chapter 3 Supplementary material

Table of all GAMMs run, AIC, BIC and adjusted R² values.

Model name	Model specification	AIC	BIC	R ² Adj.
Full GAMM	logNASC ~ s(logChlorA_m_14daylag, k = 3) + s(sqrt_current_ms, k = 3) + s(sst_centigrade, k = 3) + s(gebco_depth_m, k = 3) + s(dist_to_coast_km, k = 3) + s(hours_light, k = 3) + s(MaxSealce_Perc, k = 3) + daynight	16008.49	16141.90	0.577
Full GAMM - Chl	logNASC ~ s(sqrt_current_ms, k = 3) + s(sst_centigrade, k = 3) + s(gebco_depth_m, k = 3) + s(dist_to_coast_km, k = 3) + s(hours_light, k = 3) + s(MaxSealce_Perc, k = 3) + daynight	16022.41	16141.00	0.573
Full GAMM - GeoCurr	logNASC ~ s(logChlorA_m_14daylag, k = 3) + s(sst_centigrade, k = 3) + s(gebco_depth_m, k = 3) + s(dist_to_coast_km, k = 3) + s(hours_light, k = 3) + s(MaxSealce_Perc, k = 3) + daynight	16021.52	16140.10	0.571
Full GAMM - SST	logNASC ~ s(logChlorA_m_14daylag, k = 3) + s(sqrt_current_ms, k = 3) + s(gebco_depth_m, k = 3) + s(dist_to_coast_km, k = 3) + s(hours_light, k = 3) + s(MaxSealce_Perc, k = 3) + daynight	16461.58	16580.17	0.455
Full GAMM - Depth	logNASC ~ s(logChlorA_m_14daylag, k = 3) + s(sqrt_current_ms, k = 3) + s(sst_centigrade, k = 3) + s(dist_to_coast_km, k = 3) + s(hours_light, k = 3) + s(MaxSealce_Perc, k = 3) + daynight	16008.25	16126.83	0.577

Chapter 3 Supplementary material

Table of all GAMMs run, AIC, BIC and adjusted R² values (continued).

Model name	Model specification	AIC	BIC	R ² Adj.
Full GAMM - DistToCoast	logNASC ~ s(logChlorA_m_14daylag, k = 3) + s(sqrt_current_ms, k = 3) + s(sst_centigrade, k = 3) + s(gebco_depth_m, k = 3) + s(hours_light, k = 3) + s(MaxSealce_Perc, k = 3) + daynight	16053.30	16171.88	0.569
Full GAMM - DHr	logNASC ~ s(logChlorA_m_14daylag, k = 3) + s(sqrt_current_ms, k = 3) + s(sst_centigrade, k = 3) + s(gebco_depth_m, k = 3) + s(dist_to_coast_km, k = 3) + s(MaxSealce_Perc, k = 3) + daynight	16302.37	16420.95	0.505
Full GAMM - SIP	logNASC ~ s(logChlorA_m_14daylag, k = 3) + s(sqrt_current_ms, k = 3) + s(sst_centigrade, k = 3) + s(gebco_depth_m, k = 3) + s(dist_to_coast_km, k = 3) + s(hours_light, k = 3) + daynight	16144.20	16262.78	0.545
Full GAMM - DayNight	logNASC ~ s(logChlorA_m_14daylag, k = 3) + s(sqrt_current_ms, k = 3) + s(sst_centigrade, k = 3) + s(gebco_depth_m, k = 3) + s(dist_to_coast_km, k = 3) + s(hours_light, k = 3) + s(MaxSealce_Perc, k = 3)	16009.78	16135.77	0.577
SST only GAMM	logNASC ~ s(sst_centigrade, k = 3)	16457.11	16494.16	0.437
DHr only GAMM	logNASC ~ s(hours_light, k = 3)	16879.02	16916.08	0.211
SIP only GAMM	logNASC ~ s(MaxSealce_Perc, k = 3)	16846.36	16883.41	0.242
SST, DHr and SIP GAMM	logNASC ~ s(sst_centigrade, k = 3) + s(hours_light, k = 3) + s(MaxSealce_Perc, k = 3)	16077.38	16144.09	0.556

Chapter 4

How many fish are in the Scotia Sea?

An acoustic biomass estimate of
mesopelagic fish

4.1 Abstract

The oceans mesopelagic zone, 200-1000 m below sea level, holds vast resources of fish. These typically small yet abundant fishes play important roles in biogeochemical cycling, are prey for charismatic and commercially important higher predators, and are of interest for future exploitation to meet humanities growing needs. Despite a recent increase in research focussed on the ecology of mesopelagic fish of the Southern Ocean, they remain one of the least investigated components of the Antarctic ecosystem. Sampling challenges have led to considerable uncertainty regarding the magnitude of mesopelagic fish resources and this limits our ability to monitor fish populations or quantify their contribution to ecosystem function. This study aims to derive a mesopelagic fish biomass estimate for the Scotia Sea and wider Southern Ocean, using a combination of catch data from net sampling, target strength modelling of important Scotia Sea mesopelagic fish species, and models of broad-scale patterns of acoustic backscatter. The results indicate that the Scotia Sea mesopelagic fish assemblage has an estimated biomass of 51.75 Mt, and Southern Ocean biomass estimate of 703.76 Mt, which are considerably higher than previous net-based estimates. In addition, the model predicts a relatively high proportion of mesopelagic fish biomass in colder polar waters, which non-groundtruthed acoustic surveys are likely to overlook. This study highlights the importance of validating acoustic data with knowledge of the species present and their unique backscattering properties.

4.2 Introduction

Mesopelagic fish inhabit the twilight zone of the world's oceans, 200 m to 1000 m below sea level. These typically small (<20 cm) fish are the most abundant vertebrates on earth, and their communities are often dominated by lanternfish (family Myctophidae) in terms of number and biomass (Gjøsaeter and Kawaguchi, 1980). Mesopelagic fish play a vital role in biogeochemical cycling through extensive diel vertical migration, where large proportions of the community ascend into nutrient rich surface waters to feed under the cover of darkness, before returning to the relative safety of deeper darker water during daylight (Brierley, 2014). In the Southern Ocean myctophids are a key prey item of many charismatic higher predators, including king penguins *Aptenodytes patagonicus* (Duhamel, 1998), Antarctic fur seals *Arctocephalus gazelle* (Lea et al., 2002) and elephant seals *Mirounga leonina* (Cherel et al., 2008, Guinet et al., 2014). They are also an important component of the diet of the commercially-important Patagonian toothfish *Dissostichus eleginoides* (Collins et al., 2007).

While past forays into commercial exploitation of mesopelagic fish have been undertaken with varying degrees of success and viability (FAO, 1997, Valinassab et al., 2007, FAO, 2019), there has been a renewed interest in the opportunities the mesopelagic zone has to offer, as we consider new ways to sustainably meet the needs of our ever growing human population (St. John et al., 2016, European Commission, 2018). However, there is considerable uncertainty regarding the abundance and biomass of mesopelagic fishes, both globally and in the Southern Ocean. This limits our ability to fully comprehend both the extent of the role mesopelagic fish play in ecosystem functioning and carbon sequestration, and their potential as an exploitable resource.

Traditional net sampling provides valuable data on species community composition, life history, and the relative abundance of Southern Ocean mesopelagic fishes. However, patchy species distributions, net avoidance behaviour and the limited spatial and temporal coverage of net sampling all contribute to uncertainty when estimating mesopelagic fish biomass (Kaartvedt et al., 2012, Warren, 2012). Globally net-based biomass estimates for mesopelagic fish stand at ~1000 million tonnes (Gjøsaeter and Kawaguchi, 1980). However, acoustic studies suggest actual biomass may be at least an order of magnitude higher (Gjøsaeter and Kawaguchi, 1980, Irigoien et al., 2014). Within the highly productive Scotia Sea region of the Southern Ocean, net sampling provides a conservative myctophid biomass estimate of 4.5 million tonnes (Collins et al., 2012). Southern Ocean mesopelagic fish biomass estimates are in the region of 70 to 191 million tonnes (Lancraft et al., 1989).

In contrast to net sampling, active underwater acoustics provides us with the ability to collect open-ocean data of unrivalled spatial and temporal resolution, with acoustic transects spanning ocean basins and data collection possible throughout the mesopelagic zone using frequencies of 38 kHz and below (Kloser et al., 2009). Analysis of acoustic data has revealed a decrease in backscatter towards the pole (Proud et al., 2017, Dornan et al., 2019), concurrent with a change in mesopelagic fish community composition (Escobar-Flores et al., 2018b, Dornan et al., 2019). This poleward change in community is likely to contribute to the reduction in acoustic signal, as the dominant species in colder high latitude waters tend to lose the highly reflective gas component in their swimbladder, making them weak acoustic targets (Dornan et al., 2019).

To interpret acoustic data and realistically monitor the pelagic community, we require data on biological community composition, habitat occupation and the scattering properties

of species present (Simmonds and MacLennan, 2005, Davison, 2011). Taxon-specific metrics such as swimbladder gas component and tissue density are required to model the acoustic backscatter properties or 'Target Strength' (TS) of species, which is crucial for estimating abundance and biomass. However, absence of such data for Antarctic mesopelagic fish has hampered our ability to develop such species-specific backscatter models. Moreover, a detailed knowledge of intraspecific changes in morphology can be important, as some Southern Ocean mesopelagic fish species have a high degree of swimbladder variability with some losing the gas component in adulthood (Marshall, 1960, Dornan et al., 2019). Since the gas in a swimbladder can account for up to 95% of the backscatter from a fish (Foote, 1980b), the loss of gas with increasing body size results in a non-linear effect in a species' backscattering response, where larger fish may return a considerably lower acoustic signal than smaller gas-bearing individuals. Partitioning the observed acoustic backscatter among species is therefore clearly necessary to realistically interpret acoustic data and derive biomass estimates.

Using a combination of active acoustics and net derived data this study aims to produce a biomass estimate for mesopelagic fish in the Scotia Sea and wider Southern Ocean, to facilitate ecosystem modelling and inform management and monitoring of key mesopelagic fish resources. First, taxon-specific estimates of TS are made for key Southern Ocean mesopelagic fish species, using information on tissue density and swimbladder gas presence/absence. Second, environmental climatologies are used to predict large-scale patterns of acoustic backscatter for the Southern Ocean. Third, net catch data is used to identify and assign the proportions of acoustic backscatter observed to specific mesopelagic fish taxa. Finally, using these apportioned backscatter data, I estimate biomass of mesopelagic fish in both the Scotia Sea and Southern Ocean.

4.3 Methods

4.3.1 Net sampling

Depth-stratified (surface to 1000 m) RMT25 net sampling of the Scotia Sea mesopelagic fish community was undertaken aboard the RRS James Clark Ross. Fish were sampled on five cruises, between 2006 and 2017 (Supplement S.1), at locations spanning the major fronts and water masses of the Scotia Sea (see Dornan et al., 2019). On early cruises (JR161 and JR177) fish were sampled day and night at each location, but sampling was subsequently restricted to night-time only (JR200, JR15004 and JR16003), as daylight net avoidance was assumed to be responsible for reduced catches (Collins et al., 2012). To remove bias from daytime net avoidance, only stratified night-time RMT25 nets data were used in the statistical analysis of species abundance (see Fig. 4.1 for locations, Supplement S.1). All net sample data was standardised for tow speed and duration prior to statistical analysis. Once fish were brought on-board, whenever possible total catch weight and standard length to the nearest mm were recorded. Fish were then taken for further measurements or were frozen at -20°C for future analysis.

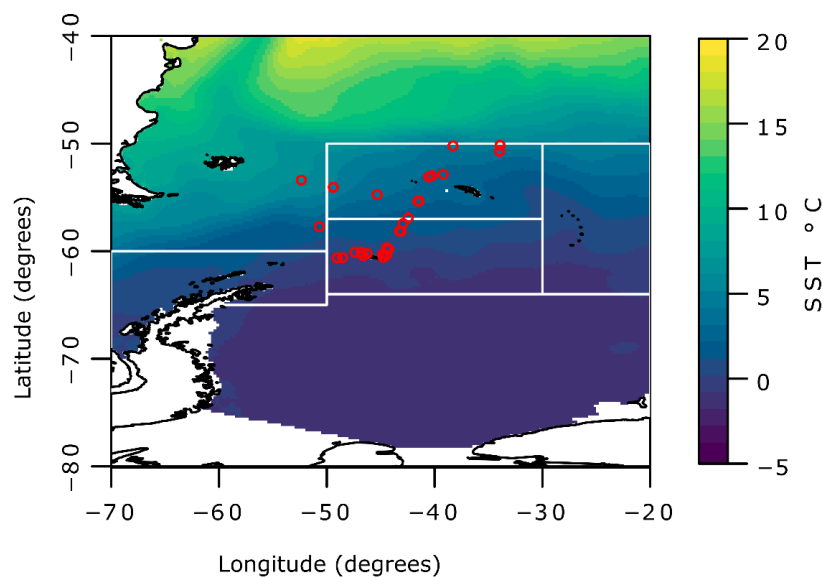


Figure 4.1 Location of night-time RMT25 net samples (red circles), used in assessment of relative abundance of mesopelagic fish taxa in relation to sea surface temperature in the Scotia Sea. Projection WGS84, produced in R version 3.5.1. Sea surface temperature (SST) climatology covers months of Oct-Apr, 2005-2017, from World Ocean Database (Locarnini et al., 2018). White boxes indicate Commission for the Conservation of Antarctic Marine Living Resources (CCAMLR) area 48 boundaries.

4.3.2 Fish properties for TS modelling

4.3.2.1 Samples analysed

Whole specimens were analysed from both day and night RMT25 net samples, plus one full depth net sample (JR16003, event 112). These specimens were used for measuring tissue density, establishing length-frequency distributions, and determining length-weight relationships. To ensure the widest possible number of species were available for tissue density experiments during cruise JR16003, additional fish were sampled from RMT8 and MOCNESS nets (see Supplement S.2). The analyses focussed on 11 taxa that collectively dominate the mesopelagic fish fauna of the Scotia Sea (Dornan et al. 2019; Table 4.1).

Table 4.1 Overview of fish taxa included in mesopelagic fish biomass assessment. Gas status source: [1] Dornan et al. (2019). [2] Marshall (1960), [3] Post (1990). Current study: ✓ indicates new data collected and/or analysed during this study's assessment of fish acoustic properties, 'Est.' indicates value was estimated from current study data, 'Lit.' indicates value was derived from literature. Where ρ_f is fish tissue density and equivalent spherical radius of gas volume for neutral buoyancy, LW_{reg} is Length-Weight regression, LW_{rat} is Length-Width ratio, TS is target strength model.

Family	Taxon	Swimbladder gas [source]	Current study			
			ρ_f	LW_{reg}	LW_{rat}	TS
Myctophidae	<i>Electrona antarctica</i>	< 51.378 mm – Gas [1]	✓	✓	✓	✓
		≥ 51.378 mm – No gas [1]	✓	✓	✓	✓
	<i>Electrona carlsbergi</i>	Gas [1]	✓	✓	✓	✓
	<i>Gymnoscopelus braueri</i>	Regressed – No gas [1]	✓	✓	✓	✓
	<i>Gymnoscopelus fraseri</i>	Regressed – No gas [1]	✓	✓	✓	✓
	<i>Gymnoscopelus nicholsi</i>	Regressed – No gas [1]	Est.	✓	✓	✓
	<i>Protomyctophum bolini</i>	Gas [1]	✓	✓	✓	✓
	<i>Protomyctophum tenisoni</i>	Gas [2]	Est.	✓	✓	✓
	<i>Krefflichthys anderssoni</i>	Gas [1]	✓	✓	✓	✓
Bathylagidae	<i>Bathylagus</i> spp.	No swimbladder – No gas [2]	✓	✓	✓	✓
Gonostomatidae	<i>Cyclothone</i> spp.	Fat invested – No gas [2]	Est.	✓	Est.	✓
Paralepididae	<i>Notolepis</i> spp.	No swimbladder – No gas [3]	Est.	Lit.	Est.	✓

4.3.2.2 Tissue density measurements

During cruise JR16003, the specific gravity (ratio of density relative to freshwater) of 81 fish from seven species was measured (Supplement S.2), following a modified density bottle method (Davison, 2011, Dornan, 2017). In preparation for analyses, solutions of glycerol (98%, extra pure; Fisher) and seawater were initially mixed at room temperature (~18/19°C), in 0.0025 specific gravity unit increments ranging from 1.025 to 1.090 using hydrometers (precision 0.002). Solutions were then chilled, along with a batch of filtered seawater, to cold room temperature (4°C ± 1°C), where specific gravity was re-recorded.

As soon as possible after capture, fish were retained on ice and standard length was recorded to the nearest mm, before being transferred to the cold room at ~4°C. Fish were dissected underwater to release any gas in the swimbladder and body cavity. Fish were then placed sequentially from low density to higher density glycerol-seawater solutions to determine the point of neutral buoyancy and fish specific gravity. When a fish was neutrally buoyant, the solution code was recorded. Alternatively, neutral buoyancy was calculated as the average of the specific gravity of the last solution the fish sank in and the first one in which it floated. Fish were then rinsed in seawater and gently blotted to remove excess water prior to being placed in individually labelled zip-lock bags for storage at -20°C. Mid-way through the experiment, solutions were checked and corrected for any change in specific gravity due to evaporation or dilution, and were found to be within ±0.0025 units. Specific gravity of fish tissue was converted to density g ml⁻¹ at 4°C, using equations derived from hydrometer calibration (see Supplement S.3 for hydrometer calibration).

Linear regression was used to test for relationships between fish standard length and tissue density. As not all fish length-density relationships were significant, the mean density of each taxon was used in all TS calculations. As no density measurements were taken for *Gymnoscopelus nicholsi*, *Notolepis* spp. and *Cyclothone* spp., their density was assigned as the mean of the three non-gas bearing species mean densities (*Bathylagus* spp., *Gymnoscopelus braueri* and *Gymnoscopelus fraseri*). Gas-bearing *Protomyctophum tenisoni* was assigned the mean density of the three gas-bearing species (*Protomyctophum bolini*, *Electrona carlsbergi* and *Krefflichthys anderssoni*).

4.3.2.3 Standard length and length to width ratio

Standard length data for all eleven study taxa was taken from all RMT25 day and night nets during cruises JR161, JR177, JR200, JR15004 and JR16003 (Supplement S.1). Length-width ratio was derived using laboratory measurements from cruises JR161, JR177 and JR200, for all species with the exception of *Bathylagus* spp., which was measured from digital photographs taken immediately after capture, and *Notolepis* spp. and *Cyclothone* spp., which were assigned the mean Length-Width ratio of all nine other taxa in the study.

4.3.2.4 Wet weight and length weight regressions

Frozen fish were weighed, and with the exception of *Notolepis* spp., length-weight regressions were calculated for each of the study taxa from RMT25 day and night stratified net data (see Supplement S.4 for results). The following equation was used to convert standard length (SL in mm) to biomass (wet weight *WW* in g).

$$WW = a SL^b \quad 4.1$$

For *Notolepis* species, length-weight regression parameters were taken from FishBase (*Notolepis coatsi*) (Froese et al., 2014). Standard length was first converted from SL in mm to total length (TL) in cm, using the conversion factor for the closely-related *Arctozenus risso* (Froese and Pauly, 2019), where:

$$TL = \frac{SL}{10 \times 1.065} \quad 4.2$$

4.3.2.5 Fish swimbladder gas volume

Estimation of the TS of a gas-bearing swimbladder fish requires knowledge of the size of the swimbladder. Following Davison (2011) fish wet weight (g) and density values (g ml⁻¹) were used to calculate the theoretical equivalent gas volume (EGV in ml, equation 4.3) that would be required for a fish to achieve neutral buoyancy in the density of surrounding seawater at atmospheric pressure. Gas volume was calculated at atmospheric pressure, as fish densities were measured at atmospheric pressure, and it is assumed that the same gas volume will be maintained at depth (Benoit-Bird et al., 2003). EGV was then converted to equivalent spherical radius (ESR in mm, equation 4.4) of gas-bearing fish species (Table 4.1).

$$EGV = WW_f \times \left(\frac{1}{\rho_{sw}} - \frac{1}{\rho_f} \right) \quad 4.3$$

$$ESR = \left(\left(3 \frac{EGV}{4\pi} \right)^{\frac{1}{3}} \right) \times 10 \quad 4.4$$

Where, WW_f is wet weight of fish in g, ρ_{sw} and ρ_f are density of seawater and fish tissue in g ml^{-1} respectively. Density of surrounding seawater was estimated as the mean total water column (surface to 1000 m) density from the nearest JR16003 Conductivity Temperature Depth (CTD, Sea-Bird SBE911Plus) sample to the net sample location (Supplement S.2).

4.3.3 Modelling fish TS

The TS ($\text{dB re } 1\text{m}^2$) for each of the eleven mesopelagic fish taxa was modelled using either a finite cylinder model for non-gas bearing fish or the prolate spheroid model for fish with a gas-filled swimbladder. The prolate spheroid model was also used to investigate the effect of depth on resonance and backscatter (Andreeva, 1964, Holliday, 1972, Kloser et al., 2002). See Supplement S.5 for resonance results. The TS was modelled for each species using its mean, median, 25th and 75th percentile standard lengths.

4.3.3.1 Finite cylinder model – Non-gas bearing fish

For fish lacking a gas-filled swimbladder, a fixed finite cylinder model was used to calculate TS following (Stanton et al., 1993), equations 4.5 – 4.13, with slight modifications to annotation (see Supplement S.6 for R code used and algebraic transformation). Stanton's (1993) model, originally developed for zooplankton, considers cylinder tapering, is independent of the degree of curvature, and is effective on a range of angles of orientation. Whilst the model is limited when the acoustic wavelength is much smaller than the cross sectional radius of the object being modelled (in this case half the width of the fish body), this was negligible as a 38 kHz frequency wave has a wavelength of ~ 39.5 mm in seawater and the micronekton, which are the focus of this study are typically small animals. Target strength was calculated as:

$$TS = 10 \log_{10}(\sigma_{bs}) \quad 4.5$$

$$\sigma_{bs} = A_{ij} \mathcal{R}_{12}^2 \langle |I_0|^2 \rangle_L \beta^{-1} \bar{L}^2 \quad 4.6$$

$$\langle |I_0|^2 \rangle_L = 2 \{ 1 - \exp[-8(k\bar{a}s)^2] \cos(4k\bar{a} + \mu_{p=2}) \} \quad 4.7$$

$$\beta = \frac{L}{a} \quad 4.8$$

$$k = \frac{2\pi f}{c_{sw}} \quad 4.9$$

$$s = \frac{sL}{\bar{L}} \quad 4.10$$

$$\mathcal{R}_{1,2} = \frac{g \times h - 1}{g \times h + 1} \quad 4.11$$

$$g = \frac{\rho_f}{\rho_{sw}} \quad 4.12$$

$$h = \frac{c_f}{c_{sw}} \quad 4.13$$

Where, σ_{bs} is the acoustic backscattering cross-section in m^2 , k is wave number, f is acoustic frequency in Hz. The reflection coefficient $\mathcal{R}_{1,2}$ is the plane wave/plane interface reflection coefficient between seawater and fish tissue. g is density contrast between fish tissue density and seawater density, where ρ_{sw} and ρ_f are density of seawater and fish tissue in g ml^{-1} respectively, h is sound speed contrast between fish and seawater, c_{sw} and c_f are sound speed ms^{-1} in seawater and fish respectively.

sL is the standard deviation of fish length, L and \bar{L} is standard length and mean standard length of fish, a and \bar{a} are the cross sectional and mean cross sectional radius i.e. half of fish body width. Length-Width ratios were used to calculate radius a from fish length. Constant values were used for $A_{ij} = 0.08$, sound speed of fish tissue $c_f = 1510 \text{ ms}^{-1}$ based on measured c_f for the myctophid *Stenobrachius leucopsarus* at 4°C (Yasuma et al., 2006), s is the relative standard deviation of length (standard deviation of length/length) and was set at 0.1 to minimise nulls (Stanton et al., 1993). Density of seawater ρ_{sw} (1.0274 g ml^{-1}) and speed of sound in seawater c_{sw} (1465.836 ms^{-1}) were estimated from CTD data from the same cruise (JR16003) as the density experiment, which was used to calculate fish ESR (see Supplement S.2).

4.3.3.2 Prolate spheroid model – Gas bearing fish

A prolate spheroid scattering model (Andreeva, 1964, Holliday, 1972, Kloser et al., 2002) was used to calculate TS for the gas component of equivalent spherical radius (ESR) for each of the

five gas-bearing mesopelagic fish species: *Electrona carlsbergi*, small *Electrona antarctica* (< 51.378 mm), *Krefftichthys anderssoni*, *Protomyctophum bolini* and *Protomyctophum tenisoni*. Target strength was calculated as:

$$TS = 10 \log_{10}(\sigma_{bs}) \quad 4.14$$

$$\sigma_{bs} = a_{es}^2 \left(\left(\left(\frac{f_p}{f} \right)^2 - 1 \right)^2 + \frac{1}{Q^2} \right)^{-1} \quad 4.15$$

$$f_p = f_o 2^{\frac{1}{2}} e^{-\frac{1}{3}} (1 - e^2)^{\frac{1}{4}} \left\{ \ln \left(\frac{1 + (1 - e^2)^{\frac{1}{2}}}{1 - (1 - e^2)^{\frac{1}{2}}} \right) \right\}^{-\frac{1}{2}} \quad 4.16$$

$$f_o = \frac{1}{2\pi a_{es}} \left(\frac{3\gamma P + 4\mu_1}{\rho_f} \right)^{\frac{1}{2}} \quad 4.17$$

$$P = (1 + 0.103D)10^5 \quad 4.18$$

Where, σ_{bs} is the acoustic backscattering cross section in m^2 and a_{es} is the equivalent spherical radius (ESR) of gas volume in m. f is acoustic frequency in Hz, f_p and f_o prolate and spherical resonant frequencies respectively, P is hydrostatic pressure in Pascals at fish depth D in metres, ρ_f is fish tissue density in $kg\ m^{-3}$. Prolate spheroid roundness e , is the ratio between minor semi-axis and major semi-axis of gas bubble, this was fixed at 0.3 based on measurements from CT scans of *Krefftichthys anderssoni* (n=4).

Following Holliday (1972) and Kloser (2002), assumed values were used for resonance quality factor $Q = 5$; the real part of the complex shear modulus of fish tissue $\mu_1 = 10^5$ Pa; and the ratio of specific heats for swimbladder gas $\gamma = 1.4$.

4.3.4 Basin scale backscatter, species abundance and biomass prediction

4.3.4.1 Acoustic backscatter estimation

Basin-scale predictions of the NASC (Nautical Area Scattering Coefficient), an acoustically-derived proxy for biomass, were predicted using a generalised additive mixed model (GAMM) approach. The model was derived from sea surface temperature (SST), daylight hours and sea

ice data, which have previously been determined as strong predictors of NASC in the Scotia Sea region (Chapter 3). Environmental climatology data were derived for the period of 2005-2017, and therefore representative of the period during which net samples and acoustic data were collected (JR161 Oct 2006 – JR16003 Jan 2017). SST data (Locarnini et al., 2018) and mean daylight hours covered the period from Oct-Apr. Mean sea ice concentration data (Fetterer et al., 2017), covered the month of September when peak sea ice occurs. NASC was predicted for the Southern Ocean in 0.25° lat-lon grid cells using a GAMM trained on six years of \log_e transformed NASC using the R package ‘mgcv’ (Wood, 2019; Chapter 3). The predict.gam function was then used to project the model to basin scale (Figure 4.2), and predicted NASC data were back-transformed prior to abundance calculations. Data processing flow, from net and environmental data to biomass estimation, is summarised in Figure 4.3.

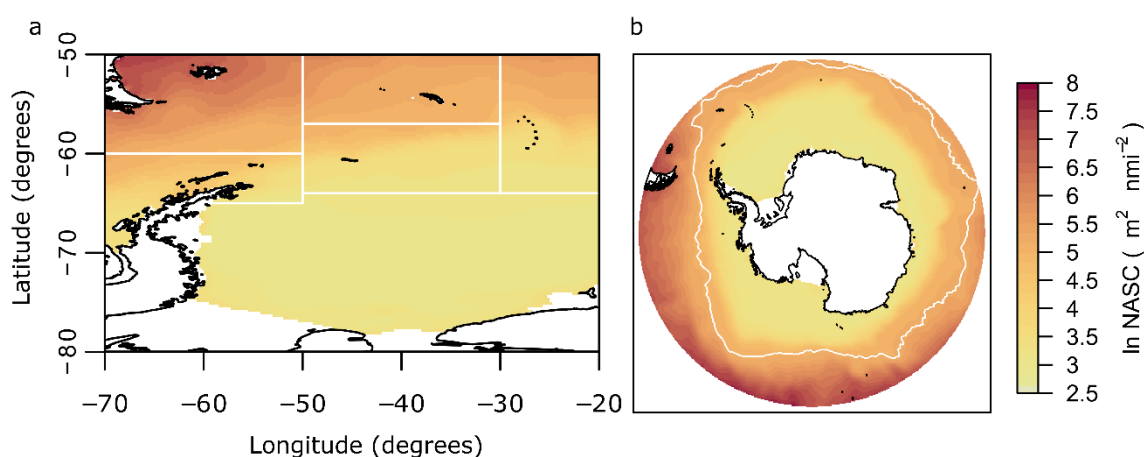


Figure 4.2 (a) Predicted \log_e NASC for Scotia Sea. CCAMLR areas bounded by white boxes. (b) Southern ocean \log_e NASC, white line indicates approximate mean position of the Polar Front (PF).

4.3.4.2 Determining fish community composition across the basin.

The proportion of each of the eleven key fish taxa in each 0.25° cell, was assigned as follows. Each net sample was allocated into one of seven 1°C SST groups (range -1°C to 6°C), using the same SST data as the NASC prediction model, with R package ‘raster’ (Hijmans, 2018). Mean species abundance was then calculated for each 1°C SST groups (Table 4.2), and therefore each 0.25° cell was assigned a proportional fish community composition on the basis of the SST group to which it belonged.

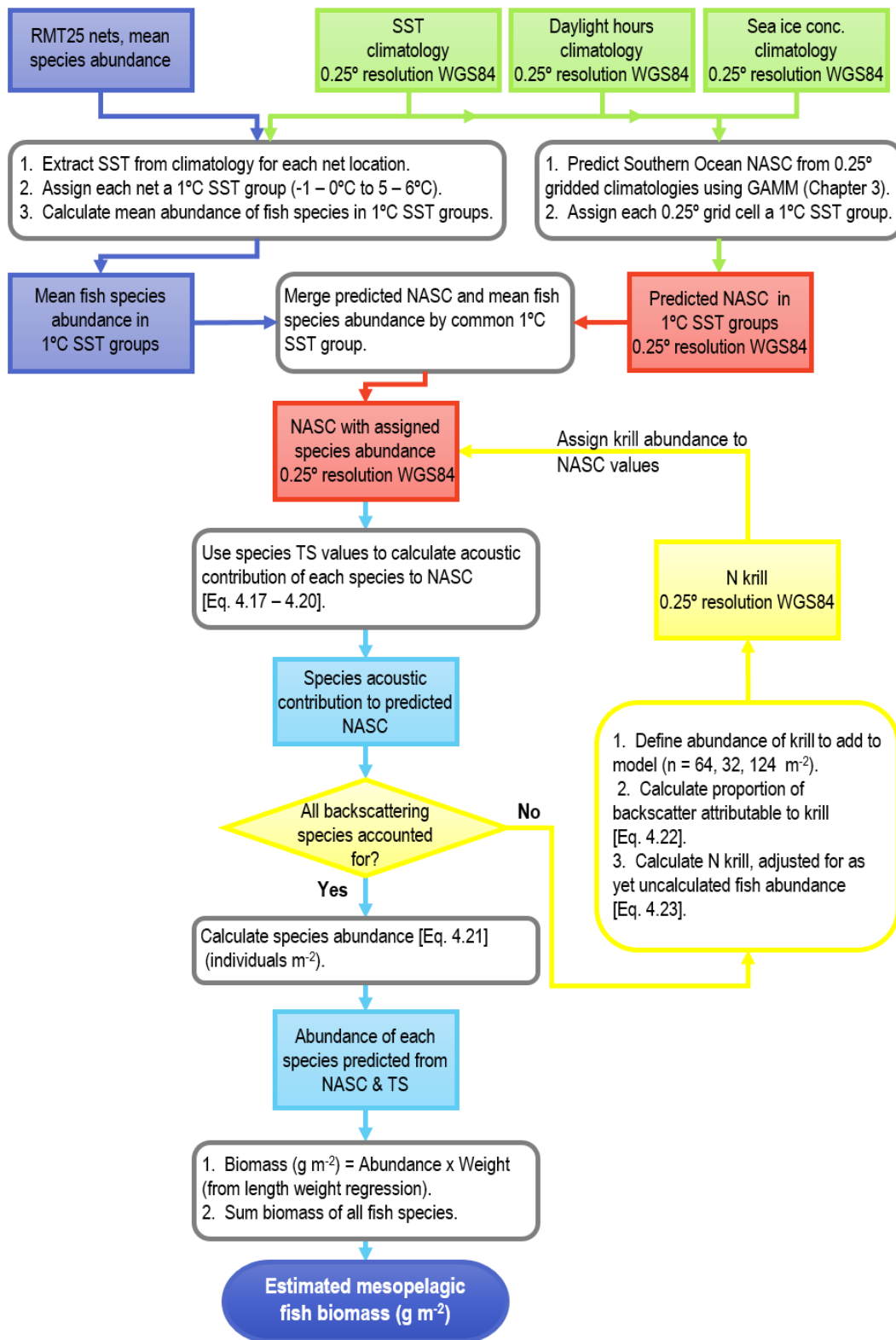


Figure 4.3 Data processing flow to calculate estimated mesopelagic fish biomass from raw RMT25 night, surface – 1000 m net data and environmental climatologies. SST: sea surface temperature Oct-Apr 2005-2017, mean Daylight hours Oct-Apr, Sea ice conc.: mean sea ice concentration Sept only 2005-2017 (see Chapter 3 supplement S.7 for further details on climatology data). Filled rectangles = data sets, unfilled rounded rectangles = processing step.

Table 4.2 Mean abundance of ind. m⁻² from RMT25 night-time total water column net samples, in each 1°C SST groups. Data were used to apportion predicted Southern Ocean NASC values among species in each 0.25° grid square. BAX – *Bathylagus* spp., ELC – *E. carlsbergi*, ELN L – *E. antarctica* (> 51.378 mm), ELN S – *E. antarctica* (< 51.378 mm), GYF - *G. fraseri*, GYN – *G. nicholsi*, GYR – *G. braueri*, KRA – *K. anderssoni*, NOE – *Notolepis* spp., PRE – *P. tenisoni*, PRM – *P. bolini*, YTX – *Cyclothone* spp.

SST	BAX	ELC	ELN L	ELN S	GYF	GYN	GYR	KRA	NOE	PRE	PRM	YTX
-1,0	0.1735	0.0000	0.3320	0.0308	0.0012	0.0030	0.1365	0.0000	0.0187	0.0000	0.0058	0.0353
0,1	0.2369	0.0000	0.4345	0.0442	0.0000	0.0181	0.2450	0.0015	0.0070	0.0000	0.0156	0.0269
1,2	0.1572	0.0633	0.1456	0.0399	0.0015	0.0069	0.2297	0.0713	0.0053	0.0073	0.0469	0.0445
2,3	0.0545	0.0662	0.0853	0.0160	0.0158	0.0091	0.1221	0.1336	0.0213	0.0213	0.0832	0.0554
3,4	0.0432	0.0366	0.0492	0.0162	0.0419	0.0258	0.2676	0.1847	0.0088	0.0537	0.1818	0.1218
4,5	0.0714	0.0033	0.0130	0.0060	0.0348	0.0076	0.1677	0.2285	0.0049	0.0337	0.2308	0.2714
5,6	0.0150	0.0000	0.0000	0.0057	0.0269	0.0383	0.0735	0.2025	0.0000	0.2062	0.1208	0.0803

4.3.4.3 Acoustics to biomass

Species-specific abundance estimates were calculated from predicted NASC values for the Scotia Sea and Southern Ocean. This was achieved by apportioning each NASC value into species-specific acoustic backscatter, based on a combination of the species abundance and their individual target strengths.

The proportional contribution of each species to the acoustic signal (NASC) was calculated for each cell using the abundance of species and the species-specific TS models. Where the TS of each species i was converted into the linear domain i.e. the backscattering cross-section (σ_{bs}) of species i :

$$\sigma_{bs_i} = 10^{TS_i/10} \quad 4.19$$

Backscatter from multiple individuals within each species was found by multiplying backscattering cross section of each species by mean species abundance N :

$$N_i \times \sigma_{bs_i} \quad 4.20$$

Total backscatter for all species was obtained by summing contribution backscatter from all species, where n is number of fish species:

$$\sigma_{bs_{total_fish}} = \sum_{i=1}^n N_i \times \sigma_{bs_i} \quad 4.21$$

Proportion of species i contribution to backscatter is calculated by dividing total linear backscatter of species i by total linear backscatter of all species:

$$\sigma_{bsprop_i} = \frac{N_i \times \sigma_{bs_i}}{\sigma_{bs_{total_fish}}} \quad 4.22$$

Abundance (ρ_a ind. m^{-2}) of species i is obtained by multiplying NASC by proportion of species i contribution to backscatter, then dividing by the backscattering cross-section of species i .

$$\rho_{a_i} = \frac{NASC \times \sigma_{bsprop_i}}{\sigma_{bs_i} \times 4 \times \pi \times 1852^2} \quad 4.23$$

Once fish abundance was calculated from NASC, the biomass of each species in $g\ m^{-2}$ was calculated by multiplying each predicted species abundance by the wet weight of a median length fish, calculated from length weight regressions.

To obtain total Scotia Sea and Southern Ocean biomass estimates, each 0.25° lat-lon biomass estimate ($g\ m^{-2}$), was multiplied by the area of the 0.25° lat-lon resolution cell using R package ‘raster’ (Hijmans, 2018), and all cell values within the Scotia Sea or Southern Ocean region were summed, excluding no data cells.

4.3.5 Sensitivity analysis

4.3.5.1 Altering fish TS – Standard length adjustment

Assuming that all of the backscatter in the Southern Ocean was attributable to fish, the effect of increasing TS was investigated by modelling species contribution to backscatter at the TS of fish at the 25th, mean, median and 75th percentile standard length for each individual species.

4.3.5.2 Other species - Krill adjustment

Since fish are not the only contributors to acoustic backscatter, Antarctic krill (*Euphausia superba*, hereafter krill) was incorporated into the model. Individual krill are relatively weak sound scatterers at 38 kHz, however, their abundance and swarming behaviour can make them ‘visible’ in the acoustic signal. Southern Ocean krill abundance estimates were taken from literature, and applied at a mean value of 64 krill m^{-2} throughout the Southern Ocean (Atkinson et al., 2004). A sensitivity analysis of the influence of their abundance on the estimates of fish biomass was undertaken by halving and doubling this value. Krill length

frequencies from cruises JR161, JR177 and JR200 were extracted from *Krillbase* (Atkinson et al., 2017) and used to calculate the mean, median, 25th and 75th percentiles of krill lengths in the Scotia Sea. Estimated krill TS for each length, derived using the stochastic distorted wave borne approximation (SDWBA) TS model (McGehee et al., 1998, Demer and Conti, 2005), parameterised for orientation, speed of sound and density contrast according to Fielding et al. (2011).

To adjust the fish proportion of backscatter to include krill, the krill net abundance N_{krill} (value = 64 krill) was back calculated using Equations 4.22-4.23:

$$\sigma_{bspropkrill} = \frac{N_{krill} \times \sigma_{bskrill} \times 4 \times \pi \times 1852^2}{NASC} \quad 4.24$$

$$N_{krill} = \frac{\sigma_{bspropkrill} \times \sigma_{bstotal_fish}}{\sigma_{bskrill} - (\sigma_{bskrill} \times \sigma_{bspropkrill})} \quad 4.25$$

4.4 Results

4.4.1 Fish morphological properties

Median tissue density of the gas-bearing species *P. bolini* (1.0613 g ml⁻¹), *E. carlsbergi* (1.0619 g ml⁻¹) and *K. anderssoni* (1.0374 g ml⁻¹) were all relatively higher than the non-gas bearing taxa *G. braueri* (1.0277 g ml⁻¹) and *Bathylagus* spp. (1.0358 g ml⁻¹). However, the non-gas bearing myctophid *G. fraseri* also had a high median tissue density (1.0656 g ml⁻¹). The myctophid *E. antarctica*, which had a median density of 1.0368 g ml⁻¹, showed a significant decline in density with increasing standard length, coincident with the shift from a gas-filled to non-gas filled swimbladder. Linear regressions of tissue density against standard length revealed statistically significant ($p < 0.05$) negative relationships between density and standard length for the non-gas bearing *Bathylagus* spp. and *G. braueri*, as well as gas-bearing *P. bolini* (Figure 4.4, Table 4.3).

The mean ESR (± 1 S.D.) of the gas volume required to make a fish neutrally buoyant in surrounding seawater ranged from 1.31 mm (± 0.24) for *E. antarctica* to 3.57 mm ± 0.20 for

E. carlsbergi (Table 4.3). The ESR for *E. antarctica* was calculated based on the tissue density values of all but the largest fish (standard length = 95 mm), as all of the other individuals were found to have a gas-filled swimbladder. The mean percentage volume of gas in relation to total fish volume (± 1 S.D.) ranged from 1.02% ± 0.95 for smaller *E. antarctica*, to 3.2% ± 0.34 for *E. carlsbergi*.

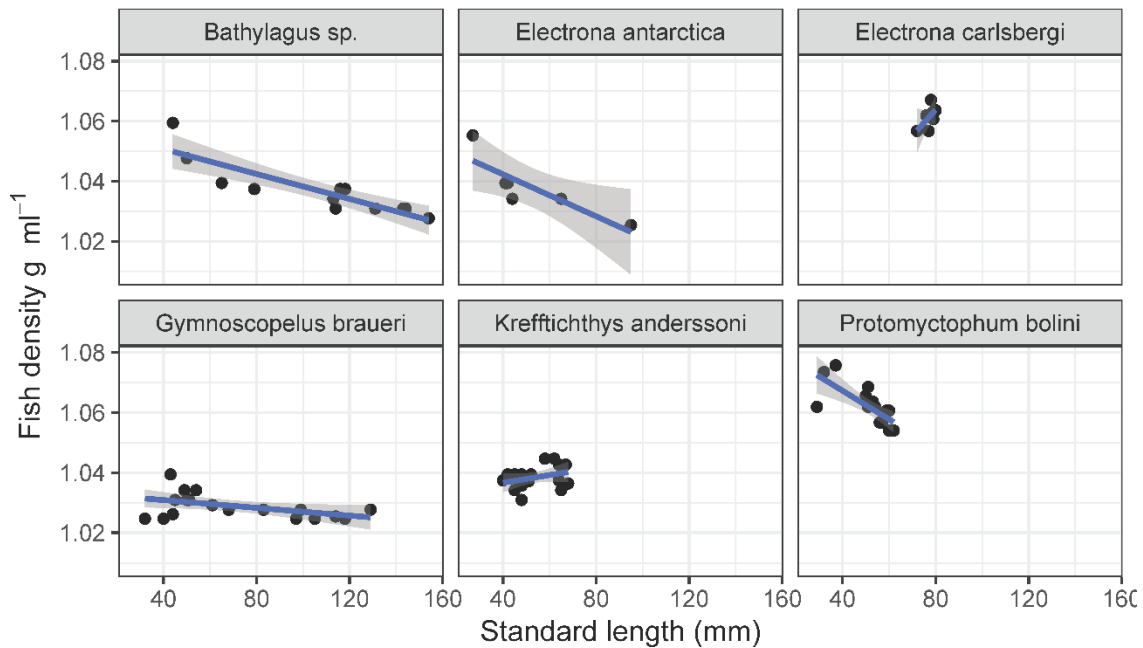


Figure 4.4 Mesopelagic fish density relationships in relation to standard length. Linear regression lines and 95% confidence interval. *Gymnoscopelus fraseri* (n=3) is not shown.

Chapter 4

Table 4.3 Linear regression fits for fish density in relation to standard length, plus summary stats for theoretical equivalent spherical radius of gas bubble required to achieve neutral buoyancy in surrounding sea water at atmospheric pressure. Values in 'red' are set to zero as these fish do not possess gas-bearing bladders in these size classes or at all in the case of *Bathylagus* spp., ELN summary contains fish in both small (gas-bearing swimbladder) and large (non-gas swimbladder) size classes.

Species	Intercept	Slope	F statistic	P value	Residual standard error	DF	Adjusted R ²	n	Min SL mm	Max SL mm	Mean SL mm ±1 S.D.	Mean tissue density g ml ⁻¹ ±1 S.D.	Mean Gas Total % vol ±1 S.D.	Mean ESR mm ±1 S.D.
BAX	1.0590	-2.08E-04	33.391	<0.001	0.004469	10	0.746	12	44	154	105.9 ±37.5	1.0370 ±0.0089	0 0 0 0	
ELN	1.0563	-3.49E-04	10.682	0.031	0.005778	4	0.659	6	27	95	52.3 ±24.2	1.0380 ±0.0099	1.02 ±0.95 1.31 ±0.24	
ELC	0.9951	8.59E-04	3.034	0.142	0.003248	5	0.253	7	72	80	77.3 ±2.7	1.0614 ±0.0038	3.20 ±0.34 3.57 ±0.20	
GYR	1.0330	-6.47E-05	4.861	0.042	0.003831	17	0.177	19	32	129	70.1 ±30.8	1.0289 ±0.0042	0 0 0 0	
GYF	1.0530	1.41E-04	0.026	0.897	0.007468	1	-0.948	3	75	86	79.0 ±6.1	1.0641 ±0.0054	0 0 0 0	
KRA	1.0310	1.29E-04	1.906	0.186	0.003566	16	0.051	18	40	68	53.6 ±9.2	1.0384 ±0.0037	1.07 ±0.35 1.61 ±0.38	
PRM	1.0863	-4.76E-04	17.06	0.001	0.004591	14	0.517	16	29	62	51.8 ±10.3	1.0617 ±0.0066	3.23 ±0.60 2.32 ±0.42	

4.4.2 Target strength estimates

The mean TS estimates for gas-swimbladdered species ranged from -57.70 dB re 1 m² for small *E. antarctica* to -48.85 dB re 1 m² for *E. carlsbergi*, the largest and densest of the gas-bearing species (see Table 4.4 for full results). TS is on a logarithmic scale, with each 3 dB increase or decrease in TS resulting in a doubling or halving of acoustic signal respectively. Consequently, the signal from the larger *E. carlsbergi* is theoretically ~ 7.5 times stronger than that from the smaller *E. antarctica*. This difference in signal is particularly notable when comparing non-gas bearing taxa and size classes, which ranged from -86.23 dB re 1 m² for small non-gas *Cyclothone* species to -69.11 dB re 1 m² for *G. nicholsi*, the largest of the myctophids in this study, a 17.12 dB difference i.e. a factor of ~50. Comparing gas to non-gas taxa, the difference in TS between the weakest scattering non-gas *Cyclothone* spp. and the strongest scattering gas-bearing *E. carlsbergi* is 37.38 dB, resulting in a factor of ~5,500 increase in signal between species.

Theoretical relative frequency responses for a range of swimbladder radii (0.2 – 4 mm) were assessed for potential effects of resonance, a depth related phenomenon that results in a disproportionately high level of backscatter resulting from a soundwave encountering a swimbladder diameter approximately equal to the insonifying wavelength (see Supplement S.5). Above an equivalent spherical radius of 1 mm, the effect of resonance throughout the surface to 1000 m depth range was limited. As the gas equivalent spherical radius of all of the gas-bearing species in this study was greater than 1 mm, the effect of resonance was not deemed a considerable source of bias and was not modelled within TS estimates.

Chapter 4

Table 4.4 Table of species morphological parameters and estimated target strengths used in biomass estimation. Taxa: KRA – *K. anderssoni*, PRM- *P. bolini*, PRE – *P. tenisoni*, ELC – *E. carlsbergi*, ELN_S – *E. antarctica* (< 51.378 mm), ELN_L *E. antarctica* (> 51.378 mm), GYR – *G. braueri*, GYF – *G. fraseri*, GYN – *G. nicholsi*, BAX – *Bathylagus* spp., NOE – *Notolepis* spp., YTX – *Cyclothone* spp., KRI – *Euphausia superba* (krill). Mean fish density derived from laboratory measurements with the exception of * which use the mean density of gas or non-gas fish as appropriate. LWR length to width ratio taken from laboratory measurements (the same values were used for both large and small ELN, †digital images, or ‡estimated mean of all other taxa. Gas is gas status assigned to taxon. Model PS – Prolate Spheroid model for gas bubble (Andreeva, 1964, Holliday, 1972, Kloser et al., 2002), FC is Finite Cylinder model for fish body in non-gas taxa (Stanton et al., 1993). Krill Stochastic Distorted Wave Borne Approximation (SDWBA) model data was taken from (Fielding et al., 2011).

Taxon	Mean fish density kg m ⁻³	LWR (n)	Standard length (SL) mm						Target strength at SL (dB re 1 m ²)				Gas	Model
			25 th			75 th			25 th		75 th			
			n	percentile	Mean	Median	percentile	percentile	Mean	Median	percentile			
KRA	1038.39	12.42 (365)	964	35.00	45.09	43.00	58.50	-59.98	-57.68	-58.11	-55.32	Gas	PS at 500m	
PRM	1061.67	11.36 (289)	619	37.00	43.94	45.00	51.00	-55.60	-54.09	-53.89	-52.79	Gas	PS at 500m	
PRE	*1053.83	11.39 (58)	145	33.00	39.33	42.00	47.00	-57.25	-55.85	-55.33	-54.44	Gas	PS at 500m	
ELC	1061.44	9.13 (112)	251	73.00	75.64	76.00	78.00	-49.39	-49.10	-49.06	-48.85	Gas	PS at 500m	
ELN_S	1038.00	10.14 (1133)	335	42.00	44.75	46.00	49.00	-58.28	-57.70	-57.45	-56.87	Gas	PS at 500m	
ELN_L			2220	64.00	74.48	74.00	84.00	-80.99	-78.13	-78.25	-76.00	Non-Gas	FC	
GYR	1028.94	11.91 (484)	1493	67.00	84.22	86.00	103.00	-84.69	-80.27	-79.89	-76.71	Non-Gas	FC	
GYF	1064.14	10.86 (66)	118	59.00	65.46	66.00	76.00	-79.44	-77.37	-77.21	-74.51	Non-Gas	FC	
GYN	*1043.38	9.51 (46)	100	116.00	122.68	137.00	149.00	-69.65	-69.11	-68.33	-68.10	Non-Gas	FC	
BAX	1037.05	†8.08 (6)	1578	76.00	96.19	94.00	114.00	-75.09	-71.88	-72.15	-70.41	Non-Gas	FC	
NOE	*1043.38	‡10.53 (-)	185	63.75	76.07	72.00	83.00	-80.57	-77.21	-78.23	-75.64	Non-Gas	FC	
YTX	*1043.38	‡10.53 (-)	669	40.00	48.23	45.00	57.00	-90.19	-86.23	-87.68	-82.80	Non-Gas	FC	
KRI	NA	NA NA	NA	40.00	44.00	45.00	50.00	-82.35	-80.36	-79.90	-77.79	Non-Gas	SDWBA	

4.4.3 Fish abundance and biomass

Fish abundance and biomass was estimated for the Scotia Sea region (CCAMLR convention areas 48.2, 48.3 and 48.4, bounded by a northern latitude of -50° , southern latitude of -64° , and between longitudes of -50° and -20°), and all areas south of -50° for entire Southern Ocean (Figure 4.5). Whilst predicted NASC values were available throughout these regions, abundance and biomass estimates were restricted to regions with a temperature range of -1°C to 6°C based on available net samples.

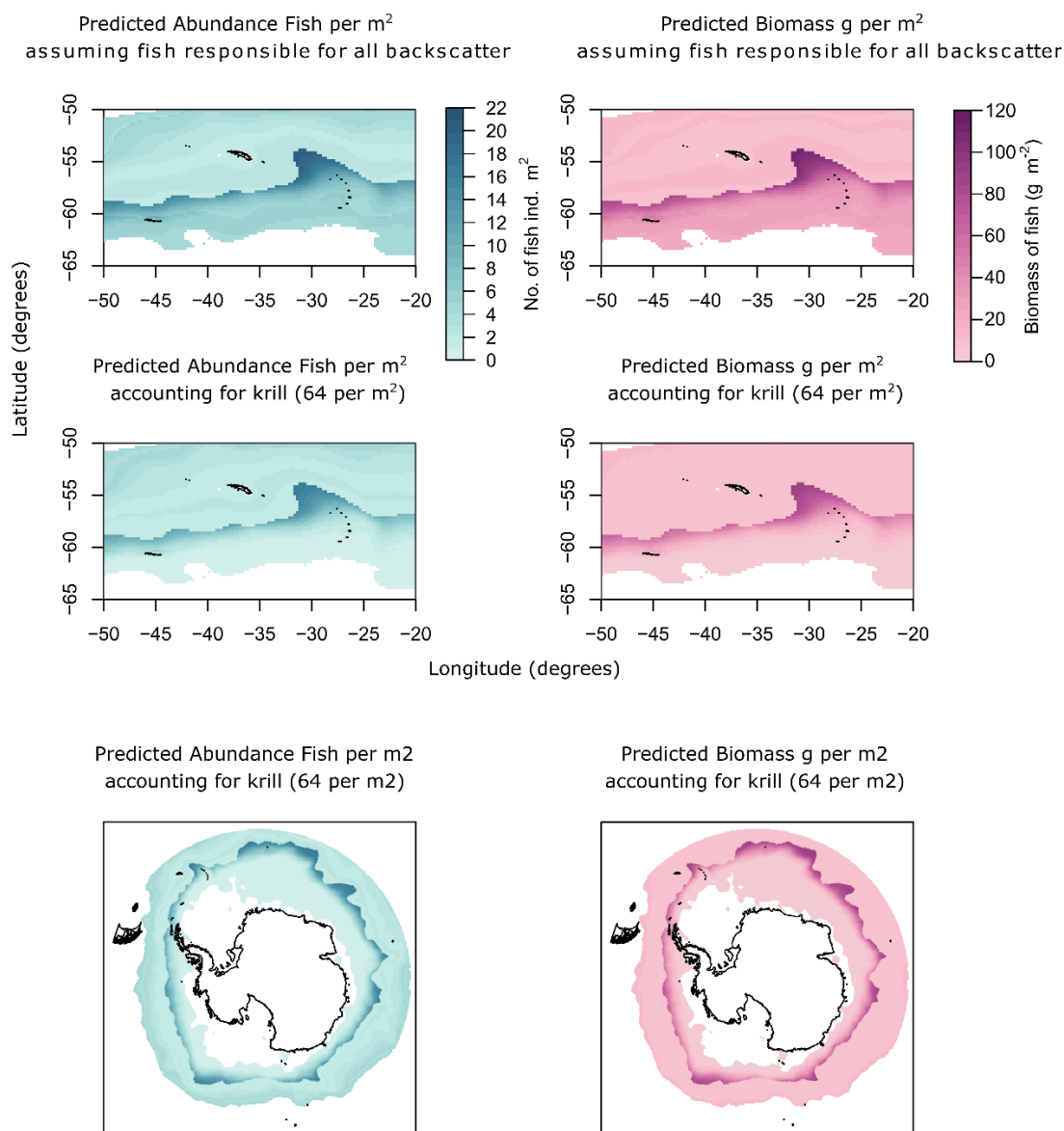


Figure 4.5 Predicted Scotia Sea abundance (left) and biomass (right) of mesopelagic fish. Top plots assume that all backscatter is from mesopelagic fish. Middle and bottom plots assume that krill contribute to backscatter at a rate of 64 krill m^{-2} , in the Scotia Sea and Southern Ocean respectively. White regions indicate no data.

Based on the TS of the median standard-length fish in each taxon, and assuming that fish are responsible for all of the acoustic backscatter, the estimated mean abundance and mean biomass (interquartile range) of mesopelagic fish in the Scotia Sea are 4.68 fish m^{-2} (2.39 – 5.27 fish m^{-2}) and 21.44 g m^{-2} (9.31 – 26.65 g m^{-2}) respectively. For the Southern Ocean mean abundance and biomass estimates rise to 5.09 fish m^{-2} (2.53 – 5.43 fish m^{-2}) and 23.82 g m^{-2} (9.60 – 27.46 g m^{-2}), see Table 4.5 for full summary.

There are notable peaks in biomass broadly tracing the path of the Southern Antarctic Circumpolar Current Front (SACCF) and Southern Boundary (see Supplement S.7). These biomass peaks are prominent in regions where SST is low ($\leq 1^{\circ}C$) and therefore dominated by non-gas bearing species, but beyond the sea ice zone and so having marginally higher NASC values. The nonlinear effect of swimbladder gas, which is a disproportionately strong reflector of acoustic signal, is demonstrated in Figure 4.6, where high levels of acoustic backscatter predicted in the model are largely driven by gas-bearing fish, rather than high biomass.

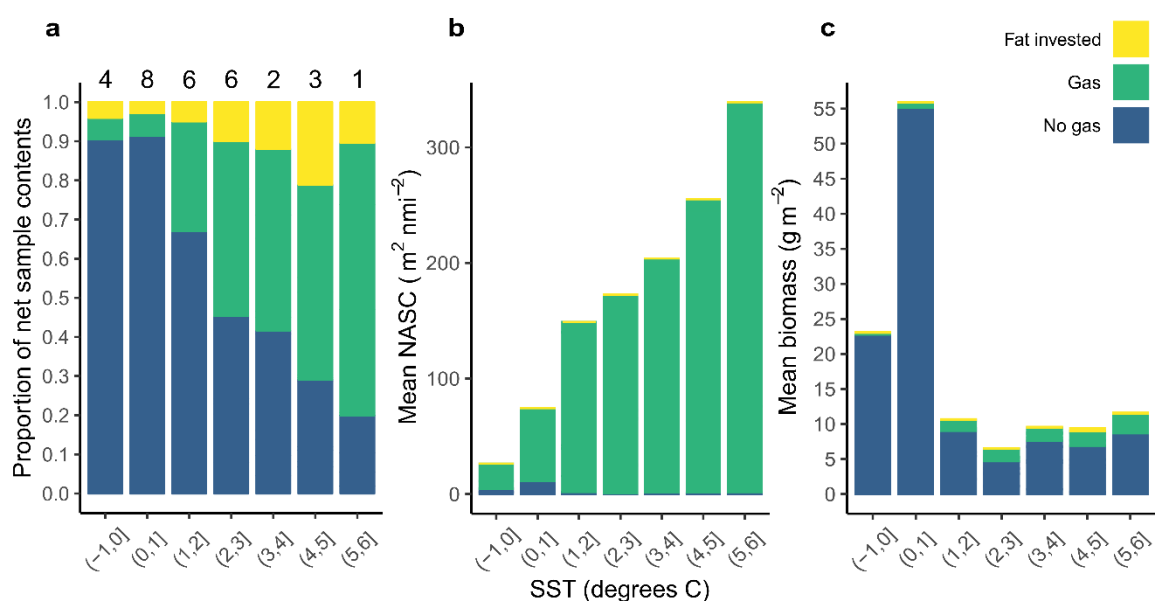


Figure 4.6 (a) Proportions of fish by swimbladder contents in net samples within 1°C sea surface temperature (SST) groups. Numbers above bars indicate the number of total water column samples in each 1°C group. (b) Acoustic contribution of fish species to mean predicted NASC in 1°C SST groups by swimbladder contents. Acoustic contribution is calculated using species-specific target strength values for median length fish. (c) Relative proportions of gas and non-gas swimbladder fish species contributing to Southern Ocean mean biomass ($g m^{-2}$) as estimated from acoustic backscatter and net proportion data, in 1°C sea surface temperature (SST) groups. Notice that relative proportion of gas bearing species is highest at warmer temperatures but overall contributes less to biomass because of the non-linear effect of gas contribution to backscatter.

4.4.3.1 Sensitivity analysis - Impact of altering fish standard length (TS)

Reducing the standard length of each taxon to the 25th percentile of samples in nets resulted in an increase in mean fish abundance in the Scotia Sea to 6.37 fish m⁻², but a biomass decrease to a mean of 15.75 g m⁻². When standard length was increased to the 75th percentile, estimated mean abundance was reduced to 3.67 fish m⁻², but there was a biomass increase to 28.76 g m⁻² (see Table 4.5). Therefore, the impact of increasing TS (size of fish) resulted in fewer individuals but overall higher fish biomass. Similar mean values were found across the Southern Ocean. Notably there was disparity between the median biomass values for the Scotia Sea and Southern Ocean. Median biomass in the Scotia Sea for each of the TS scenarios (median 11.06 g m⁻², range 7.68-15.60 g m⁻²) were considerably lower than those predicted for the wider Southern Ocean (median 17.95 g m⁻², range 13.25-24.41-29.43 g m⁻²) and well below mean values.

Table 4.5 Abundance and biomass estimates for median and interquartile range of fish standard lengths (TSs) in the Scotia Sea and the Southern Ocean, assuming that fish are responsible for all of the acoustic backscatter.

Values	<u>Abundance (fish per m²)</u>						<u>Biomass (g per m²)</u>					
	<u>Scotia Sea</u>			<u>Southern Ocean</u>			<u>Scotia Sea</u>			<u>Southern Ocean</u>		
	SL 0.25	SL Median	SL 0.75	SL 0.25	SL Median	SL 0.75	SL 0.25	SL Median	SL 0.75	SL 0.25	SL Median	SL 0.75
Min.	1.61	1.36	1.15	1.21	1.02	0.87	4.00	6.06	7.91	3.01	4.39	5.72
1 st Qu	2.82	2.39	2.02	2.99	2.53	2.08	6.76	9.31	11.82	6.90	9.60	12.08
Median	5.96	4.13	2.93	5.82	4.11	3.14	7.68	11.06	15.60	13.25	17.95	24.41
Mean	6.37	4.68	3.67	6.97	5.09	3.99	15.75	21.44	28.76	17.59	23.82	31.92
3 rd Qu	7.35	5.27	4.18	7.52	5.43	4.31	19.71	26.65	36.25	20.30	27.46	37.36
Max.	28.82	20.78	16.38	29.41	21.21	16.72	83.48	112.27	150.21	85.20	114.57	153.29

4.4.3.2 Sensitivity analysis - Impact of adding krill

To assess the impact of other fauna on fish abundance and biomass estimates, krill was added to the model at rates of 32, 64 and 128 krill m⁻². As expected, increasing the number of krill contributing to the acoustic backscatter decreased both abundance and biomass of fish (see Table 4.6). Where it is assumed that krill contribute to the acoustic backscattered signal at a relatively high abundance of 64 individual krill m⁻², the mean biomass of mesopelagic fish was 11.31 g m⁻², within the Scotia Sea, and 12.08 g m⁻² across the Southern Ocean, almost halving the fish contribution.

Table 4.6 Abundance and biomass estimates for median fish in the Scotia Sea and the Southern Ocean when varying abundance of median sized krill m^{-2} .

Values Location	Abundance (fish per m^2)						Biomass (g per m^2)					
	Scotia Sea			Southern Ocean			Scotia Sea			Southern Ocean		
	32	64	128	32	64	128	32	64	128	32	64	128
Var.	krill m^{-2}	krill m^{-2}	krill m^{-2}	krill m^{-2}	krill m^{-2}	krill m^{-2}	krill m^{-2}	krill m^{-2}	krill m^{-2}	krill m^{-2}	krill m^{-2}	krill m^{-2}
Min.	1.14	0.00	0.00	0.80	0.00	0.00	5.14	0.00	0.00	3.62	0.00	0.00
1 st Qu	2.08	1.44	0.00	1.84	0.65	0.00	8.58	5.36	0.00	8.12	3.26	0.00
Median	2.65	1.94	1.37	2.55	1.90	1.29	10.09	8.06	5.24	9.85	7.83	4.76
Mean	3.65	2.64	1.70	3.84	2.73	1.74	16.31	11.31	6.73	17.60	12.08	7.15
3 rd Qu	3.97	2.96	2.22	4.16	3.54	2.26	14.71	9.43	7.39	15.47	9.69	7.37
Max.	18.82	16.86	12.94	19.25	17.29	13.37	101.68	91.10	69.93	103.99	93.40	72.23

The addition of krill at a rate of 64 krill m^{-2} and 128 krill m^{-2} (Atkinson et al., 2004) resulted in negative values for fish abundance and hence biomass in some areas because the level of predicted backscatter was lower than the backscatter 64 krill would have produced. To prevent negative down weighting of biomass estimates, all negative abundances of fish were set to 0 prior to calculating summary statistics for fish abundance and biomass (Figure 4.7).

Location of -ve fish values (64 krill m^{-2})

Location of -ve fish values (128 krill m^{-2})

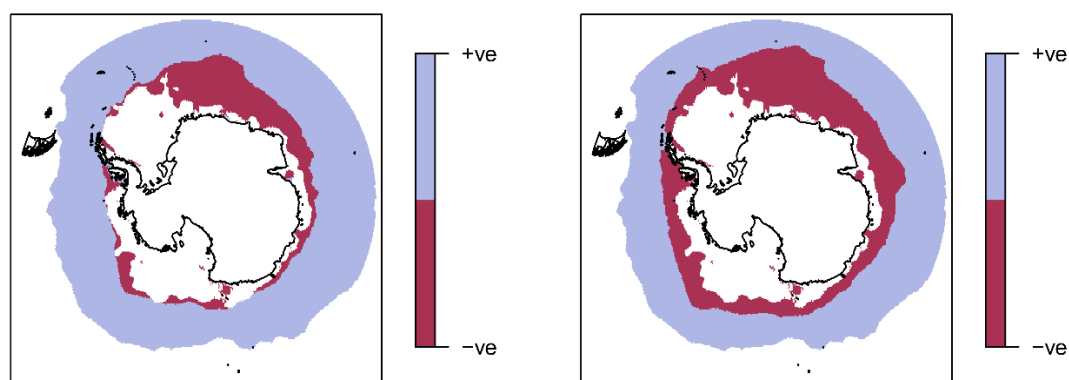


Figure 4.7 Predicted locations of 'negative' abundances of fish when the model is forced to apply krill at rates of 64 krill m^{-2} (left) and 128 krill m^{-2} (right). All negative values for fish abundance were set to 0 to calculate mean values for fish abundance and biomass.

4.4.3.3 Basin and ocean scale mesopelagic biomass estimates

Assuming fish are responsible for all of the acoustic backscatter, and based on the TS of a median length fish, total mesopelagic fish biomass for the Scotia Sea is estimated is 51.75

million tonnes (range 38.01 Mt – 69.30 Mt based on the 25th and 75th percentile TS respectively). When the relationship between community composition, NASC and SST are extrapolated to the Southern Ocean, the Southern Ocean biomass estimate is 703.76 million tonnes (range 519.75 Mt – 941.28 Mt). Biomass estimates are based on a Scotia Sea area of 2,497,593 km² and a Southern Ocean area of 30,300,113 km². See Table 4.7 for additional myctophid only biomass estimates. Some of the areas within the defined Scotia Sea and Southern Ocean were missing biomass estimates as species distributions were only modelled for locations within a -1°C to 6°C sea surface temperature range.

Table 4.7 Total regional mesopelagic fish and myctophid biomass estimates in million tonnes (Mt), derived by summing the product of each gridded biomass estimate by cell area. Biomass values calculated from target strength (TS) as a function of fish standard length at the median, 25th and 75th percentiles.

Taxa	Region	Area (km ²)	Total Biomass (Mt)		
			Median TS	25th percentile TS	75th percentile TS
All fish	Scotia Sea	2,497,593	51.75	38.01	69.30
	Southern Ocean	30,300,113	703.76	519.75	941.28
Myctophidae	Scotia Sea	2,497,593	37.63	29.03	46.76
	Southern Ocean	30,300,113	508.61	395.23	630.07

Where it is assumed that krill contribute to the acoustic signal at an abundance of 64 krill m⁻², the Scotia Sea fish biomass (based on median TS fish) is estimated to be 28.47 million tonnes (range 39.98 Mt – 17.37 Mt if krill abundance is halved or doubled respectively). For the Southern Ocean this rises to 377.08 million tonnes (range (531.44 Mt – 230.17 Mt, if krill abundance is halved or doubled respectively).

4.5 Discussion

Active acoustic methods indicate that our existing net based mesopelagic fish biomass estimates are likely to be vastly underestimated (Irigoiien et al., 2014, Anderson et al., 2018). However, validating acoustic data requires knowledge of the acoustic scattering properties of the local community (Davison, 2011). This study aimed to address these knowledge gaps by modelling the TS of the dominant mesopelagic fish species in the Southern Ocean, using locally derived measurements of species acoustic properties. By combining these TS values

and relative species abundance with modelled acoustic data, I have derived an acoustic biomass estimate for the Scotia Sea and wider Southern Ocean, which indicates that there is likely to be considerably higher fish biomass than previous net-based estimates suggest. In addition, there are notable spatial differences, which suggest potentially sizeable biomass in colder polar waters, which non-groundtruthed acoustic surveys are likely to overlook.

4.5.1 Biomass at the basin and oceanic scale

Challenges exist around the interpretation of previous Southern Ocean mesopelagic fish biomass estimates, as research papers are often not in the public domain or may have incomplete methodology, making direct comparisons difficult (see Supplement S.8). Within the Scotia Sea, net-based estimates of myctophid species biomass stands at 2.23 g m^{-2} (Collins et al., 2012). Using a combination of acoustic modelling and net derived community composition data, I have calculated a Scotia Sea mesopelagic fish (myctophids plus other species) biomass estimate of 21.44 g m^{-2} , almost an order of magnitude higher. For the Southern Ocean my mean mesopelagic fish biomass estimate rises to 23.82 g m^{-2} . A previous mesopelagic fish biomass estimate for the Southern Ocean, when scaled to the same area ($30.3 \times 10^6 \text{ km}^2$) as my study is 151.9 Mt (Lancraft et al., 1989). My acoustic estimate of 703.76 Mt , is ~ 4.6 higher.

Several studies have suggested that net-based estimates are likely to be considerably lower than actual biomass. Irigoien et al. (2014) proposed that global mesopelagic fish biomass were likely to be underestimated by at least an order of magnitude, whereas Anderson et al. (2018), incorporating primary productivity into an ecosystem-flow model, suggested that net based estimates were likely to be underestimated by a factor of ~ 2.4 . While my revised estimates are not in the regions of those suggested by Irigoien et al. (2014) it is worth noting that, their study applied a single median value of TS for mesopelagic fish globally, whereas the current study uses locally measured and derived TS estimates for each of the fish species. In this study species-specific TS estimates, which were applied across the Southern Ocean through a fish community relationship with SST, demonstrate the effect of differences in backscattering communities varying with location, which result in distinctly different scattering regimes. Further research into the energetic flow within the Southern Ocean ecosystem would help to investigate the extent to which mesopelagic fish contribute to the flow of carbon and refine the current biomass estimate.

A notable effect of the observed latitudinal change in mesopelagic community composition (Chapter 2; Dornan et al. 2019), is a predicted peak in biomass in the region between the ice-edge and $SST \leq 1^{\circ}C$, despite an overall decline in acoustic backscatter at higher latitudes. Escobar-Flores (2017), modelled similar levels of biomass in the west pacific sector of the Southern Ocean region, where changes in community resulted in a decrease in backscatter but an increase in predicted biomass. While Escobar-Flores (2017) study covered a larger latitudinal range (approximately $45^{\circ}S$ to $75^{\circ}S$) with differing community composition, the highest mean biomass in the central region (most comparable to the peak biomass region in my study) was 39.31 g m^{-2} (95% confidence intervals $20.52 - 70.25 \text{ g m}^{-2}$), higher than my current estimate but within confidence interval boundaries. Discrepancies between these two studies may have arisen from Escobar-Flores (2017) using TS values from ecologically-similar species, and treating all *Electrona* species as gas-bearing rather than using species-specific values. Moreover, Escobar-Flores (2017) assigned the scattering community based on 1500 m shelf break south of New Zealand, and used different modelling techniques, both of which may have influenced the outcome.

4.5.2 Sources of uncertainty

Demer (2004), summarised the causes of uncertainty that are liable to produce errors in biomass estimates from acoustic data, considering data collection, calibration, processing, and environmental conditions (temperature and salinity affecting sound speed). Demer (2004), identified that the largest sources of error are likely to derive from species identification, TS measurements and fish vertical migration, which may alter the backscatter from fish as they change swimming behaviour, orientation, or as a result of resonance with changing depth (Simmonds and MacLennan, 2005).

To identify the species contributing to acoustic backscatter, Scotia Sea net sample data was used to locate scattering communities by common SST values, which were extrapolated to the wider Southern Ocean. As species are known to have a circumpolar distribution (Gon and Heemstra, 1990), this approach seems biologically reasonable. However, further net samples from different regions would facilitate the testing of this hypothesis at the oceanic scale. Net systems are also known to have a degree of bias, as systems and mesh sizes are selected to specifically target the community of interest, which may miss strongly scattering species such as gas-bearing siphonophores, which are poorly sampled by our RMT25 nets (Kloser et al., 2016, Proud et al., 2018b). Proud et al. (2018) have conducted a sensitivity analysis into the

effect of varying siphonophore abundance on acoustic biomass estimates, which provides a framework for adjusting mesopelagic fish biomass estimates. However, we currently lack sufficient data on siphonophore distribution and abundance, to account for them at this time. Mesopelagic fish are also known to exhibit net avoidance (Kaartvedt et al., 2012), which may favour the capture of slower individuals (Pakhomov and Yamamura, 2010), potentially skewing community composition. However, in spite of this, net samples are still the best current method for collecting data on the relative abundance of the community to species level.

While sensitivity analysis revealed that altering species TS based on small or large individuals had limited effect in overall biomass, errors in the ratio of gas- to non-gas bearing species are likely to have considerably more impact. To minimise errors in TS, species-specific TS estimates were made based on knowledge of the local communities' swimbladder gas status and tissue density. Changes in the volume of swimbladder gas or change in gas pressure, can result in resonance, which is particularly problematic in small gas-bearing species during DVM, when using the lower frequencies that are required to sample mesopelagic depths (Kloser et al., 2002, Simmonds and MacLennan, 2005, Godø et al., 2009). Within this study, fish migration is of limited impact, as both day and night data was used to train the GAMM model, in addition, as climatologies used for prediction were averaged over multiple years and seasons any diel cycle and resonance response is likely to have been de-trended.

4.5.3 Implications for the ecosystem

This study reveals that by applying locally derived TS estimates to the dominant species, biomass is predicted to be sustained at high latitudes with a peak in biomass in the region of the ice edge. While foraging by land-breeding higher predators in the vicinity of the polar front zone is well documented (Bost et al., 1997, Trathan et al., 2008), there is considerable evidence that the regions further south, and close to the ice-edge are a hotspot for a variety of fish consumers. King penguins, which specialise on myctophids, have been tracked preferentially foraging further south and away from the PF (Pistorius et al., 2017). Tracking data reveals that when king penguin chicks are in the crèche stage adults preferentially forage away from the PF, travelling up to 1,600 km, reaching the latitudes of this studies predicted biomass peak, presumably to access rich food resources (Charrassin and Bost, 2001). While there is no existing data on the species they are consuming it seems likely that these would be the biomass dominant *Electrona antarctica* (Charrassin and Bost, 2001). In addition, the ice-

edge and Weddell-Scotia confluence (where outflowing water from the Weddell gyre meets the eastward ACC in the Scotia Sea), are known to be important foraging zones for number of seabirds, with *Electrona antarctica* being a main prey item (Ainley et al., 1991). Elephant seals are also known to exploit this potentially high biomass region throughout the year, with king and macaroni penguins, elephant and fur seals known to forage down towards the ice edge in winter (Reisinger et al., 2018).

Studies have predicted a poleward shift in mesopelagic fish species in response to future ocean warming (Freer et al., 2019). In addition, acoustic modelling has predicted a global increase in acoustic backscatter, which is cautiously interpreted as an increase in biomass (Proud et al., 2017). The results of this study indicate that while we may see an increase in acoustic backscatter as a result of a poleward shift in species, this may reflect a decrease in polar mesopelagic fish biomass, which could have a significant negative impact on the success of the higher predators that preferentially feed on fish at high latitudes.

4.6 Conclusions

This study has provided a revised mesopelagic fish biomass estimate for the Southern Ocean, which suggest an increase on previous net-based assessments by a factor of ~4.6. In particular, these results indicate a relatively high polar mesopelagic fish biomass, supporting large populations of higher predators, which is at risk under future warming scenarios. Further work is required to verify these results at the regional level, via net sampling at different locations in the Southern Ocean, to ensure the appropriate assignment of the backscattering community to the acoustic model output. It is also imperative that periodic net sample monitoring is implemented, as there is a risk that an increase in acoustic signal may indicate a decrease in the biomass of these vital mid-trophic species, which has implications for Antarctic ecosystem function.

Chapter 4

Supplementary material

Chapter 4 Supplementary material

S.1 Summary of net sample locations

Table S.1.1 summary of net sample locations used to collect fish samples and estimate relative abundance. TWC group – code of stratified RMT25 nets which together sample the total water column (1000 m to surface) in the same location, code format is cruise number, followed by event numbers i.e. cruise_event_event. Lat and Lon are the mean latitude and mean longitude respectively of net sample tow locations in decimal degrees. Sample regime indicate if the sample was taken in day or night. Non-stratified sample 'TWC night' sampled the total water column, towed open from surface - 1000 m – surface, and 'PWC night' sampled the partial water column (400 m – surface), these latter two were the source of some samples for density experiment and length weight regression only.

TWC group	Lat	Lon	Sample regime
JR16003_129_130	-54.62316	-45.15590	Night
JR16003_146_147	-53.94665	-49.22128	Night
JR16003_163_164	-53.27934	-52.18621	Night
JR16003_112	-55.26142	-41.25934	TWC night
JR16003_171	-56.71931	-56.85779	PWC night
JR15004_60_61	-59.98448	-47.21586	Night
JR15004_65_66	-60.00494	-46.62482	Night
JR15004_72_73	-60.11098	-46.07252	Night
JR15004_91_96	-60.29788	-46.44657	Night
JR200_17_18	-60.47902	-48.35652	Night
JR200_42_43	-60.26909	-44.28923	Night
JR200_55_56	-59.72112	-44.11384	Night
JR200_81_82	-58.02024	-42.93323	Night
JR200_100_101	-58.01202	-43.09128	Night
JR200_115_127	-56.78163	-42.26636	Night
JR200_141_142	-55.23331	-41.37658	Night
JR200_225_226	-50.04378	-33.74582	Night
JR200_235_236	-50.59429	-33.78504	Night
JR177_74_75_78	-60.54424	-48.27988	Day
JR177_123_124	-60.19128	-44.64590	Night
JR177_158_161	-59.69697	-44.09373	Night
JR177_165_166	-59.68210	-44.09211	Day
JR177_198_199	-58.01637	-43.04677	Night
JR177_205_206_207	-58.02262	-43.05350	Day
JR177_250_251	-55.21812	-41.27436	Day
JR177_254_255	-55.21386	-41.25581	Night
JR177_295_305	-52.86233	-40.07592	Night
JR177_300_301	-52.87498	-40.14300	Day
JR177_328_329	-52.73305	-39.01788	Night
JR177_334_335	-52.63693	-39.09611	Day
JR161_42_43_56	-57.59868	-50.51684	Night
JR161_58_59	-57.72445	-50.42456	Day
JR161_73_84	-60.50366	-48.87095	Night
JR161_91_92	-60.59061	-49.03184	Day

Chapter 4 Supplementary material

JR161_106_118	-60.45036	-44.59176	Night
JR161_114_115	-60.44190	-44.55088	Day
JR161_134_136	-59.57060	-44.25345	Night
JR161_142_143	-59.54251	-44.26010	Day
JR161_157_159	-57.32181	-42.75052	Night
JR161_199_214	-55.24943	-41.27878	Night
JR161_217_218	-55.29389	-41.36310	Day
JR161_253_269	-52.98467	-40.35246	Night
JR161_273_275	-50.09308	-38.11088	Night
JR161_282_283	-49.98505	-38.09780	Day

Chapter 4 Supplementary material

S.2 Density and CTD data

Table S2.1 of densities measured during JR16003 using modified density bottle method. ρ_f is density of fish tissue (g ml^{-1}), EGV is equivalent gas volume (mm^3) required to make fish neutrally buoyant in surrounding sea water at atmospheric pressure (see CTD cast number and CTD table S2.2 for sea water values), ESR equivalent spherical radius (mm) of gas volume, PGV percentage gas volume of fish. Gas values in 'red' are hypothetical as individuals are non-gas bearing species or size classes.

Species	SL mm	WW g	ρ_f g ml^{-1}	EGV mm^3	ESR mm	PGV %	Net event	Net no.	Net type	CTD cast
KRA	40	0.8	1.0374	7.596	1.219	0.975	146	2	RMT25	20
KRA	42	0.9	1.0394	10.214	1.346	1.166	143	2	MOCNESS	20
KRA	45	1.2	1.0342	7.760	1.228	0.664	146	2	RMT25	20
KRA	45	1.0	1.0394	11.349	1.394	1.166	146	2	RMT25	20
KRA	48	1.1	1.0394	12.484	1.439	1.166	147	1	RMT25	20
KRA	48	1.1	1.0374	10.445	1.356	0.975	147	1	RMT25	20
KRA	48	1.2	1.0357	9.452	1.312	0.809	147	1	RMT25	20
KRA	48	1.2	1.0309	4.264	1.006	0.365	164	2	RMT25	21
KRA	49	1.3	1.0374	12.344	1.434	0.975	147	1	RMT25	20
KRA	51	1.4	1.0372	12.983	1.458	0.953	146	2	RMT25	20
KRA	52	1.6	1.0394	18.159	1.631	1.166	146	2	RMT25	20
KRA	58	2.0	1.0447	32.632	1.982	1.676	171	1	RMT25	21
KRA	62	2.9	1.0447	46.930	2.238	1.662	146	1	RMT25	20
KRA	64	2.6	1.0427	37.333	2.073	1.475	146	1	RMT25	20
KRA	64	3.1	1.0374	29.849	1.924	0.989	171	1	RMT25	21
KRA	65	3.1	1.0342	20.461	1.697	0.678	171	1	RMT25	21
KRA	67	3.2	1.0427	46.376	2.229	1.489	171	1	RMT25	21
KRA	68	3.8	1.0364	32.549	1.981	0.880	146	1	RMT25	20
PRM	29	0.2	1.0619	6.295	1.145	3.234	89	1	MOCNESS	10
PRM	32	0.4	1.0735	16.808	1.589	4.316	164	2	RMT25	21
PRM	37	0.6	1.0757	26.365	1.846	4.514	164	2	RMT25	21
PRM	50	1.7	1.0656	59.715	2.425	3.608	164	2	RMT25	21
PRM	51	1.5	1.0686	56.057	2.374	3.840	39	2	RMT8	2
PRM	51	1.7	1.0619	54.161	2.347	3.273	164	2	RMT25	21
PRM	53	1.9	1.0637	62.888	2.467	3.401	129	2	RMT25	16
PRM	54	1.9	1.0619	60.533	2.436	3.273	164	2	RMT25	21
PRM	56	2.4	1.0568	65.073	2.495	2.785	147	2	RMT25	20
PRM	57	2.5	1.0568	67.398	2.525	2.770	129	2	RMT25	16
PRM	57	2.5	1.0568	67.784	2.529	2.785	147	2	RMT25	20
PRM	59	2.5	1.0607	76.585	2.634	3.147	147	2	RMT25	20
PRM	60	2.7	1.0607	82.294	2.698	3.132	129	2	RMT25	16
PRM	60	2.7	1.0540	66.635	2.515	2.535	147	2	RMT25	20
PRM	61	2.6	1.0540	63.765	2.478	2.520	129	2	RMT25	16
PRM	62	3.1	1.0540	76.027	2.628	2.520	129	2	RMT25	16
ELC	72	5.2	1.0568	140.187	3.223	2.770	129	2	RMT25	16
ELC	76	5.8	1.0619	183.114	3.523	3.244	129	2	RMT25	16

Chapter 4 Supplementary material

ELC	77	6.2	1.0568	167.146	3.417	2.770	129	2	RMT25	16
ELC	78	6.2	1.0671	224.029	3.768	3.713	129	2	RMT25	16
ELC	79	6.7	1.0607	204.212	3.653	3.132	129	2	RMT25	16
ELC	79	6.3	1.0632	205.986	3.664	3.359	129	2	RMT25	16
ELC	80	6.8	1.0637	225.072	3.774	3.401	129	2	RMT25	16
ELN	27	0.3	1.0553	7.743	1.227	2.651	143	1	MOCNESS	20
ELN	41	0.6	1.0394	6.890	1.180	1.179	171	1	RMT25	21
ELN	42	0.9	1.0394	10.334	1.351	1.179	171	1	RMT25	21
ELN	44	0.9	1.0342	5.623	1.103	0.642	39	2	RMT8	2
ELN	65	3.3	1.0342	20.831	1.707	0.649	129	2	RMT25	16
ELN	95	10.2	1.0254	-19.746		-0.199	129	2	RMT25	16
GYR	32	0.2	1.0247	-0.471		-0.242	171	1	RMT25	21
GYR	40	0.3	1.0247	-0.706		-0.242	171	1	RMT25	21
GYR	43	0.4	1.0394	4.593	1.031	1.179	171	1	RMT25	21
GYR	44	0.5	1.0262	-0.464		-0.095	171	1	RMT25	21
GYR	45	0.6	1.0309	1.959	0.776	0.335	129	2	RMT25	16
GYR	49	0.6	1.0342	3.787	0.967	0.649	129	2	RMT25	16
GYR	49	0.7	1.0342	4.620	1.033	0.678	171	1	RMT25	21
GYR	50	0.7	1.0309	2.286	0.817	0.335	129	2	RMT25	16
GYR	51	0.8	1.0309	2.612	0.854	0.335	129	2	RMT25	16
GYR	54	0.9	1.0342	5.940	1.124	0.678	171	1	RMT25	21
GYR	61	1.4	1.0292	2.274	0.816	0.167	129	2	RMT25	16
GYR	68	2.1	1.0277	1.021	0.625	0.050	164	2	RMT25	21
GYR	83	3.6	1.0277	0.715	0.555	0.020	129	1	RMT25	16
GYR	97	7.2	1.0247	-19.025		-0.271	129	1	RMT25	16
GYR	99	6.0	1.0277	1.191	0.658	0.020	129	1	RMT25	16
GYR	105	9.4	1.0247	-23.385		-0.256	146	2	RMT25	20
GYR	114	11.1	1.0254	-21.489		-0.199	129	1	RMT25	16
GYR	118	11.3	1.0247	-29.858		-0.271	129	1	RMT25	16
GYR	129	15.8	1.0277	5.578	1.100	0.036	147	1	RMT25	20
GYF	75	3.71	1.0686	139.955	3.221	3.875	164	2	RMT25	21
GYF	76	3.93	1.0582	112.162	2.992	2.932	164	2	RMT25	21
GYF	86	5.53	1.0656	194.249	3.593	3.608	164	2	RMT25	21
BAX	44	0.4	1.0595	11.721	1.409	3.011	112	1	RMT25	12
BAX	50	0.8	1.0477	15.138	1.535	1.944	146	2	RMT25	20
BAX	65	1.7	1.0394	19.294	1.664	1.166	146	2	RMT25	20
BAX	79	3.5	1.0374	32.417	1.978	0.952	112	1	RMT25	12
BAX	113	12.3	1.0342	76.675	2.635	0.641	112	1	RMT25	12
BAX	114	14.0	1.0309	44.610	2.200	0.327	112	1	RMT25	12
BAX	116	13.9	1.0374	131.984	3.158	0.975	143	1	MOCNESS	20
BAX	118	9.6	1.0374	88.915	2.769	0.952	112	1	RMT25	12
BAX	131	27.0	1.0309	92.331	2.804	0.351	146	2	RMT25	20
BAX	143	40.2	1.0309	137.470	3.202	0.351	146	2	RMT25	20
BAX	144	31.3	1.0309	99.736	2.877	0.327	112	1	RMT25	12
BAX	154	40.0	1.0277	4.794	1.046	0.012	112	1	RMT25	12

Table S.2.2 Summary of oceanographic data collected by Conductivity Temperature Depth profiler during cruise JR16003 for use in fish gas volume calculations. Mean values were calculated from total water column (TWC). Mean of all six CTD cast density and sound speed were used in TS modelling.

CTD cast	CTD latitude	CTD longitude	Mean density of seawater (g ml⁻¹)	Mean in-situ temperature (°C)	Mean sound speed (ms⁻¹)
12	-55.24859	-41.26209	1.027565	1.707793	1464.151
16	-54.53799	-45.09371	1.027482	1.722665	1464.039
20	-53.90491	-49.27398	1.027319	2.673288	1468.015
21	-53.29432	-52.18519	1.027178	3.283250	1470.462
10	-52.80868	-40.11375	1.027584	1.783169	1464.472
2	-53.49266	-39.25101	1.027550	1.673574	1463.875

S.3 Hydrometer calibration

Hydrometers were calibrated in the laboratory post-cruise using density bottles and six solutions of glycerol and Milli-Q®, plus one of pure Milli-Q® water, covering specific gravity ranges of on board measurements. Volumes of density bottles were calculated using pure Milli-Q® water and balances to 4 dp. Solutions were thoroughly mixed at room temperature and placed in a controlled chiller cabinet set at 4°C (approximate temperature of JCR cold room) to equilibrate and allow gas to settle. Balances were set up in a cold room, where mass and specific gravity readings were measured. Density bottles were covered with parafilm prior to chilling along with other equipment, to prevent moisture being drawn into vessel during transfer between lab, chiller and cold room. In the cold room, solutions were carefully pipetted into density bottles, where mass of bottle and solution was recorded. The specific gravity reading of the hydrometer being calibrated was taken at the same time. The following correction factors were calculated for each hydrometer used to measure specific gravity of fish at 4°C and applied to calculate actual fish tissue density (see Figure S.3.1).

Hydrometer 1 (specific gravity range 1.000-1.050)

$$\text{Density (g ml}^{-1}\text{)} = 0.9997 \times \text{Specific Gravity}$$

Hydrometer 2 (specific gravity range 1.050-1.100)

$$\text{Density (g ml}^{-1}\text{)} = 0.9859 \times \text{Specific Gravity} + 0.01170$$

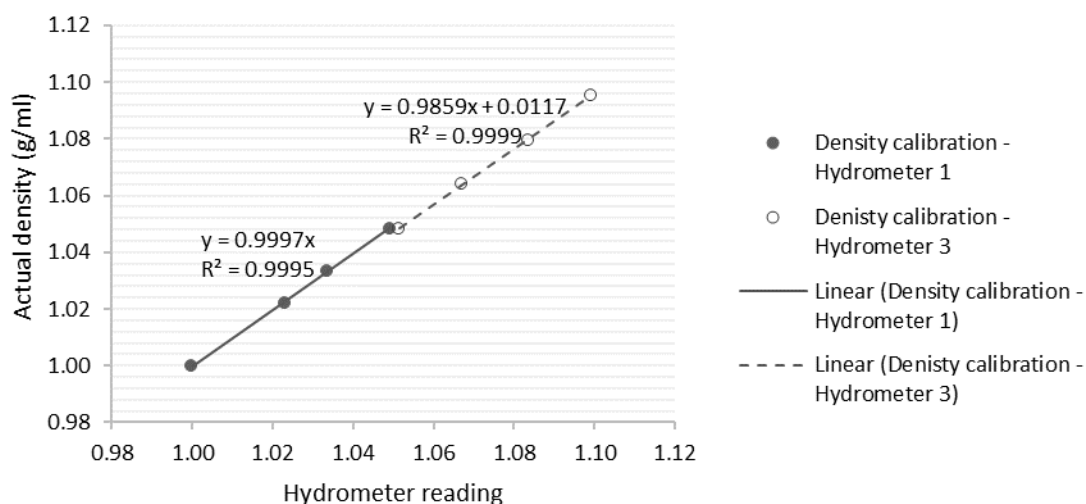


Figure S.3.1. Hydrometer calibration results. Equations of the line were used to convert specific gravity readings of mesopelagic fish species at 4°C to density measurements in g ml⁻¹.

Chapter 4 Supplementary material

S.4 Mesopelagic fish length-weight regression

Table S.4.1 Length-weight regression parameters calculated for key mesopelagic taxa. Standard length (SL, mm) to biomass (wet weight, g), $WW = a SL^b$. *Notolepis* spp. (NOE) data from Fishbase applies to fish total length (TL, cm), where $TL = SL/10.65 \times 10$.

<i>Species</i>	<i>N</i>	<i>Min</i> <i>SL</i> <i>(mm)</i>	<i>Max</i> <i>SL</i> <i>(mm)</i>	<i>Mean</i> <i>SL</i> <i>(mm)</i>	<i>a</i>	<i>2.5%</i> <i>CI</i>	<i>97.5%</i> <i>CI</i>	<i>b</i>	<i>2.5%</i> <i>CI</i>	<i>97.5%</i> <i>CI</i>	<i>R</i> ²
BAX	11	44	154	105.0	4.43E-07	9.99E-08	1.96E-06	3.639	3.315	3.963	0.986
ELC	200	66	89	75.6	3.57E-05	1.42E-05	8.96E-05	2.787	2.574	3.000	0.771
ELN_L	1204	52	113	74.6	3.54E-06	3.05E-06	4.12E-06	3.291	3.256	3.326	0.966
ELN_S	180	24	51	45.1	6.51E-06	4.14E-06	1.02E-05	3.140	3.021	3.259	0.939
GYF	74	37	108	66.6	3.57E-06	1.98E-06	6.44E-06	3.253	3.112	3.393	0.967
GYN	51	33	166	126.2	4.42E-06	3.31E-06	5.90E-06	3.174	3.114	3.235	0.996
GYR	654	31	131	83.8	3.54E-06	2.95E-06	4.24E-06	3.180	3.138	3.221	0.972
KRA	517	24	70	46.2	6.23E-06	5.24E-06	7.41E-06	3.137	3.092	3.183	0.973
PRE	58	40	53	47.1	3.21E-05	8.80E-06	1.17E-04	2.744	2.408	3.080	0.827
PRM	315	21	63	46.2	1.20E-05	8.17E-06	1.78E-05	3.017	2.915	3.118	0.916
YTX	5	43	56	48.8	1.08E-06	7.31E-09	1.59E-04	3.309	2.023	4.595	0.957
NOE	-	-	-	-	0.00324	0.00123	0.00854	3.080	2.850	3.310	-

S.5 Resonance scattering from prolate spheroid model

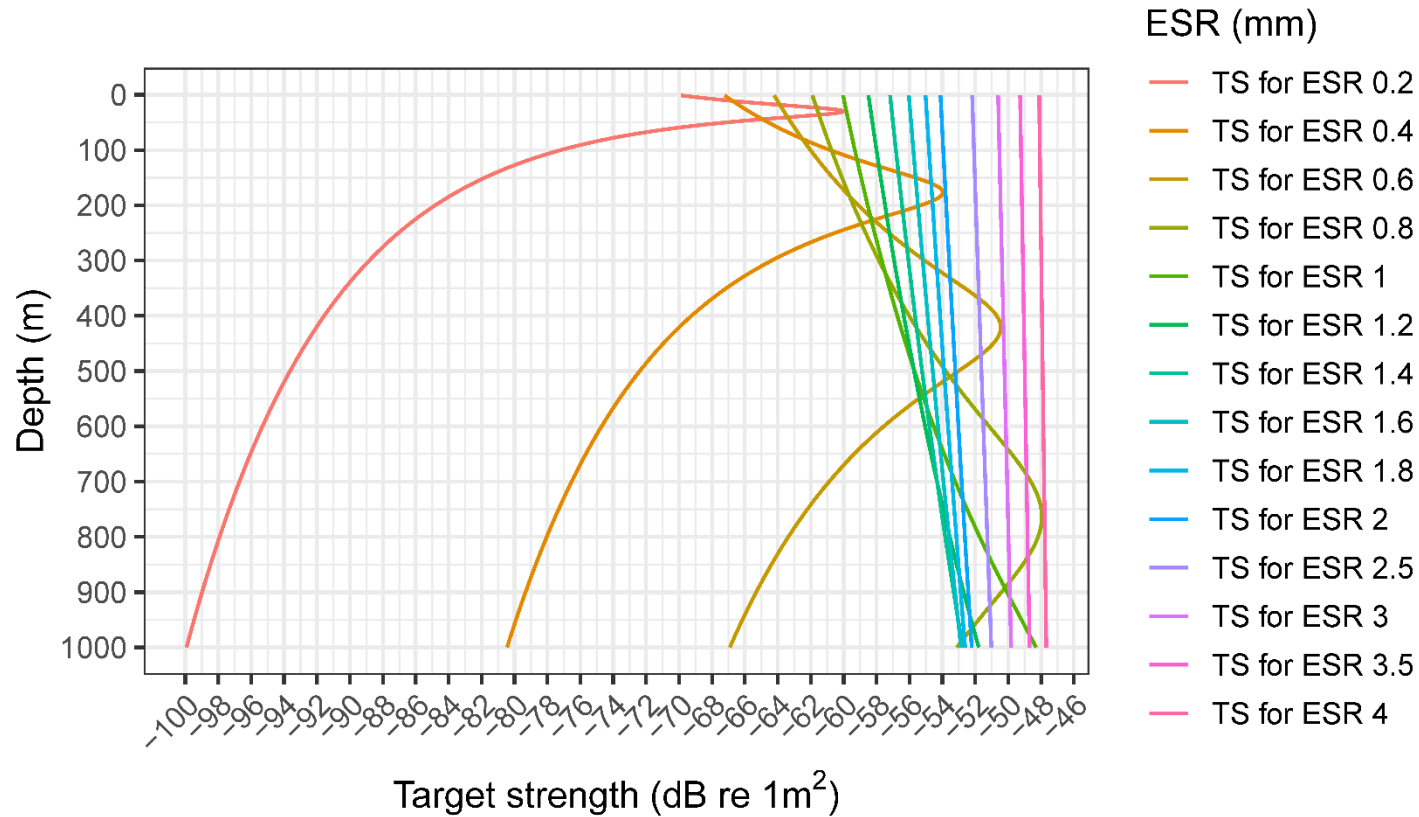


Figure S.5.1 Frequency response plot for fish with theoretical range of swimbladder gas volumes at 38 kHz. Equivalent spherical radius (ESR) in mm. Model has fixed parameters of fish density at 1.054 g ml⁻¹ (the mean density for gas-bearing fish species from this study) and prolate spheroid roundness of 0.3 (the average for *Krefflichthys anderssoni* measured from computed tomography scans, n=4).

S.6 Finite cylinder model code

For fish without a gas-filled swimbladder, a fixed finite cylinder model was used following Stanton et al. (1993). R code used based on simple algebraic transformation of Stanton et al.'s (1993) model:

$$TS = 10 \log_{10}(\sigma_{bs})$$

$$\sigma_{bs} = (0.08 \times ref^2 \times SL^2 \times bd^{-1}) \times step2$$

$$step2 = (1 - \exp(-8 \times \pi^2 \times f^2 \times tempdfl^2 \times s^2 \times c^{-2})) \times step1$$

$$step1 = \cos(\pi \times f \times dfl \times c^{-1} \times (4 - 0.5 \times \pi \times (\pi \times f \times dfl \times c^{-1} + 0.4)^{-1}))$$

$$ref = \frac{g \times h - 1}{g \times h + 1}$$

$$g = \frac{\rho_{fish}}{\rho_{seawater}}$$

$$h = \frac{c_{fish}}{c_{seawater}}$$

Where:

dfl is fish length / Length-Width ratio, ref is the reflection coefficient, g is density contrast between fish tissue density and seawater density, h is sound speed contrast between fish and seawater, c is sound speed in ms^{-1} . Sound speed of fish tissue was assumed to be $1510 ms^{-1}$, based on measured c_{fish} for the myctophid *Stenobrachius leucopsarus* at $4^\circ C$ (Yasuma et al, 2006).

bd is the length to width ratio of fish body dimensions, a mean value of 10.8 was used for all Scotia Sea non-gas bearing fish based on laboratory measurements.

How to transform from Stanton et al. (1993) equations to R code...

Main equation on page 3468, second to last paragraph:

$$\langle |I_0|^2 \rangle_L = 2 \{ 1 - \exp[-8(k\bar{a}s)^2] \cos(4k\bar{a} + \mu_{p=2}) \}$$

Substitute in $k = \frac{2\pi f}{c}$

$$\langle |I_0|^2 \rangle_L = 2 \left\{ 1 - \exp \left[-8 \left(\frac{2\pi f}{c} \bar{a} s \right)^2 \right] \cos \left(4 \frac{2\pi f}{c} \bar{a} + \mu_{p=2} \right) \right\}$$

Dealing with left part of equation first, square exponent bracketed section

$$\langle |I_0|^2 \rangle_L = 2 \left\{ 1 - \exp \left[-8 \left(\frac{2^2 \pi^2 f^2}{c^2} \bar{a}^2 s^2 \right) \right] \cos \left(4 \frac{2\pi f}{c} \bar{a} + \mu_{p=2} \right) \right\}$$

And multiply it all on one line

$$\langle |I_0|^2 \rangle_L = 2 \left\{ 1 - \exp[-8(2^2 \pi^2 f^2 \bar{a}^2 s^2 c^{-2})] \cos \left(4 \frac{2\pi f}{c} \bar{a} + \mu_{p=2} \right) \right\}$$

Substitute in $\bar{a} = \frac{dfl}{2}$

$$\langle |I_0|^2 \rangle_L = 2 \left\{ 1 - \exp \left[-8 \left(2^2 \pi^2 f^2 \frac{dfl^2}{2^2} s^2 c^{-2} \right) \right] \cos \left(4 \frac{2\pi f}{c} \bar{a} + \mu_{p=2} \right) \right\}$$

Cancel out the 2²

$$\langle |I_0|^2 \rangle_L = 2 \left\{ 1 - \exp[-8(\pi^2 f^2 dfl^2 s^2 c^{-2})] \cos \left(4 \frac{2\pi f}{c} \bar{a} + \mu_{p=2} \right) \right\}$$

Continuing with the section after to cosine

Substitute in $\mu_{p=2} = \frac{-\frac{\pi}{2} k_1 a}{k_1 a + 0.4}$

$$\langle |I_0|^2 \rangle_L = 2 \left\{ 1 - \exp[-8\pi^2 f^2 dfl^2 s^2 c^{-2}] \cos \left(4 \frac{2\pi f}{c} \bar{a} + \frac{-\frac{\pi}{2} k_1 a}{k_1 a + 0.4} \right) \right\}$$

Substitute in $\bar{a} = \frac{dfl}{2}$

$$\langle |I_0|^2 \rangle_L = 2 \left\{ 1 - \exp[-8\pi^2 f^2 dfl^2 s^2 c^{-2}] \cos \left(4 \frac{2\pi f}{c} \frac{dfl}{2} + \frac{-\frac{\pi}{2} k_1 a}{k_1 a + 0.4} \right) \right\}$$

Chapter 4 Supplementary material

Cancel out the 2's and simplify $-\frac{\pi}{2}$ to -0.5π , and $1/c$ to c^{-1}

$$\langle |I_0|^2 \rangle_L = 2 \left\{ 1 - \exp[-8\pi^2 f^2 dfl^2 s^2 c^{-2}] \cos\left(4 \frac{\pi f}{c} dfl + \frac{-0.5\pi k_1 a}{k_1 a + 0.4}\right) \right\}$$

Simplify c

$$\langle |I_0|^2 \rangle_L = 2 \left\{ 1 - \exp[-8\pi^2 f^2 dfl^2 s^2 c^{-2}] \cos\left(4 \pi f dfl c^{-1} + \frac{-0.5\pi k_1 a}{k_1 a + 0.4}\right) \right\}$$

Substitute in $k_1 = \frac{2\pi f}{c}$ and $\bar{a} = \frac{dfl}{2}$

$$\langle |I_0|^2 \rangle_L = 2 \left\{ 1 - \exp[-8\pi^2 f^2 dfl^2 s^2 c^{-2}] \cos\left(4 \pi f dfl c^{-1} + \frac{-0.5\pi \frac{2\pi f}{c} \frac{dfl}{2}}{\frac{2\pi f}{c} \frac{dfl}{2} + 0.4}\right) \right\}$$

Cancel out 2's and transpose c's to top of equation i.e. $1/c$ to c^{-1}

$$\langle |I_0|^2 \rangle_L = 2 \left\{ 1 - \exp[-8\pi^2 f^2 dfl^2 s^2 c^{-2}] \cos\left(4 \pi f dfl c^{-1} + \frac{-0.5\pi \pi f dfl c^{-1}}{\pi f dfl c^{-1} + 0.4}\right) \right\}$$

Simplify by moving the $\pi f dfl c^{-1}$ outside brackets

$$\langle |I_0|^2 \rangle_L = 2 \left\{ 1 - \exp[-8\pi^2 f^2 dfl^2 s^2 c^{-2}] \cos\left(\pi f dfl c^{-1} \left(4 + \frac{-0.5\pi}{\pi f dfl c^{-1} + 0.4}\right)\right) \right\}$$

Simply to single line for coding

$$\langle |I_0|^2 \rangle_L = 2 \{ 1 - \exp[-8\pi^2 f^2 dfl^2 s^2 c^{-2}] \cos(\pi f dfl c^{-1} (4 - 0.5\pi (\pi f dfl c^{-1} + 0.4)^{-1})) \}$$

Major coding is now complete, this needs to be slotted into the back-scattering cross section segment.

NOTE that the $2 \{ \dots \}$ is still present encompassing all of calculation above, this is about to cancel out in the next formula...

$$\langle \sigma_{bs} \rangle_{\theta,L} / \bar{L}^2 = A_{ij} \mathcal{R}_{12}^2 \langle |I_0|^2 \rangle_L \beta^{-1}$$

Multiply both sides by \bar{L}^2

$$\langle \sigma_{bs} \rangle_{\theta,L} = A_{ij} \mathcal{R}_{12}^2 \langle |I_0|^2 \rangle_L \beta^{-1} \bar{L}^2$$

Where $\beta = \frac{L}{a}$ and $bd = \frac{L}{2a} = \frac{1L}{2a} = \frac{1}{2} \beta$ therefore $\beta = 2bd$ and $\beta^{-1} = 2bd^{-1}$

Now substitute in $2bd^{-1}$ for β^{-1} , because the $\langle |I_0|^2 \rangle_L$ was = $2\{\dots\}$

$$\langle \sigma_{bs} \rangle_{\theta,L} = A_{ij} \mathcal{R}_{12}^2 \langle |I_0|^2 \rangle_L bd^{-1} \bar{L}^2$$

I_0 = term describing interference between echoes from front and back faces of cylinder at angle of incidence $\theta = 0$.

k = wavenumber

f = frequency in Hertz

c = sound speed in ms^{-1}

dfl = Fish Length / LW ratio = fish width

$LWratio$ = Fish length / Fish width

bd = fish width (body diameter, measured dorsally)

The reflection coefficient $\mathcal{R}_{1,2}$ is the plane wave/plane interface reflection coefficient within the medium surrounding the body (ie seawater) and the body (ie tissue).

$\mathcal{R}_{1,2} = ref$ in R code, where:

$$ref = \frac{g \times h - 1}{g \times h + 1}$$

$$g = \frac{\rho_{fish}}{\rho_{seawater}}$$

$$h = \frac{c_{fish}}{c_{seawater}}$$

Stanton et al. (1993) calculated A_{ij} as a constant of 0.08, for all bent and straight cylinders of Gaussian and uniformly distributed oriented cylinders.

S.7 Southern Ocean variable plots with mean front positons.

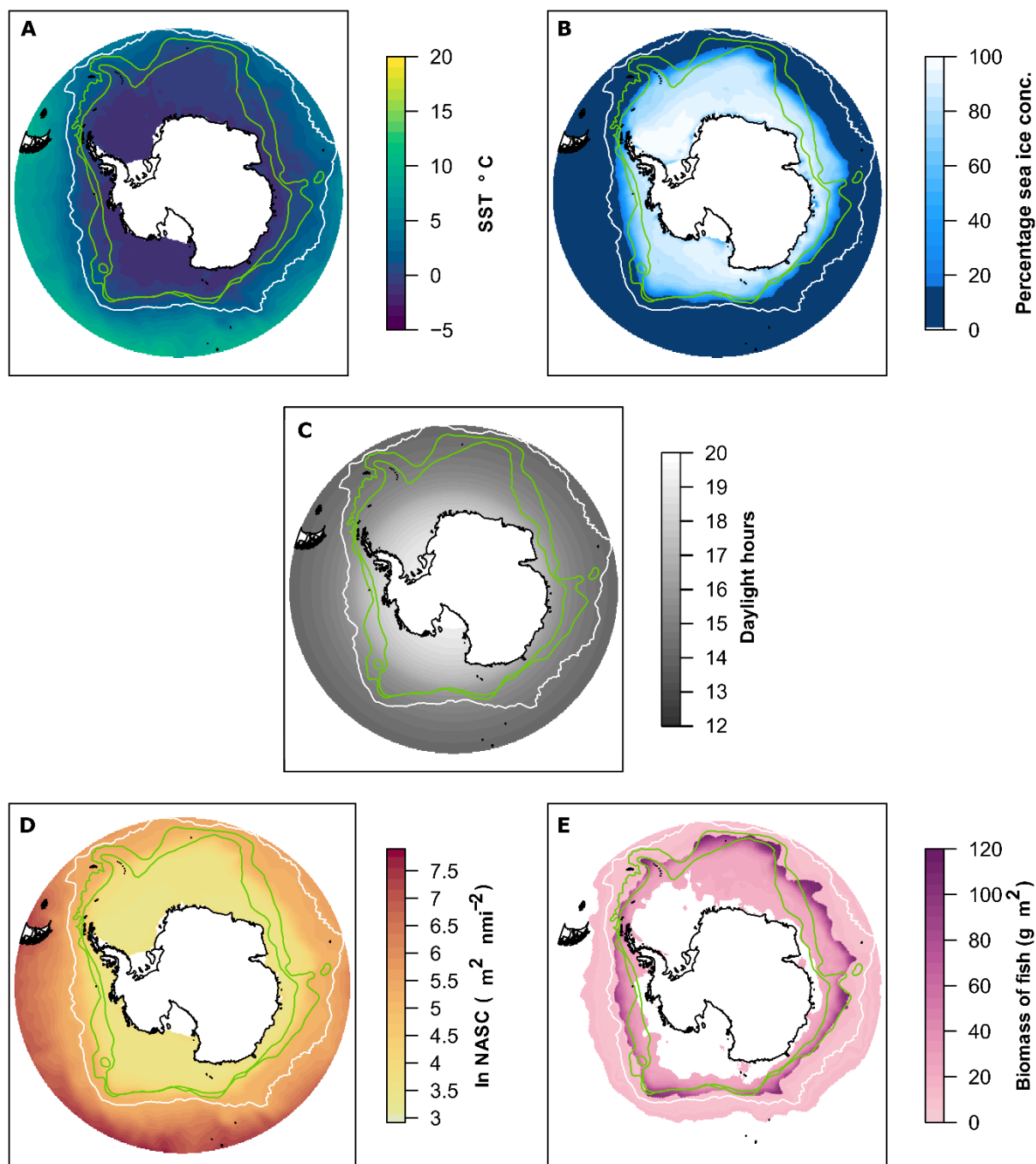


Figure S.7.1 Southern Ocean variable plots with mean front positons. (a) Sea surface temperature climatology (Oct-Apr 2005-2017), (b) Sea ice concentration climatology (Sep 2005-2017) and (c) mean daylight hours (Oct-Apr), as used in NASC prediction. (d) Predicted acoustics backscatter (\log_e NASC). (e) Predicted mesopelagic fish biomass, based on the target strength of a median length fish in each of the eleven mesopelagic study species and assuming fish are responsible for all backscatter. White regions indicate no data. Fronts: from north to south, Antarctic Polar Front (white), Southern Antarctic Circumpolar Current Front and Southern Boundary (both green).

S.8 Previous fish biomass estimates

Challenges exist around the interpretation of previous Southern Ocean mesopelagic fish biomass, as research papers are often not in the public domain or may have incomplete methodology, making direct comparisons difficult. A commonly cited source for myctophid biomass is that of Lubimova et al. (1987), which is not publicly available. The following publications do have biomass estimates listed, though only Lancraft et al. (1989) is primary research.

Table S.8.1 Summary of mesopelagic fish biomass estimate sources, and areas of uncertainty. **Bold** citations are publicly available papers which were reviewed.

Source	Taxa	Area	Biomass (Mt)	Data type/ methodology	Uncertainty
Kock, 1987	Mesopelagic fish	South of Antarctic Polar Front	140 – 190	“Soviet investigations” (undefined)	Original papers not cited.
Lancraft et al, 1989	Mesopelagic fish	Southern Ocean (38.1 x 10 ⁶ km ²)	133 – 191	Net samples (0 – 1000 m) from Scotia & Weddell Sea	Method for calculating total biomass unclear.
Tseitlin, 1982, cited in: Lubimova et al, 1983, cited in: Sabourenkov, 1991	Mesopelagic myctophids*	South of 40°S	337 212 – 396**	Survey data (undefined) Modelling (undefined)	Original papers not in the public domain. * ‘myctophid’ likely to be typographical error.
Lubimova, 1985, and Lubimova, 1983, in: Sabourenkov, 1991	Myctophids	As above?	70 – 130 100 – 200	Unclear: possibly based on 1/3 to 1/2 of 212-396**	Original papers not in the public domain.

Chapter 5

General discussion

5.1 General conclusions

Mesopelagic fish contribute to the vertical transport of carbon, and occupy a key mid-trophic position in the Antarctic marine food web, as predators of zooplankton and prey for marine megafauna. Yet, biomass estimates are rare and are typically based on net samples, which are broadly recognised to underestimate actual biomass (Kaartvedt et al., 2012). There is increasing interest in the use of mesopelagic resources to sustainably support the growing human population (St. John et al., 2016, European Commission, 2018), therefore it is essential that we find methods of quantifying and monitoring change in mesopelagic fish populations. Active acoustics facilitates the collection of relatively large amounts of data throughout the mesopelagic depth zone at unrivalled spatial and temporal scales. However, to reliably interpret acoustic data we require additional information on the species present, and their unique backscattering properties (Davison, 2011). However, such data have been lacking for Southern Ocean mesopelagic fish species.

In this thesis I aimed to address knowledge gaps to facilitate the interpretation of acoustic data and shed light on mesopelagic fish behaviour and abundance at the basin scale. Given that gas-filled swimbladders are major reflectors of acoustic signal, I have assessed the morphology of swimbladders of dominant mesopelagic fish species from the Scotia Sea to determine the extent that they contribute to acoustic backscatter signals. I have revealed how the species composition of the mesopelagic fish community changes with latitude, and shown how species with gas-filled swimbladders become less prominent in the community towards the Antarctic landmass. I have tested for evidence of diel vertical migration (DVM), using 38 kHz acoustic data as a proxy for mesopelagic fish, and explored the environmental drivers of changes in acoustic backscatter at the ocean basin scale. I have calculated the first Target Strength estimates for eleven of the most common mesopelagic fish taxa in the Scotia Sea from empirical and literature derived data. I have used these measures of Target Strength alongside net sample abundance data to calculate mesopelagic fish biomass within the Scotia Sea and Southern Ocean.

In Chapter 2, I aimed to identify the strong and weak acoustic backscattering species within the Scotia Sea mesopelagic fish community, to assess if any systematic change in community composition could bias acoustic signal interpretation. By assessing the presence or absence of gas in the swimbladders of the dominant myctophid species in the Scotia Sea, I revealed that as we travel north to south towards the Antarctic continent, there is a gradual

decline in the abundance of gas-bearing species. As acoustic signal return from a fish with a gas-filled bladder is particularly strong (Foote, 1980b), this north-south shift from gas- to non-gas species in colder polar waters is likely to contribute to the ubiquitous decline in acoustic backscatter that we see in the Scotia Sea towards the continent. Change in fish community composition paralleling a reduction in acoustic backscatter has been reported in other sectors of the Southern Ocean (Escobar-Flores et al., 2018), suggesting the pattern we observe in the Scotia Sea is a circumpolar trend. As acoustic backscatter is commonly used as a proxy for biomass (Irigoiien et al., 2014, Proud et al., 2017), a decline in acoustic backscatter may be interpreted as a decrease in biomass. However, my analysis indicates that within the Southern Ocean this is more likely to reflect a change in community rather than a decrease in biomass. Knowledge of the species present and their individual backscattering properties is therefore essential for measuring mesopelagic fish abundance (Davison, 2011). My research indicates that periodic validation of acoustic data with knowledge of species present and their relative contribution to the overall backscatter, should enable managers to account for potentially sizable assemblages of species that contribute only weakly to the overall signal detected by active acoustic methods.

As the DVM behaviour of mesopelagic fish is understood to contribute to the vertical transport of carbon (Davison et al., 2013, Belcher et al., 2019), a key aim of this thesis was to evaluate to what extent DVM occurred and if latitudinal variation in DVM behaviour can be detected in the Scotia Sea. My analysis of 38 kHz acoustic data in Chapter 3 revealed clear evidence for DVM from the mesopelagic into the epipelagic zone at night north of 57°S. However, just as the acoustic signal weakens as we transit south, so does the signal of DVM, which seems to be vertically suppressed occurring within the mesopelagic zone only, south of 57°S – the approximate location of the Antarctic Polar Front. Suppression of vertical migration below the epipelagic zone appears to be consistent at both poles, with light understood to be a strong contributing factor (Norheim et al., 2016, Langbehn et al., 2019), conceivably coupled with a temperature barrier from surface intrusion of colder water (Collins et al., 2012). A suppression in DVM behaviour would limit the extent of mesopelagic fish contribution to the active sequestration of carbon in the colder polar waters. However, polar specialists such as the myctophid *Electrona antarctica*, are known to occur throughout the water column, indicating that there is likely to be a degree of vertical migration that may be masked by poor acoustic reflectivity as a result of the loss of the gas in their swimbladder, or may involve brief

asynchronous forays to feed in surface waters (Pearre, 2003, Dypvik et al., 2012, Saunders et al., 2018).

A further aim was to assess the importance of key environmental drivers for explaining horizontal spatial patterns in acoustic backscatter at the ocean basin scale. Modelling revealed that acoustic backscatter was positively correlated with sea surface temperature and negatively correlated with daylight hours and sea ice concentration, resulting in a predictable decrease in acoustic backscatter towards and into the sea ice zone. This relationship between temperature and acoustic backscatter, also parallels the change in mesopelagic fish community composition. In agreement with Longhurst's (2007) principles of ecological provinces, my research indicates a Southern Ocean mesopelagic fish community, driven by water mass properties, which are fundamentally reflected in changes of acoustic backscatter at the ocean basin scale.

The final aim of this thesis was to produce a biomass estimate for mesopelagic fish in the Scotia Sea and wider Southern Ocean. Using the relationships between sea surface temperature and (i) the backscattering fish community coupled with locally derived measurements of fish acoustic scattering properties, and (ii) modelled acoustic backscatter, I have demonstrated that Southern Ocean mesopelagic fish biomass is likely to be considerably higher than previous net-based estimates. Irigoien et al. (2014) used a median Target Strength value for all mesopelagic fish (gas and non-gas) and a single circumglobal acoustic transect, to model global backscatter based on a relationship with primary productivity. Their estimate of mesopelagic fish biomass (between latitudes of 40° N and 40° S) indicated that biomass may be at least an order of magnitude higher than net based estimates (Irigoien et al., 2014). However, ecosystem modelling suggests that mesopelagic fish biomass is more likely to be closer to ~2.4 times net based estimates (Anderson et al., 2018). My study adds to this existing body of work by providing a biomass estimate for the Southern Ocean, which uniquely takes into account multiple acoustic transects across the Scotia Sea, and applies species-specific Target Strength estimates for the dominant species. My modelled fish biomass estimate of ~52 Mt (38 – 69 Mt) in the Scotia Sea and ~704 Mt (520 – 941 Mt) for the Southern Ocean, is approximately 4.6 times higher than net-based estimates, with a potential peak in biomass in the region of the sea ice edge.

5.2 From limitations to solutions

Target identification is the largest source of uncertainty in my biomass estimate, which is based on mesopelagic fish being responsible for all of the acoustic backscatter. However, fish make up only a portion of the mesopelagic community. At 38 kHz many of the smaller zooplankton would be unlikely to contribute to the signal, but high-density swarms of Antarctic krill (*Euphausia superba* hereafter krill) could. I conducted a sensitivity analysis by adding krill to the backscattering community, which at a mean rate of 64 krill m⁻² throughout my modelled area, resulted in a halving of my fish biomass estimate. However, a halving of predicted biomass is likely to be conservative, since krill distribution is patchy (Atkinson et al., 2004). Gas-bearing siphonophores also have considerable potential to contribute to the acoustic signal. Proud et al. (2018b) conducted a study into the effect of siphonophores on acoustic biomass estimates. Under a scenario where fish were assumed to be gas-bearing as juveniles, and a proportion maintained gas-filled bladders as adults, and siphonophores were assumed to contribute 50% of the acoustic signal, fish biomass was again halved. However, there is a paucity of data on the abundance and distribution of siphonophores across the Scotia Sea and Southern Ocean, which needs resolving before they can be appropriately accounted for. As environmental DNA methods improve, in the future it may be possible to ground-truth acoustic data by generating a quantitative estimate of the abundance of both fish and invertebrate taxa. However, net samples will still be required to measure length-frequency distributions and determine the presence or absence of gas in species with regressed swimbladders.

Limited spatial and temporal data coverage is another important limiting factor. My models were parameterised using multiple years of acoustic transect and net data spanning the Scotia Sea, prior to extrapolating these relationships to the wider Southern Ocean. The justification for extrapolation is based on the assumption that the mesopelagic species of the Scotia Sea tend to have a circumpolar distribution (Gon and Heemstra, 1990), with patterns in community composition and hence swimbladder gas condition, linked to temperature. Additional acoustic data, alongside complementary net samples, for the wider Southern Ocean, would enable the validation of these assumptions.

My thesis has focused on large basin-scale descriptions of mesopelagic fish distribution and estimates of biomass. As sampling in the Southern Ocean is challenging and costly, multiple years of acoustic and net data were combined in this study to build a spatially

comprehensive dataset for analysis and modelling. However, combining multiyear data has precluded the ability to look at annual and seasonal trends in the acoustic data or changes in the mesopelagic community over the duration of the study period. The current biomass estimate should therefore be refined by further work. To elucidate patterns in mesopelagic community backscatter at a finer scale, a concerted acoustic and net sampling protocol is required, similar to the Commission for the Conservation of Antarctic Marine Living Resources (CCAMLR) synoptic krill survey, where acoustic sampling is completed in a parallel transect pattern with concurrent net data (Trathan et al., 2001, Fielding et al., 2016), enabling fine-scale detail of spatial patterns to be revealed. However, these large-scale surveys are effort and cost intensive. For example the CCAMLR synoptic surveys involved four international research vessels surveying for 1 month, and logistical constraints mean that they take place very infrequently (Hewitt et al., 2004). Nevertheless, we are entering an era where fishing vessels are starting to collect calibrated acoustic data (Watkins et al., 2016, Haris and Kloser, 2018), and compilations of such data have the potential to contribute to our knowledge of the spatial and temporal patterns of acoustic signal across the Southern Ocean.

The vertical ranges of some mesopelagic species, which extend into the epipelagic zone, indicate that diel vertical migration behaviour south of 57° S may not be fully resolved. The use of an array of upward facing echosounders on fixed moorings at fixed depths would facilitate the capture of fine-scale migration behaviour of the mesopelagic community, and the detection of seasonal changes in migration behaviour (La et al., 2015). Simultaneous collection of data on downwelling light and temperature would enable the relative impact of environmental variables as drivers of DVM behaviour to be quantitatively investigated.

5.3 Exploitation – potential and challenges

This thesis has identified a potential mesopelagic fish biomass of ~52 Mt (38 – 69 Mt) in the Scotia Sea (area ~2.5 million km²), with a peak in biomass predicted in the region of the sea ice edge. In comparison to an estimated krill biomass of 60.3 Mt (area ~2 million km²) (Fielding et al., 2011), mesopelagic fish are a potentially considerable resource. While this magnitude of fish may offer opportunities as a viable fishery, nontrivial questions around the sustainability and catchability of these species remain, which need to be resolved before we can begin to model the impacts of fishing on the mesopelagic fish population or ecosystem functioning.

Sustainable yield is built on the principle that a portion of a resource can be harvested at a rate that will be naturally replenished without negatively affecting the standing stock. Within the CCAMLR convention area, a precautionary approach to fisheries has been adopted (Constable, 2000). This includes a requirement for fisheries to ensure that (i) balance is maintained within the ecosystem, taking into account the role of the target species as both predator and prey, (ii) the sustainable yield of the target species stock is not reduced, and stable recruitment is safeguarded, and (iii) harvesting does not negatively impact on the marine ecosystem, directly or indirectly (Constable, 2000). I will now look at these principles to highlight areas of further research required to fulfil the criteria of precautionary approach to fisheries and assess commercial viability.

To manage an ecosystem, good baseline data on the species present, their trophic interactions, energetic requirements, and the external factors that may cause their populations to naturally fluctuate is required. In the previous section I highlighted the sources of uncertainty yet to be resolved in my current mesopelagic fish biomass estimate. Narrowing the uncertainties in the current biomass estimate is important to generate a robust pre-exploitation baseline and facilitate ongoing monitoring. Beyond the effects of fishing mortality on the fish population, mesopelagic fish are recognised as consumers of krill, and prey for higher predators. Larger myctophids are major consumers of Antarctic krill, a keystone species in the food web of the Scotia Sea (Saunders et al., 2019). It seems reasonable to assume that a mesopelagic fishery would be likely to target larger individuals, in turn releasing krill from a degree of predation pressure which may result in an initial increase in krill density. However, the longer-term effects of mesopelagic fish extraction would need to be monitored in both the fish and krill fisheries.

The impact of mesopelagic fish extraction on higher predators is likely to be less favourable. While we know that mesopelagic fish, in particular myctophids, are a key component in the diet of many higher predators, a lack of predator biomass and fish consumption data at the ocean basin scale limits our ability to estimate predator requirements. In addition, mesopelagic fish are known to provide an alternative food source to krill consumers, when krill are scarce (Murphy et al., 2007). Given that krill distributions are changing in response to climatic warming (Atkinson et al., 2019), the extent to which mesopelagic fish can fill this gap is yet to be resolved.

Much remains unknown about the life cycles or reproductive strategies of the majority of mesopelagic fish species in the Southern Ocean, which is of particular importance in estimating their potential as a sustainable resource and safeguarding stable recruitment. For example *Electrona antarctica*, the dominant species in colder polar waters, are thought to have a lifespan of ~3.5 years, only reproducing in the final year (Greely et al., 1999). However, questions remain as to its reproductive cycle, the conditions required for effective larval recruitment, and fecundity, which is generally considered to be low in mesopelagic species (Gjøsaeter and Kawaguchi, 1980). Low rates of fecundity make species particularly vulnerable to overexploitation, so further research is required to ensure appropriate management for stable recruitment. Given that a fishery is likely to harvest larger individuals, the spawning stock is at particular risk of exploitation and the spatial extent of any fishery needs to be limited to avoid conservation issues. In *E. antarctica* both adults and larvae are known to occur in the sea ice sector (Moteki et al., 2017), which is also the location of the highest predicted biomass (and hence most productive fishing grounds), and a common foraging area for higher predators. Therefore, there is clear potential for a fishery based in this sector to remove spawning individuals from the stock, and impact directly on higher trophic levels.

For any fishery to be economically viable the catch per unit effort must be high enough that the value of fish biomass justifies the effort to capture it. While the biomass of fish may be sufficient, myctophid fisheries have previously existed and closed (FAO, 1997). Exploratory research was conducted into a potential myctophid (*Benthosema pterotum*) fishery in the Oman Sea, but failed to capture sufficient fish to be viable (Valinassab et al., 2007). In addition, a number of species, including *E. antarctica*, are known to be high in wax esters, which has industrial uses but makes them less suitable for direct human consumption (Phleger et al., 1997). The high lipid content also makes them difficult to process (FAO, 1997). Given that mesopelagic fish are prone to exhibit net avoidance (Kaartvedt et al., 2012), there may be also be fishing gear design issues to overcome before any commercial exploitation can be considered.

5.4 Climate change and mesopelagic fish

There is a two-way interaction between climate and mesopelagic fish, where (i) mesopelagic fish provide an ecosystem service by actively sequestering carbon during DVM (Robinson et al., 2010), and (ii) climate change is predicted to affect the distribution, and hence community structure, of mesopelagic fish (Freer et al., 2019).

Models predict that projected climate change will increase acoustic backscatter that is generally interpreted as an increase in biomass (Proud et al., 2017). In addition the majority of Southern Ocean myctophid species are predicted to shift towards the Antarctic continent, and those species with a cooler thermal niche are likely to experience a reduction in suitable habitat (Freer et al., 2019). The Scotia Sea mesopelagic fish community is dominated by myctophids, which appear to comply with Bergmann's rule, where larger animals are found in colder environments (Meiri, 2011, Saunders and Tarling, 2018). As a result there is a strong likelihood that as ocean temperatures rise that larger species may be displaced by smaller species (Freer et al., 2019), which according to results in this thesis would be likely to result in an overall decrease in Southern Ocean mesopelagic fish biomass.

Using a relationship between mesopelagic fish community structure and SST, my modelled fish biomass is predicted to be highest in the vicinity of the sea ice edge, with relatively high biomass south of the Southern Boundary. Under a warming ocean scenario, where larger weak-scattering fish species are replaced by small strong-scattering species, this would likely result in an overall decrease in fish biomass, whilst we see an increase in acoustic signal as predicted by Proud et al. (2017). My research indicates that the use of active acoustics for monitoring the mesopelagic community is likely to be a useful method of detecting this initial change in community structure, which can be verified through the use of net samples.

Through DVM and respiration at depth, mesopelagic fish are able to actively sequester carbon into the deep ocean faster than passive sinking would (Belcher et al., 2019). Respiration rates of larger mesopelagic fish are predicted to be higher than in smaller myctophids, based on larger body mass (Belcher et al., 2019). As a result if the larger fish species typical of the more southerly latitudes are replaced by smaller species in response to rising ocean temperatures, it follows that overall respiration would decrease. This has serious implications for active carbon transport between the epipelagic and mesopelagic zones. However, my results indicate that while the signal of DVM is stronger at lower latitudes where smaller species are more common, it is suppressed farther south. It is therefore unclear the extent to which larger mesopelagic fish at more southerly latitudes are contributing to carbon sequestration. If larger fish are not migrating into the surface to feed and respiring at depth, they may provide little in the way of active vertical carbon transport, in comparison to smaller species which may migrate more readily. Before we can quantify their role in the carbon cycle or begin to predict changes to the provision of this ecosystem service if communities are

restricted in response to climate change, further work is required, on a community or species-specific basis, to assess the extent of vertical migration.

5.5 Future work

Along with the areas for improvement I have outlined above, I propose that the following research will help to advance our ability to understand mesopelagic fish distribution and behaviour.

- This research provides an initial biomass estimate for mesopelagic fish in the Scotia Sea, which is extrapolated to the Southern Ocean. There is a clear need to refine this biomass estimate regionally and at greater temporal resolution, and to develop ocean wide monitoring so that changes in the mesopelagic fish community can be detected. In the first instance, the collection of net sample and acoustic data from data poor regions in the Southern Ocean would help to validate the biomass estimate predicted here for regions beyond the Scotia Sea.
- Expanding computed tomography scanning to smaller size classes of mesopelagic fish than were available for this study would help reveal the length at which mesopelagic species gain and lose the gas within their swimbladders, and to test if there were regional differences in swimbladder morphology, which would aid in the validation of biomass and monitoring of mesopelagic community at the regional and oceanic scale. There are also interesting questions around why species in colder waters tend to lack the gas component in their swimbladders, and what selective ecological pressures have promoted this loss over evolutionary time. A summary table, grouping species by common geographical, ecological and physiological characteristics, is provided in Supplement S.1, which frames broader ecological questions about the mesopelagic fish community.
- A strategy to monitor change in the mesopelagic community could be built around the combined use of active acoustics and net sample data. To refine biomass estimates at a regional scale, acoustic data could be gathered as part of a concerted sampling regime consisting of parallel gridded transects, alongside concurrent net sampling, to facilitate geostatistical analysis (Petitgas, 1993). However, as previously highlighted there are considerable time and cost implications associated with the collection of contemporaneous acoustic and net sample data.

- One future solution to the collection of acoustic data is to engage the use of echosounders on commercial fishing and research vessels already in the Southern Ocean, where these ships of opportunity could have their echosounders periodically calibrated to facilitate the conversion of the acoustic signal to biomass (Watkins et al., 2016, Haris and Kloser, 2018). While these would not solve the issue of species identification (Kloser et al., 2009), resources could then be focussed on validating knowledge of the community present, as my current research has indicated a link between the scattering community and SST which may be useful in other locations for inferring the backscattering community.
- Much of our available data in the Southern Ocean is restricted to the summer field season, when vessels can access ice free waters. Arrays of fixed moorings, fitted with wideband autonomous transceivers, have the ability to assess temporal trends in the backscattering mesopelagic community (Urmy et al., 2012, De Robertis et al., 2018). This will help to quantify changes in DVM behaviour both at different locations and over annual cycles.
- Ideally the *in-situ* measurement of free swimming mesopelagic fish, identified to species level would help to refine Target Strength (TS) estimates. Drop down camera acoustic systems have enabled the capture of TS measurements, but have lacked the ability to identify fauna to species level (Kloser et al., 2016). Net-mounted combined camera and acoustic systems have been used on larger fauna, but do not yet have the optical resolution required for the study of mesopelagic fish (Ryan et al., 2009). As underwater technology develops the study of mesopelagic fish behaviour and recording of acoustic properties may help to refine biomass estimates, by accounting for species swimming behaviour.

The composition of the Scotia Sea mesopelagic fish community is intrinsically shaped by changes in sea temperature and seasonal sea ice. By combining knowledge of these unique communities and their backscattering properties, my research has revealed a potentially high biomass of fish in colder polar waters than is commonly interpreted from the acoustic signal. It would appear that there are indeed plenty more fish in the sea¹.

¹ In comparison to previous net-based biomass estimates.

Chapter 5

Supplementary material

Supplement S.1

Table 5.1 Summary of mesopelagic fauna groups as defined by common ecological and physiological characteristics. This study: Yes - all values measured and used in analyses, Partial - some values measured and some mean and/or literature values used, Lit - all values taken from literature, No - species not included in analysis (low abundances). Dist NB and Dist SB - northern and southern frontal boundaries of core distribution range respectively. Depth UB and Depth LB - upper and lower depth boundaries (m) of core vertical range. Max SL is the maximum standard length (mm) as recorded on FishBase (Froese et al., 2014), for *E. antarctica* (small) max SL in red is based on logistic regression for presence of gas in swimbladder. SB is swimbladder status: No SB – no swimbladder, Gas to none – has gas in smaller size classes, Regressed – no gas in size classes studied, Fat - fat invested (no gas). Density is mean tissue density in kg m⁻³, where * denotes estimated value from mean density of similar swimbladder species. Mean SL is mean standard length (mm) of species in this study, and Mean TS is estimated mean target strength of fauna. NOTE: Lower abundances of fauna can be found outside of core range boundaries.

Group	Species	This study	Dist NB	Dist SB	Depth UB m	Depth LB m	Max SL (FB) mm	Lifespan years	SB	Density kg m ⁻³	Mean SL mm	Mean TS dB re 1m ²
Sea ice	<i>Antarctic krill (E. superba)</i>	Lit	PF	SIZ	0	200	>60		No SB	NA	44.00	-80.36
	<i>Electrona antarctica</i> (Small)	Yes	PF	SIZ	0	1000	51	4	Gas to none	1038	44.75	-57.70
	<i>Electrona antarctica</i> (Large)	Yes	PF	SIZ	0	1000	115	4	Gas to none	1038	74.48	-78.13
	<i>Bathylagus</i> spp.	Yes	STF	SIZ	0	1000	217		No SB	1037.05	96.19	-71.88
	<i>Gymnoscopelus nicholsi</i>	Partial	STF	SIZ	0	1000	161	7	Regressed	*1043.38	122.68	-69.11
	<i>Gymnoscopelus braueri</i>	Yes	STF	SIZ	0	1000	132	4	Regressed	1028.94	84.22	-80.27
	<i>Notolepis</i> spp.	Partial	PF	SIZ	200	1000	380		No SB	*1043.38	76.07	-77.21
	<i>Bathylagus antarcticus</i>	Yes	PF	SIZ	200	1000	170		No SB	1037.05	96.19	-71.88
	<i>Gymnoscopelus opisthopterus</i>	No	STF	SIZ	400	1000	162	5	Regressed	NA	NA	NA
	<i>Cyclothone</i> spp.	Partial	STF	SIZ	400	1000	76		Fat	*1043.38	48.23	-86.23
Transitional	<i>Protomyctophum choriodon</i>	No	STF	SACCF	0	400	95	4	Gas	NA	NA	NA
	<i>Protomyctophum bolini</i>	Yes	STF	SACCF	200	700	67	2	Gas	1061.67	43.94	-54.09
	<i>Krefflichthys anderssoni</i>	Yes	STF	SACCF	200	1000	71	3	Gas	1038.39	45.09	-57.68
Northern	<i>Electrona carlsbergi</i>	Yes	STF	PF	0	400	112	5	Gas	1061.44	75.64	-49.10
	<i>Gymnoscopelus fraseri</i>	Yes	STF	PF	0	400	88	3	Regressed	1064.14	65.46	-77.37
	<i>Protomyctophum tenisoni</i>	Partial	STF	PF	0	700	54	2	Gas	*1053.83	39.33	-55.85
	<i>Nannobrachium achirus</i>	No	STF	PF	200	1000	162	4	NA	NA	NA	NA

Sea ice group: Fauna with a core distance range that extends into the Sea ice zone (SIZ)

The 'sea ice' group includes both polar specialists and broadly Antarctic species with an extended northerly range.

- There is an ontogenetic loss of swimbladder gas (or complete lack of swimbladder) in all of the fauna in this group, as well as a relatively low mean tissue density.
- As has previously been noted (Saunders and Tarling, 2018), fish in these colder waters predominantly attain a larger maximum standard length.
- Myctophids in this group have a lifespan ≥ 4 years.
- All of these fish taxa occupy the deepest depth zones of the mesopelagic, down to 1000 m.
- Some taxa (*Bathylagus antarcticus*, *Notolepis* spp, *Cyclothone* spp. and *Gymnoscopelus opisthopterus*) are predominantly found deeper than the epipelagic zone, where undercooled Antarctic winter water (WW) may act as a temperature barrier.
- However, other species, specifically *E. antarctica* and *G. braueri*, can be found in the epipelagic zone suggesting these animals do tolerate a degree of undercooling whilst passing through WW, though how often these fauna would cross this potential barrier is unclear.
- Questions remain as to whether the loss of swimbladder gas is in response to large scale migrations, or if water temperature is a barrier to maintaining gas in a swimbladder. Unlike the majority of myctophid species, both adult and juvenile *E. antarctica* are found in the Scotia Sea, however it is unclear if there is any depth stratification of this species based on swimbladder condition.

Transitional group: Fauna with a core distance range extending south to the SACCF

The 'transitional' group includes both south temperate and broadly Antarctic species rarely found south of the SACCF. This region is the farthest south to support smaller myctophid species, with max standard length <100 mm.

- The species in this group maintain a functional (gas bearing) swimbladder throughout their lifespan.
- Similar to some fauna in the sea ice group *Krefflichthys anderssoni* and *Protomyctophum bolini*, also have depth ranges predominantly deeper than 200 m, though there is evidence of surface feeding in both species.
- In contrast *Protomyctophum choriodon*, which was not part of the current study as it occurs in low abundances, is also likely to be gas bearing and occupies a relatively shallow depth range (0-400 m).
- *K. anderssoni* has a relatively low tissue density in comparison to other gas-bearing taxa. There is evidence that KRA depth of occupation is progressively deeper from spring (~200 m at night) through to autumn (700-1000 m at night), with younger size classes in surface water (Lourenço et al., 2016).
- Questions remain as to the feeding strategies of these fauna, how body condition relates to depth of occupation and vertical migration, and what the benefits are of maintaining a gas filled swimbladder in smaller myctophids.

Northern group: Fauna with a core distance range extending south to the PF

The 'northern' group is the most diverse, including south temperate and broadly Antarctic species. This cosmopolitan region supports species from the 'transitional' and 'sea ice' groups, with a corresponding range of size classes, core depth habitat, and swimbladder adaptations, indicating the potential for niche partitioning.

- *G. fraseri* and *E. carlsbergi* occupy similar depths (0-400 m) but deploy different buoyancy mechanisms, while there is an overlap in prey taken by these species, they are exploited in different quantities (Saunders et al., 2019).
- Notably, *G. fraseri* (a regressed swimbladder species) maintains a relatively high tissue density in comparison *Gymnoscopelus* species, which may be linked to alternative feeding strategy. Further work is required to elucidate the drivers of high tissue density of *G. fraseri*.
- There are also unanswered questions around the reproductive strategies of Southern Ocean myctophids, as smaller larval individual of the majority of species are not found in the Scotia Sea.

References

- AINLEY, D. G., FRASER, W. R., SMITH, W. O., HOPKINS, T. L. & TORRES, J. J. 1991. The structure of upper level pelagic food webs in the Antarctic: Effect of phytoplankton distribution. *Journal of Marine Systems*, 2, 111-122.
- AINLEY, D. G., FRASER, W. R., SULLIVAN, C. W., TORRES, J. J., HOPKINS, T. L. & SMITH, W. O. 1986. Antarctic mesopelagic micronekton: Evidence from seabirds that pack ice affects community structure. *Science*, 232, 847-849.
- ANDERSON, C. I. H., BRIERLEY, A. S. & ARMSTRONG, F. 2005. Spatio-temporal variability in the distribution of epi- and meso-pelagic acoustic backscatter in the Irminger Sea, North Atlantic, with implications for predation on *Calanus finmarchicus*. *Marine Biology*, 146, 1177-1188.
- ANDERSON, T. R., MARTIN, A. P., LAMPITT, R. S., TRUEMAN, C. N., HENSON, S. A. & MAYOR, D. J. 2018. Quantifying carbon fluxes from primary production to mesopelagic fish using a simple food web model. *ICES Journal of Marine Science*, 76, 690-701.
- ANDERSON, V. C. 1950. Sound scattering from a fluid sphere. *The Journal of the Acoustical Society of America*, 22, 426-431.
- ANDREEVA, I. B. 1964. Scattering of sound by air bladders of fish in deep sound-scattering ocean layers. *Soviet Physics Acoustics*, 10, 17-20.
- ARRIGO, K. R., VAN DIJKEN, G. L. & BUSHINSKY, S. 2008. Primary production in the Southern Ocean, 1997–2006. *Journal of Geophysical Research: Oceans*, 113, C08004.
- ATKINSON, A., HILL, S. L., PAKHOMOV, E. A., SIEGEL, V., ANADON, R., CHIBA, S., DALY, K. L., DOWNIE, R., FIELDING, S., FRETWELL, P., GERRISH, L., HOSIE, G. W., JESSOPP, M. J., KAWAGUCHI, S., KRAFFT, B. A., LOEB, V., NISHIKAWA, J., PEAT, H. J., REISS, C. S., ROSS, R. M., QUETIN, L. B., SCHMIDT, K., STEINBERG, D. K., SUBRAMANIAM, R. C., TARLING, G. A. & WARD, P. 2017. KRILLBASE: A circumpolar database of Antarctic krill and salp numerical densities, 1926–2016. *Earth System Science Data*, 9, 193-210.
- ATKINSON, A., HILL, S. L., PAKHOMOV, E. A., SIEGEL, V., REISS, C. S., LOEB, V. J., STEINBERG, D. K., SCHMIDT, K., TARLING, G. A., GERRISH, L. & SAILLEY, S. F. 2019. Krill (*Euphausia superba*) distribution contracts southward during rapid regional warming. *Nature Climate Change*, 9, 142-147.
- ATKINSON, A., NICOL, S., KAWAGUCHI, S., PAKHOMOV, E., QUETIN, L., ROSS, R., HILL, S., REISS, C., SIEGEL, V. & TARLING, G. 2012a. Fitting *Euphausia superba* into Southern Ocean food-web models: a review of data sources and their limitations. *CCAMLR Science*, 19, 219-245.
- ATKINSON, A., SIEGEL, V., PAKHOMOV, E. & ROTHERY, P. 2004. Long-term decline in krill stock and increase in salps within the Southern Ocean. *Nature*, 432, 100-103.
- ATKINSON, A., SIEGEL, V., PAKHOMOV, E. A., ROTHERY, P., LOEB, V., ROSS, R. M., QUETIN, L. B., SCHMIDT, K., FRETWELL, P., MURPHY, E. J., TARLING, G. A. &

- FLEMING, A. H. 2008. Oceanic circumpolar habitats of Antarctic krill. *Marine Ecology Progress Series*, 362, 1-23.
- ATKINSON, A., WARD, P., HUNT, B. P. V., PAKHOMOV, E. A. & HOSIE, G. W. 2012b. An overview of Southern Ocean zooplankton data: abundance, biomass, feeding and functional relationships. *CCAMLR Science*, 19, 171-218.
- BAKER, A. D. C., CLARKE, M. R. & HARRIS, M. J. 1973. The N.I.O. combination net (RMT 1 + 8) and further developments of rectangular midwater trawls. *Journal of the Marine Biological Association of the United Kingdom*, 53, 167-184.
- BALLS, R. 1948. Herring fishing with the echometer. *Journal du Conseil*, 15, 193-206.
- BARHAM, E. G. 1966. Deep scattering layer migration and composition: observations from a diving saucer. *Science*, 151, 1399-403.
- BATES, D., MAECHLER, M., BOLKER, B. & WALKER, S. 2015. Fitting Linear Mixed-Effects Models using lme4. *Journal of Statistical Software*, 67, 1-48.
- BELCHER, A., SAUNDERS, R. A. & TARLING, G. A. 2019. Respiration rates and active carbon flux of mesopelagic fishes (Family Myctophidae) in the Scotia Sea, Southern Ocean. *Marine Ecology Progress Series*, 610, 149-162.
- BELCHIER, M. & LAWSON, J. 2013. An analysis of temporal variability in abundance, diversity and growth rates within the coastal ichthyoplankton assemblage of South Georgia (sub-Antarctic). *Polar Biology*, 36, 969-983.
- BENOIT-BIRD, K. J. & AU, W. W. L. 2001. Target strength measurements of Hawaiian mesopelagic boundary community animals. *The Journal of the Acoustical Society of America*, 110, 812-819.
- BENOIT-BIRD, K. J., AU, W. W. L., KELLEY, C. D. & TAYLOR, C. 2003. Acoustic backscattering by deepwater fish measured in situ from a manned submersible. *Deep-Sea Research Part I: Oceanographic Research Papers*, 50, 221-229.
- BENOIT-BIRD, K. J., AU, W. W. L. & WISDOMA, D. W. 2009. Nocturnal light and lunar cycle effects on diel migration of micronekton. *Limnology and Oceanography*, 54, 1789-1800.
- BENOIT-BIRD, K. J. & LAWSON, G. L. 2016. Ecological insights from pelagic habitats acquired using active acoustic techniques. *Annual Review of Marine Science*, 8, 463-90.
- BIANCHI, D., GALBRAITH, E. D., CAROZZA, D. A., MISLAN, K. A. S. & STOCK, C. A. 2013a. Intensification of open-ocean oxygen depletion by vertically migrating animals. *Nature Geoscience*, 6, 545-548.
- BIANCHI, D., STOCK, C., GALBRAITH, E. D. & SARMIENTO, J. L. 2013b. Diel vertical migration: Ecological controls and impacts on the biological pump in a one-dimensional ocean model. *Global Biogeochemical Cycles*, 27, 478-491.
- BIVAND, R. & LEWIN-KOH, N. 2018. maptools: Tools for handling spatial objects. R package version 0.9-4 ed.

- BIVAND, R. & RUNDEL, C. 2018. rgeos: Interface to Geometry Engine - Open Source ('GEOS'). R package version 0.4-2 ed.
- BOERSCH-SUPAN, P. H., ROGERS, A. D. & BRIERLEY, A. S. 2017. The distribution of pelagic sound scattering layers across the southwest Indian Ocean. *Deep-Sea Research Part II: Topical Studies in Oceanography*, 136, 108-121.
- BOST, C. A., GEORGES, J. Y., GUINET, C., CHEREL, Y., PÜTZ, K., CHARRASSIN, J. B., HANDRICH, Y., ZORN, T., LAGE, J. & LE MAHO, Y. 1997. Foraging habitat and food intake of satellite-tracked king penguins during the austral summer at Crozet Archipelago. *Marine Ecology Progress Series*, 150, 21-33.
- BRIERLEY, A. S. 2014. Diel vertical migration. *Current Biology*, 24, R1074-R1076.
- BUTLER, J. L. & PEARCY, W. G. 1972. Swimbladder morphology and specific gravity of Myctophids off Oregon. *Journal of the Fisheries Board of Canada*, 29, 1145-1150.
- CADE, D. E. & BENOIT-BIRD, K. J. 2015. Depths, migration rates and environmental associations of acoustic scattering layers in the Gulf of California. *Deep-Sea Research Part I: Oceanographic Research Papers*, 102, 78-89.
- CATUL, V., GAUNS, M. & KARUPPASAMY, P. K. 2011. A review on mesopelagic fishes belonging to family Myctophidae. *Reviews in Fish Biology and Fisheries*, 21, 339-354.
- CHARRASSIN, J.-B. & BOST, C.-A. 2001. Utilisation of the oceanic habitat by king penguins over the annual cycle. *Marine Ecology Progress Series*, 221, 285-298.
- CHEREL, Y., DUCATEZ, S., FONTAINE, C., RICHARD, P. & GUINET, C. 2008. Stable isotopes reveal the trophic position and mesopelagic fish diet of female southern elephant seals breeding on the Kerguelen Islands. *Marine Ecology Progress Series*, 370, 239-247.
- CLARK, C. W. & LEVY, D. A. 1988. Diel vertical migrations by juvenile sockeye salmon and the antipredation window. *The American Naturalist*, 131, 271-290.
- CLAY, C. S. & HORNE, J. K. 1994. Acoustic models of fish: The Atlantic cod (*Gadus morhua*). *The Journal of the Acoustical Society of America*, 96, 1661-1668.
- COLLINS, M. A., ROSS, K. A., BELCHIER, M. & REID, K. 2007. Distribution and diet of juvenile Patagonian toothfish on the South Georgia and Shag Rocks shelves (Southern Ocean). *Marine Biology*, 152, 135-147.
- COLLINS, M. A., STOWASSER, G., FIELDING, S., SHREEVE, R., XAVIER, J. C., VENABLES, H. J., ENDERLEIN, P., CHEREL, Y. & VAN DE PUTTE, A. 2012. Latitudinal and bathymetric patterns in the distribution and abundance of mesopelagic fish in the Scotia Sea. *Deep-Sea Research Part II: Topical Studies in Oceanography*, 59, 189-198.
- COLLINS, M. A., XAVIER, J. C., JOHNSTON, N. M., NORTH, A. W., ENDERLEIN, P., TARLING, G. A., WALUDA, C. M., HAWKER, E. J. & CUNNINGHAM, N. J. 2008. Patterns in the distribution of myctophid fish in the northern Scotia Sea ecosystem. *Polar Biology*, 31, 837-851.
- CONNAN, M., CHEREL, Y. & MAYZAUD, P. 2007. Lipids from stomach oil of procellariiform seabirds document the importance of myctophid fish in the Southern Ocean. *Limnology and Oceanography*, 52, 2445-2455.

- CONSTABLE, A. 2000. Managing fisheries to conserve the Antarctic marine ecosystem: practical implementation of the Convention on the Conservation of Antarctic Marine Living Resources (CCAMLR). *ICES Journal of Marine Science*, 57, 778-791.
- CROXALL, J. P., REID, K. & PRINCE, P. A. 1999. Diet, provisioning and productivity responses of marine predators to differences in availability of Antarctic krill. *Marine Ecology Progress Series*, 177, 115-131.
- CULLINS, T. L., DEVRIES, A. L. & TORRES, J. J. 2011. Antifreeze proteins in pelagic fishes from Marguerite Bay (Western Antarctica). *Deep-Sea Research Part II: Topical Studies in Oceanography*, 58, 1690-1694.
- DAVISON, P. 2011. The specific gravity of mesopelagic fish from the northeastern Pacific Ocean and its implications for acoustic backscatter. *ICES Journal of Marine Science*, 68, 2064-2074.
- DAVISON, P. C., CHECKLEY, D. M., KOSLOW, J. A. & BARLOW, J. 2013. Carbon export mediated by mesopelagic fishes in the northeast Pacific Ocean. *Progress in Oceanography*, 116, 14-30.
- DAVISON, P. C., KOSLOW, J. A. & KLOSER, R. J. 2015. Acoustic biomass estimation of mesopelagic fish: backscattering from individuals, populations, and communities. *ICES Journal of Marine Science*, 72, 1413-1424.
- DE ROBERTIS, A. & HIGGINBOTTOM, I. 2007. A post-processing technique to estimate the signal-to-noise ratio and remove echosounder background noise. *ICES Journal of Marine Science*, 64, 1282-1291.
- DE ROBERTIS, A., LEVINE, R. & WILSON, C. D. 2018. Can a bottom-moored echo sounder array provide a survey-comparable index of abundance? *Canadian Journal of Fisheries and Aquatic Sciences*, 75, 629-640.
- DEMER, D. A. 2004. An estimate of error for the CCAMLR 2000 survey estimate of krill biomass. *Deep-Sea Research Part II: Topical Studies in Oceanography*, 51, 1237-1251.
- DEMER, D. A., BERGER, L., BERNASCONI, M., BETHKE, E., BOSWELL, K., CHU, D. D., REKA, DUNFORD, A., FÄSSLER, S., GAUTHIER, S., HUFNAGLE, L. T., JECH, J. M., BOUFFANT, N., LEBOURGES-DHAUSSY, A., LURTON, X., MACAULAY, G. J., PERROT, Y., RYAN, T., PARKER-STETTER, S., STIENESSEN, S., WEBER, T. & WILLIAMSON, N. 2015. Calibration of acoustic instruments. In: ANDERSON, E. D. (ed.) *ICES Cooperative Research Report*. Copenhagen, Denmark: International Council for the Exploration of the Sea.
- DEMER, D. A. & CONTI, S. G. 2005. New target-strength model indicates more krill in the Southern Ocean. *ICES Journal of Marine Science*, 62, 25-32.
- DEMER, D. A. & HEWITT, R. P. 1995. Bias in acoustic biomass estimates of *Euphausia superba* due to diel vertical migration. *Deep-Sea Research Part I: Oceanographic Research Papers*, 42, 455-475.
- DEMER, D. A., KLOSER, R. J., MACLENNAN, D. N. & ONA, E. 2009. An introduction to the proceedings and a synthesis of the 2008 ICES Symposium on the Ecosystem Approach

- with Fisheries Acoustics and Complementary Technologies (SEAFACETS). *ICES Journal of Marine Science*, 66, 961–965.
- DIETZ, R. S. 1962. The sea's deep scattering layers. *Scientific American*, 207, 44-51.
- DONNELLY, J., TORRES, J. J., HOPKINS, T. L. & LANCRAFT, T. M. 1990. Proximate composition of Antarctic mesopelagic fishes. *Marine Biology*, 106, 13-23.
- DORNAN, T. 2017. Morphometric analysis of mesopelagic fish fauna. *RRS James Clark Ross JR16003 – Cruise summary report*.
- DORNAN, T., FIELDING, S., SAUNDERS, R. A. & GENNER, M. J. 2019. Swimbladder morphology masks Southern Ocean mesopelagic fish biomass. *Proceedings of the Royal Society B: Biological Sciences*, 286, 20190353.
- DOWLE, M. & SRINIVASAN, A. 2018. data.table: Extension of `data.frame`. R package version 1.11.8 ed.
- DUHAMEL, G. 1998. The pelagic fish community of the Polar Front Zone off the Kerguelen Islands. In: DI PRISCO, G., PISANO, E. & CLARK, M. (eds.) *Fishes of Antarctica: A biological overview*. Milan, Italy: Springer-Verlag.
- DYPVIK, E., ROSTAD, A. & KAARTVEDT, S. 2012. Seasonal variations in vertical migration of glacier lanternfish, *Benthoosema glaciale*. *Marine Biology*, 159, 1673-1683.
- EL-SAYED, S. Z. 1994. History, organization and accomplishments of the BIOMASS Programme. In: EL-SAYED, S. Z. (ed.) *Southern Ocean ecology : the BIOMASS perspective*. Cambridge: Cambridge University Press.
- ESCOBAR-FLORES, P., O'DRISCOLL, R. L. & MONTGOMERY, J. C. 2013. Acoustic characterization of pelagic fish distribution across the South Pacific Ocean. *Marine Ecology Progress Series*, 490, 169-183.
- ESCOBAR-FLORES, P. C. 2017. *The use of acoustics to characterise mid-trophic levels of the Southern Ocean pelagic ecosystem*. PhD Thesis, University of Auckland
- ESCOBAR-FLORES, P. C., O'DRISCOLL, R. L. & MONTGOMERY, J. C. 2018a. Predicting distribution and relative abundance of mid-trophic level organisms using oceanographic parameters and acoustic backscatter. *Marine Ecology Progress Series*, 592, 37-56.
- ESCOBAR-FLORES, P. C., O'DRISCOLL, R. L. & MONTGOMERY, J. C. 2018b. Spatial and temporal distribution patterns of acoustic backscatter in the New Zealand sector of the Southern Ocean. *Marine Ecology Progress Series*, 592, 19-35.
- EUROPEAN COMMISSION 2018. Horizon 2020 - Work Programme 2018-2020. *Food security, sustainable agriculture and forestry, marine, maritime and inland water research and the bioeconomy*. European Commission.
- FAO 1997. Review of the state of world fishery resources: Marine fisheries. Rome: Food and Agriculture Organization of the United Nations.
- FAO 2019. Fishery and Aquaculture Statistics. Global capture production 1950-2017 (FishstatJ). Rome: FAO Fisheries and Aquaculture Department.

- FERNANDES, P. G., GERLOTTO, F., HOLLIDAY, D. V., NAKKEN, O. & SIMMONDS, E. J. 2002. Acoustic applications in fisheries science: the ICES contribution. *ICES Marine Science Symposia*, 215, 483-492.
- FETTERER, F., KNOWLES, K., MEIER, W., SAVOIE, M. & WINDNAGEL, A. K. 2017. Sea ice Index, Version 3. Boulder, Colorado USA: NSIDC: National Snow and Ice Data Center.
- FIELDING, S., COSSIO, A., COX, M., REISS, C., SKARET, G., DEMER, D., WATKINS, J. & ZHAO, X. 2016. A condensed history and document of the method used by CCAMLR to estimate krill biomass (B0) in 2010.
- FIELDING, S., WATKINS, J., COSSIO, A., REISS, C., WATTERS, G., CALISE, L., SKARET, G., TAKAO, Y., ZHAO, X., AGNEW, D., RAMM, D. & REID, K. 2011. The ASAM 2010 assessment of krill biomass for area 48 from the Scotia Sea CCAMLR 2000 synoptic survey. Hobart, Australia: CCAMLR.
- FIELDING, S., WATKINS, J. L., COLLINS, M. A., ENDERLEIN, P. & VENABLES, H. J. 2012. Acoustic determination of the distribution of fish and krill across the Scotia Sea in spring 2006, summer 2008 and autumn 2009. *Deep-Sea Research Part II: Topical Studies in Oceanography*, 59, 173-188.
- FIELDING, S., WATKINS, J. L., TRATHAN, P. N., ENDERLEIN, P., WALUDA, C. M., STOWASSER, G., TARLING, G. A. & MURPHY, E. J. 2014. Interannual variability in Antarctic krill (*Euphausia superba*) density at South Georgia, Southern Ocean: 1997–2013. *ICES Journal of Marine Science*, 71, 2578-2588.
- FIRING, Y. L., MCDONAGH, E. L., KING, B. A. & DESBRUYÈRES, D. G. 2017. Deep temperature variability in Drake Passage. *Journal of Geophysical Research: Oceans*, 122, 713-725.
- FLORES, H., ATKINSON, A., KAWAGUCHI, S., KRAFFT, B. A., MILINEVSKY, G., NICOL, S., REISS, C., TARLING, G., WERNER, R., REBOLLEDO, E., CIRELLI, V., CUZIN-ROUDY, J., FIELDING, S., GROENEVELD, J., HARALDSSON, M., LOMBANA, A., MARSCHOFF, E., MEYER, B., PAKHOMOV, E., ROMBOLA, E., SCHMIDT, K., SIEGEL, V., TESCHKE, M., TONKES, H., TOULLEC, J., TRATHAN, P., TREMBLAY, N., VAN DE PUTTE, A. P., VAN FRANEKER, J. & WERNER, T. 2012. Impact of climate change on Antarctic krill. *Marine Ecology Progress Series*, 458, 1-19.
- FLYNN, A. J. & KLOSER, R. J. 2012. Cross-basin heterogeneity in lanternfish (family Myctophidae) assemblages and isotopic niches ($\delta^{13}\text{C}$ and $\delta^{15}\text{N}$) in the southern Tasman Sea abyssal basin. *Deep-Sea Research Part I: Oceanographic Research Papers*, 69, 113-127.
- FOOTE, K. G. 1980a. Effect of fish behaviour on echo energy: the need for measurements of orientation distributions. *ICES Journal of Marine Science*, 39, 193-201.
- FOOTE, K. G. 1980b. Importance of the swimbladder in acoustic scattering by fish: a comparison of gadoid and mackerel target strengths. *The Journal of the Acoustical Society of America*, 67, 2084-2089.
- FOOTE, K. G. 1982. Optimizing copper spheres for precision calibration of hydroacoustic equipment. *The Journal of the Acoustical Society of America*, 71, 742-747.

- FOOTE, K. G., KNUDSEN, H. P., VESTNES, G., MACLENNAN, D. N. & SIMMONDS, E. J. 1987. Calibration of acoustic instruments for fish density estimation: a practical guide. *Cooperative research report*. Copenhagen: International Council for the Exploration of the Sea.
- FOOTE, K. G. & STANTON, T. K. 2000. Acoustical methods. *ICES Zooplankton Methodology Manual*. Elsevier.
- FRANCOIS, R. E. & GARRISON, G. R. 1982. Sound absorption based on ocean measurements: Part I: Pure water and magnesium sulfate contributions. *The Journal of the Acoustical Society of America*, 72, 896-907.
- FREER, J. J., TARLING, G. A., COLLINS, M. A., PARTRIDGE, J. C. & GENNER, M. J. 2019. Predicting future distributions of lanternfish, a significant ecological resource within the Southern Ocean. *Diversity and Distributions*, 25, 1259-1272.
- FROESE, R. & PAULY, D. 2019. FishBase. World Wide Web electronic publication.
- FROESE, R., THORSON, J. T. & REYES, R. B. 2014. A Bayesian approach for estimating length-weight relationships in fishes. *Journal of Applied Ichthyology*, 30, 78-85.
- GAMA, J. 2016. sonar: Fundamental formulas for sonar. R package version 1.0.2 ed.
- GARABATO, A. C. N., POLZIN, K. L., KING, B. A., HEYWOOD, K. J. & VISBECK, M. 2004. Widespread intense turbulent mixing in the Southern Ocean. *Science*, 303, 210-213.
- GEBCO 2014. The GEBCO_2014 Grid.
- GEBCO COMPILATION GROUP 2019. GEBCO 2019 Grid.
- GILLY, W. F., BEMAN, J. M., LITVIN, S. Y. & ROBISON, B. H. 2013. Oceanographic and biological effects of shoaling of the oxygen minimum zone. *Annual Review of Marine Science*, 5, 393-420.
- GJØSÆTER, H., WIEBE, P. H., KNUTSEN, T. & INGVALDSEN, R. B. 2017. Evidence of diel vertical migration of mesopelagic sound-scattering organisms in the Arctic. *Frontiers in Marine Science*, 4, 332.
- GJØSAETER, J. & KAWAGUCHI, K. 1980. A review of the world resources of mesopelagic fish. *FAO Fisheries Technical Paper*, 193, 123-134.
- GODØ, O. R., HANDEGARD, N. O., BROWMAN, H. I., MACAULAY, G. J., KAARTVEDT, S., GISKE, J., ONA, E., HUSE, G. & JOHNSEN, E. 2014. Marine ecosystem acoustics (MEA): quantifying processes in the sea at the spatio-temporal scales on which they occur. *ICES Journal of Marine Science*, 71, 2357-2369.
- GODØ, O. R., PATEL, R. & PEDERSEN, G. 2009. Diel migration and swimbladder resonance of small fish: some implications for analyses of multifrequency echo data. *ICES Journal of Marine Science*, 66, 1143-1148.
- GOHIN, F., DRUON, J. N. & LAMPERT, L. 2002. A five channel chlorophyll concentration algorithm applied to SeaWiFS data processed by SeaDAS in coastal waters. *International Journal of Remote Sensing*, 23, 1639-1661.

- GON, O. & HEEMSTRA, P. C. (eds.) 1990. *Fishes of the Southern Ocean*, Grahamstown: J.L.B. Smith Institute of Ichthyology.
- GOODALL, R. N. P., BAKER, A. N., BEST, P. B., MEYER, M. & MIYAZAKI, N. 1997. On the biology of the hourglass dolphin, *Lagenorhynchus cruciger* (Quoy and Gaimard, 1824). In: DONOVAN, G. P. (ed.) *Forty-Seventh Report of the International Whaling Commission*. Cambridge: The International Whaling Commission.
- GREELY, T. M., GARTNER JR, J. V. & TORRES, J. J. 1999. Age and growth of *Electrona antarctica* (Pisces: Myctophidae), the dominant mesopelagic fish of the Southern Ocean. *Marine Biology*, 133, 145-158.
- GUINEHUT, S., DHOMPS, A. L., LARNICOL, G. & LE TRAON, P. Y. 2012. High resolution 3D temperature and salinity fields derived from in situ and satellite observations. *Ocean Science*, 8, 845-857.
- GUINEHUT, S., LE TRAON, P. Y., LARNICOL, G. & PHILIPPS, S. 2004. Combining Argo and remote-sensing data to estimate the ocean three-dimensional temperature fields - A first approach based on simulated observation. *Journal of Marine Systems*, 46, 85-98.
- GUINET, C., VACQUIE-GARCIA, J., PICARD, B., BESSIGNEUL, G., LEBRAS, Y., DRAGON, A. C., VIVIAN, M., ARNOULD, J. P. Y. & BAILLEUL, F. 2014. Southern elephant seal foraging success in relation to temperature and light conditions: insight into prey distribution. *Marine Ecology Progress Series*, 499, 285-301.
- GUISAN, A., EDWARDS, T. C. & HASTIE, T. 2002. Generalized linear and generalized additive models in studies of species distributions: setting the scene. *Ecological Modelling*, 157, 89-100.
- HARIS, K. & KLOSER, R. 2018. Acoustic data from vessels of opportunity. Report from the EU-H2020 MESOPP project.
- HAYS, G. C. 2003. A review of the adaptive significance and ecosystem consequences of zooplankton diel vertical migrations. *Hydrobiologia*, 503, 163-170.
- HEWITT, R. P., WATKINS, J., NAGANOBU, M., SUSHIN, V., BRIERLEY, A. S., DEMER, D., KASATKINA, S., TAKAO, Y., GOSS, C., MALYSHKO, A., BRANDON, M., KAWAGUCHI, S., SIEGEL, V., TRATHAN, P., EMERY, J., EVERSON, I. & MILLER, D. 2004. Biomass of Antarctic krill in the Scotia Sea in January/February 2000 and its use in revising an estimate of precautionary yield. *Deep-Sea Research Part II: Topical Studies in Oceanography*, 51, 1215-1236.
- HEYWOOD, K. J., SCHMIDTKO, S., HEUZE, C., KAISER, J., JICKELLS, T. D., QUESTE, B. Y., STEVENS, D. P., WADLEY, M., THOMPSON, A. F., FIELDING, S., GUIHEN, D., CREED, E., RIDLEY, J. K. & SMITH, W. 2014. Ocean processes at the Antarctic continental slope. *Philosophical Transactions of the Royal Society A-Mathematical Physical and Engineering Sciences*, 372, 20130047.
- HIJMANS, R. J. 2018. raster: Geographic data analysis and modeling. R package version 2.8-4 ed.
- HIJMANS, R. J. 2019. geosphere: Spherical Trigonometry. R package version 1.5-10. ed.

- HOLLIDAY, D. V. 1972. Resonance structure in echoes from schooled pelagic fish. *The Journal of the Acoustical Society of America*, 51, 1322-1332.
- HU, C. M., LEE, Z. & FRANZ, B. 2012. Chlorophyll *a* algorithms for oligotrophic oceans: A novel approach based on three-band reflectance difference. *Journal of Geophysical Research-Oceans*, 117, C01011.
- HULLEY, A. P. 1990. Family Myctophidae. In: GON, O. & HEEMSTRA, P. C. (eds.) *Fishes of the Southern Ocean*. Grahamstown: J.L.B. Smith Institute of Ichthyology.
- IRIGOIEN, X., KLEVJER, T. A., ROSTAD, A., MARTINEZ, U., BOYRA, G., ACUNA, J. L., BODE, A., ECHEVARRIA, F., GONZALEZ-GORDILLO, J. I., HERNANDEZ-LEON, S., AGUSTI, S., AKSNES, D. L., DUARTE, C. M. & KAARTVEDT, S. 2014. Large mesopelagic fishes biomass and trophic efficiency in the open ocean. *Nature Communications*, 5, 3271.
- JECH, J. M., HORNE, J. K., CHU, D., DEMER, D. A., FRANCIS, D. T., GORSKA, N., JONES, B., LAVERY, A. C., STANTON, T. K., MACAULAY, G. J., REEDER, D. B. & SAWADA, K. 2015. Comparisons among ten models of acoustic backscattering used in aquatic ecosystem research. *The Journal of the Acoustical Society of America*, 138, 3742-64.
- JECH, J. M. & MICHAELS, W. L. 2006. A multifrequency method to classify and evaluate fisheries acoustics data. *Canadian Journal of Fisheries and Aquatic Sciences*, 63, 2225-2235.
- JONES, G. 2005. Echolocation. *Curr Biol*, 15, R484-8.
- JPL MUR MEASURES PROJECT 2015. GHRSSST Level 4 MUR Global Foundation Sea Surface Temperature Analysis (v4.1). 4.1 ed. PO.DAAC, CA, USA.
- KAARTVEDT, S., STABY, A. & AKSNES, D. L. 2012. Efficient trawl avoidance by mesopelagic fishes causes large underestimation of their biomass. *Marine Ecology Progress Series*, 456, 1-6.
- KLEVJER, T. A., IRIGOIEN, X., ROSTAD, A., FRAILE-NUEZ, E., BENITEZ-BARRIOS, V. M. & KAARTVEDT, S. 2016. Large scale patterns in vertical distribution and behaviour of mesopelagic scattering layers. *Scientific Reports*, 6, 19873.
- KLOSER, R. J., RYAN, T., SAKOV, P., WILLIAMS, A. & KOSLOW, J. A. 2002. Species identification in deep water using multiple acoustic frequencies. *Canadian Journal of Fisheries and Aquatic Sciences*, 59, 1065-1077.
- KLOSER, R. J., RYAN, T. E., KEITH, G. & GERSHWIN, L. 2016. Deep-scattering layer, gas-bladder density, and size estimates using a two-frequency acoustic and optical probe. *ICES Journal of Marine Science*, 73, 2037-2048.
- KLOSER, R. J., RYAN, T. E., YOUNG, J. W. & LEWIS, M. E. 2009. Acoustic observations of micronekton fish on the scale of an ocean basin: Potential and challenges. *ICES Journal of Marine Science*, 66, 998-1006.
- KOCK, K. H. 1987. Marine consumers - fish and squid. *Environment International*, 13, 37-45.
- KORNELIUSSEN, R. 2003. Synthetic echograms generated from the relative frequency response. *ICES Journal of Marine Science*, 60, 636-640.

- KORNELIUSSEN, R. J. 2000. Measurement and removal of echo integration noise. *ICES Journal of Marine Science*, 57, 1204-1217.
- LA, H. S., HA, H. K., KANG, C. Y., WÅHLIN, A. K. & SHIN, H. C. 2015. Acoustic backscatter observations with implications for seasonal and vertical migrations of zooplankton and nekton in the Amundsen shelf (Antarctica). *Estuarine, Coastal and Shelf Science*, 152, 124-133.
- LAM, V. W. Y. & PAULY, D. 2005. Mapping the global biomass of mesopelagic fishes. *Sea Around Us Project Newsletter*, 30, 4-4.
- LANCRAFT, T. M., TORRES, J. J. & HOPKINS, T. L. 1989. Micronekton and macrozooplankton in the open waters near Antarctic ice edge zones (AMERIEZ 1983 and 1986). *Polar Biology*, 9, 225-233.
- LANGBEHN, T. J., AKSNES, D. L., KAARTVEDT, S., FIKSEN, Ø. & JØRGENSEN, C. 2019. Light comfort zone in a mesopelagic fish emerges from adaptive behaviour along a latitudinal gradient. *Marine Ecology Progress Series*, 623, 161-174.
- LEA, M. A., CHEREL, Y., GUINET, C. & NICHOLS, P. D. 2002. Antarctic fur seals foraging in the Polar Frontal Zone: inter-annual shifts in diet as shown from fecal and fatty acid analyses. *Marine Ecology Progress Series*, 245, 281-297.
- LEGENDRE, P. 1993. Spatial autocorrelation: trouble or new paradigm? *Ecology*, 74, 1659-1673.
- LENTH, R. 2019. emmeans: Estimated Marginal Means, aka Least-Squares Means. R package version 1.3.2 ed.
- LOCARNINI, R. A., MISHONOV, A. V., BARANOVA, O. K., BOYER, T. P., ZWENG, M. M., GARCIA, H. E., REAGAN, J. R., SEIDOV, D., WEATHERS, K., PAVER, C. R. & SMOLYAR, I. 2018. World Ocean Atlas 2018, Volume 1: Temperature. A. Mishonov Technical Ed. *NOAA Atlas NESDIS 81*.
- LOEB, V. J., KELLERMANN, A. K., KOUBBI, P., NORTH, A. W. & WHITE, M. G. 1993. Antarctic larval fish assemblages: A review. *Bulletin of Marine Science*, 53, 416-449.
- LONGHURST, A. R. 2007. *Ecological geography of the sea*, Elsevier Science & Technology.
- LOURENÇO, S., SAUNDERS, R. A., COLLINS, M., SHREEVE, R., ASSIS, C. A., BELCHIER, M., WATKINS, J. L. & XAVIER, J. C. 2016. Life cycle, distribution and trophodynamics of the lanternfish *Krefftichthys anderssoni* (Lönnerberg, 1905) in the Scotia Sea. *Polar Biology*, 40, 1229-1245.
- LUBIMOVA, T. G., SHUST, K. V. & POPKOV, V. V. 1987. Specific features in the ecology of Southern Ocean mesopelagic fish of the family Myctophidae. (In Russian). *Biological resources of the Arctic and Antarctic (collected papers)*, 320-327.
- MACKENZIE, K. V. 1981. Nine-term equation for sound speed in the ocean. *Journal of the Acoustic Society of America*, 70, 807-812.
- MACLENNAN, D. N., FERNANDES, P. G. & DALEN, J. 2002. A consistent approach to definitions and symbols in fisheries acoustics. *ICES Journal of Marine Science*, 59, 365-369.

- MAPSTONE, G. M. 2014. Global diversity and review of Siphonophorae (Cnidaria: Hydrozoa). *PLOS ONE*, 9, e87737.
- MARSHALL, J. & SPEER, K. 2012. Closure of the meridional overturning circulation through Southern Ocean upwelling. *Nature Geoscience*, 5, 171-180.
- MARSHALL, N. B. 1950. Air bladder structure and vertical distribution in deep-sea fishes. *Annual Report of the Challenger Society*, 3, 26-27.
- MARSHALL, N. B. 1960. Swimbladder structure of deep-sea fishes in relation to their systematics and biology. *Discovery Reports*, 31, 1-122.
- MARTIN, J. H., GORDON, R. M. & FITZWATER, S. E. 1990. Iron in Antarctic waters. *Nature*, 345, 156-158.
- MASSOM, R. A. & STAMMERJOHN, S. E. 2010. Antarctic sea ice change and variability – Physical and ecological implications. *Polar Science*, 4, 149-186.
- MCGEHEE, D. E., O'DRISCOLL, R. L. & TRAYKOVSKI, L. V. M. 1998. Effects of orientation on acoustic scattering from Antarctic krill at 120 kHz. *Deep-Sea Research Part II: Topical Studies in Oceanography*, 45, 1273-1294.
- MEIRI, S. 2011. Bergmann's Rule – what's in a name? *Global Ecology and Biogeography*, 20, 203-207.
- MISUND, O. A. & BELTESTAD, A. K. 1996. Target-strength estimates of schooling herring and mackerel using the comparison method. *ICES Journal of Marine Science*, 53, 281-284.
- MITSON, R. B. & WOOD, R. J. 1961. An automatic method of counting fish echoes. *Journal du Conseil*, 26, 281-291.
- MOORE, J. K., ABBOTT, M. R. & RICHMAN, J. G. 1999. Location and dynamics of the Antarctic Polar Front from satellite sea surface temperature data. *Journal of Geophysical Research: Oceans*, 104, 3059-3073.
- MOTEKI, M., FUJII, K., AMAKASU, K., SHIMADA, K., TANIMURA, A. & ODATE, T. 2017. Distributions of larval and juvenile/adult stages of the Antarctic myctophid fish, *Electrona antarctica*, off Wilkes Land in East Antarctica. *Polar Science*, 12, 99-108.
- MULET, S., RIO, M. H., MIGNOT, A., GUINEHUT, S. & MORROW, R. 2012. A new estimate of the global 3D geostrophic ocean circulation based on satellite data and in-situ measurements. *Deep-Sea Research Part II: Topical Studies in Oceanography*, 77-80, 70-81.
- MURPHY, E. J., WATKINS, J. L., TRATHAN, P. N., REID, K., MEREDITH, M. P., THORPE, S. E., JOHNSTON, N. M., CLARKE, A., TARLING, G. A., COLLINS, M. A., FORCADA, J., SHREEVE, R. S., ATKINSON, A., KORB, R., WHITEHOUSE, M. J., WARD, P., RODHOUSE, P. G., ENDERLEIN, P., HIRST, A. G., MARTIN, A. R., HILL, S. L., STANILAND, I. J., POND, D. W., BRIGGS, D. R., CUNNINGHAM, N. J. & FLEMING, A. H. 2007. Spatial and temporal operation of the Scotia Sea ecosystem: a review of large-scale links in a krill centred food web. *Philosophical Transactions of the Royal Society B: Biological Sciences*, 362, 113-148.

- NAKKEN, O. & DOMMASNES, A. 1975. The application of an echo integration system in investigations on the stock strength of the Barents Sea capelin (*Mallotus Villosus*, Müller) 1971-1974. *ICES CM 1975/B:25*, 20.
- NAKKEN, O. & OLSEN, K. 1977. Target strength measurements of fish. *Rapports et Procès-Verbaux des Réunions*, 170, 52-69.
- NETBURN, A. N. & ANTHONY KOSLOW, J. 2015. Dissolved oxygen as a constraint on daytime deep scattering layer depth in the southern California current ecosystem. *Deep-Sea Research Part I: Oceanographic Research Papers*, 104, 149-158.
- NORHEIM, E., KLEVJER, T. A. & AKSNES, D. L. 2016. Evidence for light-controlled migration amplitude of a sound scattering layer in the Norwegian Sea. *Marine Ecology Progress Series*, 551, 45-52.
- OPDAL, A. F., GODØ, O. R., BERGSTAD, O. A. & FIKSEN, Ø. 2008. Distribution, identity, and possible processes sustaining meso- and bathypelagic scattering layers on the northern Mid-Atlantic Ridge. *Deep-Sea Research Part II: Topical Studies in Oceanography*, 55, 45-58.
- ORSI, A. H., WHITWORTH, T. & NOWLIN, W. D. 1995. On the meridional extent and fronts of the Antarctic Circumpolar Current. *Deep-Sea Research Part I: Oceanographic Research Papers*, 42, 641-673.
- PAKHOMOV, E. A., PERISSINOTTO, R. & MCQUAID, C. D. 1996. Prey composition and daily rations of myctophid fishes in the Southern Ocean. *Marine Ecology Progress Series*, 134, 1-14.
- PAKHOMOV, E. A. & YAMAMURA, O. 2010. Report of the advisory panel on micronekton sampling inter-calibration experiment. *PICES Scientific Report No. 38*. Sidney, B.C., Canada: North Pacific Marine Science Organization (PICES).
- PARADIS, E. & SCHLIEP, K. 2018. ape 5.0: an environment for modern phylogenetics and evolutionary analyses in R. *Bioinformatics*, 35, 526-528.
- PARKINSON, C. L. 2019. A 40-y record reveals gradual Antarctic sea ice increases followed by decreases at rates far exceeding the rates seen in the Arctic. *Proceedings of the National Academy of Sciences*, 116, 14414-14423.
- PARKINSON, C. L. & CAVALIERI, D. J. 2012. Antarctic sea ice variability and trends, 1979-2010. *The Cryosphere*, 6, 871-880.
- PEARRE, S. 2003. Eat and run? The hunger/satiation hypothesis in vertical migration: history, evidence and consequences. *Biological Reviews of the Cambridge Philosophical Society*, 78, 1-79.
- PERRY, A. L., LOW, P. J., ELLIS, J. R. & REYNOLDS, J. D. 2005. Climate change and distribution shifts in marine fishes. *Science*, 308, 1912-1915.
- PETITGAS, P. 1993. Geostatistics for fish stock assessments: a review and an acoustic application. *ICES Journal of Marine Science*, 50, 285-298.

- PHILLIPS, K. L., JACKSON, G. D. & NICHOLS, P. D. 2001. Predation on myctophids by the squid *Moroteuthis ingens* around Macquarie and Heard Islands: stomach contents and fatty acid analyses. *Marine Ecology Progress Series*, 215, 179-189.
- PHLEGER, C. F., NICHOLS, P. D. & VIRTUE, P. 1997. The lipid, fatty acid and fatty alcohol composition of the myctophid fish *Electrona antarctica*: high level of wax esters and food-chain implications. *Antarctic Science*, 9, 258-265.
- PIATKOWSKI, U., RODHOUSE, P. G., WHITE, M. G., BONE, D. G. & SYMON, C. 1994. Nekton community of the Scotia Sea as sampled by the RMT 25 during austral summer. *Marine Ecology Progress Series*, 112, 13-28.
- PINHEIRO, J. C. & BATES, D. M. 2000. *Mixed-Effects Models in S and S-PLUS*, New York, Springer.
- PISTORIUS, P., HINDELL, M., CRAWFORD, R., MAKHADO, A., DYER, B. & REISINGER, R. 2017. At-sea distribution and habitat use in king penguins at sub-Antarctic Marion Island. *Ecology and Evolution*, 7, 3894-3903.
- POLLARD, R., TRÉGUER, P. & READ, J. 2006. Quantifying nutrient supply to the Southern Ocean. *Journal of Geophysical Research*, 111, C05011.
- POLOCZANSKA, E. S., BROWN, C. J., SYDEMAN, W. J., KIESSLING, W., SCHOEMAN, D. S., MOORE, P. J., BRANDER, K., BRUNO, J. F., BUCKLEY, L. B., BURROWS, M. T., DUARTE, C. M., HALPERN, B. S., HOLDING, J., KAPPEL, C. V., O'CONNOR, M. I., PANDOLFI, J. M., PARMESAN, C., SCHWING, F., THOMPSON, S. A. & RICHARDSON, A. J. 2013. Global imprint of climate change on marine life. *Nature Climate Change*, 3, 919-925.
- POST, A. 1990. Paralepididae. In: GON, O. & HEEMSTRA, P. C. (eds.) *Fishes of the Southern Ocean*. Grahamstown, South Africa: J.L.B. Smith Institute of Ichthyology.
- POST, A. L., MEIJERS, A. J. S., FRASER, A. D., MEINERS, K. M., AYERS, J., BINDOFF, N. L., GRIFFITHS, H. J., VAN DE PUTTE, A. P., O'BRIEN, P. E., SWADLING, K. M. & RAYMOND, B. 2014. Environmental Setting. In: DE BROYER, C., KOUBBI, P., GRIFFITHS, H. J., RAYMOND, B., D'UDEKEM D'ACOS, C., VAN DE PUTTE, A. P., DANIS, B., DAVID, B., GRANT, S., GUTT, J., HELD, C., HOSIE, G., HUETTMANN, F., POST, A. & ROPERT-COUDERT, Y. (eds.) *Biogeographic Atlas of the Southern Ocean*. Cambridge UK: Scientific Committee on Antarctic Research.
- PRIEDE, I. G. 2017. Adaptations to the Deep Sea. In: PRIEDE, I. G. (ed.) *Deep-Sea Fishes: Biology, Diversity, Ecology and Fisheries*. Cambridge: Cambridge University Press.
- PROUD, R., COX, M. J. & BRIERLEY, A. S. 2017. Biogeography of the global ocean's mesopelagic zone. *Current Biology*, 27, 113-119.
- PROUD, R., COX, M. J., LE GUEN, C. & BRIERLEY, A. S. 2018a. Fine-scale depth structure of pelagic communities throughout the global ocean based on acoustic sound scattering layers. *Marine Ecology Progress Series*, 598, 35-48.
- PROUD, R., COX, M. J., WOTHERSPOON, S. & BRIERLEY, A. S. 2015. A method for identifying Sound Scattering Layers and extracting key characteristics. *Methods in Ecology and Evolution*, 6, 1190-1198.

- PROUD, R., HANDEGARD, N. O., KLOSER, R. J., COX, M. J. & BRIERLEY, A. S. 2018b. From siphonophores to deep scattering layers: uncertainty ranges for the estimation of global mesopelagic fish biomass. *ICES Journal of Marine Science*, 76, 718–733.
- PUSCH, C., HULLEY, P. A. & KOCK, K. H. 2004. Community structure and feeding ecology of mesopelagic fishes in the slope waters of King George Island (South Shetland Islands, Antarctica). *Deep-Sea Research Part I: Oceanographic Research Papers*, 51, 1685–1708.
- R CORE TEAM 2018. R: A language and environment for statistical computing. Vienna, Austria: R Foundation for Statistical Computing.
- REID, K., DAVIS, D. & STANILAND, I. J. 2006. Spatial and temporal variability in the fish diet of Antarctic fur seal (*Arctocephalus gazella*) in the Atlantic sector of the Southern Ocean. *Canadian Journal of Zoology*, 84, 1025–1037.
- REISINGER, R. R., RAYMOND, B., HINDELL, M. A., BESTER, M. N., CRAWFORD, R. J. M., DAVIES, D., DE BRUYN, P. J. N., DILLEY, B. J., KIRKMAN, S. P., MAKHADO, A. B., RYAN, P. G., SCHOOMBIE, S., STEVENS, K., SUMNER, M. D., TOSH, C. A., WEGE, M., WHITEHEAD, T. O., WOTHERSPOON, S., PISTORIUS, P. A. & SCHOEMAN, D. 2018. Habitat modelling of tracking data from multiple marine predators identifies important areas in the Southern Indian Ocean. *Diversity and Distributions*, 24, 535–550.
- RINTOUL, S., HUGHES, C. & OLBERS, D. 2001. The Antarctic Circumpolar Current system *In: SIEDLER, G., CHURCH, J. & GOULD, J. (eds.) Ocean Circulation and Climate*. New York: Academic Press.
- RINTOUL, S. R., SPARROW, M., MEREDITH, M. P., WADLEY, V., SPEER, K., HOFMANN, E., SUMMERHAYES, C., URBAN, E. & BELLERBY, R. (eds.) 2012. *The Southern Ocean Observing System: initial science and implementation strategy: SCAR and SCOR*.
- ROBINSON, C., STEINBERG, D. K., ANDERSON, T. R., ARÍSTEGUI, J., CARLSON, C. A., FROST, J. R., GHIGLIONE, J.-F., HERNÁNDEZ-LEÓN, S., JACKSON, G. A., KOPPELMANN, R., QUÉGUINER, B., RAGUENEAU, O., RASSOULZADEGAN, F., ROBISON, B. H., TAMBURINI, C., TANAKA, T., WISHNER, K. F. & ZHANG, J. 2010. Mesopelagic zone ecology and biogeochemistry – a synthesis. *Deep-Sea Research Part II: Topical Studies in Oceanography*, 57, 1504–1518.
- ROBISON, B. H. 2003. What drives the diel vertical migrations of Antarctic midwater fish? *Journal of the Marine Biological Association of the United Kingdom*, 83, 639–642.
- RYAN, T. E., DOWNIE, R. A., KLOSER, R. J. & KEITH, G. 2015. Reducing bias due to noise and attenuation in open-ocean echo integration data. *ICES Journal of Marine Science*, 72, 2482–2493.
- RYAN, T. E., KLOSER, R. J. & MACAULAY, G. J. 2009. Measurement and visual verification of fish target strength using an acoustic-optical system attached to a trawl net. *ICES Journal of Marine Science*, 66, 1238–1244.
- SABOURENKOV, E. N. 1991. Mesopelagic fish of the Southern Ocean - Summary results of recent Soviet studies. *CCAMLR Science, Selected Scientific Papers, SC-CAMLR-SSP/7 (1990)*, 433–457.

- SAUNDERS, R. A., COLLINS, M. A., FOSTER, E., SHREEVE, R., STOWASSER, G., WARD, P. & TARLING, G. A. 2014a. The trophodynamics of Southern Ocean *Electrona* (Myctophidae) in the Scotia Sea. *Polar Biology*, 37, 789-807.
- SAUNDERS, R. A., COLLINS, M. A., SHREEVE, R., WARD, P., STOWASSER, G., HILL, S. L. & TARLING, G. A. 2018. Seasonal variation in the predatory impact of myctophids on zooplankton in the Scotia Sea (Southern Ocean). *Progress in Oceanography*, 168, 123-144.
- SAUNDERS, R. A., COLLINS, M. A., STOWASSER, G. & TARLING, G. A. 2017. Southern Ocean mesopelagic fish communities in the Scotia Sea are sustained by mass immigration. *Marine Ecology Progress Series*, 569, 173-185.
- SAUNDERS, R. A., COLLINS, M. A., WARD, P., STOWASSER, G., HILL, S. L., SHREEVE, R. & TARLING, G. A. 2015a. Predatory impact of the myctophid fish community on zooplankton in the Scotia Sea (Southern Ocean). *Marine Ecology Progress Series*, 541, 45-64.
- SAUNDERS, R. A., COLLINS, M. A., WARD, P., STOWASSER, G., SHREEVE, R. & TARLING, G. A. 2014b. Distribution, population structure and trophodynamics of Southern Ocean *Gymnoscopelus* (Myctophidae) in the Scotia Sea. *Polar Biology*, 38, 287-308.
- SAUNDERS, R. A., COLLINS, M. A., WARD, P., STOWASSER, G., SHREEVE, R. & TARLING, G. A. 2015b. Trophodynamics of *Protomyctophum* (Myctophidae) in the Scotia Sea (Southern Ocean). *Journal of Fish Biology*, 87, 1031-58.
- SAUNDERS, R. A., FIELDING, S., THORPE, S. E. & TARLING, G. A. 2013. School characteristics of mesopelagic fish at South Georgia. *Deep-Sea Research Part I: Oceanographic Research Papers*, 81, 62-77.
- SAUNDERS, R. A., HILL, S. L., TARLING, G. A. & MURPHY, E. J. 2019. Myctophid fish (Family Myctophidae) are central consumers in the food web of the Scotia Sea (Southern Ocean). *Frontiers in Marine Science*, 6, 530.
- SAUNDERS, R. A. & TARLING, G. A. 2018. Southern Ocean mesopelagic fish comply with Bergmann's Rule. *American Naturalist*, 191, 343-351.
- SCHEFFER, A., BOST, C. A. & TRATHAN, P. N. 2012. Frontal zones, temperature gradient and depth characterize the foraging habitat of king penguins at South Georgia. *Marine Ecology Progress Series*, 465, 281-297.
- SCHMIDTKO, S., STRAMMA, L. & VISBECK, M. 2017. Decline in global oceanic oxygen content during the past five decades. *Nature*, 542, 335-339.
- SHREEVE, R. S., COLLINS, M. A., TARLING, G. A., MAIN, C. E., WARD, P. & JOHNSTON, N. M. 2009. Feeding ecology of myctophid fishes in the northern Scotia Sea. *Marine Ecology Progress Series*, 386, 221-236.
- SILK, J. R. D., THORPE, S. E., FIELDING, S., MURPHY, E. J., TRATHAN, P. N., WATKINS, J. L. & HILL, S. L. 2016. Environmental correlates of Antarctic krill distribution in the Scotia Sea and southern Drake Passage. *ICES Journal of Marine Science*, 73, 2288-2301.
- SIMMONDS, J. & MACLENNAN, D. N. 2005. *Fisheries Acoustics: Theory and Practice*, Wiley-Blackwell.

- ST. JOHN, M. A., BORJA, A., CHUST, G., HEATH, M., GRIGOROV, I., MARIANI, P., MARTIN, A. P. & SANTOS, R. S. 2016. A dark hole in our understanding of marine ecosystems and their services: Perspectives from the mesopelagic community. *Frontiers in Marine Science*, 3, 31.
- STANTON, T. K. 1988. Sound scattering by cylinders of finite length. I. Fluid cylinders. *The Journal of the Acoustical Society of America*, 83, 55-63.
- STANTON, T. K., CHU, D., JECH, J. M. & IRISH, J. D. 2010. New broadband methods for resonance classification and high-resolution imagery of fish with swimbladders using a modified commercial broadband echosounder. *ICES Journal of Marine Science*, 67, 365-378.
- STANTON, T. K., CHU, D., WIEBE, P. H. & CLAY, C. S. 1993. Average echoes from randomly oriented random-length finite cylinders: zooplankton models. *Journal of the Acoustical Society of America*, 94, 3463-3472.
- STANTON, T. K., WIEBE, P. H., CHU, D. Z., BENFIELD, M. C., SCANLON, L., MARTIN, L. & EASTWOOD, R. L. 1994. On acoustic estimates of zooplankton biomass. *ICES Journal of Marine Science*, 51, 505-512.
- STAT, M., HUGGETT, M. J., BERNASCONI, R., DIBATTISTA, J. D., BERRY, T. E., NEWMAN, S. J., HARVEY, E. S. & BUNCE, M. 2017. Ecosystem biomonitoring with eDNA: metabarcoding across the tree of life in a tropical marine environment. *Scientific Reports*, 7, 12240.
- STEIN, M. & HEYWOOD, R. B. 1994. Antarctic environment - physical oceanography: the Antarctic Peninsula and Southwest Atlantic region of the Southern Ocean. In: EL-SAYED, S. Z. (ed.) *Southern Ocean ecology: the BIOMASS perspective*. Cambridge: Cambridge University Press.
- STOWASSER, G., ATKINSON, A., MCGILL, R. A. R., PHILLIPS, R. A., COLLINS, M. A. & POND, D. W. 2012. Food web dynamics in the Scotia Sea in summer: A stable isotope study. *Deep-Sea Research Part II: Topical Studies in Oceanography*, 59, 208-221.
- STRAND, E., JØRGENSEN, C. & HUSE, G. 2005. Modelling buoyancy regulation in fishes with swimbladders: bioenergetics and behaviour. *Ecological Modelling*, 185, 309-327.
- SUND, O. 1935. Echo sounding in fishery research. *Nature*, 135, 953.
- SUNDAY, J. M., BATES, A. E. & DULVY, N. K. 2012. Thermal tolerance and the global redistribution of animals. *Nature Climate Change*, 2, 686-690.
- TAKI, K., YABUKI, T., NOIRI, Y., HAYASHI, T. & NAGANOBU, M. 2008. Horizontal and vertical distribution and demography of euphausiids in the Ross Sea and its adjacent waters in 2004/2005. *Polar Biology*, 31, 1343-1356.
- TARLING, G. A. & FIELDING, S. 2016. Swarming and Behaviour in Antarctic Krill. In: SIEGEL, V. (ed.) *Biology and Ecology of Antarctic Krill*. Cham: Springer International Publishing.
- TARLING, G. A., THORPE, S. E., FIELDING, S., KLEVJER, T., RYABOV, A. & SOMERFIELD, P. J. 2018. Varying depth and swarm dimensions of open-ocean Antarctic krill *Euphausia*

- superba* Dana, 1850 (Euphausiacea) over diel cycles. *Journal of Crustacean Biology*, 38, 716-727.
- THOMPSON, D. W. J. & SOLOMON, S. 2002. Interpretation of recent southern hemisphere climate change. *Science*, 296, 895-899.
- THOMPSON, D. W. J., SOLOMON, S., KUSHNER, P. J., ENGLAND, M. H., GRISE, K. M. & KAROLY, D. J. 2011. Signatures of the Antarctic ozone hole in Southern Hemisphere surface climate change. *Nature Geoscience*, 4, 741-749.
- THORPE, S. E., HEYWOOD, K. J., BRANDON, M. A. & STEVENS, D. P. 2002. Variability of the southern Antarctic Circumpolar Current front north of South Georgia. *Journal of Marine Systems*, 37, 87-105.
- TOGGWEILER, J. R. & RUSSELL, J. 2008. Ocean circulation in a warming climate. *Nature*, 451, 286-288.
- TORRES, J., LANCRAFT, T., WEIGLE, B., ROBISON, B. & HOPKINS, T. 1985. Distribution and abundance of fishes and salps in relation to the marginal ice-zone of the Scotia Sea, November and December 1983. *Antarctic Journal of the United States*, 19, 117-119.
- TORRES, J. & SOMERO, G. 1988. Vertical distribution and metabolism in Antarctic mesopelagic fishes. *Comparative Biochemistry and Physiology Part B: Comparative Biochemistry*, 90, 521-528.
- TRATHAN, P. N., BISHOP, C., MACLEAN, G., BROWN, P., FLEMING, A. & COLLINS, M. A. 2008. Linear tracks and restricted temperature ranges characterise penguin foraging pathways. *Marine Ecology Progress Series*, 370, 285-294.
- TRATHAN, P. N., WATKINS, J. L., MURRAY, A. W. A., BRIERLEY, A. S., EVERSON, I., GOSS, C., PRIDDLE, J., REID, K., WARD, P., HEWITT, R., DEMER, D., NAGANOBU, M., KAWAGUCHI, S., SUSHIN, V., KASATKINA, S. M., HEDLEY, S., KIM, S. & PAULY, T. 2001. The CCAMLR-2000 Krill Synoptic Survey: A description of the rationale and design. *CCAMLR Science*, 8, 1-23.
- TRENBERTH, K. E., LARGE, W. G. & OLSON, J. G. 1990. The mean annual cycle in global ocean wind stress. *Journal of Physical Oceanography*, 20, 1742-1760.
- TURNER, J. R., WHITE, E. M., COLLINS, M. A., PARTRIDGE, J. C. & DOUGLAS, R. H. 2009. Vision in lanternfish (Myctophidae): Adaptations for viewing bioluminescence in the deep-sea. *Deep-Sea Research Part I: Oceanographic Research Papers*, 56, 1003-1017.
- TYACK, P. L. (ed.) 1997. *Studying how cetaceans use sound to explore their environment*: Springer.
- URMY, S. S., HORNE, J. K. & BARBEE, D. H. 2012. Measuring the vertical distributional variability of pelagic fauna in Monterey Bay. *ICES Journal of Marine Science*, 69, 184-196.
- VALINASSAB, T., PIERCE, G. J. & JOHANNESSON, K. 2007. Lantern fish (*Benthosema pterotum*) resources as a target for commercial exploitation in the Oman Sea. *Journal of Applied Ichthyology*, 23, 573-577.

- VAN WAEREBEEK, K., LEAPER, R., BAKER, A. N., PAPASTAVROU, V., THIELE, D., FINDLAY, K., DONOVAN, G. & ENSOR, P. 2010. Odontocetes of the Southern Ocean sanctuary. *Journal of Cetacean Research and Management*, 11, 315-346.
- VENABLES, H., MEREDITH, M. P., ATKINSON, A. & WARD, P. 2012. Fronts and habitat zones in the Scotia Sea. *Deep-Sea Research Part II: Topical Studies in Oceanography*, 59, 14-24.
- VENABLES, H. & MOORE, C. M. 2010. Phytoplankton and light limitation in the Southern Ocean: Learning from high-nutrient, high-chlorophyll areas. *Journal of Geophysical Research*, 115, C02015.
- WARD, P., ATKINSON, A., MURRAY, A. W. A., WOOD, A. G., WILLIAMS, R. & POULET, S. A. 1995. The summer zooplankton community at South Georgia: biomass, vertical migration and grazing. *Polar Biology*, 15, 195-208.
- WARD, P., ATKINSON, A., VENABLES, H. J., TARLING, G. A., WHITEHOUSE, M. J., FIELDING, S., COLLINS, M. A., KORB, R., BLACK, A., STOWASSER, G., SCHMIDT, K., THORPE, S. E. & ENDERLEIN, P. 2012. Food web structure and bioregions in the Scotia Sea: A seasonal synthesis. *Deep-Sea Research Part II: Topical Studies in Oceanography*, 59, 253-266.
- WARRANT, E. J. & LOCKET, N. A. 2004. Vision in the deep sea. *Biological Reviews*, 79, 671-712.
- WARREN, J. 2001. In situ measurements of acoustic target strengths of gas-bearing siphonophores. *ICES Journal of Marine Science*, 58, 740-749.
- WARREN, J. D. 2012. Counting critters in the sea using active acoustics. *Acoustics Today*, 8, 25-34.
- WATKINS, J. & BRIERLEY, A. S. 2002. Verification of the acoustic techniques used to identify Antarctic krill. *ICES Journal of Marine Science*, 59, 1326-1336.
- WATKINS, J. L., REID, K., RAMM, D., ZHAO, X. Y., COX, M., SKARET, G., FIELDING, S., WANG, X. L. & NIKLITSCHKE, E. 2016. The use of fishing vessels to provide acoustic data on the distribution and abundance of Antarctic krill and other pelagic species. *Fisheries Research*, 178, 93-100.
- WATSON, A. J., MEREDITH, M. P. & MARSHALL, J. 2014. The Southern Ocean, carbon and climate. *Philosophical Transactions of the Royal Society of London A: Mathematical, Physical and Engineering Sciences*, 372, 20130057.
- WICKHAM, H. 2016. ggplot2: Elegant graphics for data analysis. R package version 3.1.0 ed.
- WILKE, C. O. 2018. cowplot: Streamlined plot theme and plot annotations for 'ggplot2'. R package version 0.9.3 ed.
- WOOD, S. 2019. mgcv: Mixed GAM computation vehicle with automatic smoothness estimation. R package version 1.8-26 ed.
- YASUMA, H., SAWADA, K., TAKAO, Y., MIYASHITA, K. & AOKI, I. 2010. Swimbladder condition and target strength of myctophid fish in the temperate zone of the Northwest Pacific. *ICES Journal of Marine Science*, 67, 135-144.

- YASUMA, H., TAKAO, Y., SAWADA, K., MIYASHITA, K. & AOKI, I. 2006. Target strength of the lanternfish, *Stenobrachius leucopsarus* (family Myctophidae), a fish without an airbladder, measured in the Bering Sea. *ICES Journal of Marine Science*, 63, 683-692.
- ZASEL'SLIY, V., KUDRIN, B., POLETAYEV, V. & CHECHENIN, S. C. 1985. Some features of the biology of *Electrona carlsbergi* (Taning)(Myctophidae) in the Atlantic sector of the Antarctic. *Journal of Ichthyology*, 25, 163-166.
- ZUUR, A. F., IENO, E. N., WALKER, N., SAVELIEV, A. A. & SMITH, G. M. 2009. *Mixed effects models and extensions in ecology with R*, New York, Springer.

Appendix I

Research



Cite this article: Dornan T, Fielding S, Saunders RA, Genner MJ. 2019 Swimbladder morphology masks Southern Ocean mesopelagic fish biomass. *Proc. R. Soc. B* **286**: 20190353.
<http://dx.doi.org/10.1098/rspb.2019.0353>

Received: 11 February 2019
Accepted: 2 May 2019

Subject Category:

Ecology

Subject Areas:

ecology, environmental science

Keywords:

ecosystem, myctophid, mesopelagic fish, acoustics, biomass, Southern Ocean

Author for correspondence:Tracey Dornan
e-mail: td15166@bristol.ac.uk

Electronic supplementary material is available online at <https://dx.doi.org/10.6084/m9.figshare.c.4498925>.

Swimbladder morphology masks
Southern Ocean mesopelagic fish biomassTracey Dornan^{1,2}, Sophie Fielding¹, Ryan A. Saunders¹ and Martin J. Genner²¹British Antarctic Survey, High Cross, Madingley Road, Cambridge CB3 0ET, UK²School of Biological Sciences, University of Bristol, Life Sciences Building, 24 Tyndall Avenue, Bristol BS8 1TQ, UK

TD, 0000-0001-8265-286X

Within the twilight of the oceanic mesopelagic realm, 200–1000 m below sea level, are potentially vast resources of fish. Collectively, these mesopelagic fishes are the most abundant vertebrates on Earth, and this global fish community plays a vital role in the function of oceanic ecosystems. The biomass of these fishes has recently been estimated using acoustic survey methods, which rely on echosounder-generated signals being reflected from gas-filled swimbladders and detected by transducers on vessels. Here, we use X-ray computed tomography scans to demonstrate that several of the most abundant species of mesopelagic fish in the Southern Ocean lack gas-filled swimbladders. We also show using catch data from survey trawls that the fish community switches from fish possessing gas-filled swimbladders to those lacking swimbladders as latitude increases towards the Antarctic continent. Thus, the acoustic surveys that repeatedly show a decrease in mesopelagic fish biomass towards polar environments systematically overlook a large proportion of fish species that dominate polar seas. Importantly, this includes lanternfish species that are key prey items for top predators in the region, including king penguins and elephant seals. This latitudinal community switch, from gas to non-gas dominance, has considerable implications for acoustic biomass estimation, ecosystem modelling and long-term monitoring of species at risk from climate change and potential exploitation.

1. Introduction

Mesopelagic fish inhabit the twilight zone of the world's oceans, 200–1000 m below sea level. This global community of typically small (less than 20 cm) fish is often dominated by myctophids, commonly known as lanternfishes (Family Myctophidae) by both abundance and biomass [1]. Debate surrounds the magnitude of mesopelagic fish biomass, with global estimates ranging from 1 to 19.5 gigatonnes [1–3]. A key issue underlying this uncertainty is that many mesopelagic fish, including lanternfishes, exhibit net avoidance behaviour, potentially resulting in an underestimation of biomass [4].

Active acoustics provides a more informative method of studying these animals at the oceanic scale. Acoustic surveys are routinely used to estimate the biomass of commercially important fish stocks [5]. The underlying principle of active acoustics is to transmit a pulse of sound of known frequency and duration into the water column from an echosounder; when the sound-wave encounters something of a different acoustic impedance, such as gas in the swimbladder of a fish, it is reflected or scattered back to the transducer. The quantity of reflected signal or 'echo' is then integrated throughout the water column, and is commonly used as a proxy for biomass [2,6]. However, the interpretation of acoustic data into meaningful biology is complex, and requires ancillary information on species distribution, behaviour and fish

morphology [7], as well as knowledge of how a specific target organism backscatters the acoustic signal at a given acoustic frequency [6].

Gas in the swimbladders of fish can account for up to 95% of reflected acoustic 'backscatter' signal [8]; thus the swimbladder morphology of fish is critical for determining the effectiveness of active acoustics for estimating fish biomass. It has been known for over 50 years that mesopelagic fishes can differ in swimbladder morphology [9], with species showing both intra- and interspecific variability. For example, some species can maintain a gas-filled swimbladder throughout their lifespan, while some species may never have a gas-filled swimbladder, and others lose the gas component in adulthood [9]. Net sampling is regularly used to ground-truth acoustic data, providing knowledge of the species present and their morphological characteristics [10]. However, this is challenging to undertake comprehensively at the ocean basin scale [11] and adequate net sampling has generally focused on commercially harvested species at smaller regional scales.

In the Southern Ocean, 35 species of myctophids are known to occur [12], where they form a key component of the Antarctic ecosystem, acting as both predators of zooplankton [13–15] and prey for higher predators, including seabirds and seals [16–19]. In this food web, which is typically dominated by krill (*Euphausia superba*), myctophids have elevated importance for higher-trophic-level species during the years when krill are scarce [20]. Additionally, these myctophid species play a key role in carbon transport through the water column during diel vertical migration (DVM), which may contribute up to 17% of total carbon export from the system [21]. Assessment of the biomass of these species is important for our understanding of ecosystem function and carbon sequestration, both regionally and globally. However, the utility of active acoustics for this assessment has been hampered by limited data on swimbladder morphology both within and among key myctophid species. Specifically, it has been unclear if the reported latitudinal decline in backscatter towards the Antarctic continent [22,23] is a consequence of a decrease in fish biomass, or instead a consequence of the coincidental change in mesopelagic fish community composition [23].

Here, we report a detailed exploration of the potential influence of swimbladder morphology on estimates of mesopelagic fish biomass in the Southern Ocean, which for the purposes of this study we define as the region south of 50° S. We first use multiple acoustic transects to confirm a pattern of declining acoustic backscatter towards the Antarctic landmass in the South Atlantic, in agreement with observations from the South Pacific sector [23]. We then analyse the swimbladder condition of the common myctophid species in the region using X-ray imaging of fresh specimens, dissection of fresh specimens and X-ray micro-computed tomography (CT) of preserved specimens. Finally, we use net data to describe the change in the mesopelagic community towards higher latitudes. We conclude that the reduction in backscatter with latitude towards Antarctica is strongly influenced by a shift in community structure from gas-bladdered to non-gas bladdered species. We consider this result from the perspective of acoustic biomass assessment, and discuss the potential underlying ecological and evolutionary drivers of the observed shift in myctophid community composition and morphology.

2. Methods

(a) Acoustic surveys

We quantified nautical area scattering coefficient (NASC, $\text{m}^2 \text{nmi}^{-2}$), a measure of mean water column acoustic backscatter and a proxy for biomass, in relation to latitude. Six acoustic transects from five individual cruises between the Falkland Islands and the South Orkneys were conducted aboard the RRS *James Clark Ross*, covering Austral spring to autumn (figure 1). An EK60 split-beam hull-mounted transducer was used to collect 38 kHz data to depths of 1000 m on all cruises with the exception of JR161 and JR200, where data were collected to 800 m and 990 m, respectively. All data were calibrated, processed and integrated in 1 km distance by 10 m depth bins in ECHOVIEW (v. 8.0.95, Echoview Software Pty Ltd, Hobart, Australia). Prior to integration, bad or unwanted data such as false bottom echoes, seabed, surface near-field, intermittent noise and attenuated signal were set to 'no-data' and excluded from the analyses. Non-transit data, where vessel speed slowed below 4 knots to undertake alternative science operations, were not included in the analysis. After integration, data collected in water shallower than 1000 m were excluded from analysis to constrain the study to mesopelagic waters. Total water column NASC was calculated in R (v. 3.5.1) [27] and \log_e -transformed prior to fitting a linear regression model using latitude as a predictor variable. To verify that high NASC values were valid and not noise, the top 1% of NASC values were visually scrutinized on echograms. Less than 10% of these were suspected to be noise-biased, and the biased NASC values were removed from further analysis. Both day and night collected acoustic data were used in the analysis. To confirm that DVM did not introduce bias, linear regressions were also carried out on separate day and night data, and all reported trends remained consistent (electronic supplementary material, figure S1).

(b) Net sampling

Stratified net sampling was undertaken on six cruises, between 2004 and 2017, at locations spanning the major frontal positions and water masses of the Scotia Sea (figure 1). Nets were deployed day and night during early cruises (JR161 and JR177). These were later restricted to night only sampling (JR200, JR15004 and JR16003) due to comparatively low fish abundance within daylight catches, presumably due to net avoidance behaviour.

Samples were collected using an opening and closing rectangular mid-water trawl net system (RMT25) [28]. The RMT25 is equipped with two nets, with an aperture of 25 m^2 , and cod-end mesh of 5 mm. To sample the mesopelagic and epipelagic regions, each haul was stratified into four depth zones: 1000–700 m, 700–400 m, 400–200 m and 200 m–surface. Nets were towed obliquely in each zone at a towing speed of approximately 2.5 knots, for a duration of 30–60 min. All nets were closed during deployment and recovery, to minimize contamination from different depth zones. Once on deck, cod-end samples were transferred to fresh seawater. The total catch weight of all fauna by species was recorded whenever possible. Fish were then placed on ice for identification, and the standard length (SL) measured, before either further morphological analysis on board the research vessel or preservation by freezing at -20°C .

Fish from these surveys were used for soft tissue X-ray and/or dissection (freshly caught specimens), or X-ray CT (frozen specimens). Additional fish for morphological analysis were sampled opportunistically from RMT8 and multiple opening/closing net and environmental sensing system (MOCNESS) nets deployed during the same cruises (electronic supplementary material, table S1).

(c) Swimbladder gas assessment

The swimbladders of seven of the eight most common species of myctophid (based on the net data) were assessed for the presence

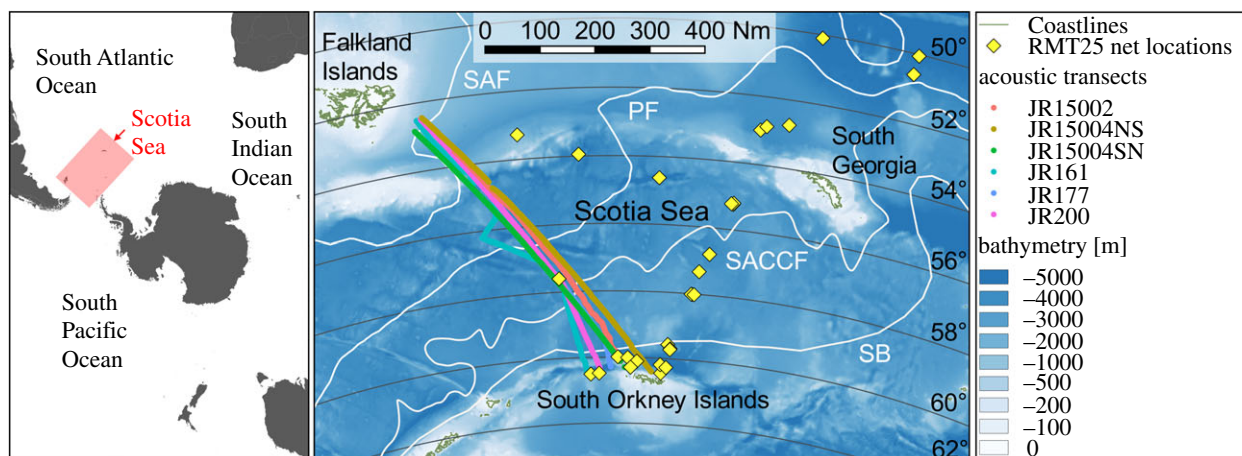


Figure 1. Study location in the Scotia Sea, Atlantic sector of the Southern Ocean. RMT25 surface to 1000 m depth net sample locations (yellow diamond). Acoustic transects between the Falkland Islands and the South Orkney Islands (coloured lines): spring cruises, JR161 (October 2006), JR15002 (November 2015); summer cruises JR177 (January 2008), JR15004 (January and February 2016); autumn cruise, JR200 (March 2009). Mean frontal positions are represented in white. SAF, Sub-Antarctic Front; PF, Polar Front; SACCF, Southern Antarctic Circumpolar Current Front; SB, Southern ACC Boundary [24–26]. Also shown are the 2° latitudinal bands used in analysis. Map generated in QUANTUM GIS v. 2.18 (www.qgis.org). (Online version in colour.)

or absence of gas: *Electrona antarctica* ($n = 56$), *Electrona carlsbergi* ($n = 28$), *Gymnoscopelus braueri* ($n = 21$), *Gymnoscopelus fraseri* ($n = 12$), *Gymnoscopelus nicholsi* ($n = 14$), *Krefftichthys anderssoni* ($n = 39$) and *Protomyctophum bolini* ($n = 32$). Assessment of individual fish was conducted using one of three methods: (a) visual inspection following dissection, (b) soft tissue X-ray scanning and (c) X-ray CT scans.

For visual inspection following dissection, freshly captured samples were dissected and the swimbladder punctured under water to record presence or absence of swimbladder gas. All dissections occurred within 8 h of capture, with fish stored in individual sealed bags at approximately 4°C prior to dissection.

All soft tissue X-ray images were captured using an Ultra-power 100 veterinary X-ray unit. Lateral and dorsal X-rays were taken with the film cassette positioned 0.88 m from the radiography unit. Exposure time and peak voltage (kVp) were set depending on the size and thickness of the animals being imaged, from small species being exposed for 0.08 s at 44 kVp, to larger species exposed for 0.09 s at 50 kVp.

Fish subjected to X-ray CT were scanned using one of two methods: (a) fish were freshly defrosted, held on ice in the CT facility, and mounted in polyethylene and foam to minimize movement in the scanner; and (b) fish were fixed in 5% formalin, stained with Potassium Iodide IKI, rinsed and scanned in distilled water; using a Nikon XTH225ST CT scanner. Fish were scanned in batches or individually depending on the size of the fish; and settings were adjusted between scans to capture the maximum detail while retaining all of the fish in view.

Swimbladders were considered to be gas-filled if they were found to contain gas or if the swimbladder was visibly ruptured on X-ray CT images, soft tissue X-ray images or during dissection. Fish were classed as non-gas-filled if they did not contain gas, or when gas was only present in the oesophagus/gut, indicative of ingestion of gas on hauling. Damaged fish, or those for which CT images were inconclusive, were excluded from analysis. Electronic supplementary material, tables S2 and S3 have detailed information on how gas presence or absence was determined from X-ray CT images.

Species not assessed for gas component as part of this study were assigned swimbladder status from the literature. *Protomyctophum tenisoni* was assigned as gas bearing, based on previously published analyses [9]. Non-myctophid Bathylagidae [29] and *Notolepis* spp. [30] do not possess swimbladders and so were not assessed for gas. As *Cyclothone* species were only identified

to genus level, all were treated as ‘fat invested’ (for justification see electronic supplementary material, table S4).

(d) Statistical analysis

Community composition was determined from only the night-sampled, surface–1000 m depth stratified, RMT25 net samples, which were standardized for tow speed and duration. Analyses focussed on 11 of the most dominant Scotia Sea fishes, which accounted for greater than 94% of all fish captured by abundance in RMT25 net data (electronic supplementary material, table S4). A depth-integrated abundance of each species was assessed for each sampling event, by calculating the average abundance across the four depth zones. Latitudinal community change was assessed by calculating mean species abundance in 2° latitudinal bands. Fish biomass for each of the 11 fish species was derived directly from the same net samples as the abundance data. Where catch weights were missing, abundance of each species was multiplied by a mean weight for each species (calculated from combined JR161, JR177 and JR200 data). Swimbladder gas status was assigned, from either this study or literature as described above, to each individual in the net based on species, and SL where relevant. All statistical analyses were conducted in R (v. 3.5.1) [27].

3. Results

(a) Acoustic backscatter declines with latitude

Significant declines in \log_e NASC with increasing latitude were evident in all six acoustic transects (figures 1 and 2). The transect with the greatest variability along the linearly decreasing trend was undertaken during the late Austral spring cruise JR15002 (figure 2), where visual inspection of echograms revealed high, patchy levels of backscatter in the upper water column. To confirm that the declining trend in NASC was not associated with a decreasing biomass in general, the total biomass of all fauna (both fish and invertebrates) and fish (study species only), captured in each stratified net sample, standardized for tow speed and duration, were plotted against latitude. This revealed that there was no decrease in biomass with increasing latitude in net samples (electronic supplementary material, figure S2 and S3).

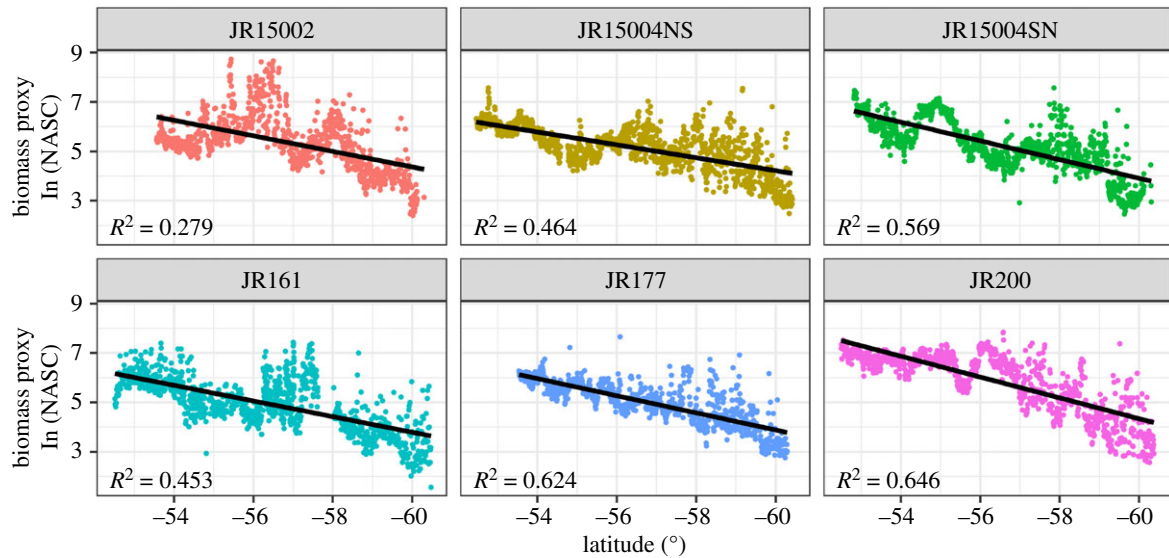


Figure 2. Relationship between the nautical area scattering coefficient (NASC, $\text{m}^2 \text{nmi}^{-2}$), a proxy for biomass, and increasing latitude by cruise number. JR15004 had both north to south (NS) and south to north (SN) transits, all others are one way only. All data shown were collected in water greater than 1000 m depth. Linear regressions (black lines) are statistically significant ($p < 0.001$). (Online version in colour.)

(b) Gas presence and absence of key mesopelagic fish species

Electrona carlsbergi (SL 70–86 mm, $n = 28$), *K. anderssoni* (SL 30–70 mm, $n = 39$) and *P. bolini* (SL 29–62 mm, $n = 32$) all showed evidence of gas-filled swimbladders across all lengths assessed, indicative of gas presence throughout their lifespans. *Gymnoscopelus braueri* (SL 68–123 mm, $n = 21$), *G. nicholsi* (SL 124–153 mm, $n = 14$) and *G. fraseri* (SL 55–84 mm, $n = 12$) showed no evidence of swimbladder gas.

There was an apparent ontogenetic loss of swimbladder gas in *E. antarctica* (SL 27–103 mm, $n = 56$), with SL a highly significant predictor of the presence of gas ($p < 0.001$), and the modelled shift in probability of gas presence to absence estimated at SL 51.4 mm (electronic supplementary material, figure S4). Both dissection and X-ray CT images (figure 3a) revealed the swimbladder tissue to be thickened in larger specimens with no gas retained.

The swimbladder of *K. anderssoni* was thick-walled and possessed a fine transparent membraned oval structure at the anterior side, which was commonly inflated with a bubble-like appearance on dissected and CT-scanned specimens (figure 3b). Swimbladders of *E. carlsbergi* and *P. bolini* were apparently thin walled as they were commonly ruptured on hauling with gas filling abdominal cavity.

(c) Changing community structure

The mesopelagic fish community was dominated by Myctophidae by abundance, accounting for 75.07% of fishes captured with the RMT25, with Bathylagidae and Gonostomatidae accounting for 14.41% and 6.30%, respectively. The eleven most commonly occurring mesopelagic taxa were selected for community assessment accounted for greater than 94% of individuals captured (electronic supplementary material, table S4). There was an overall reduction in species richness of mesopelagic fishes with increasing latitude, and a switch in the dominant species from the gas-bearing *P. bolini* and *K. anderssoni* at lower latitudes, to the regressed and non-gas-bearing swimbladder *E. antarctica* and *G. braueri* at higher latitudes (figure 3c).

(d) Effects of changing community on acoustic signal—less backscatter, not fewer fish

Mean fish abundance (mean 0.867 individuals 1000 m^{-3} , range 0.751–0.920 individuals 1000 m^{-3}) and biomass (median 3.993 g 1000 m^{-3} , range 1.520–5.922 g 1000 m^{-3}) as estimated using RMT25 trawl samples were consistent across the latitudinal gradient of the Scotia Sea (figure 4a,b). To examine change in morphology with latitude all *Gymnoscopelus* species, *E. antarctica* > 51.4 mm, Bathylagidae [29] and *Notolepis* spp. [30] were assigned ‘no gas’ status. All *E. carlsbergi*, *P. bolini*, *K. anderssoni*, *E. antarctica* < 51.4 mm and *P. tenisoni* [9] were assigned as ‘gas’. Cyclothone were assigned as ‘fat invested’. This categorization revealed a clear latitudinal shift in the community from strongly scattering gas-bladdered species in the north of the sampled area, to acoustically cryptic non-gas bearing fish southwards towards the Antarctic continent (figure 4c).

4. Discussion

Active acoustics can be an invaluable method for monitoring and understanding ecosystems [10]. Since acoustic data are commonly used as a proxy for biomass, a change in the fish community structure, where strong scattering fish are replaced by weak scattering fish, could have considerable implications for ecosystem assessment and modelling of trophic interactions. It has previously been reported that there is a north to south shift in fish community composition in the Scotia Sea [31,32]. This study has confirmed a poleward shift in mesopelagic community structure that parallels a decline in acoustic backscatter. We suggest that the decline is most likely to reflect a shift in the morphological and physiological properties of the fish community present towards the Antarctic continent, rather than a systematic change in total fish biomass.

(a) Poleward loss of gas-filled swimbladders

The apparent loss of gas-filled swimbladders in fish species with increasing latitude raises interesting questions about

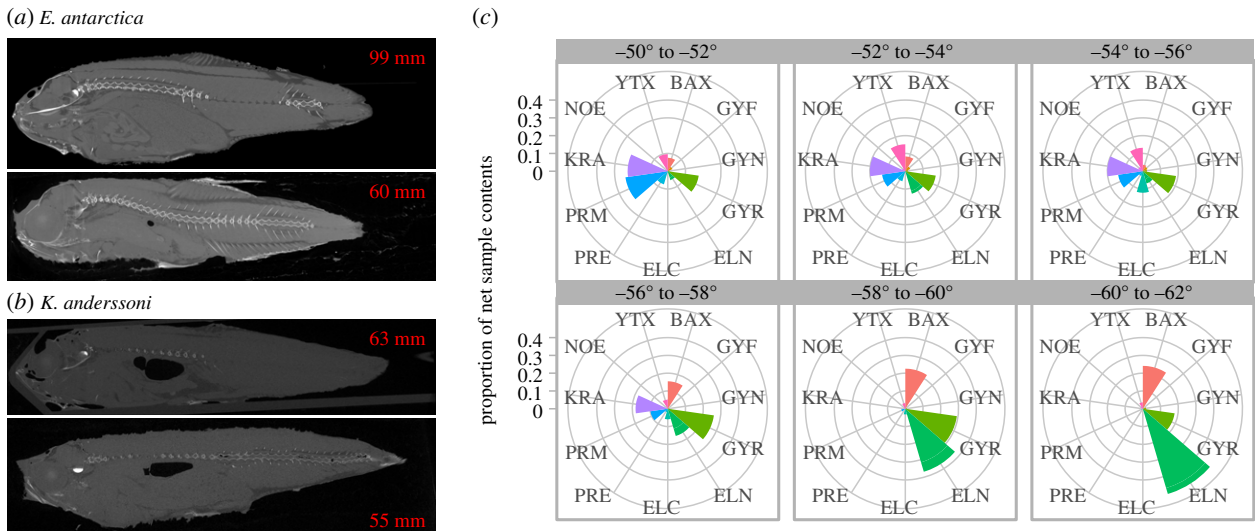


Figure 3. Single slice computed tomography scans of (a) *Electrona antarctica* showing loss of swimbladder gas and (b) *Krefflichthys anderssoni* showing gas presence (dark regions in tissue). Fish standard lengths shown in mm. (c) Polar plots of standardized proportions of species captured in 2° latitude bins, each colour segment proportionally corresponds to the abundance of individual species. (Online version in colour.)

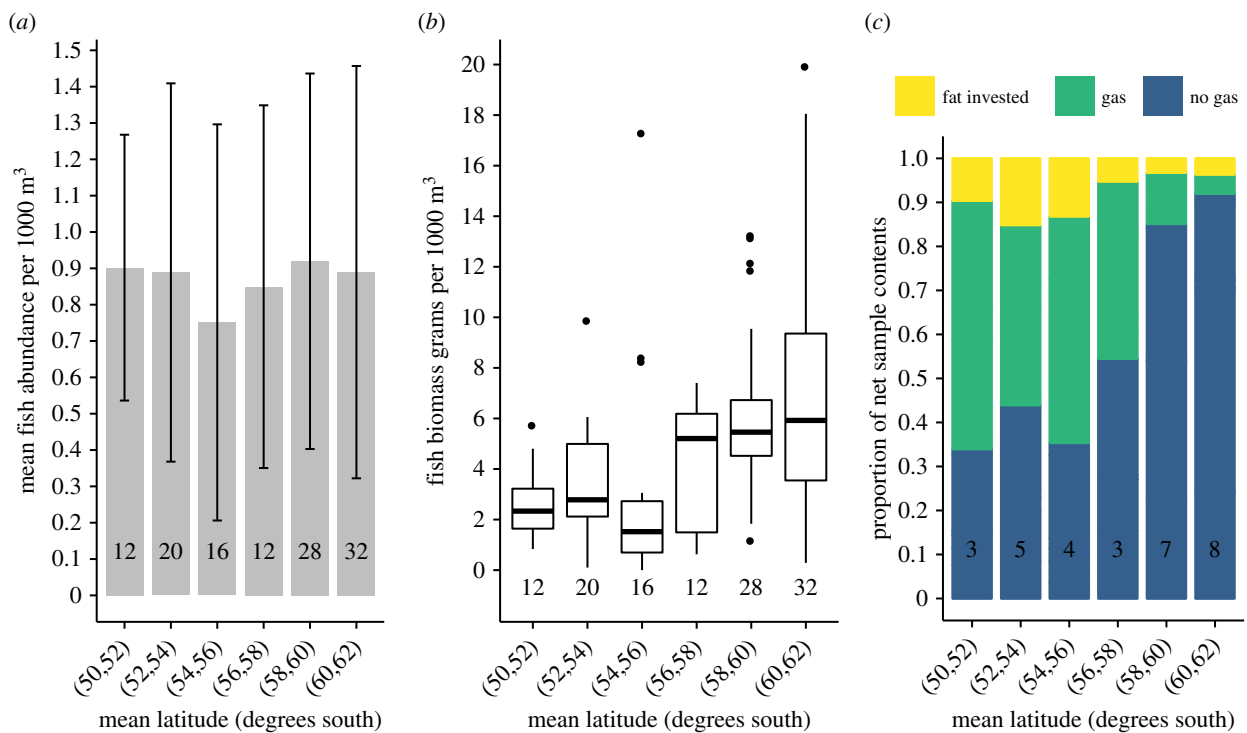


Figure 4. (a) Mean abundance of fish (individuals per 1000 m³) in RMT25 net samples by latitude. Bars indicate standard deviation between net samples and numbers in columns indicate numbers of individual net strata samples included. (b) Biomass of fish (grams per 1000 m³) in RMT25 net samples by latitude, box spans interquartile range (IQR), horizontal line is the median, whiskers include values up to 1.5 × IQR, outlying values plotted individually. (c) Relative proportions of fish by swimbladder contents in net samples at latitude. Numbers in columns are the individual number of total water column samples (each consisting of 4 depth strata) used in analysis. (Online version in colour.)

the ecology of the system, and the evolutionary drivers of shifts in swimbladder properties. Typically, mesopelagic fishes undertake large-scale DVM (mean approx. 590 m per cycle) [33], to enable them to forage on abundant near-surface zooplankton at night, while avoiding shallow-water predators during daytime [34]. However, at extreme polar latitudes, DVM is apparently reduced relative to lower latitude habitats [35]. A key underlying factor could be a poleward shift in the light environment, which is known to be an important stimulus of DVM behaviour [36]. It is

therefore plausible that the observed shift in swimbladder morphology is associated with a change in physiological requirements to enable large-scale diurnal depth changes. Species occupying higher latitudes may have a reduced need to alter buoyancy dynamically using a gas-filled swimbladder, instead relying upon buoyancy provided by lipids and avoiding the physiological costs of rapid secretion and resorption of gas. Testing this hypothesis would require modelling of energetic costs of DVM using alternative gas and lipid buoyancy strategies across the depth ranges,

temperatures, water densities and behaviours where diurnal migration takes place in the Southern Ocean [37].

(b) Ontogenetic shifts in distribution and swimbladder morphology

Data on the presence or absence of gas in swimbladders were restricted to larger size classes of myctophids captured, because small (less than 40 mm) individuals of most species are rarely taken in the Scotia Sea. Saunders *et al.* [38] discussed the absence of larval myctophids in wider Scotia Sea net samples and suggested that many myctophid species of the Scotia Sea could be expatriates from sub-Antarctic, or temperate latitudes that migrate southwards during ontogeny, possibly in search of food hotspots. The main exceptions are *K. anderssoni*, which appears to produce larvae in the coastal waters around South Georgia (Cumberland Bay) [39], and *E. antarctica*, the larvae of which are present in waters towards the Antarctic continental shelf in other regions of the Southern Ocean (Indian Ocean sector) [40]. Whether expatriated myctophids return to waters further north to reproduce remains unclear and requires further investigation.

Unlike the other Southern Ocean myctophids, *E. antarctica* is regarded as a polar specialist that is confined to waters south of the Antarctic Polar Front. This species appears to have a close association with sea ice in some regions of the Southern Ocean (Indian Ocean sector), with the marginal sea ice zone seemingly important for larval development [40]. At present, it is unclear if an ontogenetic habitat shift from sea ice margin to open ocean of *E. antarctica* has favoured the loss of gas-filled swimbladders with increasing body size, but it is plausible that loss of gas represents an adaptation to changing habitat occupancy and DVM behaviour during ontogeny. The observed ontogenetic shift could have importance for interpretation of acoustic data, as any seasonal increase in larval *E. antarctica* with small gas-bearing swimbladders could lead to increased resonance on echograms. Further sampling of smaller individuals of the species in this assemblage, coupled with analyses of their morphology and buoyancy strategies, would clarify if the ontogenetic regression of the swimbladder we observed in *E. antarctica* is unique to that species, or instead more widespread across myctophid species of the region. In particular, further study should examine abundant *Gymnoscopelus* species as we could not rule out gas presence in earlier life stages. It would be advisable to chemically fix larvae and juveniles immediately on capture for later staining and CT scanning, as freezing of such small specimens can lead to tissue damage.

(c) Challenges for acoustic studies of mesopelagic fish

As in other large-scale surveys of mesopelagic fish biomass [2], we used 38 kHz acoustic data as it generally has sufficient depth resolution to sample the mesopelagic zone. However, the Scotia Sea supports a diverse community of mesopelagic species [41] and single frequency acoustic data lack the detailed information to distinguish between taxa, presenting two main sources of bias. First, fluid-like Antarctic krill *Euphausia superba* would be undetectable individually, but collectively the extensive dense aggregations would be readily detected by echosounders. Second, colonial siphonophores, many species of which bear a gas-filled pneumatophore,

have been shown to be strong acoustic targets with the potential to resonate [3,42,43]. Of 18 siphonophore species known to occur south of 50° S only five are physonect (gas bearing) [44]. While only limited data exist on the abundance of siphonophores in the region, there is evidence that both siphonophores and krill are more prevalent in the south of the Scotia Sea [45–47]. Thus, it seems unlikely that the pattern of a southward reduction in NASC in this study is driven by shifts in the abundance of either krill or physonect siphonophores, but there is a clear need for focused research on the distribution and abundance patterns of siphonophores in the Southern Ocean [3].

Our study shows that reliable interpretation of acoustic biomass survey data requires additional biological information that can be derived by net sampling [7]. Ideally, net sampling and acoustic data collection would occur concurrently. However, limited ship time requires that a balance is achieved between obtaining consistent acoustic transects and acquiring sufficient net data. While much of the acoustic and net sample data used in this study are from longitudinally offset locations and a relatively small regional scale, both datasets span the same major Southern Ocean fronts and water masses (shown in figure 1). This study reveals latitudinal trends in both the acoustics and community structure, which are consistent with other Southern Ocean regions [23]. From an ecological perspective, this is unsurprising as the most common mesopelagic fish typically have circumpolar distributions [12], resulting from broadly analogous latitudinal water masses and habitats [24]. We therefore suggest that the trends revealed in this study may be broadly applicable to the wider Southern Ocean ecosystem. Further net sample and acoustic data would enable tests of the generality of our findings, particularly in the South West Atlantic, South Indian Ocean and South West Pacific Sectors.

It has been noted that there is a markedly greater acoustic backscatter in low latitude mesopelagic habitats relative to those at higher latitudes [22]. A comparison between the Southern Ocean and what are known to be highly productive low latitude sub-tropical regions was not the focus of the current study. Nevertheless, it would be interesting to determine how the morphology of species contrasts between these latitudinal realms, and if fish scattering properties more generally are able to influence patterns of acoustic backscatter across larger global spatial scales.

(d) Implications for monitoring and modelling

Recent modelling based on acoustic data predicts an increase in mesopelagic biomass under future warming scenarios [22]. Our results indicate that a proportion of the Southern Ocean mesopelagic community is dominated by acoustically cryptic species and therefore polar biomass may be underestimated. It is therefore important that complementary methods of accounting for potential ‘missing’ biomass are employed, including ground-truthing through net validation. However, such net sampling requires extensive investment in sampling resources, and would be challenging for larger basin- and global-scale surveys [11]. It is possible that the need for such extensive surveys could be partially mitigated by knowledge of basin-scale trends in community composition, as well as backscatter properties of species present, that would enable the development of geographical correction factors that can be applied to acoustics-based estimates. Future solutions may

also lie in the development and refinement of environmental DNA techniques, where acoustic data may be validated and adjusted for through assessment of community composition within water samples [48]. In the meantime, active acoustics in combination with net sampling will remain a powerful combination of methods for the collection of temporal and spatial data for assessment of mesopelagic communities.

5. Conclusion

There has been recent interest in the potential exploitation of abundant mesopelagic fish to meet growing human needs, but to achieve this sustainably requires a solid understanding of the impacts on the wider ecosystem [49]. An inability to detect key species during acoustic monitoring presents a particular risk to fish stocks, where species could be exploited beyond sustainable levels. In addition, many fish species have shifted poleward to maintain their optimum thermal tolerance [50–52] as sea temperatures warm, and further shifts are projected. Development of reliable sampling methods, including acoustics, can only enhance our ability to monitor changes in population dynamics of myctophids, informing long-term management of the wider Antarctic ecosystem.

References

- Gjøsaeter J, Kawaguchi K. 1980 A review of the world resources of mesopelagic fish. *FAO Fish. Tech. Pap.* **193**, 123–134.
- Irigoin X *et al.* 2014 Large mesopelagic fishes biomass and trophic efficiency in the open ocean. *Nat. Commun.* **5**, 3271. (doi:10.1038/ncomms4271)
- Proud R, Handegard NO, Kloser RJ, Cox MJ, Brierley AS. 2018 From siphonophores to deep scattering layers: uncertainty ranges for the estimation of global mesopelagic fish biomass. *ICES J. Mar. Sci.* fsy037. (doi:10.1093/icesjms/fsy037)
- Kaartvedt S, Staby A, Aksnes DL. 2012 Efficient trawl avoidance by mesopelagic fishes causes large underestimation of their biomass. *Mar. Ecol. Prog. Ser.* **456**, 1–6. (doi:10.3354/meps09785)
- Fernandes PG, Gerlotto F, Holliday DV, Nakken O, Simmonds EJ. 2002 Acoustic applications in fisheries science: the ICES contribution. *ICES J. Mar. Sci.* **215**, 483–492.
- Simmonds J, MacLennan DN. 2005 *Fisheries acoustics: theory and practice*, 2nd edn. Chichester, UK: Wiley-Blackwell.
- Davison PC, Koslow JA, Kloser RJ. 2015 Acoustic biomass estimation of mesopelagic fish: backscattering from individuals, populations, and communities. *ICES J. Mar. Sci.* **72**, 1413–1424. (doi:10.1093/icesjms/fsv023)
- Foote KG. 1980 Importance of the swimbladder in acoustic scattering by fish: a comparison of gadoid and mackerel target strengths. *J. Acoust. Soc. Am.* **67**, 2084–2089. (doi:10.1121/1.384452)
- Marshall NB. 1960 Swimbladder structure of deep-sea fishes in relation to their systematics and biology. *Discov. Rep.* **31**, 1–122.
- Benoit-Bird KJ, Lawson GL. 2016 Ecological insights from pelagic habitats acquired using active acoustic techniques. *Ann. Rev. Mar. Sci.* **8**, 463–490. (doi:10.1146/annurev-marine-122414-034001)
- Kloser RJ, Ryan TE, Young JW, Lewis ME. 2009 Acoustic observations of micronekton fish on the scale of an ocean basin: potential and challenges. *ICES J. Mar. Sci.* **66**, 998–1006. (doi:10.1093/icesjms/fsp077)
- Hulley AP. 1990 Family Myctophidae. In *Fishes of the Southern Ocean* (eds O Gon, PC Heemstra), pp. 146–178. Grahamstown, South Africa: JLB Smith Institute of Ichthyology.
- Pakhomov EA, Perissinotto R, McQuaid CD. 1996 Prey composition and daily rations of myctophid fishes in the Southern Ocean. *Mar. Ecol. Prog. Ser.* **134**, 1–14. (doi:10.3354/meps134001)
- Saunders RA, Collins MA, Shreeve R, Ward P, Stowasser G, Hill SL, Tarling GA. 2018 Seasonal variation in the predatory impact of myctophids on zooplankton in the Scotia Sea (Southern Ocean). *Prog. Oceanogr.* **168**, 123–144. (doi:10.1016/j.pocean.2018.09.017)
- Shreeve RS, Collins MA, Tarling GA, Main CE, Ward P, Johnston NM. 2009 Feeding ecology of myctophid fishes in the northern Scotia Sea. *Mar. Ecol. Prog. Ser.* **386**, 221–236. (doi:10.3354/meps08064)
- Connan M, Cherel Y, Mayzaud P. 2007 Lipids from stomach oil of procellariiform seabirds document the importance of myctophid fish in the Southern Ocean. *Limnol. Oceanogr.* **52**, 2445–2455. (doi:10.4319/lo.2007.52.6.2445)
- Duhamel G. 1998 The pelagic fish community of the Polar Front Zone off the Kerguelen Islands. In *Fishes of Antarctica: A biological overview* (eds G di Prisco, E Pisano, M Clark), pp. 63–74. Milan, Italy: Springer.
- Guinet C, Vacquie-Garcia J, Picard B, Bessigneul G, Lebras Y, Dragon AC, Viviant M, Arnould JPY, Bailleul F. 2014 Southern elephant seal foraging success in relation to temperature and light conditions: insight into prey distribution. *Mar. Ecol. Prog. Ser.* **499**, 285–301. (doi:10.3354/meps10660)
- Lea MA, Cherel Y, Guinet C, Nichols PD. 2002 Antarctic fur seals foraging in the Polar Frontal Zone: inter-annual shifts in diet as shown from fecal and fatty acid analyses. *Mar. Ecol. Prog. Ser.* **245**, 281–297. (doi:10.3354/meps245281)
- Murphy EJ *et al.* 2007 Spatial and temporal operation of the Scotia Sea ecosystem: a review of large-scale links in a krill centred food web. *Phil. Trans. R. Soc. B.* **362**, 113–148. (doi:10.1098/rstb.2006.1957)
- Davison PC, Checkley DM, Koslow JA, Barlow J. 2013 Carbon export mediated by mesopelagic fishes in the northeast Pacific Ocean. *Prog. Oceanogr.* **116**, 14–30. (doi:10.1016/j.pocean.2013.05.013)
- Proud R, Cox MJ, Brierley AS. 2017 Biogeography of the global ocean's mesopelagic zone. *Curr. Biol.* **27**, 113–119. (doi:10.1016/j.cub.2016.11.003)
- Escobar-Flores PC, O'Driscoll RL, Montgomery JC. 2018 Spatial and temporal distribution patterns of acoustic backscatter in the New Zealand sector of the Southern Ocean. *Mar. Ecol. Prog. Ser.* **592**, 19–35. (doi:10.3354/meps12489)
- Orsi AH, Whitworth T, Nowlin WD. 1995 On the meridional extent and fronts of the Antarctic circumpolar current. *Deep-Sea Res. I* **42**, 641–673. (doi:10.1016/0967-0637(95)00021-W)

25. Moore JK, Abbott MR, Richman JG 1999 Location and dynamics of the Antarctic Polar Front from satellite sea surface temperature data. *J. Geophys. Res.-Oceans* **104**, 3059–3073. (doi:10.1029/1998jc900032).
26. Thorpe SE, Heywood KJ, Brandon MA, Stevens DP 2002 Variability of the southern Antarctic circumpolar current front north of South Georgia. *J. Marine Syst.* **37**, 87–105. (doi:10.1016/S0924-7963(02)00197-5)
27. R Core Team. 2018 *R: a language and environment for statistical computing*. Vienna, Austria: R Foundation for Statistical Computing.
28. Baker AdC, Clarke MR, Harris MJ. 1973 The NIO combination net (RMT 1 + 8) and further developments of rectangular midwater trawls. *J. Mar. Biol. Assoc. UK* **53**, 167–184. (doi:10.1017/S0025315400056708)
29. Marshall NB. 1950 Air bladder structure and vertical distribution in deep-sea fishes. *Ann. Rep. Challenger. Soc.* **3**, 26–27.
30. Post A. 1990 Paralepididae. In *Fishes of the Southern Ocean* (eds O Gon, PC Heemstra), pp. 138–141. Grahamstown, South Africa: JLB Smith Institute of Ichthyology.
31. Collins MA, Stowasser G, Fielding S, Shreeve R, Xavier JC, Venables HJ, Enderlein P, Chereil Y, Van de Putte A. 2012 Latitudinal and bathymetric patterns in the distribution and abundance of mesopelagic fish in the Scotia Sea. *Deep-Sea Res. II* **59**, 189–198. (doi:10.1016/j.dsr2.2011.07.003)
32. Saunders RA, Tarling GA. 2018 Southern Ocean mesopelagic fish comply with Bergmann's rule. *Am. Nat.* **191**, 343–351. (doi:10.1086/695767)
33. Klejver TA, Irigoien X, Rostad A, Fraile-Nuez E, Benitez-Barrios VM, Kaartvedt S. 2016 Large scale patterns in vertical distribution and behaviour of mesopelagic scattering layers. *Sci. Rep.* **6**, 19873. (doi:10.1038/srep19873)
34. Pearre S. 2003 Eat and run? The hunger/satiation hypothesis in vertical migration: history, evidence and consequences. *Biol. Rev. Camb. Phil.* **78**, 1–79. (doi:10.1017/s146479310200595x)
35. Proud R, Cox MJ, Le Guen C, Brierley AS. 2018 Fine-scale depth structure of pelagic communities throughout the global ocean based on acoustic sound scattering layers. *Mar. Ecol. Prog. Ser.* **598**, 35–48. (doi:10.3354/meps12612)
36. Brierley AS. 2014 Diel vertical migration. *Curr. Biol.* **24**, R1074–R1076. (doi:10.1016/j.cub.2014.08.054)
37. Strand E, Jørgensen C, Huse G. 2005 Modelling buoyancy regulation in fishes with swimbladders: bioenergetics and behaviour. *Ecol. Model.* **185**, 309–327. (doi:10.1016/j.ecolmodel.2004.12.013)
38. Saunders RA, Collins MA, Stowasser G, Tarling GA. 2017 Southern Ocean mesopelagic fish communities in the Scotia Sea are sustained by mass immigration. *Mar. Ecol. Prog. Ser.* **569**, 173–185. (doi:10.3354/meps12093)
39. Belchier M, Lawson J. 2013 An analysis of temporal variability in abundance, diversity and growth rates within the coastal ichthyoplankton assemblage of South Georgia (sub-Antarctic). *Polar Biol.* **36**, 969–983. (doi:10.1007/s00300-013-1321-9)
40. Moteki M, Fujii K, Amakasu K, Shimada K, Tanimura A, Odate T. 2017 Distributions of larval and juvenile/adult stages of the Antarctic myctophid fish, *Electrona antarctica*, off Wilkes Land in East Antarctica. *Polar Sci.* **12**, 99–108. (doi:10.1016/j.polar.2017.02.004)
41. Piatkowski U, Rodhouse PG, White MG, Bone DG, Symon C. 1994 Nekton community of the Scotia Sea as sampled by the RMT 25 during austral summer. *Mar. Ecol. Prog. Ser.* **112**, 13–28. (doi:10.3354/meps112013)
42. Warren J. 2001 In situ measurements of acoustic target strengths of gas-bearing siphonophores. *ICES J. Mar. Sci.* **58**, 740–749. (doi:10.1006/jmsc.2001.1047)
43. Kloser RJ, Ryan TE, Keith G, Gershwin L. 2016 Deep-scattering layer, gas-bladder density, and size estimates using a two-frequency acoustic and optical probe. *ICES J. Mar. Sci.* **73**, 2037–2048. (doi:10.1093/icesjms/fsv257)
44. Mapstone GM. 2014 Global diversity and review of Siphonophorae (Cnidaria: Hydrozoa). *PLoS ONE* **9**, e87737. (doi:10.1371/journal.pone.0087737)
45. Fielding S, Watkins JL, Collins MA, Enderlein P, Venables HJ. 2012 Acoustic determination of the distribution of fish and krill across the Scotia Sea in spring 2006, summer 2008 and autumn 2009. *Deep-Sea Res. II* **59**, 173–188. (doi:10.1016/j.dsr2.2011.08.002)
46. Ward P *et al.* 2012 Food web structure and bioregions in the Scotia Sea: a seasonal synthesis. *Deep-Sea Res. II* **59**, 253–266. (doi:10.1016/j.dsr2.2011.08.005)
47. Atkinson A *et al.* 2019 Krill (*Euphausia superba*) distribution contracts southward during rapid regional warming. *Nat. Clim. Change* **9**, 142–147. (doi:10.1038/s41558-018-0370-z)
48. Stat M, Huggett MJ, Bernasconi R, DiBattista JD, Berry TE, Newman SJ, Harvey ES, Bunce M. 2017 Ecosystem biomonitoring with eDNA: metabarcoding across the tree of life in a tropical marine environment. *Sci. Rep.* **7**, 12240. (doi:10.1038/s41598-017-12501-5)
49. St. John MA, Borja A, Chust G, Heath M, Grigorov I, Mariani P, Martin AP, Santos RS. 2016 A dark hole in our understanding of marine ecosystems and their services: perspectives from the mesopelagic community. *Front. Mar. Sci.* **3**, 31. (doi:10.3389/fmars.2016.00031)
50. Perry AL, Low PJ, Ellis JR, Reynolds JD. 2005 Climate change and distribution shifts in marine fishes. *Science* **308**, 1912–1915. (doi:10.1126/science.1111322)
51. Poloczanska ES *et al.* 2013 Global imprint of climate change on marine life. *Nat. Clim. Change* **3**, 919–925. (doi:10.1038/nclimate1958)
52. Sunday JM, Bates AE, Dulvy NK. 2012 Thermal tolerance and the global redistribution of animals. *Nat. Clim. Change* **2**, 686–690. (doi:10.1038/nclimate1539)